Technology Collaboration Programme
by iea

International Energy Agency
Photovoltaic Power Systems Programme

Task 17 PV & Transport

PVPS

# PV-Powered Charging Stations: Sizing, Optimization and Control

2026

Report IEA-PVPS T17-8:2026

# What is IEA PVPS TCP?

The International Energy Agency (IEA), founded in 1974, is an autonomous body within the framework of the Organization for Economic Cooperation and Development (OECD). The Technology Collaboration Programme (TCP) was created with a belief that the future of energy security and sustainability starts with global collaboration. The programme is made up of 6.000 experts across government, academia, and industry dedicated to advancing common research and the application of specific energy technologies.

The IEA Photovoltaic Power Systems Programme (IEA PVPS) is one of the TCP's within the IEA and was established in 1993. The mission of the programme is to "enhance the international collaborative efforts which facilitate the role of photovoltaic solar energy as a cornerstone in the transition to sustainable energy systems." In order to achieve this, the Programme's participants have undertaken a variety of joint research projects in PV power systems applications. The overall programme is headed by an Executive Committee, comprised of one delegate from each country or organisation member, which designates distinct 'Tasks,' that may be research projects or activity areas.

The 28 IEA PVPS participating countries are Australia, Austria, Belgium, Canada, China, Denmark, Finland, France, Germany, India, Israel, Italy, Japan, Korea, Lithuania, Malaysia, Morocco, the Netherlands, Norway, Portugal, South Africa, Spain, Sweden, Switzerland, Thailand, Türkiye, the United Kingdom and the United States of America. The European Commission, Solar Power Europe and the Solar Energy Research Institute of Singapore are also members.

**Visit us at: www.iea-pvps.org**

# What is IEA PVPS Task 17?

The objective of Task 17 of the IEA Photovoltaic Power Systems Programme is to deploy PV in the transport, which will contribute to reducing $CO_2$ emissions of the transport and enhancing PV market expansions. The results contribute to clarifying the potential of utilization of PV in transport and to proposal on how to proceed toward realising the concepts.

Task 17's scope includes PV-powered vehicles such as PLDVs (passenger light duty vehicles), LCVs (light commercial vehicles), HDVs (heavy duty vehicles) and other vehicles, as well as PV applications for electric systems and infrastructures, such as charging infrastructure with PV, battery and other power management systems.


## Authors

- **Main Content:** Bruno Robisson, Fadi Agha Kassab, Miguel C. Brito, Nathanael Dougier, Saleh Cheikh-Mohamad
- **Editors:** Amalie Alchami, Manuela Sechilariu





**SUGGESTED CITATION**

Sechilariu M. (2025, Ed.), Celik B. (2025), Robisson B. (2023), Ngo V.L. (2023), Kassab F. A. (2024), Cheikh-Mohamad S. (2023), Brito M.C (2024), Locment F. (2025), Dougier N. (2023) and Alchami A. (Ed.) *PV-Powered Charging Stations: Sizing, Optimization and Control* (Report No. T17-8:2026). IEA PVPS Task 17. https://iea-pvps.org/key-topics/pv-charging-stations-2026//

**COVER PICTURE**

STELLA, Smart Transport and Energy Living LAb, Innovation Center of Université de Technologie de Compiègne, France

INTERNATIONAL ENERGY AGENCY

PHOTOVOLTAIC POWER SYSTEMS PROGRAMME

# PV-Powered Charging Stations:
## Sizing, Optimization and Control

**IEA PVPS**
**Task 17**
**PV and Transport**

Report IEA-PVPS T17-8:2026
January - 2026

ISBN 978-1-7642902-5-8
DOI 10.69766/HEJY2778

# AUTHORS


## Main Authors

Bruno Robisson, CEA Cadarache, France

Fadi Agha Kassab, Avenues, Université de Technologie de Compiègne, France

Miguel C. Brito, Faculdade de Ciências da Universidade de Lisboa, Portugal

Nathanael Dougier, Avenues, Université de Technologie de Compiègne, France

Saleh Cheikh-Mohamad, Avenues, Université de Technologie de Compiègne, France

## Contributing Author

Antonio Vallera, Faculdade de Ciências da Universidade de Lisboa, Portugal

Berk Celik, Avenues, Université de Technologie de Compiègne, France

Fabrice Locment, Avenues, Université de Technologie de Compiègne, France

Manuela Sechilariu, Avenues, Université de Technologie de Compiègne, France

Van-Lap Ngo, CEA Cadarache, France

## Editors

Amalie Alchami, Avenues, Université de Technologie de Compiègne, France

Manuela Sechilariu, Avenues, Université de Technologie de Compiègne, France

# TABLE OF CONTENTS

Acknowledgements ..... 6
List of abbreviations ..... 7
Executive summary ..... 7
1 Sizing for EV Workplace Charging Station ..... 10
1.1 An Empirical Study in France ..... 11
2 Technical economic and environmental co-optimization of PVCS ..... 36
2.1 Optimal sizing and energy management for a microgrid: A joint MILP approach for minimization of energy cost and carbon emission ..... 37
2.2 Optimizing Microgrid Sizing, Energy Management, and Electric Vehicle Integration ..... 60
3 PVCS: Intelligent Control and new Services ..... 73
3.1 Energy Cost Optimization via V2G Services ..... 74
3.2 Solar charging swappable EV batteries ..... 99
4 Electric bus charging stations ..... 104
4.1 Modelling of Electric Bus Operation and Charging Process: Potential Contribution of Local Photovoltaic Production ..... 105
Conclusions and future works ..... 129

# ACKNOWLEDGEMENTS

This paper has received valuable contributions from several IEA-PVPS Task 17 members and other international experts. Many thanks to all of them.

The French contribution was funded by ADEME France, project T-IPV, grant number #2308D0002 and project PV2E_Mobility grant number #1905C0043.

The Portuguese contribution was funded by the Portuguese Fundação para a Ciência e a Tecnologia (FCT) I.P./MCTES through national funds UIDB/50019/2020, UIDP/50019/2020 and LA/P/0068/2020.

# LIST OF ABBREVIATIONS

| | |
|---|---|
| 3G | Third Generation |
| AC | Alternating current |
| BES | Battery Energy Storage |
| BESS | Battery Energy Storage Systems |
| BMS | Battery Management System |
| BSS | Battery Swapping Stations |
| CAPEX | Capital Expenditures |
| CEA | Commissariat à l'Energie Atomique et aux Énergies Alternatives |
| $CO_2$ | Carbon dioxide |
| CPO | Charging Point Operator |
| DC | Direct Current |
| DSO | Distribution System Operator |
| E-bus(es) | Electric Bus (Buses) |
| EG | Electrical Grid |
| ESEV | Energy Supplier of Electric Vehicles |
| ESPV | Energy Supplier of Photovoltaics |
| EV | Electric Vehicle |
| FS/PFS | Feasibility Study / Prefeasibility Study |
| GA | Genetic Algorithm |
| GCMG | Grid Connected Microgrid |
| GEV | Generalized Extreme Value |
| GHG | Green House Gas |
| GTFS | General Transit Feed Specification |
| HMI | Human Machine Interface |
| HVAC | Heating, Ventilation, and Air Conditioning |
| ICE | Internal Combustion Engine |
| ID | Identification |
| IGM | Isolated Microgrid |
| LCE | Life Cycle Emissions |
| LCOE | Levelized Cost of Energy |
| Li-Ion | Lithium-Ion |
| MILP | Mixed-Integer Linear Programming |
| MPPT | Maximum Power Point Tracking |
| NOCT | Normal Operating Cell Temperature |
| OCPP | Open Charge Point Protocol |
| OPEX | Operating Expenses |
| PDF | Probability Density Functions |
| PHEV | Plug-in Hybrid Electric Vehicle |
| PV | Photovoltaic |
| PVCS | Photovoltaic Charging Station |

| | |
|---|---|
| PVO | Photovoltaic Operator |
| RES | Renewable Energy Sources |
| RFID | Radio-Frequency Identification |
| SCR/SPR | Self-Consumption Ratio / Self-Production Ratio |
| SOC | State of Charge |
| STC | Standard Test Condition |
| TOU | Time of Use |
| TSO | Transmission System Operator |
| V2G | Vehicle to Grid |
| V2H | Vehicle to Home |

# EXECUTIVE SUMMARY

Electric mobility is accelerating worldwide, increasing the demand for cleaner and more sustainable charging solutions. Among the most promising options are photovoltaic (PV)-powered charging stations (PVCS), which integrate solar energy production with electric vehicle (EV) charging infrastructure. These systems are becoming increasingly common in both urban and rural settings, reflecting a global shift toward renewable energy integration and greater energy autonomy.

However, the effective deployment of PVCS involves more than simply installing solar panels and chargers. Key challenges include the dimensioning of PV generation and storage systems to meet local energy demands, the management of energy flows between the PV source, the grid, and potential battery storage, and the control of EV charging to ensure system stability, operational efficiency, and user satisfaction. Without proper coordination, PVCS may face issues such as overloading, underutilization, or intermittent service availability.

Building on the initial IEA Task 17 Subtask 2 report—which examined the feasibility and fundamental requirements of PVCS – and a second report that addressed technical solutions and societal impacts, this third report advances the work further. It explores the deployment of PVCS within microgrid-based architectures, the integration of smart energy management and charging systems, and the incorporation of emerging services such as Vehicle-to-Grid (V2G) and battery swapping. It also considers the specific requirements and challenges related to charging electric buses with solar energy.

Effectively addressing these technical and operational aspects is essential to fully realize the potential of PV-powered charging, ensuring not only environmental sustainability, but also system reliability and economic viability.

### A. *Sizing for EV Workplace Charging Station*

This goal is to maximize on-site solar energy for charging electric vehicles via a dedicated control system. A modular sizing methodology was developed that separates the sizing problem into four relationships, allowing business model, charging strategy, and demand profile to vary independently, giving stakeholders flexibility to adapt the approach to different real-world scenarios. Results show that aligning charging with PV generation can greatly reduce infrastructure needs and costs. Workplace parking lots are especially suitable, as EV demand often matches predictable daytime solar production.

### *B. PVCS: Sizing and Energy Cost Optimization*

The optimal sizing and operation of PVCS in microgrid contexts involve complex trade-offs among technical, economic, and environmental objectives. A multi-objective framework based on MILP was developed to minimize both the levelized cost of energy (LCOE) and life cycle emissions (LCE) over the station's economic lifespan. Results show that while high solar irradiation improves both LCOE and LCE, site-specific conditions (e.g., climate, energy demand, grid availability) necessitate customized designs. The choice of PV and battery technologies plays a crucial role in achieving balanced outcomes.

### *C. PVCS: Integration of Vehicle-to-Grid (V2G) Services*

Since EVs are parked for extended periods, V2G services offer mutual benefits for grid operators and EV owners. A MILP-based optimization algorithm was designed to schedule EV battery charging and discharging, aiming to minimize energy costs while maximizing solar

utilization. Simulations demonstrated that dynamic scheduling strategies outperform static ones, yielding economic benefits without compromising driver requirements.

***D. PVCS for Electric Buses***

The deployment of electric buses in public transport highlights both their environmental advantages and deployment challenges. A case study in Compiègne, France, evaluated the impacts of various charging strategies – depot-only, terminal, and opportunity charging – on grid performance and service reliability. The integration of PV generation was assessed for its role in reducing emissions and grid stress. Results show significant trade-offs among strategies, affecting battery sizing, operational flexibility, and infrastructure demands. Although opportunity charging reduces battery size and energy consumption, it also imposes stress on the grid and requires costly infrastructure. Seasonal variability also limits solar potential in winter, reinforcing the need for energy storage.

## KEY FINDINGS

**A.** ***Sizing for EV Workplace Charging Station:***

- Using the Mean Power strategy instead of Plug and Charge halved (≈50 % reduction) the size of the required PV plant.
- Using the Solar Smart Charging strategy reduced the needed PV peak power to about one-third compared to the basic Plug and Charge scenario.
- The modular approach means that once the four relationships are computed for a “representative” site, other similar sites can be sized in hours instead of weeks—this is valuable for a CPO managing many workplace charging stations.

***A. PVCS Sizing and Energy Management:***

- Off-grid setups require larger components to handle low-sun periods;
- Higher battery capacity is associated with lower LCE; more PV panels improve LCOE;
- Economically optimal systems require higher initial investments, while environmentally optimal setups lead to increased long-term replacement costs;
- Greater grid interaction improves both economic and environmental outcomes;
- In the French case study, 54% of energy was locally produced, with the rest supplied primarily by the nuclear-dominated public grid.

***B. V2G Integration:***

- Small-scale V2G (e.g., residential) has limited impact but contributes to flexibility;
- Large-scale implementations (e.g., 100 EVs in a campus setting) provide better returns and support grid services more effectively.

***C. Electric Buses and PVCS:***

- Electric Buses reduce tailpipe emissions and contribute to urban air quality improvement;
- Depot-only charging: Simple, but leads to night-time grid peaks and larger battery requirements;

- Terminal + Depot charging: Reduces peak demand but needs more infrastructure;
- Opportunity charging: Cuts battery size by 83% and energy consumption by 9.4%, but stresses the grid due to high-power demands;
- PV integration lowers $CO_2$ emissions and eases peak demand, especially during high-use periods;
- Solar contribution is limited in winter, requiring battery storage for consistency.

# 1 SIZING FOR EV WORKPLACE CHARGING STATION

Electrification of transportation and the rise of EVs are driving the need for smart, sustainable charging infrastructure. Integrating PV into workplace charging stations offers a strategic solution: solar energy can directly supply EV demand, reducing reliance on the grid and enhancing environmental sustainability.

This study proposes a versatile and modular methodology to aid Charging Point Operators (CPOs) in optimally sizing PVCS, particularly in workplace environments. Recognizing that a CPO may oversee multiple sites, the authors emphasize an efficient workflow: sizing begins with a representative station and extrapolates to others – transforming a process that might take weeks into one executable in mere hours.

Their approach is grounded in an extensive empirical dataset from a research complex in Southern France: over 32 000 charging events spanning six years, 350 unique EV users, and 80 charging points. The study examines three different charging strategies, coupled with a business model aiming to maximize self-consumption of generated PV power.

By highlighting the synergy between solar generation and EV charging under real-world conditions, this chapter aims to guide CPOs, energy planners, and policymakers in designing efficient, solar-powered workplace charging infrastructure – paving the way for greener mobility and optimized renewable energy use.

## 1.1 An Empirical Study in France

PVCS are gaining traction due to the natural synergy between solar energy and electric vehicles. This study introduces a flexible methodology to help CPOs size key components of PVCS based on customizable factors like EV charging demand, strategy, and business model. By first applying the method to a representative site, CPOs can significantly reduce the time required to size additional stations. Applied to a real-world case in southern France with over 32 000 transactions, the results show that smart charging strategies, particularly Solar Smart Charging, can dramatically reduce PV system size requirements[1,2,3].

### 1.1.1 Introduction

On 4 November 2022, the French Senate enacted legislation mandating that exterior parking areas for light-duty vehicles exceeding 1 500 square meters allocate at least 50% of their surface area to solar panels [1]. The French government has also introduced a series of financial incentives to accelerate the transition towards a sustainable transportation sector, covering both the purchase of electric vehicles and the installation of charging infrastructure. These legal obligations and incentives collectively pave the way for the widespread adoption of energy systems that integrate both photovoltaic (PV) and electric vehicle (EV) technologies. Reviews of all possible interactions between these two technologies are provided in [2] – [5].

Among these possible interactions, large PV-powered charging stations (PVCS) for EV near workplaces are considered to be one of the most promising use cases. From a technical standpoint, in such scenarios, EV charging demand – which typically spans the entire working day – is found to be nearly concurrent with PV production. Additionally, if the number of EVs is sufficiently large, this demand becomes relatively predictable. As a result, the optimization of PV energy use is a priori facilitated by these two factors. This use case is also recognized as one of the simplest in terms of stakeholder interactions, allowing cooperation to be made more feasible, as demonstrated by proven experiments described in [6] and, on a larger scale, ten years later in [7]. Furthermore, when PVCS are made sufficiently large – both in terms of PV capacity and the number of charging points – economies of scale are achieved. Finally, when PV panels are installed as car park canopies, the user experience is enhanced (through vehicle shading and EV charging services), and the energy transition is supported.

In the context of large PVCS, several technical and financial stakeholders interact [2]. A PVCS with multiple charging points is managed by a Charging Point Operator (CPO). For simplicity, it is assumed that the EV driver interacts directly with the CPO, although, in practice, a third-party stakeholder known as the e – Mobility Service Provider may act as an intermediary. In the vicinity of the PVCS, ground-mounted PV plants and/or solar carports are installed and operated by a Photovoltaic Operator (PVO). To remain as generic as possible, the PVO and

---

[1] This chapter is based on the following publication: B. Robisson, V.-L. Ngo, L. Marchadier, M.-F. Bouaziz, and A. Mignonac, 'PV Sizing for EV Workplace Charging Stations – An Empirical Study in France', Applied Sciences, vol. 13, no. 18, 2023, https://doi.org/10.3390/app131810128.

[2] The content has been adapted to suit the context of this document.

[3] This work was supported by ADEME France, project PV2E_Mobility (grant number #1905C0043) and project T-IPV (grant number #2308D0002) and by the French National Program "Programme d'Investissements d'Avenir-INES.2S" (grant number ANR-10-IEED-0014-01).

CPO are assumed to be separate legal entities. It is also considered that the PV plant and charging stations are both connected to the distribution network, managed by the Distribution System Operator (DSO), but each has its own connection point (i.e., separate power meters). These power connections are used to serve a dual function: they supply electricity to the EV stations when PV generation is insufficient and allow surplus PV energy to be injected into the grid during periods of excess production.

Sizing PVCS at the earliest design stage is critical, especially for the CPO, as this will form the basis for subsequent design phases. However, this step is particularly challenging. First, by nature, the technical details of the final PVCS – such as the IT and power architecture and EV charging control algorithms (if any) – are unknown. Thus, during the sizing phase, the designer must select models that are not only approximate (i.e., lacking technical detail) but also reflective of feasible and practical technical solutions. Second, data on EV demand (e.g., arrival/departure times and energy needed to charge EV batteries) over a significant time horizon (at least six months to a year) is crucial for sizing the PVCS. However, such data is often unavailable or of poor quality at this stage. Third, various potential business interactions among stakeholders make the development of a generic sizing method particularly complex.

The objective of this study is to propose a method that addresses these challenges. First, the simplified models of PVCS used in this work are based on over ten years of experience analysing PV–EV interactions at CEA. Notably, this research considers three different EV charging strategies, the most complex of which has been validated with real users in two separate locations [6],[7]. Second, the method is built around four relationships that can be analyzed independently. One of these determines what proportion of EV annual consumption is supplied by PV, based on the number of EVs, a charging strategy, and the size of the PV plant. This relationship is derived from a large empirical dataset collected over more than six years (from 1 June 2016 to 31 August 2022), involving 350 EV users and 80 charging points at a workplace. Although calculating this relationship is resource-intensive, it can be reused for PVCS in similar contexts (i.e., large workplace car parks). The reuse of such pre-computations significantly reduces the time required to apply the method – from several days to a few hours. This feature is especially valuable for a CPO responsible for sizing multiple stations with comparable EV charging demands. Third, one of the four relationships, is specific to a particular financial arrangement among stakeholders. This relationship can be easily adapted to various business models without modifying the others. To the best of current knowledge, the proposed method is unique in offering this combination of properties.

The remainder of the chapter is structured as follows: Section 1.1.2 reviews the state of the art in this field and highlights the main contributions. Section 1.1.3 summarizes the proposed methodology, including its context, input data, and variables. Section 1.1.4 details the computation of the relationships between inputs and variables. These relationships pertain to 1.1.4.1 business models (i.e., stakeholders and their interactions), 1.1.4.2 EV consumption, 1.1.4.3 PV production and forecasting, and 1.1.4.4 charging strategies. Section 1.1.5 presents numerical examples of the methodology, while Section 1.1.6 provides an overview of the results and outlines the study's broader implications.

## 1.1.2 State of the Art

### *1.1.2.1 Research Positioning*

There are four stages in the project development process of an energy system [8]:

- The first one is the “idea development.” It consists of “brainstorming and idea generation activities to give the project a more rounded shape”;

- The second one is the “concept development” which describes the scope of the project (case descriptions, investment context, system and stakeholder overviews, etc.). It also specifies the resources required and estimates key financial (such as revenue stream, CAPEX, OPEX, etc.) and technical figures. Amongst them, the size of the main components of the system is determined. For example, the sizing of PVCS consists in determining one or all of the following quantities: the maximum power that the PV plant may deliver (also called “peak power”), the number of charging points (and possibly the maximum power that each of these charging points may deliver), the number of EVs that may be charged on the PVCS, or the capacity and the maximum power of the storage system. For such sizing studies, EV demand (number of daily EVs and their arrival and departure time), users’ behaviour, and vehicles’ characteristics are the most imperative type of input data. Other types of input data are also required, such as incentives, taxes, grid codes, PV potential, etc. The concept development phase also determines the project risks, its social and environmental impacts and its profitability;
- The third stage is called “business development” and outlines all the actions needed to make “real” the system sketched during the previous phase. During this phase, the system is first designed in detail and an operation plan to build it is provided;
- The last stage is dedicated to the project execution. This phase entails the construction and installation of the final system, plus any other civil work needed for the project operations.

The concept development phase typically comprises a prefeasibility study (PFS) and a feasibility study (FS). As described in [8], “the PFS scans a series of options and determines the best one in the set. The FS analyses in depth the best solution from the prefeasibility phase. The PFS reduces the number of options that are chosen to proceed with a more detailed fs and eventually with business development, ultimately saving time and money.”

The objective of this study is to propose a method for sizing PVCS during the early stages – specifically, the PFS – of the concept development phase. As emphasized in [9], such sizing is particularly crucial for the CPO, as it provides a strong foundation for the business development stage. However, performing this sizing at such an early stage is a particularly challenging task due to the limited availability and reliability of essential input data.

For example, key data required to size a PVCS is often unavailable or of low quality during the PFS. To address this, EV demand can be synthesized from statistical distributions based on experimental datasets [10]. However, due to daily and seasonal variability, these datasets must span a substantial time horizon (at least six months to one year) to be meaningful. Additionally, the technical specifications of the future power infrastructure, IT architecture, and control system are generally not known at this stage.

In this context, the term “control system” refers to the set of algorithms – classified into scheduling, clustering, and forecasting as in [11] – and the IT and power system interactions that collectively aim to optimize PVCS operation according to financial, efficiency, or environmental objectives [4]. Therefore, the concept development phase must employ simplified models of these control systems that can reasonably predict the performance of the final system while remaining sufficiently abstract to allow exploration of a wide range of design alternatives [12].

The following section reviews the state of the art concerning sizing during the concept development phase of energy systems that integrate at least both EVs and PV – whether in the context of a microgrid or not. Notably, studies that focus solely on the design of control

algorithms are excluded; readers can find such references in Table 1.1-1 of [9], under the column “optimal control.”

#### *1.1.2.2 Sizing PVCS at the Concept Development Step:*

The study in [9] details the sizing of the main components of a system comprising a household, a battery, a PV plant, and bidirectional EV chargers. It considers three EVs with identical weekday parking schedules (08:00 A.M – 06:00 P.M). The authors integrate the sizing problem into the optimal power management framework by treating component ratings as decision variables in addition to the power profiles of the EVs and batteries. These variables include battery energy storage (BES) capacity (kWh), BES and EV charger power ratings (kW), PV system peak power (kW), and inverter power rating (kW). The power management strategy aims to minimize total costs, including battery degradation, while accounting for network and component constraints. These constraints enable the implementation of advanced business models based on self-consumption, energy arbitrage, and frequency containment reserve market participation. The optimization problem is formulated and implemented using the Generic Algebraic Modeling System [13].

The authors in [14] propose an optimal sizing-control methodology for residential microgrids where EVs are modelled as controllable loads. The microgrid includes PV, wind turbines (WT), a bidirectional inverter, and a local BES. The optimization algorithm, based on Mixed Integer Linear Programming (MILP), is solved using CPLEX [15] and aims to minimize the annual electricity cost. Component sizes and the dispatched power profile serve as decision variables. In this study, the number of EVs is fixed and thus not treated as a sizing parameter. EV mobility data consist of deterministic behaviour for three EVs.

In [16], the authors identify the optimal sizes of PV, WT, and BES for a smart home microgrid in a vehicle-to-home context. The energy management system minimizes annual electricity costs using rule-based logic, while the sizing optimization employs the Particle Swarm Optimization technique [17]. Meteorological and EV mobility data (for a single vehicle) are synthetically generated using probabilistic distribution functions derived from existing datasets.

The authors in [18] investigate a workplace microgrid consisting of an EV charging station, BES, and PV plant. The system is controlled using expert rules designed to minimize grid interaction. The methodology determines the optimal PV tilt and BES size under two scenarios and across eight charging profiles. Optimal values are obtained through a “parametric analysis,” where parameters are tested within predefined ranges – for example, BES capacities from 5 kWh to 75 kWh in 5 kWh increments.

In [12], the system includes a PV plant and bidirectional EV chargers. One scenario considers a 2.64 MWp PV plant and 184 EVs. The charge/discharge control algorithm minimizes the deviation between day-ahead PV production commitments and actual production. The optimization is formulated as a linear problem with deterministic EV demand – vehicles are assumed to be available from 09:00 A.M to 06:00 P.M. The study also analyses different EV – to – PV ratios.

An economic study in [19] explores EV parking lots at workplaces equipped with PV in Ohio and California. It assesses the financial viability of such systems under varying PV capacities and economic assumptions. Vehicle mobility data (arrival and parking times) are statistically simulated using probability distributions derived from empirical data at Ohio State University’s parking garage. The analysis accounts for diverse incentives and tax deductions across jurisdictions. MATLAB™ is used for EV demand and grid emissions modeling, while PV output and financial analysis are performed using the System Advisor Model [20],[21]. A constant

charging power of 6.6 kW is assumed. A follow-up study by the same authors introduces a more advanced charging algorithm based on dynamic programming and optimization [22]. This algorithm maximizes PV energy utilization and minimizes grid impact while fulfilling EV energy needs. Parametric studies examine how various factors (PV size, installation cost, incentives, electricity rates, parking fees) influence financial outcomes, especially payback time.

The methodology in [23] focuses on sizing the PV system, stationary battery, and transformer in a PVCS microgrid. These component sizes, along with operational constraints, are included in an optimization model aimed at minimizing total system costs. The initial state-of-charge of EVs is modelled with a Gaussian distribution between 0.2 and 0.5. Other parameters, such as EV battery capacities, number of daily EVs, and arrival times, are also generated using Gaussian distributions. One numerical example considers a system with four 40 kW chargers, a 300 kWp PV system, a 600-kWh battery, and a 200-kW transformer. The study concludes that an optimal configuration with PV is more cost-effective than one without.

In [24], the authors present a simple, multi-phase methodology for sizing a microgrid comprising a PV system, BES, and EV charging infrastructure. Implemented via a customizable Excel tool, the method is designed for use by various stakeholders. Users can adjust EV charging profiles, physical dimensions, and financial parameters to evaluate system performance from different perspectives. The energy management strategy mirrors a realistic deployment approach: grid energy is used when PV and BES outputs are insufficient; surplus PV energy is stored or exported to the grid to avoid overloading and ensure high PV utilization.

The study in [25] examines PV and EV integration in an office building in southern Italy. One EV is charged during working hours under four different driving needs (from 0 km/day to 120 km/day). Two charging modes are compared: uncontrolled AC charging and controlled DC charging, which prioritizes the use of surplus PV energy. The analysis evaluates self-consumption and self-production metrics across four PV capacities (4.5 kWp to 9 kWp) and various charger sizes.

In [26], the authors analyze long-term EV – PV integration in a household over a ten-year period, accounting for battery and PV aging. Scenarios vary based on annual driving distance (10 000– 25 000 km/year), charging strategy (uncontrolled or basic controlled charging), and PV system characteristics (location and size ranging from 2 kWp to 10 kWp). User profiles are also considered: a "commuter" not home during workdays versus a "private user" who returns home several times a day. EV charging profiles for these user types are synthesized from statistics found in [27].

#### *1.1.2.3 Synthesis*

The authors in [2] propose classifying systems that integrate PV and EV based on three main criteria:

- Spatial configuration: Systems may be deployed at different scales, including households, buildings, charging stations, or broader territories. An extension of this criterion is proposed by also considering the size of the PV plant and the number of EV users;
- Technological environment: This refers to the various technological components that are included in or added to the system. These components can include BES, WT, Heating, Ventilation, and Air Conditioning systems, and network technologies such as DC microgrids;
- Smart control strategy: Strategies are further categorized by their objectives, which may be:

- Economic, such as minimizing electricity costs or maximizing revenues;
- Energy-related, such as improving self-consumption or reducing grid impact;
- Environmental, such as lowering $CO_2$ emissions.

Additionally, the coordination method – i.e., the mathematical formulation of the strategy – is a key distinction. These methods may include:

- Optimization methods (e.g., MILP);
- Heuristic methods (e.g., rule-based expert systems);
- Hybrid methods, which combine heuristic and optimization approaches.

As described in Section 1.1.2.1, prefeasibility studies are designed to explore a wide range of potential solutions, while feasibility studies focus on evaluating the most promising ones in greater detail. In practice, these phases differ primarily in terms of complexity, particularly regarding the data required and the level of technical expertise involved. This expertise often concerns the complexity of the charging schedule algorithms and the software used for implementation. Heuristic methods are commonly employed during the prefeasibility phase, while optimization methods are more typical in feasibility studies.

Table 1.1-1 summarizes the reviewed studies in Section 1.1.2.2 using the criteria mentioned above, as well as additional dimensions: the targeted project development stage, EV fleet and PV plant size, EV mobility data, sizing methods, and the variables/parameters being sized.

**Table 1.1-1 Summary of literature review**

| | [9] | [14] | [16] | [18] | [12] | [22] | [23] | [24] | [25] | [26] | This work |
|---|---|---|---|---|---|---|---|---|---|---|---|
| **Development Stage** | FS | FS | PFS | PFS | FS | FS | PFS | PFS | PFS | PFS | PFS |
| **Spatial Configuration** | Household | Residential Microgrid | Household | CS | CS | CS | CS | CS | Office | Household | CS |
| **Fleet Size** | 3 EVs | Hundreds of EVs | 1 EV | 1 EV | Dozens to hundreds of EVs | Dozens to hundreds of EVs | Several EVs | Several EVs | 1 EV | 1 EV | Dozens to hundreds of EVs |
| **PV Size** | Up to 50 kWp | Hundreds kWp | Several kWp | Several kWp | Dozens to hundreds of kWp | Dozens to hundreds of kWp | Hundreds kWp | Several kWp | 4.5 - 9 kWp | Several kWp | Dozens to hundreds of kWp |
| **EV Mobility Data** | Deterministic | Deterministic | Probabilistic | Deterministic | Deterministic | Probabilistic | Probabilistic | User-defined | Deterministic | Probabilistic | Empirical |
| **Components** | PV, BES, EV Charger | PV, WT, BES | PV, WT, BES | PV, BES | PV, EV | PV, EV | PV, BES, Transformer | PV, BES, EV | Building, PV, HVAC, EV | PV, EV | PV, EV |
| **Control Algorithm** | Nonlinear Optimization | MILP | Rule-based | Rule-based | LP | DP | MILP | Rule-based | Rule-based | Rule-based | Rule-based |
| **Sizing Algorithm** | Nonlinear Optimization | MILP | Optimization PSO | Parametric Analysis | Parametric Analysis | Parametric Analysis | MILP | Parametric Analysis | Parametric Analysis | Parametric Analysis | Parametric Analysis |
| **Sized Variables** | PV, BES, EV Charger Ratings | PV, WT, BES sizes | PV, WT, BES Ratings | BES Ratings | PV Ratings #EVs | PV Ratings | PV, BES,EV Transformer Ratings | PV, BES Charger Ratings | PV,EV Charger Ratings | PV Ratings | PV, #EV |
| **Tool** | GAMS | CPLEX | – | – | – | Matlab, SAM | – | Customized tool | TRNSYS | PVSOL | Matlab |

Abbreviations: FS = Feasibility Study, PFS = Prefeasibility Study, CS = Charging Station, HVAC= Heating, Ventilation, and Air Conditioning, MILP = Mixed Integer Linear Programming, LP = Linear Programming, DP = Dynamic Programming, PSO = Particle Swarm Optimization, GAMS = Generic Algebraic Modeling System SAM = System Advisor Model.

### *1.1.2.4 Contribution*

EV charging demand data is considered to be among the most important input parameters in PFS and FS. More precisely, it is believed that, in order to obtain accurate results, this EV charging demand must be as representative as possible of the use case under study. In particular, it should reflect both the variability of EV users' behaviour over an extended period and the technical characteristics of the EVs and the charging infrastructure.

It is also believed that standard EV charging demand profiles can be defined to correspond to typical scenarios, such as:

- Workplace parking lots, where EVs remain plugged in during work hours;
- Shopping centres, where users arrive throughout the day and stay for a few hours;
- Residential areas, where users arrive in the evening and leave in the morning;
- Delivery fleets, where EVs arrive and depart at fixed times during the day.

The workplace parking lot use case is the focus of this study. Empirical data has been collected over more than six years at an industrial and research complex in southern France. As detailed in Section 1.1.4.2, the dataset is composed of over 32 000 charging transactions, 350 EV users, more than 40 EV models, and 80 charging points. Based on the literature review and to the best of current knowledge, this study is believed to be the first to describe a sizing procedure based on such a large, real-world EV charging dataset.

Furthermore, the computational logic of the proposed methodology is structured around four key relationships between input data and internal variables (defined in Section 1.1.3.3). Of these, Relationship 4 – which links the self-production ratio to the production-to-consumption ratio – is the most complex. To derive it, the designer must

- collect and process input data (mainly EV demand and PV production/forecast);
- perform simulations, and;
- aggregate the simulation results.

Relationship 1 connects energy price and self-production rate and can be readily adapted to business models that aim to increase self-production. Relationships 2 and 3 are relatively easy to compute.

Thus:

- When the PVCS designer assumes that EV charging demand follows a standard profile, the pre-computed values of Relationship 4 can be reused. The designer may also adjust Relationship 1 if a different business model is considered. In both cases, the required effort is minimal (i.e., a few hours of work for a non-specialist);
- For specific or non-standard use cases, the pre-processed data provided in this research cannot be reused. All four relationships must be recomputed. This enables the most precise estimation of project performance but requires significantly more effort. It is estimated that 3 to 4 weeks of work with solid programming skills are needed.

In summary, the modular structure of the method allows business models to be modified independently of other parameters, and intermediate results to be pre-computed. Once these pre-computations are completed, the sizing procedure is made quick and straightforward. To the best of current knowledge, no other method is known to possess such properties.

This approach is particularly useful, for example, for a CPO who needs to size multiple charging stations with similar demand profiles. In that case, the CPO would compute the relationships once, based on a representative charging station, and then reuse them – especially Relationship 4 – to significantly accelerate the sizing of the remaining stations.

## 1.1.3 Context and Methodology

### *1.1.3.1 Use-Case: CEA Cadarache EV Charging Infrastructure (EVCI) and PV Plant*

The data collection took place at the Cadarache research centre of the French Alternative Energies and Atomic Energy Commission (CEA, the French acronym for Commissariat à l'Énergie Atomique et aux Énergies Alternatives), located near Aix-en-Provence. This research centre has its own water, heating, lighting, and electricity distribution network, within which it operates as the DSO. A private bus service is provided for employees to commute and to travel between laboratories and canteens. A taxi service is also available for intra-site transportation. Thus, the Cadarache centre can be seen as a privately-owned town with a population of approximately 5 000, managed by the CEA.

The CEA also set up an Electric Vehicle Charging Infrastructure (EVCI) during the summer of 2016. It consists of 40 Diva-type terminals, produced and installed by G²Mobility, which was acquired by TotalEnergies in 2018. Each Diva terminal includes two 22 kW AC charging points. Each charging point is equipped with a Type 2 socket for mode 3 connections and a Type E socket for mode 1 and 2 connections. These charging stations were installed either individually or in groups of up to four Diva terminals, forming 30 charging stations spread throughout the centre. Each station has an embedded IoT gateway that communicates via 3G networks using Open Charge Point Protocol (OCPP) commands. As soon as an EV is plugged in, it charges at its nominal power. In other words, the EVCI enables vehicles to charge as rapidly as possible from the moment they are connected. This charging strategy, referred to as the "Plug and Charge" strategy in this work, is generally the default approach used by most commercial charging points.

The CEA also conducts research at Cadarache in collaboration with INES on solar thermal energy and PV. In particular, it tests and evaluates innovative PV systems (such as Tandem Perovskite-Silicon PV, bifacial PV, and single- and dual-axis solar trackers) ranging in size from individual modules to systems of several tens of kilowatts. The energy produced by this equipment – aggregating up to 50 kWP – is injected into the CEA's private power network. Furthermore, the CEA plans to install additional PV plants, either ground-mounted or building-integrated, as well as PV solar canopies. In the latter case, these PV installations will be designed for a self-consumption scheme, described in the following section.

### *1.1.3.2 Collective Self-Consumption Scheme*

As explained in the introduction and visualized in Figure 1.1-1, the general case is considered, in which the EVCI and the PV installation are managed by two separate entities, namely the Charging Point Operator and PV Operator (CPO and PVO). The CPO has to manage the charging of a certain number of EVs while utilizing the production from the PV plant, characterized by a certain peak power, noted $P_{peak}^{PV}$. It is also considered that an agreement on the exchange of PV energy is established between them. Without loss of generality, this agreement could be a partnership with a 'third party' called Legal Person (LP), or 'Personne Morale Organisatrice' in French, according to the scheme called "collective self-consumption" in France. This LP entity plays the role of a facilitator for the financial as well as power flows between the CPO and the PVO. The CPO also contracts with an energy supplier (ESEV) that provides supplementary energy to the charging stations when PV production is insufficient to the EV charging consumption. In the meantime, the PVO also establishes a contract with another energy supplier (ESPV), which extracts the surplus PV energy produced when there is more PV production than EV consumption.

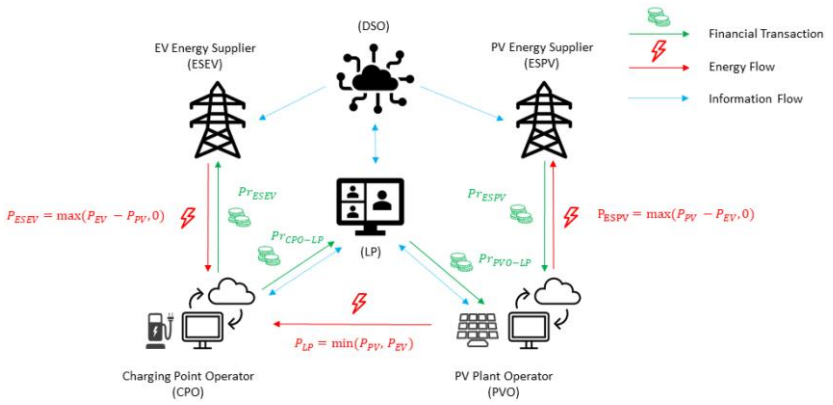


**Figure 1.1-1 Interactions of the EVCI's stakeholders.**

In this study, the power $x$ is denoted $P_x$. The energy of $P_x$ over a period $\Delta$, $E_x^\Delta$ is the integral of this power over $\Delta$: ($E_x^\Delta = \int_0^\Delta P_x dt$). The energy of the power $P_x$ calculated over a day, a month and a year are noted $E_x^d$, $E_x^m$ and $E_x^a$, respectively. The energy of the power $P_x$ computed on an arbitrary period is noted without a subscript, i.e., $E_x$ . The price per kWh that actor A pays when he buys a given amount of energy from actor B is noted $Pr_{B-A}$. It is important to note that this price may also include other services, apart from the energy production fee itself, such as transport, taxes and contributions.

With these notations (summarized in Table 1.1-2), the principle of this scheme, represented in Figure 1.1-2, is the following:

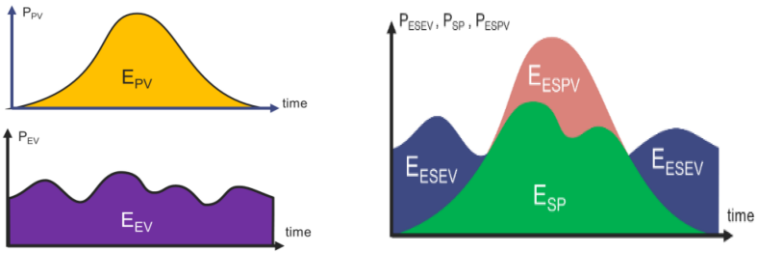


**Figure 1.1-2 Principle of collective self-consumption scheme.**

**Table 1.1-2 Nomenclature of variables used in this study.**

| Symbol | Explanation |
|---|---|
| $P_{EV}$ | Power supplied for EV Charging (kW) |
| $P_{PV}$ | Power generated by PV (kW) |
| $P_{ESEV}$ | Power extracted from the grid to charge EV (kW) |
| $P_{ESPV}$ | Power injected to the grid from PV (kW) |
| $P_{SP}$ | Power from PV for EV charging (kW) |
| $E^{\Delta}_{EV,PV,ESEV,ESPV,SP}$ | Integration of the corresponding powers over certain duration Δ (kWh) |
| $Pr_{PVO-ESPV}$ | Purchasing price of $E_{ESPV}$ by ESPV (€/MWh) |
| $Pr_{ESEV-CPO}$ | Purchasing price for $E_{ESEV}$ by CPO (€/MWh) |
| $Pr_{LP-CPO}$ | Purchasing price for $E_{SP}$ by CPO (€/MWh) |
| $Pr_{CPO}$ | Mean power price for the CPO (€/MWh) |

- The PV power ($P_{PV}$) and the corresponding energy ($E_{PV}$), produced by the PV plant during the period, are visualized in the top left part of the figure;

- The charging power ($P_{EV}$) and energy ($E_{EV}$) consumed by the EVs are represented on the bottom left diagram;
- The CPO partially charges the EVs with the power $P_{SP}$ (SP for Self-Production) such that $P_{SP} = min(P_{PV}, P_{EV})$. The CPO buys the associated energy, represented in green and noted $E_{SP}$ to the LP at a price noted $Pr_{LP-CPO}$;
- The PVO, for his part, sells $E_{SP}$ to the LP at a price noted $Pr_{PVO-LP}$;
- The CPO also charges the EVs with the power $P_{ESEV}$ that complements $P_{SP}$ when there is not enough solar power (i.e., such as $P_{ESEV} = max(P_{EV} - P_{PV}, 0)$). The CPO buys the associated energy, represented in dark blue and noted $E_{ESEV}$, to the power supplier ESEV at a price noted $Pr_{ESEV-CPO}$;
- The PVO injects in the network the power $P_{ESPV}$ , if any, produced by the PV plant but not consumed by the EVS (i.e., such as $P_{ESPV} = max(P_{PV} - P_{EV}, 0)$). The PVO sells the associated energy, represented in pink and noted $E_{ESPV}$, to the power supplier ESPV at a price $Pr_{PVO-ESPV}$.

In such a configuration, the local DSO is responsible for the virtual dispatch ("virtual" because the dispatch is performed in front of the meter); the DSO measures $E_{EV}$ and $E_{PV}$ from the power meters of the EV charging point and the PV plants, respectively. The meters are read at a frequency that depends on the market time step whose value depends on countries. The DSO computes $P_{ESPV}$, $P_{ESEV}$, $E_{SP}$ based on the following logics and transfers these values to the LP, ESPV and ESEV, respectively.

- $E_{ESPV} = max(E_{PV} - E_{EV}, 0)$ ;
- $E_{ESEV} = max(E_{EV} - E_{PV}, 0)$ ;
- $E_{SP} = min(E_{PV}, E_{EV})$ .

### *1.1.3.3 Main Internal Variables*

The ratio between the total PV production to the total EV, computed for an arbitrary period, is termed Production-to-Consumption ratio (or $PTC$).

$$PTC = \frac{E_{PV}}{E_{EV}} \quad (1.1\text{-}1)$$

The Self-Production Rate ($SPR$) and Self-Consumption Rate ($SCR$) are also considered, which represent the proportion of total EV charging demand being supplied by the PV production and the proportion of total PV production used for EV charging, respectively. These variables are, for an arbitrary period, defined as follows:

$$SPR = \frac{E_{SP}}{E_{EV}} \quad (1.1\text{-}2)$$

$$SCR = \frac{E_{SP}}{E_{PV}} \quad (1.1\text{-}3)$$

A period $d_i$ is considered during which the different prices are assumed to remain constant. The duration of such a period depends on the pricing scheme; if the prices are flat, the period is generally one year. On the contrary, if the prices are time-varying, the period is the market time step. The annual energy cost and the Mean Power Price, $Pr_{CPO}$ (€/MWh), which is the effective price of electricity that the CPO has to pay for both electricity from the PV and the electricity from the grid, are then calculated using equations (1.1-4) and (1.1-5).

$$Cost^{a}_{CPO} = \sum_{di}^{Year} E^{di}_{SP} \times Pr^{di}{}_{LP-CPO} + E^{di}_{ESEV} \times Pr^{di}{}_{ESEV-CPO} \quad (1.1\text{-}4)$$

$$Pr_{CPO} = \frac{Cost^{a}_{CPO}}{E^{a}_{EV}} \quad (1.1\text{-}5)$$

### *1.1.3.4 Methodology Description*

#### 1.1.3.4.1 Inputs/Output Data

This section describes the input data required, depending on the elements that are to be sized:

- Given a target $Pr_{CPO}$ (€/kWh) and a number of EV users, what should the PV peak power be (kWp)?
- Given a PV peak power (kWp) and a number of EV users, what should the $Pr_{CPO}$ be (€/kWh)?
- Given a PV peak power (kWp) and a target $Pr_{CPO}$, what should be the maximum number of EV users?

The row name of Table 1.1-3 represents the targeted outputs, while the columns are the input data. For example, in order to calculate the peak power of a PV plant (first line of the table), 8 out of 9 inputs (marked with an x symbol) must be collected. The CPO has to provide the price of the power from the network ($Pr_{ESEV-CPO}$) and from the PV plant ($Pr_{ESPV-CPO}$); he also needs its target of Mean Power price ($Pr_{CPO}$), obtain data about potential PV production (location of the plant, orientation, tilt angle and possibly PV production and forecast profiles), the expected number of EVs and their main characteristics (size and efficiency of the embedded charger, capacity of the battery, etc.). He also needs a charging session history that contains, for each session, the start date and the end date of the session. This history also has to contain the energy withdrawn by the car during each session. The history also has to record the name of the charging point and the user's badge number. Lastly, the CPO has to obtain the relationship between a badge and the EV model.

**Table 1.1-3 Input and Output data.**

| Input / Output | Price Network Power $Pr_{ESEV-CPO}$ | Price PV Power $Pr_{ESPV-CPO}$ | Mean Power Price $Pr_{CPO}$ | PV Potential | PV Peak Power $P_{PV}^{peak}$ | #EV Users | #EVs Characteristics | Charging Session History | Badge/EV Model |
|---|---|---|---|---|---|---|---|---|---|
| Peak Power | x | x | x | x | | x | x | x | x |
| Mean Power Price | x | x | | x | x | x | x | x | x |
| #EV users | x | x | x | x | x | | x | x | x |

#### 1.1.3.4.2 Principles

In this section, the main principles of the methodology are briefly described through four different relationships among various inputs, outputs, and variables, as illustrated in Figure 1.1-3. First, the energy exchange scheme between the CPO and the PVO needs to be specified. This scheme is then used to derive a relationship between the $SPR$ and the Mean Power price ($Pr_{CPO}$), with different prices as inputs. This first relationship is described in Section 1.1.4.1.

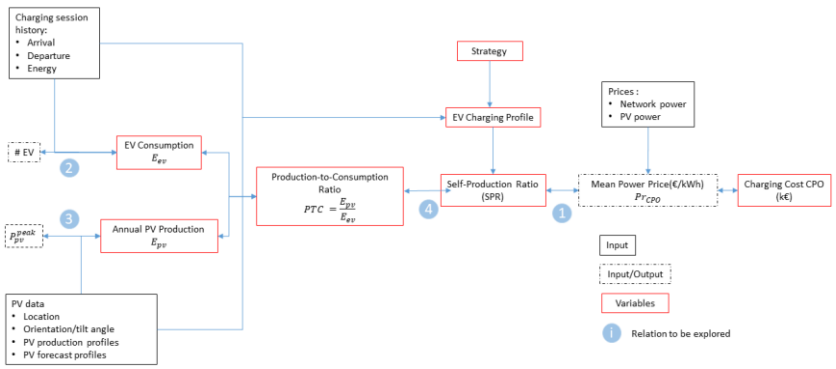


**Figure 1.1-3 Computational procedure for EV and PV sizing.**

The charging session history is then used to express the annual EV energy consumption as a function of the number of EVs. This second relationship is then given in Section 1.1.4.2.

The yearly PV production is then estimated as a function of the PV peak power $P_{PV}^{peak}$. This production depends on the solar potential that varies with the location of the PV plant, its orientation and its tilt angle. Section 1.1.4.3 will specify more details about this relationship.

Lastly, the PV production forecast profile is required, which is then combined with the charging session history to reconstruct the corresponding charging power profiles based on a given charging strategy. Based on these profiles and PV production profiles, the computation of the $SPR$ can be performed. In addition, it is also possible to compute the $PTC$. The relationship between the $SPR$ and $PTC$ is an abacus (that can then be approximated using empirical formulas as described in Appendix A[4]), which is presented in Section 1.1.4.4.

The diagram in Figure 1.1-3 describes the computational logic flow for this methodology. The black plain line boxes are inputs and the dotted ones are inputs or outputs. The red boxes represent internal variables. Lastly, the bidirectional arrows represent the reciprocal relationship between two quantities (if one is known, the other can be determined and vice versa).

## 1.1.4 Relationships Necessary for the Application of the Method

### *1.1.4.1 Business Model*

#### 1.1.4.1.1 Hypothesis

It is considered in this study that $Pr_{ESPV} = Pr_{PVO-LP}$, this means that all revenues of the PVO come with the same price, thus making its revenue independent of neither $SPR$ nor $SCR$.

#### 1.1.4.1.2 Relationship 1: Self-Production Rate versus Mean Power Price

The cost $Cost_{CPO}$ given in (1.1-4) can be rewritten by replacing $E_{ESEV}$ with $E_{ESEV} = E_{EV} - E_{SP} = E_{EV} - SPR \times E_{EV} = E_{EV} \times (1 - SPR)$:

$$Cost_{CPO} = SPR \times E_{EV} \times Pr_{LP-CPO} + (1 - SPR) \times E_{EV} \times Pr_{ESEV-CPO} \quad (1.1\text{-}6)$$

[4] https://doi.org/10.3390/app131810128.

The Mean Power price, previously given in (1.1-5), is then obtained by dividing Equation (1.1-6) by $E_{EV}$, thus establishing a linear relationship between $Pr_{CPO}$ and $SPR$:

$$Pr_{CPO} = Pr_{ESEV-CPO} - SPR \times (Pr_{ESEV-CPO} - Pr_{CPO-LP}) \quad (1.1\text{-}7)$$

When $Pr_{ESEV-CPO} > Pr_{CPO-LT}$, the Mean Power price for the $CPO$ linearly decreases with the increasing value of $SPR$. In other words, if electricity from the PV plant is more affordable then from the grid, self-production has to be prioritized. When $SPR = 0, Pr_{CPO} = E_{EV} \times Pr_{ESEV}$. This means that when there is no PV available for EV charging, the Mean Power price is equivalent to the price of the power from the grid. When $SPR = 1, Pr_{CPO} = Pr_{CPO-LP}$. This means that when there is no power coming from the network, the Mean Power price is the price of the power coming from the PV plant.

### *1.1.4.2 EV Consumption*

#### 1.1.4.2.1 Charging Periods

Data from 31 014 charging sessions were collected for more than 6 years, spanning from 1 June 2016 to 31 August 2022. Each charging session record contains the start and end time stamps of the session (noted $ST$ and $ET$, respectively), the identification number ($ID$) of the charging point, the badge number of the user and the energy that has been supplied to the EV. The transaction duration, $ET - ST$, is denoted $TD$.

Figure 1.1-4 illustrates the distributions of the start and end times of the dataset. It is observed that the start time of the charging sessions is statistically concentrated around 08:00 A.M (start of work hours), lunch time and early afternoon (after 04:00 P.M, when the business trips are terminated). There are also three main periods during which the majority of the charging sessions terminate. The first one is at 09:00 A.M when the service cars that have been connected the day before are disconnected to be used for business trips, the second one is after lunchtime and the last period is at the end of the working day (around 05:00 P.M) when employees leave the centre. The average duration and energy consumption of each charging session were 11.3 h and 17.22 kWh, respectively, and a total of 551 MWh of electricity was consumed.

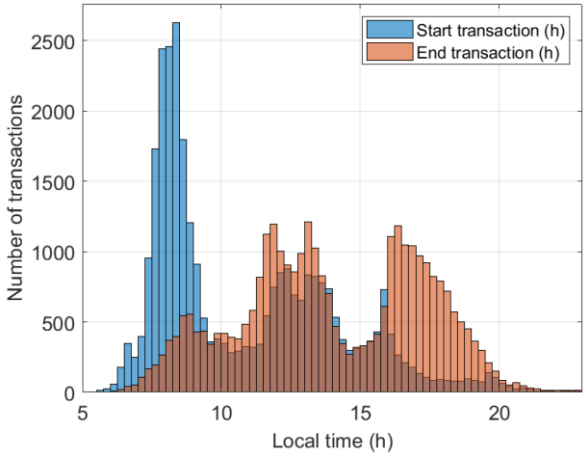


**Figure 1.1-4 Histograms of start and end times of charging sessions.**

#### 1.1.4.2.2 EV Users and EV Fleet Compositions

The number of "active" and "delivered" badges is computed from the EVCI charging session history. A badge is said to be “active” from the start of its first charging session until the end of

its last recorded session. The status “inactive” will be given otherwise. A badge is said to be “delivered” from its first connection to the ESEV. The number of active and delivered badges per day is described in Figure 1.1-5, where it can be observed that 348 RFID badges were delivered to EV (including PHEV) owners, with up to 200 active badges at the end of the considered period. Between 2021 and 2022, the number of delivered badges increased steadily by around 100 per year. At the end of the collection horizon, all the badges are inactive due to the definition of an active badge (i.e., they are all inactive after their last connection). It is also noted that there is a considerable amount of delivered inactive badges. This can be attributed to the loss of badges or to the fact that the users left them permanently or they stopped charging their EVs within the facility.

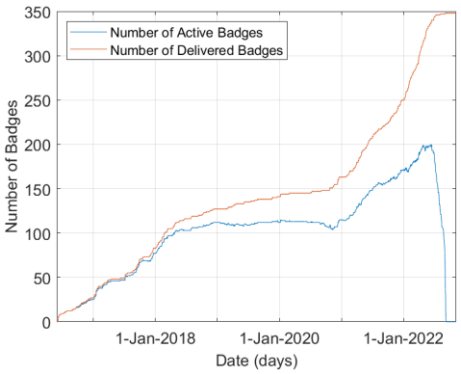


**Figure 1.1-5 Number of active and delivered badges.**

#### 1.1.4.2.3 EV Characteristics

Technical information regarding the vehicle corresponding to the badge was also recorded: vehicle model and usage category (personal, internal taxi and service car). Amongst all the delivered badges, 232 vehicles are attributed to employees’ personal vehicles, eighty-four vehicles are for facility services and three Renault ZOE for internal taxi services. An additional 29 vehicles serving external companies are also among the considered EVs. In terms of car models, there is a very clear predominance of Renault ZOE, which represents 38% of the fleet. There are also, among others, 10% of Peugeot e208, 7% of Renault Twingo, 8% of Tesla (Model + and Model S) and 5% of Nissan Leaf vehicles.

Primary characteristics of vehicles were also collected from publicly available sources, namely, the nominal power of the on-board chargers (kW) and their battery capacity (kWh). Figure 1.1-6 displays the histogram of these nominal powers and battery capacities of the considered fleet. It is observed that approximately 45%, 30% and 25% of EVs have nominal charging power at 22 kW, 11 kW and less than 11 kW, respectively. Additionally, it is observed that more than half of the EVs have a battery capacity between 45 and 55 kWh.

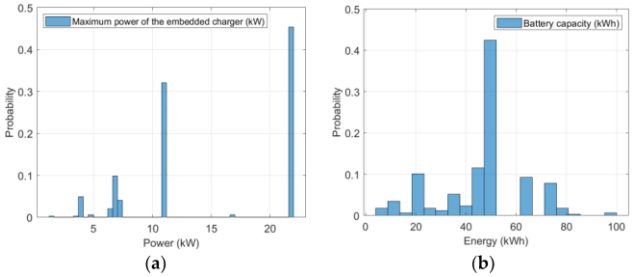


**Figure 1.1-6 Histograms of vehicles’ (a) nominal charging power and (b) battery capacity.**

#### 1.1.4.2.4 Energy Consumption

The aggregated daily, weekly, monthly, quarterly, and annual energy delivered to the EVs has been computed from the EV charging session history. Figure 1.1-7 demonstrates that the total monthly energy consumption data can be classified into four groups over the entirety of the data collection. The first period, called pre-COVID-19, started in June 2016 and terminated at the beginning of the COVID-19 crisis. The second period corresponds to the first COVID-19 lockdown in France (March 2020 – April 2020), during which very little charging service was used, leading to minimal electricity consumption. The third period (May 2020 to February 2022 has seen the introduction of the hybrid-working mode (i.e., normal onsite and work from home) and, thus, resulted in charging patterns similar to that of the first period but with slightly lower consumption. The last period of the considered horizon (March 2022 to August 2022) bears an identical context to the first period since the facility has returned to the pre-COVID-19 working mode (work from home is still available but has been exercised negligibly). It can be noticed that the electric consumption has increased significantly compared to the first and third periods. This increase can be attributed to the rise in the number of active badges during this period (as seen in Figure 1.1-5).

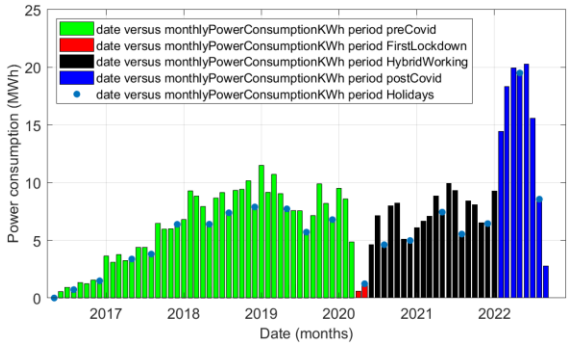


**Figure 1.1-7 Monthly energy consumption of the dataset.**

#### 1.1.4.2.5 Relationship 2: Active Badge versus Energy Consumption

Figure 1.1-8 illustrates the relationship between the monthly energy consumption (noted $E_{monthly}$, in kWh) and the number of active badges (noted $B_{monthly}$ without units) during the same month. The colours used in Figure 1.1-8 represent the same periods in Figure 1.1-7. It can be observed that there exists a simple linear dependence (represented with a dotted line) between the number of active badges and the maximum monthly energy consumption. This dependency is expressed in the following formula, which will be referred to as the second relationship in the methodology:

$$E_{monthly}[kWh] = 100 \times B_{monthly} \quad (1.1\text{-}8)$$

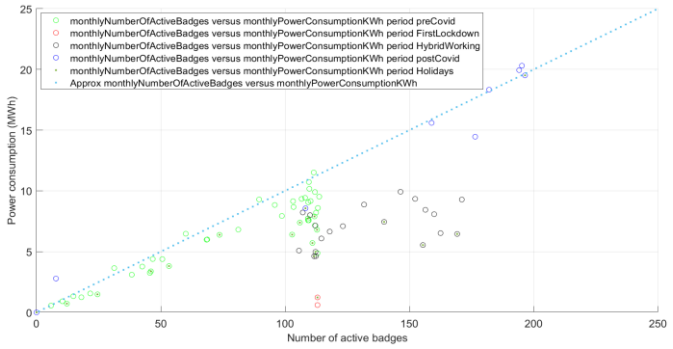


**Figure 1.1-8 Monthly EV power consumption versus monthly number of active badges.**

### *1.1.4.3 PV Production*

#### 1.1.4.3.1 Production and Forecast Profiles

The PV production forecast is based on public forecasts provided by the French Transmission System Operator (TSO): RTE. This forecast represents the aggregated French PV production and is calculated on the morning (approximately at 08:00 A.M) of the current day. The time step of the forecast is one hour. The forecast data for the considered period has been retrieved. It is represented in Figure 1.1-9 (left). As the installed PV capacity increased significantly in France during this period, the values have been corrected to obtain forecasts as if the installed capacity had been constant. These values have also been normalized to correspond to the production of a plant with a given peak power. In Figure 1.1-9 (right), this peak power is equal to 1 kWp.

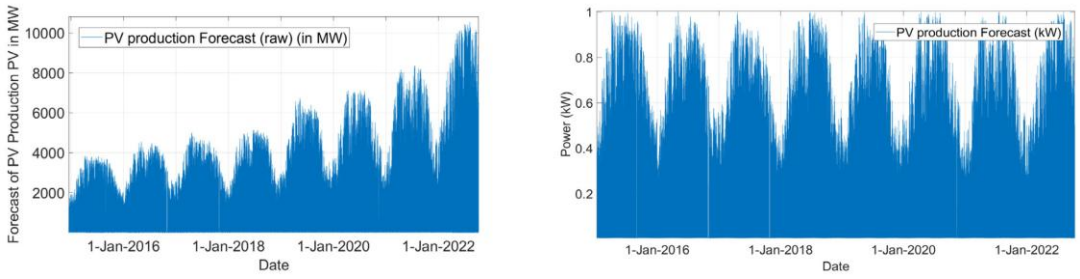


**Figure 1.1-9 Raw production forecast (left) and corrected values (right).**

In order to eliminate the effect of forecast imprecision, it is supposed that the CPO is able to perfectly forecast the PV production. Thus, the forecasted data is considered as the PV production.

#### 1.1.4.3.2 Relationship 3: Yearly PV Production versus Peak Power

There are two manners to obtain the yearly PV energy production from a peak power value for a given location as required to obtain the third relationship.

- If production profiles are available, integrating the power over a complete year gives the energy produced during this year;
- If production profiles are not available, many free software tools like PVGIS [28] estimate the annual PV production per peak power value.

### *1.1.4.4 Solar EV Charging*

#### 1.1.4.4.1 Production-to-Consumption Ratio

The $PTC$ ratio has been calculated for annual periods (each beginning on the 1st of June and ending on the 31st of May the following year) and for the period that begins on the 1st of June 2021 and ends on the 31st of August 2022. These values are summarized in Table 1.1-4, where it can be observed that the annual PV production is relatively constant while EV electricity consumption varies considerably.

**Table 1.1-4 Sum-up of the PV production, the EV consumption and the $PTC$ ratio over 6 year period.**

| Periods | Duration (Months) | Annual PV Production (100 kWp) MWh | Annual EV Consumption (MWh) | Annual *PTC* Ratio |
|---|---|---|---|---|
| 1 June 2016–31 May 2017 | 12 | 178 | 24 | 7.21 |
| 1 June 2017–31 May 2018 | 12 | 171 | 76 | 2.25 |
| 1 June 2018–31 May 2019 | 12 | 180 | 109 | 1.66 |
| 1 June 2019–31 May 2020 | 12 | 173 | 76 | 2.28 |
| 1 June 2020–31 May 2021 | 12 | 171 | 77 | 2.21 |
| 1 June 2021–31 August 2022 | 15 | 238 | 178 | 1.33 |

It is also worth noting that the total production for the PV is rather large compared to the installed peak power (i.e., ~ 1.7 kWh per kWp compared to ~ 1.6 kWh per kWp estimated with PVGIS and with optimal orientation and tilt angle). This is because the PV production has been calculated from forecast data provided by RTE, and the normalization factor used for this purpose has certainly been overestimated.

#### 1.1.4.4.2 EV Charging Strategies

The charging power profiles for individual vehicles were not recorded during the period considered. Thus, simulations are conducted with different EV charging strategies based on charging session history to reconstruct these profiles. As the charging records contain the energy withdrawn by vehicle $i$ ($E_i$) and the transaction duration ($DT$), it is supposed that this data is used by the CPO for controlling the charges. In practice, this data is not known, but it could be statistically estimated by the CPO. In this work, three charging strategies with different complexity are considered.

The first strategy is the Plug and Charge strategy described in 1.1.3.1. In that case, the charging power is limited by the nominal charging power of the embedded charger of the vehicle, noted $P^i_{max}$. The effective duration of the charging session is then equal to $E^i/P^i_{max}$.

The second strategy is called 'Mean Power'. In that case, the vehicle charges at constant power from the beginning to the end of the charging session. The duration of the charge is thus equal to $DT$ and the constant charging power for vehicle $i$ is $E^i/DT$.

The third strategy is a Smart Charging strategy, whose main objective is to increase the $SPR$. The detailed algorithm is out of the scope of the study but can be briefly explained as follows. The PV production forecast of the PV plant is considered as the power that is "available" to charge the EVs. The planning algorithm then sorts the EVs according to the alphabetical order of the badges and allocates a part of this available power to each car. The principle of this allocation is as follows. The setpoints of a car are constituted of a constant power part added to a part that is proportional to the available power. Two constraints have been considered when choosing the setpoints: the sum of the power has to be less than the maximum power of the car ($P^i_{max}$) and the integrate of the setpoints has to be equal to the energy withdrawn by the car ($E^i$).

#### 1.1.4.4.3 Load Curve Reconstruction

Figure 1.1-10 represents the simulated load curves of 11 July 2018, obtained for different strategies and with a 75 kWp PV installation. The PV production is represented in blue. The curve that corresponds to the EV consumption with the PC strategy, in red, shows a large peak of approximately 200 kW at the beginning of the day and a second peak at noon. The curve corresponding to the Mean Power strategy, in yellow, is smoother and relatively synchronized with the PV production, but it is observed that energy is consumed by the EVs during the night (due to EVs that stay connected for more than a day). The curve corresponding to the Smart Charging strategy, in purple, is aligned with the PV production. It is observed that no power consumption occurs during night-time.

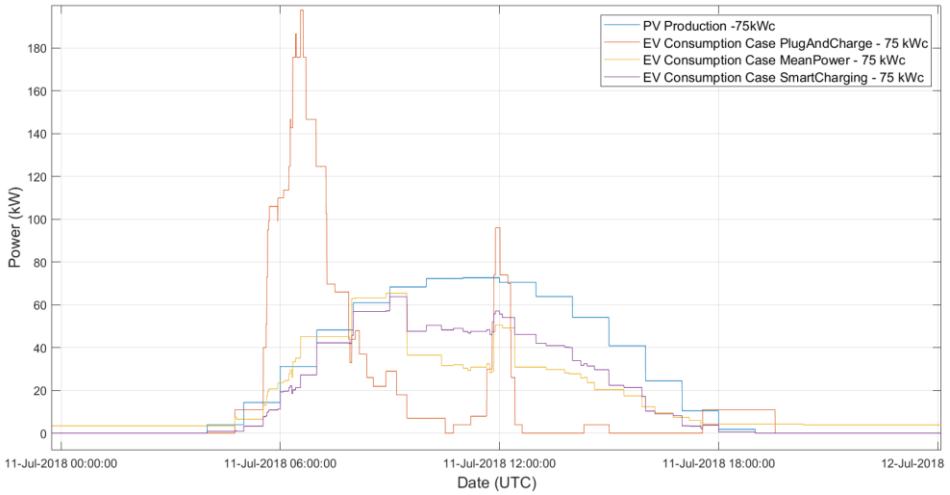


**Figure 1.1-10 Simulation results on 11th of July 2018 for a PV system of 75 kWp.**

On this particular day, the $SCR$ and $SPR$ are considerably higher for Mean Power and Smart Charging strategies than the basic Plug and Charge since their charging profiles are distributed throughout the day, in particular, when the PV production is the highest. Thus, the $SPR$ is equal to 49% with the Plug and Charge strategy, 89% with the Mean Power and 100% with the Plug and Charge strategy. The $SCR$ is equal to 31% with the Plug and Charge strategy, 62% with the Mean Power and 69% with the Plug and Charge strategy.

#### 1.1.4.4.4 Relationship 4: $PTC$ Ratio versus $SPR$

This section explores the relationship between the $PTC$ and the $SPR$, given a particular charging strategy chosen among the three described in Section 1.1.4.4.2. In order to vary the $PTC$, as the total energy consumption of the cars is independent of the charging strategy, the value of the PV production has been modified. Fifteen different sizes of the PV plant have been considered for this study:

$S_{peak} = [0{,}1{,}25{,}50{,}75{,}100{,}125{,}150{,}175{,}200{,}300{,}700{,}1\,000{,}5\,000{,}12\,000]kWp.$

First, the following 17 simulations are performed, with the horizon spanning more than a 6-year period:

- One simulation of the Plug and Charge strategy;
- One simulation of the Mean Power strategy;
- One simulation Smart charging strategy for each of the 15 different values of $S_{peak}$.

Daily $PTC$ and $SPR$ for each of these simulations and for each value of PV plant size are then calculated. Figure 1.1-11 illustrates the values of daily $PTC$ along with daily $SPR$, computed for a peak power value of 100 kWp using more than 6 years of data. This figure distinguishes between the different charging strategies: in yellow, the results with smart charging, in red with Mean Power and in blue with Plug and Charge. It is observed that the $SPR$ is the highest for the smart charging strategy and the lowest for the Plug and Charge strategy. It is also observed that very high values of $SPR$ are obtained with the SC strategy as soon as the $PTC$ exceeds 1.

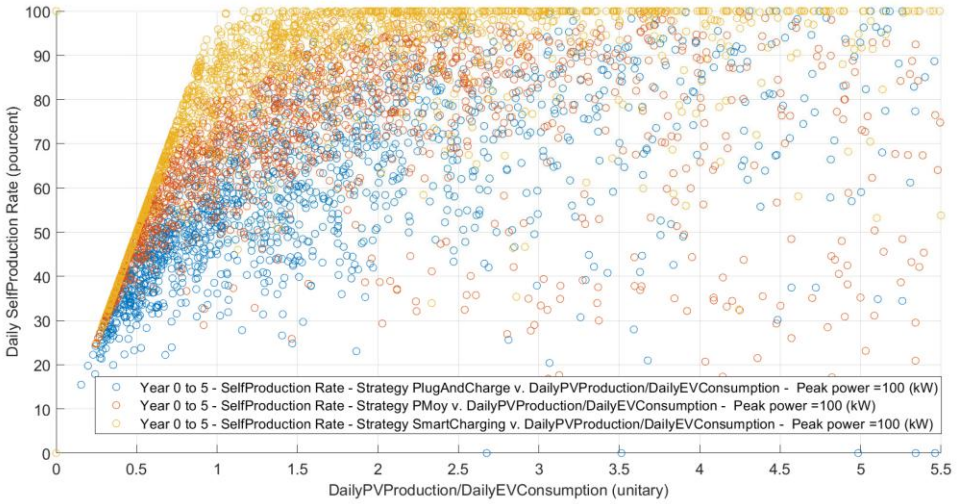


**Figure 1.1-11 Daily $SPR$ and Daily $PTC$ for every day for 6 years of the experimentation.**

In addition, the $PTC$ and $SPR$ have been computed over the entire 6 year-long period. Each point of Figure 1.1-12 has $PTC$ as the $x$-coordinate and $SPR$ as the $y$-coordinate. For the purpose of simplicity, only the $PTC$ values obtained with the 10 lowest PV peak power values 0,1,25,50,75,100,125,150,175, 200 are displayed. The colors of the points distinguish different strategies similar to those in Figure 1.1-11.

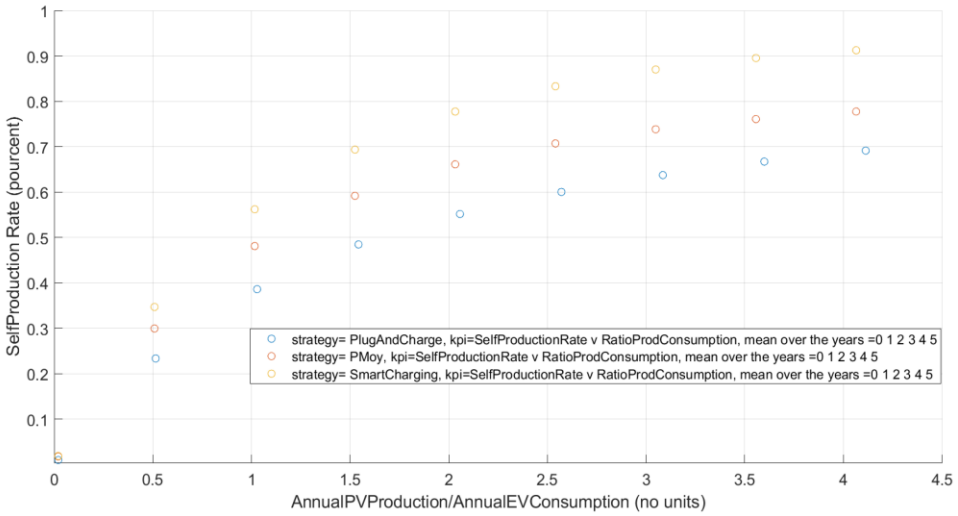


**Figure 1.1-12 Relationship 4: $PTC$ vs $SPR$, computed for different PV peak powers (0,1,25,50,75,100,125,150,175,200) over a more than 6-year period.**

It is observed that, for a given value of $PTC$, the self-production increases with the Smart Charging strategy compared to the Mean Power strategy. In the same way, the $SPR$ increases with the Mean Power strategy compared to the Plug and Charge strategy. For example, for $PTC = 1$, the $SPR$ is equal to 56% for the Smart Charging strategy, is equal to 48% for the Mean Power strategy and is equal to 38% for the Plug and Charge strategy. It can also be observed that, in order to obtain an $SPR$ of 70%, the $PTC$ has to be equal to 1.5 with the Smart Charging strategy, 2.5 with the Mean Power strategy, and 4.1 with the Plug and Charge strategy.

It should be noted that the results presented in Figure 1.1-12 allow for the simplistic aggregation of the dataset and chosen strategies into the computational procedure described in Section 1.1.3.4.2. Such a choice is discussed in Section 1.1.5.2. The following subsection exemplifies the importance of these results in a specific use-case.

## 1.1.5 Sizing Procedure Examples

### *1.1.5.1 Price Examples*

Since there are several stakeholders participating in the collective self-consumption scheme, the electricity would be billed differently according to stakeholder interactions. As assumed in Section 1.1.4.1.1, these bills are computed with flat rates and the cost of the electricity subscription is not considered.

The price of the electricity coming from the grid in this example is calculated by the Energy Regulation Commission in France for 2023 [29]. The price structure of $Pr_{ESEV-CPO}$ (424 €/MWh in total) is then composed of:

- Energy Component: 322 €/MWh corresponding to “non-residential blue” tariff (version B, power subscription less than 36 kVA, included transportation, “supplementary power case” also called ‘alloproduit’ in French), as described in Appendix B2 of [29];
- Contribution Component: 31 €/MWh corresponding to the electricity consumption tax (Taxe Intérieure sur la Consommation Finale d’Electricité) or TICFE until 31 January 2022. This contribution since then has been reduced to 1 €/MWh as a result of electricity subsidy for French consumers (called “bouclier tarifaire” in french). Such a subsidy lasts until the end of 2024;
- Tax Component: 71 €/MWh corresponding to 20% of the VAT on the energy, transport and contribution parts.

PV fit-in-tariff is a selling price also regulated by the Energy Regulation Commission and is currently at 120 €/MWh (Tariff $T_c$, $100\,kWp < P_{peak} < 500\,kWp$ in 2023) [30]. The purchase price $Pr_{PVO-LP} = Pr_{PVO-ESPV}$ is thus supposed to be equal to 120 €/MWh as well. It is considered that the energy is sold by the LP at this price (i.e., without margin) but increased with transport, contribution, and taxes. The price structure of $Pr_{LP-CPO}$(197 €/MWh in total) is as follows:

- Energy component: $Pr_{PVO-LP} = 120$ €/MWh;
- Transportation component: 13 €/MWh (as explained in [31]);
- Contribution part: 31 €/MWh corresponding to TICFE;

- Tax Component: 33 €/MWh corresponding to 20% of the VAT on the energy, transport and contribution.

A summary of these prices' structure described above is given in Table 1.1-5.

**Table 1.1-5 Electricity Prices for different stakeholder interactions. Notice that these prices are simple flat rates.**

| Interaction | Nomenclature | Prices (€/MWh) | Price Structure |
|---|---|---|---|
| PVO sells to LP | $Pr_{PVO-LP}$ | 120 | 120 Energy |
| LP sells to CPO | $Pr_{LP-CPO}$ | 197 | 120 Energy + 13 Transport + 64 (Taxes and contribution) |
| ESEV sells to CPO | $Pr_{ESEV-CPO}$ | 424 | 322 (Energy + transport), 102 (Taxes and contributions) |

### *1.1.5.2 Hypothesis*

In the following examples, it is supposed that the methodology will be applied by the CPO for PFS (i.e., with the lowest effort but at the price of relatively low precision). Its use-case has to be similar to the one described in this research in order to utilize the integrated dataset of the fourth relationship. In particular:

- The configuration of the charging points must be similar to the one presented in Section 1.1.3.1, i.e., 100% of the charging points are 22 kW AC;
- The characteristics of the EVs are identical to the presented ones (i.e., a probability distribution similar to the one of Figure 1.1-6);
- The working time and user behaviour (i.e., the statistics of the start and end date of the transaction, as depicted in Figure 1.1-4) are comparable;
- The EVCI has to be large enough to integrate new users such that there is no congestion in the charging stations.

Note that if these assumptions are not satisfied, the fourth relationship is not valid and all the simulations would have to be performed again.

### *1.1.5.3 Sizing PV Given a Targeted Number of EVs and a Targeted Mean Power Price*

As an illustration, let it be considered that the method of this research is applied by the CEA to size a PV plant located at Cadarache (near Aix-En-Provence, France) in order to charge its EV fleet in 2030. By using Figure 1.1-5, CEA observes that the number of EVs currently increases by approximately 100 per year. Thus, the number of EVs is assumed to be 1 000 in 2030 (instead of 200 in 2022). By using Equation (1.1-8), this represents an annual consumption of $12 \times 100 \times 1\,000 = 1.2\,GWh$.

Let it be considered that the target price of the CPO is $Pr_{CPO} = 265\,€/MWh$. Equation (1.1-8) gives $SPR = \frac{Pr_{CPO}-Pr_{ESEV-CPO}}{Pr_{CPO-LP}-Pr_{ESEV-CPO}} \approx 70\%$. Thanks to Figure 1.1-12, it is identified that, in order to obtain an $SPR$ of 70%, the ratio $PTC$ has to be equal to 1.5, 2.5, and 4 for Smart Charging, Mean Power, and Plug and Charge strategies, respectively.

With an EV consumption of 1.2 GWh these correspond to an annual PV production of 1.8, 3 and 4.8 GWh. Once the required annual PV production has been identified, the PV peak power can be determined using solar potential for a particular location. For example, it is estimated that the PV production is about 1.4 GWh/MWp at the location of the experiment (south orientation, tilt angle of 20° and system loss of 18%). With such hypotheses, the peak power of the PV plant has to be equal to 1.28, 2.14 and 3.42 MWp to reach the targeted $Pr_{CPO-LP}$.

#### *1.1.5.4 Estimating the Mean Power Price Given an Existing PV Installation and a Number of EVs*

Let it be supposed that the owner of an existing PV installation of 100 kWp in the same region wants to estimate the Mean Power price of the energy needed to feed 100 EVs with the smart charging strategy. The procedure for deriving this price, according to Figure 1.1-3, is the following:

- From PVGIS: Annual PV Production $E_{PV} = 100[kWp] \times 1.4 \left[\frac{MWh}{kWp}\right] = 140\ MWh$;
- From Equation (1.1-8): Annual EV Charging Consumption $E_{EV} = 12 \times 100 \left[\frac{kWh}{badge}\right] \times 100\ [badge] = 120\ MWh$;
- $PTC = \frac{E_{PV}}{E_{EV}} = 1.16$;
- SPR (for Smart Charging) according to Figure 1.1-12: $SPR = 0.6$;
- $Pr_{CPO}$ can then be estimated from Equation (1.1-6);
- $Pr_{CPO} = Pr_{ESEV-CPO} - SPR(Pr_{ESEV-CPO} - Pr_{LP-CPO}) \approx 287€/MWh$;

#### *1.1.5.5 Estimating the Number of EVs Given an Existing PV Installation and a Target Mean Power Price*

Let it be supposed that the owner of an existing PV installation of 100 kWp in the same region wants to determine the number of EVs that could be charged with the Mean Power strategy and with a targeted Mean Power price of $Pr_{CPO} = 265\ €/MWh$. The procedure for deriving the number of EVs that it can support is as follows, according to Figure 1.1-3:

- From PVGIS: Annual PV Production $E_{PV} = 100[kWp] \times 1.4 \left[\frac{MWh}{kWp}\right] = 140\ MWh$;
- From Equation (1.1-7), $SPR = \frac{Pr_{CPO} - Pr_{ESEV-CPO}}{Pr_{CPO-LP} - Pr_{ESEV-CPO}} = \frac{265-424}{197-424} \approx 0.7$;
- The $PTC$ ratio for different strategies is determined using Figure 1.1-12: $PTC_{MeanPower} = 2.5$;
- Annual EV Charging Consumption (using the Mean Power strategy) is then $E_{EV} = \frac{E_{PV}}{PTC} = \frac{140[MWh]}{2.5} = 56\ MWh$;
- From Equation (1.1-8), the optimal number of EVs is then: $\frac{E_{EV}}{(12 \times 100)} = \frac{56\ MWh}{12 \times 100\ kWh} \approx 46$.

### 1.1.6 Conclusions and Perspectives

In this study, a method was proposed for:

- Sizing the PV plant required to properly charge a certain number of EVs, given a targeted Mean Power price;
- Estimating the Mean Power price, given a PV plant size and the number of EVs to be charged;
- Estimating the number of chargeable EVs for a particular PV installation and charging price.

This method was applied to a car park located in a research centre in southern France. The main input of this study is a massive empirical dataset collected over more than 6 years with 350 EV users and 80 charging points. To generate the EV charging power profiles, simulations were conducted with different charging strategies based on historical real data.

This allowed for the simulation of EV profiles for individual power demand and for different sizes of the PV plant. The effect of implementing rule-based charging strategies (Mean Power and Solar Smart Charging) has been proven to be significantly beneficial as compared to the simple Plug and Charge mode. In one of the showcases, the PV peak power required for 1 000 vehicles to attain a charging cost of 265 €/MWh for Smart Charging, Mean Power and Plug and Charge strategies are 1.28, 2.14 and 3.42 MWp, respectively.

The main advantage of the methodology is its modularity, meaning that each key parameter (PV production, EV charging demand, business models, and EV charging strategies) can be analyzed independently of each other. Thus, when the method is fully applied once on a given case, some computations may be re-used for other “similar” cases. In some cases, as fully exemplified in the previous section, the application of the method becomes very simple and quick.

The described methodology and results offer several avenues for future expansion:

- Different simple and advanced strategies can be further integrated into this methodology, among which optimization-based methods are the most promising, in particular, MILP;
- More realistic electricity tariff schemes (time-of-use or dynamic spot price) should be considered instead of flat rates from the energy provider ESEV;
- Costs due to power subscription (in €/MW) should also be considered, in addition to the total electricity consumption (in €/MWh) as the number of EVs grows;
- This study assumes that the PV forecast is perfectly precise and omits any negative impact on the PV forecast accuracy. Hence, further studies are required to determine the impact of real PV forecast;
- Individual Battery Degradation should be considered [32].

In contrast, datasets representative of standard use cases could be openly disseminated within the research community, as suggested in [33]. Such datasets could serve as valuable resources for benchmarking purposes. Furthermore, with increasingly higher aggregated EV capacity, the EVCI is also eligible for different market participation, thus creating several revenue streams for the CPO. For example, two of these markets encompass the European frequency containment market and demand-response market.

## REFERENCES

[1] “Loi n° 2023-175 Du 10 Mars 2023 Relative à L’accéleration de la Production D’énergies Renouvelables,” Légifrance, 2023. Available : Here, Accessed: May. 23, 2023.

[2] Q. Hoarau and Y. Perez, “Interactions between Electric Mobility and Photovoltaic generation: a Review,” Renewable and Sustainable Energy Reviews, vol. 94, pp. 510–522, 2018, doi: https://doi.org/10.1016/j.rser.2018.06.039.

[3] A. R. Bhatti, Z. Salam, M. J. B. A. Aziz, and K. P. Yee, “A Critical Review of Electric Vehicle Charging Using Solar Photovoltaic,” International Journal of Energy Research, vol. 40, no. 4, pp. 439–461, 2015, doi: https://doi.org/10.1002/er.3472.


[4] L. Liu, F. Kong, X. Liu, Y. Peng, and Q. Wang, "A Review on Electric Vehicles Interacting with Renewable Energy in Smart Grid," Renewable and Sustainable Energy Reviews, vol. 51, pp. 648–661, 2015, doi: https://doi.org/10.1016/j.rser.2015.06.036.

[5] P. Nunes, R. Figueiredo, and M. C. Brito, "The Use of Parking Lots to solar-charge Electric Vehicles," Renewable and Sustainable Energy Reviews, vol. 66, pp. 679–693, 2016, doi: https://doi.org/10.1016/j.rser.2016.08.015.

[6] J. Merten, H. Guillou, L. Ha, M. Quenard, O. Wiss, and F. Barruel, "Solar mobility: Two Years of Practical Experience Charging Ten Cars with Solar Energy," in 5th International Conference on Integration of Renewable and Distributed Energy Resources, Berlin, Germany, Dec. 2012, pp. 4–6. Available: Here Accessed: May. 23, 2023.

[7] B. Robisson, S. Guillemin, L. Marchadier, G. Vignal, and A. Mignonac, "Solar Charging of Electric Vehicles: Experimental Results," Applied Sciences, vol. 12, no. 9, pp. 4523–4523, Apr. 2022, doi: https://doi.org/10.3390/app12094523.

[8] "Prefeasibility Studies Guidelines-Methodology Overview on How to Conduct a Preseasibility Assessment of Renewable Power Generation Technologies," Danish Energy Agency. Accessed: Aug. 31, 2023. [Online]. Available: https://ens.dk/media/5133/download

[9] W. Vermeer, G. R. Chandra Mouli, and P. Bauer, "Optimal Sizing and Control of a PV-EV-BES Charging System Including Primary Frequency Control and Component Degradation," IEEE Open Journal of the Industrial Electronics Society, vol. 3, pp. 236–251, 2022, doi: https://doi.org/10.1109/ojies.2022.3161091.

[10] R. Figueiredo, P. Nunes, and M. C. Brito, "The Feasibility of Solar Parking Lots for Electric Vehicles," Energy, vol. 140, pp. 1182–1197, Dec. 2017, doi: https://doi.org/10.1016/j.energy.2017.09.024.

[11] A. S. Al-Ogaili et al., "Review on Scheduling, Clustering, and Forecasting Strategies for Controlling Electric Vehicle Charging: Challenges and Recommendations," IEEE Access, vol. 7, pp. 128353–128371, 2019, doi: https://doi.org/10.1109/access.2019.2939595.

[12] R. L. G. Latimier, L. Kovaltchouk, H. Ben Ahmed, and B. Multon, "Preliminary Sizing of a Collaborative system: Photovoltaic Power Plant and Electric Vehicle Fleet," in 2014 Ninth International Conference on Ecological Vehicles and Renewable Energies (EVER), Monte Carlo, Monaco, Mar. 2014, pp. 1–9. doi: https://doi.org/10.1109/EVER.2014.6844110.

[13] "GAMS:The General Algebraic Modeling System." https://www.gams.com/. Accessed: Aug. 31, 2023.

[14] R. Atia and N. Yamada, "Sizing and Analysis of Renewable Energy and Battery Systems in Residential Microgrids," IEEE Transactions on Smart Grid, vol. 7, no. 3, pp. 1204–1213, doi: https://doi.org/10.1109/TSG.2016.2519541.

[15] "IBM CPLEX Optimizer." https://www.ibm.com/fr-fr/products/ilog-cplex-optimization-studio Accessed: Aug. 31, 2023.

[16] B. Naghibi, M. A. S. Masoum, and S. Deilami, "Effects of V2H Integration on Optimal Sizing of Renewable Resources in Smart Home Based on Monte Carlo Simulations," IEEE Power and Energy Technology Systems Journal, vol. 5, no. 3, pp. 73–84, doi: https://doi.org/10.1109/JPETS.2018.2854709.

[17] D. Sedighizadeh and E. Masehian, "Particle Swarm Optimization Methods, Taxonomy and Applications," International Journal of Computer Theory and Engineering, vol. 1, pp. 486–502, 2009, doi: http://dx.doi.org/10.7763/ijcte.

[18] G. R. Chandra Mouli, P. T. Bauer, and M. Zeman, "System Design for a Solar Powered Electric Vehicle Charging Station for Workplaces," Applied Energy, vol. 168, pp. 434–443, Apr. 2016, doi: https://doi.org/10.1016/j.apenergy.2016.01.110.

[19] P. Tulpule, V. Marano, S. Yurkovich, and G. Rizzoni, "Energy Economic Analysis of PV Based Charging Station at Workplace Parking Garage," in IEEE 2011 EnergyTech, Cleveland, OH, USA, 2011, pp. 1–6. doi: https://doi.org/10.1109/EnergyTech.2011.5948504.

[20] "MathWorks." https://fr.mathworks.com/ Accessed: Aug. 31, 2023.

[21] "NREL System Advisor Model (SAM)." https://sam.nrel.gov/ Accessed: Aug. 31, 2023.

[22] P. J. Tulpule, V. Marano, S. Yurkovich, and G. Rizzoni, "Economic and Environmental Impacts of a PV Powered Workplace Parking Garage Charging Station," Applied Energy, vol. 108, pp. 323–332, Aug. 2013, doi: https://doi.org/10.1016/j.apenergy.2013.02.068.

[23] D. Yan and C. Ma, "Optimal Sizing of a PV Based Electric Vehicle Charging Station under Uncertainties," in IECON 201945th Annual Conference of the IEEE Industrial Electronics Society, Lisbon, Portugal, 2019, pp. 4310–4315. doi: https://doi.org/10.1109/IECON.2019.8926749.

[24] Y. Krim, M. Sechilariu, and F. Locment, “PV Benefits Assessment for PV-Powered Charging Stations for Electric Vehicles,” Applied Sciences, vol. 11, no. 9, p. 4127, Apr. 2021, doi: https://doi.org/10.3390/app11094127.

[25] C. Roselli and M. Sasso, “Integration between Electric Vehicle Charging and PV System to Increase self-consumption of an Office Application,” Energy Conversion and Management, vol. 130, pp. 130–140, Dec. 2016, doi: https://doi.org/10.1016/j.enconman.2016.10.040.

[26] L.-M. Ritte, S. Mischinger, K. Strunz, and J. Eckstein, “Modeling Photovoltaic Optimized Charging of Electric Vehicles,” in 2012 3rd IEEE PES Innovative Smart Grid Technologies Europe (ISGT Europe), Berlin, Germany, 2012, pp. 1–8. doi: https://doi.org/10.1109/ISGTEurope.2012.6465792.

[27] S. Mischinger, K. Strunz, and J. Eckstein, “Modeling and Evaluation of Battery Electric Vehicle Usage by Commuters,” in 2011 IEEE Power and Energy Society General Meeting, Detroit, MI, USA, 2011, pp. 1–3. doi: https://doi.org/10.1109/PES.2011.6039645.

[28] “JRC Photovoltaic Geographical Information System (PVGIS) - European Commission,” Jan. 11, 2016. https://re.jrc.ec.europa.eu/pvg_tools/fr/ Accessed: Aug. 31, 2023.

[29] E. Wargon, A. Cellier, C. Edwige, I. Faucheux, and V. Plagnol, “Délibération De La CRE Du 19 Janvier 2023 Portant Proposition Des Tarifs Réglementés De Vente D’électricité.” Available: Here. Accessed: Jan. 19, 2023.

[30] E. Wargon, A. Cellier, C. Edwige, I. Faucheux, and V. Plagnol, “Délibération De La CRE Du 12 Octobre 2022 Portant Avis Sur Le Projet D’arrêté Modifiant L’arrêté Du 6 Octobre 2021 Fixant Les Conditions D’achat De L’électricité Produite Par Les Installations Implantées Sur bâtiment, Hangar Ou Ombrière Utilisant L’énergie Solaire Photovoltaïque.” Available: Here. Accessed: Oct. 12, 2022.

[31] “Le Tarif D’Acheminement De L’Électricité (TURPE),” Enedis. Available : Here . Accessed: Aug. 31, 2023.

[32] Y. Zheng, Z. Shao, X. Lei, Y. Shi, and L. Jian, “The Economic Analysis of Electric Vehicle Aggregators Participating in Energy and Regulation Markets considering Battery Degradation,” Journal of Energy Storage, vol. 45, p. 103770, Jan. 2022, doi: https://doi.org/10.1016/j.est.2021.103770.

[33] R. Fachrizal, M. Shepero, D. van der Meer, J. Munkhammar, and J. Widén, “Smart Charging of Electric Vehicles considering Photovoltaic Power Production and Electricity consumption: a Review,” eTransportation, vol. 4, p. 100056, May 2020, doi: https://doi.org/10.1016/j.etran.2020.100056.

# 2 TECHNICAL ECONOMIC AND ENVIRONMENTAL CO-OPTIMIZATION OF PVCS

To fully harness the potential of integrating PVCS, it is essential to focus on the technical, economic, and environmental co-optimization of these systems. Technically, this involves optimizing PV generation, energy storage management, and real-time control strategies to ensure reliable and efficient operation. Economically, co-optimization aims to minimize lifecycle costs, enhance return on investment, and identify favorable market conditions for deployment. Environmentally, it seeks to reduce greenhouse gas emissions and land use impact while maximizing the use of renewable energy. A balanced approach that jointly considers these three dimensions enables the development of smarter, cost-effective, and environmentally responsible PVCS solutions, paving the way for a cleaner and more resilient energy infrastructure.

This chapter, therefore, focuses on the optimal design and operation of microgrids by balancing technical performance, economic viability, and environmental impact. These challenges are addressed through an integrated approach that combines system sizing and energy management into a single decision-making framework. The proposed method is based on a multi-objective mixed-integer linear programming model, aimed at minimizing both the levelized cost of energy and the life cycle emissions of a microgrid composed of photovoltaic systems, battery storage, and an optional grid connection.

The first part of this chapter presents the developed methodology and its application to the city of Compiègne, France. It also includes a comparison between a grid-connected microgrid and an isolated (off-grid) microgrid.

While the second section introduces a case study of EVs into the co-optimization framework developed previously. It evaluates the algorithm by testing various combinations of technologies and applying different case studies in differents geographic locations to highlight the influence of key input parameters such as solar irradiance, temperature, and other technical constraints.

## 2.1 Optimal sizing and energy management for a microgrid: A joint MILP approach for minimization of energy cost and carbon emission

This research addresses the optimal design and operation of microgrids challenges by proposing a comprehensive approach that combines the sizing and energy management problems of a microgrid into a single decision-making framework. The study introduces a joint multi-objective mixed-integer linear programming algorithm that minimizes the levelized cost of energy (LCOE) and life cycle emissions (LCE) of the microgrid formed by photovoltaic system, battery storage, and with/without grid connections[5,6].

### 2.1.1 Introduction

#### *2.1.1.1 Context*

Climate change is a pressing issue in the 21st century, largely caused by the use of fossil fuel-based energy sources which emit high levels of $CO_2$. The Paris Agreement aims to keep global temperatures below 2°C above pre-industrial levels by reducing reliance on fossil-fuel based electricity production [1]. Renewable energy sources (RES) are a key solution to reach carbon neutrality, as they emit no $CO_2$ during energy generation. Microgrids can be defined as a compact and interconnected energy setup that combines different distributed energy resources such as solar panels, wind turbines and energy storage with local energy demands [2]. Accordingly, there is a strong connection between micro grids and RES, as microgrids provide a valuable platform for integrating RES and maximizing their compatibility with local battery energy storage system (BESS) resources [3]. Microgrids can also address the inconsistent nature of RES, such as solar and wind power, by incorporating them with BESS, demand response, and other conventional generation.

Optimal sizing of microgrid components is important because it helps to ensure that the microgrid system meets the desired performance requirements while minimizing the overall cost of the system [4]. Microgrid optimal sizing involves selecting the best size and number of components to achieve the desired level of reliability, resilience, and cost-effectiveness [5]. Microgrid system offers the ability to operate the electricity grid both as grid-connected microgrid (GCMG) and isolated microgrid (IMG) without jeopardizing the reliability and stability of the system while increasing the use of renewable energy [6] and ensuring the cost-beneficial operation of local networks [7].
One potential advantage of microgrids is their capability to adapt intelligent approaches in order to facilitate peak consumption reduction in order to improve grid reliability [8]. Peak shaving can be considered as one of the objectives while determining the optimal capacities of the microgrid components, to aid increasing energy efficiency and reliability with reduced energy cost and carbon emission release. In the context of microgrids, system efficiency and reliability

[5] This study is based on the following publication: F. A. Kassab, B. Celik, F. Locment, M. Sechilariu, S. Liaquat, and T. M. Hansen, "Optimal sizing and energy management of a microgrid: A joint MILP approach for minimization of energy cost and carbon emission," Renewable Energy, vol. 224, p. 120186, 2024, doi: https://doi.org/10.1016/j.renene.2024.120186.

[6] This work has been achieved within the framework of EE4.0 (Energie Electrique 4.0) project. EE4.0 is co-financed by European Union with the financial support of the European Regional Development Fund (ERDF), French State and the French Region of Hauts-de-France.

rely heavily on optimal sizing and energy management of the microgrid equipment. These two factors are crucial in ensuring the microgrid operation at full effectiveness.

Three microgrid types are available: AC, DC, and hybrid AC/DC. AC microgrids are compatible with diverse power sources, while AC/DC microgrids can accommodate both AC and DC loads, combining various power sources. However, a DC microgrids with photovoltaic (PV) systems and battery BESS offers several advantages over AC microgrids. These include the reduction of system losses attributed to DC power generation by these components. Notably, regulating only the voltage amplitude is necessary, and synchronization is not required. Moreover, the absence of reactive power in the DC bus allows connecting AC sources to the common DC bus, which operates solely with active power. This configuration enhances power efficiency and transfer capability. Additionally, other advantages are presented in [9].

#### *2.1.1.2 Literature review*

The majority of scientific literature and commercial software in the field of optimization studies primarily concentrate on the optimization of single-objective, which aims to minimize the overall costs of the system [10], [11] or multi-objective that are usually economic and environmental as in [12]. The studies that investigate the optimal sizing of microgrids typically fall into two main categories. In the first category, the optimization of the component's size and the energy management are separated. In that manner, the integration of RES is investigated without co-optimizing the energy management within a microgrid using heuristic rule-based approaches. In the second category, the optimal sizing of the RES components is combined with optimal energy management, where the combination of the sizing and energy management is usually done using mixed-integer linear programming (MILP).

In the first category, rule-based approaches with predefined strategies use heuristic algorithms to size microgrid components within an acceptable computation time because the optimization problem is large in terms of constraints and decision variables [13]. However, heuristic algorithms do not guarantee a global optimal solution for the optimization problem [14]. In [15], the sizing of both GCMG and IMG is achieved using a genetic algorithm (GA), with the aim of achieving the optimal levelized cost of energy (LCOE) for the microgrid formed by PV panels and BESS. In [16], a GA is also used to study a microgrid consisting of PV, wind turbines, BESS, and loads (electric vehicles and electric loads).

The objective functions aimed to minimize three factors: greenhouse gas (GHG) emissions, life cycle cost, and the non-renewable energy consumed over the life cycle of the microgrid equipment. The work presented in [17] involves the examination of a microgrid comprising PV systems, a wind turbine, and storage. This microgrid's sizing optimization is achieved using particle swarm optimization where the energy management within the system is executed through the implementation of a rule-based strategy. An IMG case that includes a PV system, wind turbine, BESS, and a diesel generator was studied in [18] with the aim of minimizing both system cost and $CO_2$ emissions. In [19], multiple microgrid configurations were explored with compromises between several indicators such as greenhouse gas emissions versus global cost or microgrid autonomy versus global cost. The study in [20] focused on sizing an autonomous AC microgrid to minimize energy and installation costs while also reducing the probability of loss of supply for improved reliability. In [21], the optimization problem aimed to minimize energy and installation costs while maximizing reliability using GA to determine the capacity of the BESS, PV, and other components. The study in [22] presents an application of the grasshopper optimization algorithm to size an autonomous microgrid composed of PV, wind, BESS, and diesel generation. The objective was to minimize cost and $CO_2$ emissions while considering battery degradation and energy management between components. The

study in [23] discusses integrating life cycle analysis into the design process of hybrid microgrids to optimize the design and minimize environmental impact while ensuring technical and economic feasibility.

In the second category, MILP is predominantly employed as a primary method. In [24], the optimization problem addressed the optimal sizing and energy dispatch of a residential microgrid consisting of PV, wind turbine, grid connection, and an electric load. In [14], a convex optimization approach was used to determine the optimal sizing and energy management of an island microgrid, considering battery degradation. The study in [25] presented a two-stage approach for determining the optimal size, service lifetime, and maximum depth of discharge of the battery. In [26], the optimal sizing, placement, and daily charge/discharge of a battery in the distribution network was studied. An IMG where a cost optimization approach is considered with the hourly dispatch, load demand, and generating power MILP method, is demonstrated in [27]. In [28], an investigation is conducted on a microgrid implemented in an island territory, which incorporated multiple technologies such as PV, wind, biomass, and geothermal sources, among others, with the objective function of minimizing the overall costs within the system. In [29], a two-stage MILP algorithm is utilized to determine the microgrid's sizing in the first stage and to execute daily energy management in the second stage considering load uncertainty. In addition to these two delineated categories, there are investigations wherein the sizing problem is addressed by employing heuristic algorithms, while the daily energy management is executed through MILP. This hybridized approach has demonstrated potential in mitigating computational simulation time [30].

The study previously cited, which performs MILP-based sizing and hourly energy management, does not include neither an analysis of the techno-economic-environmental relationship for both IMG and GCMG operation modes, nor an examination of the energy sources utilized for the local consumption from the grid energy mix. Additionally, the impact of peak shaving on LCOE and life cycle emissions (LCE) has not been evaluated. Our work extends the state-of-the-art by incorporating a joint multi-objective optimization strategy using MILP that combines system planning and energy management to minimize both the LCOE and the LCE over the project lifetime by presenting extensive Pareto front analysis. The presented optimization algorithm outperforms other algorithms discussed in the literature in terms of speed, leveraging only a single binary decision variable, and ensuring an optimal solution for energy management along with sizing, without the need for separating them into two distinct stages. Moreover, the impact of peak shaving on both the LCOE and LCE is evaluated, and the energy sources utilized from the French electricity grid are being evaluated.

#### *2.1.1.3 Objectives and contributions*

The objective of this research is to enhance the decision-making capabilities of microgrid designers by providing them with a comprehensive approach for system planning for both IMG and GCMG operation modes. By incorporating a joint multi-objective optimization strategy using MILP which ensures a global optimal solution [31], this research enables designers to make more informed and effective design choices. These choices involve evaluating various proposed solutions and striking a balance between cost and carbon emissions while considering technical constraints of energy management problem, to address the complexities and trade-offs inherent in microgrid design.
One of the key novel aspects of this work is the integration of energy management and component sizing into a unified optimization problem while ensuring an optimality gap of 0% with a decreased computation time in comparison with the existing literature. Implemented in Python and solved using CPLEX, the optimization process aims to minimize both the LCOE and the LCE. The proposed method allows to perform a comprehensive analysis by evaluating

the interdependence among components and their collective influence on the overall system performance in terms of emission and cost over the project lifetime. Additionally, by identifying the Pareto front– a set of optimal trade-off solutions– the study provides valuable insights by proposing the range of feasible solutions and the associated compromises between economic and environmental objectives.

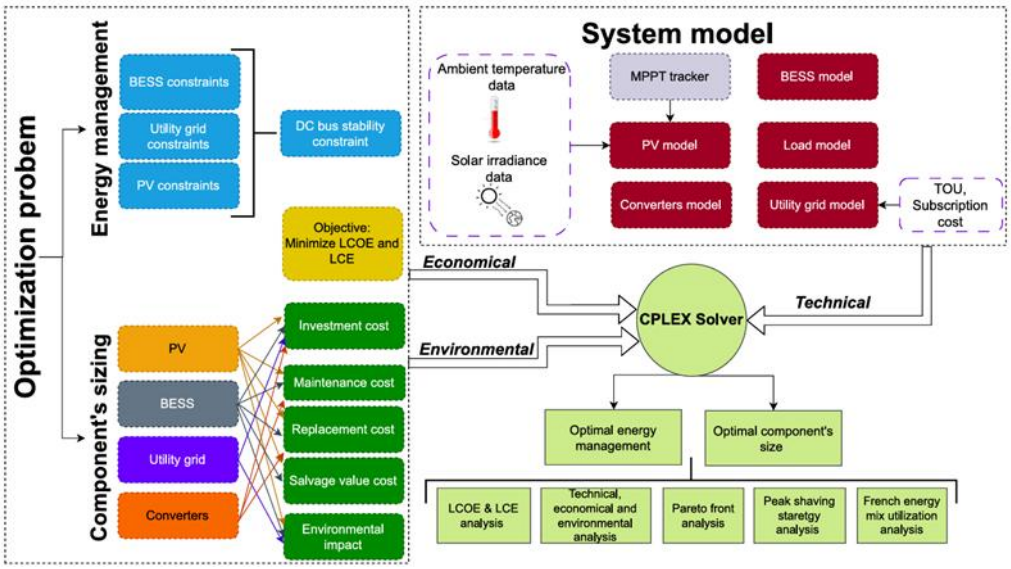


**Figure 2.1-1 General framework of the proposed multi-objective joint optimization algorithm.**

The overall structure of the study, as depicted in Figure 2.1-1, encompasses a comprehensive set of inputs, including electrical load data, ambient temperature data, solar irradiation data, time-of-use (TOU) tariffs with utility grid subscription costs, and economic and environmental data for each microgrid component. These inputs form the foundation for the system model, which incorporates the physical models of PV systems, BESS, utility grid, and the associated converters. By unifying energy management and component sizing within a single framework, the optimization problem yields the optimal energy management strategy and optimal component sizes for the microgrid system. The main contributions of this study are:

- integrating the sizing and energy management challenges within a DC microgrid framework, with due consideration to a project lifespan spanning 25 years; the focus extends to achieving hourly optimal energy management within the microgrid;
- encompassing technical, economic, and environmental dimensions in the microgrid context through the formulation of a unified multi-objective MILP algorithm. The algorithm's primary objective is to find an optimal solution, minimizing both the LCOE and the LCE of the microgrid, all while optimizing computational efficiency;
- varying the LCE constraint value to analyse and compare the Pareto front and the variation in BESS and PV capacities of the GCMG and IMG operation modes;
- evaluating the influence of peak shaving on the LCOE and LCE of the microgrid by calculating the average variation for each utility grid subscription power; and
- analysing the energy sources utilized in the French electricity grid under different LCOE and LCE scenarios where this assessment involves examining the proportional contribution of each energy source and exploring seasonal trends.

The research is organized as follows: Section 2.1.2 outlines the system modelling. Section 2.1.3 formulates the joint multi-objective optimization problem. Section 2.1.4 presents the study's results and analysis. Section 2.1.5 offers a detailed discussion, and Section 2.1.6 provides the conclusion and perspectives.

## 2.1.2 System modelling

This study analyses a university campus DC microgrid, which includes a DC bus, PV system, BESS, a connection to the utility grid, two DC/DC converters, an AC/DC converter, and a DC load. The architecture of the microgrid is shown in Figure 2.1-2, which is designed to operate with and without the utility grid connection. Excess power generated from the PV system is curtailed if the load demand is met, the BESS is fully charged, and the utility grid has reached its maximum injection limit (GCMG mode). Each component is formulated prior to determining the optimal sizing and the energy management strategy of the DC microgrid in the rest of this section. The maximum power point tracking (MPPT) mode of the PV system is accomplished through the associated converter. The efficiency of all converters is assumed to be constant for simplicity in this study.

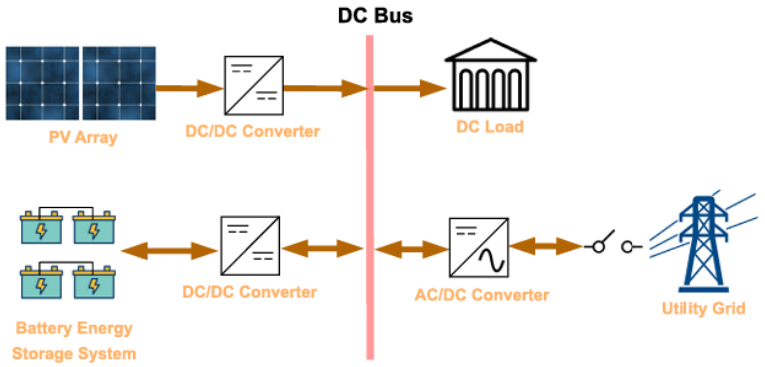


**Figure 2.1-2 The architecture of the studied DC microgrid.**

### *2.1.2.1 PV system modelling*

In this study, equation (2.1-1) is used to calculate the PV output power $p_{PV}^{MPPT}(t_i)$ at each time instant $t_i$, which depends on the solar irradiation and ambient temperature data. It is assumed that the PV system operates in MPPT mode and its power output is determined by [32]:

$$p_{PV}^{MPPT}(t_i) = p_{PV\,STC} \times g(t_i) \times 1\,000 \times \left(1 + \gamma \times (T_{PV}(t_i) - 25)\right) \times N_{PV} \quad (2.1\text{-}1)$$

$$with\ t_i = t_0, t_0 + \Delta t, \cdots, tf$$

where $p_{PV_{STC}}$ is the PV panel rated power at standard test conditions (STC). The STC stands for conditions to standardize the performance characteristics of PV panels. It typically refers to a solar irradiation of 1 000 W/m$^2$ solar spectrum of air mass 1.5, and PV cell temperature at 25°C [33]. $g(t_i)$ is the measured solar irradiation, γ is the power temperature coefficient of the PV panel, $T_{PV}(t_i)$ is the PV cell temperature, $N_{PV}$ is the number of PV panels, and $t_i$, $t_0$, $\Delta t$, and $t_f$ are the continuous time, initial time, time step, and simulation time, respectively. In equation (2.1-2), the PV cell temperature is calculated as follow [32]:

$$T_{PV}(t_i) = T_{amb}(t_i) + g(t_i) \times \frac{NOCT - 20}{800} \quad (2.1\text{-}2)$$

where $T_{amb}(t_i)$ is the ambient temperature, and $NOCT$ is the nominal operating cell temperature.

#### *2.1.2.2 Battery system modeling*

The battery is utilized as the energy storage system in the microgrid to fulfil the energy requirements in the absence of enough renew able production using stored excess PV production at high renewable production times. The energy transfer between the utility grid and the battery is prohibited in this study, hence the battery can only be charged by PV production and discharged for local load.

The battery models can be summarized in three models: the first is the charge model, which consists of modeling the state of charge ($SOC$) of the battery [34], the second is the voltage model, which focuses on modeling the terminal voltage for more detailed losses calculation [35], and the third is the lifetime model which assesses the impact of the operations on the battery lifetime [36]. These models could be independent or interdependent from each other. In this study, the charge model is considered as follows:

$$e_b(t_i) = e_b(t_{i-1}) + \left(p_b^c(t_i) + p_b^d(t_i)\right) \times \Delta t \quad (2.1\text{-}3)$$

where $e_b(t_i)$ is the quantity of energy at each instant; and $p_b^c(t_i)$, and $p_b^d(t_i)$ are the charging and discharging powers of the battery, respectively. Equation (2.1-3) represents the charge model for the battery, despite not considering the $SOC$. The reason for this choice is to maintain the linearity of the optimization problem, as the calculation of $SOC$ involves dividing two decision variables (charge/discharge powers and BESS capacity), which makes the problem formulation nonlinear.

### 2.1.3 Formulation of the joint multi-objective optimization problem

The optimization problem considers both economic and environ mental objectives and aims to find a trade-off between them. By balancing the competing objectives, the joint multi-objective optimization problem enables the design of a microgrid that integrates cost-effective solutions while reducing $CO_2$ emissions. While the constraints for both IMG and GCMG a real most similar, the IMG excludes constraints related to the utility grid. The constraints and objective functions are discussed in the following sections.

#### *2.1.3.1 Constraints*

In the optimization problem, constraints play a crucial role in defining the feasible solution space. Firstly, the quantity of BESS energy $e_b(t_i)$ is restricted by the maximum and the minimum allowed $SOC$ as follows:

$$SOC_{min} \times E_b \leq e_b(t_i) \leq SOC_{max} \times E_b \quad (2.1\text{-}4)$$

where $E_b$ is the installed capacity of the BESS in kWh; and $SOC_{min}$ and $SOC_{max}$ are the minimum and maximum $SOC$ of BESS, respectively. Ensuring a dependable energy supply for the subsequent year is of paramount importance, necessitating that the stored energy within the BESS at the end of the one-year simulation equals or surpasses the initial battery energy (taken as 50% of the storage capacity in this study). This strategic choice is implemented to guarantee a sufficiently robust BESS energy reserve capable of meeting the anticipated load demands in the forthcoming year. Omitting this constraint from the optimization algorithm could result in the BESS $SOC$ settling at the minimum $SOC$ level, potentially leading to load shedding in the subsequent year due to inadequate stored energy in the BESS. This constraint is formulated as follows:

$$e_b(t_f) \geq 0.5 \quad (2.1\text{-}5)$$

where $e_b(t_f)$ is the BESS energy at the end of the one-year simulation.

To specify the power flow of the BESS and the utility grid powers, the constraints on BESS charge/discharge powers ($p_b^c(t_i)/\ p_b^d(t_i)$) and the utility supply/inject powers ($p_g^s(t_i)\ /\ p_g^{in}(t_i)$) are established as follows:

$$p_b^c(t_i) \geq 0,\ p_b^d(t_i) \leq 0 \quad (2.1\text{-}6)$$

$$-p_g^{max} \leq p_g^s(t_i) \leq 0 \quad (2.1\text{-}7)$$

$$0 \leq p_g^{in}(t_i) \leq p_g^{max} \quad (2.1\text{-}8)$$

where $p_g^{max}$ is the maximum limit that can be supplied/injected by/into the utility grid. The convention of representing injection as positive and supply as negative is to reflect the direction of power flow. The constraints for maximum charge/discharge powers of the BESS are not included into the formulation due to the conflicting need of determining the optimal capacity of the BESS-associated converter in the sizing optimization problem. Therefore, to determine converter capacities, the nominal power value of the associated converters of the PV, BESS, and utility grid is considered to be equal or greater than electric power that flows through them as stated below:

$$p_{PV}^{MPPT}(t_i) \leq N_{PV}^{co} \quad (2.1\text{-}9)$$

$$-p_b^d(t_i) \times \mu_d + p_b^c(t_i)/\mu_c/\gamma_b^{c_0} \leq N_b^{c_0} \quad (2.1\text{-}10)$$

$$-p_g^s(t_i) + p_g^{in}(t_i)/\gamma_g^{c_0} \leq N_g^{c_0} \quad (2.1\text{-}11)$$

where $N_{PV}^{co}$ , $N_b^{co}$, and $N_g^{co}$ are the nominal power capacity of the PV, the BESS, and the utility grid converters, respectively; and $\gamma_b^{co}$ and $\gamma_g^{co}$ are the efficiency of the BESS and utility grid converters, respectively.

If the load power surpasses the PV power, the BESS should discharge and/or the utility grid should provide power. Conversely, the BESS must be charged and/or the surplus power should be fed into the utility grid. Therefore, the energy management within the microgrid typically requires the use of ‘‘if-else’’ conditions to control the power flow among each microgrid component. The ‘‘if-else’’ statements are used in programming to make decisions based on certain conditions; however, they cannot be expressed as linear equations or inequalities, hence it cannot be used directly in linear programming (LP). However, some formulations of certain problems may require the use of binary variables for the ‘‘if-else’’ statement, and in such cases alternative techniques may be used to model the optimization problem. As a solution in this study, the ‘‘Big M’’ method is employed that introduces a large constant value $M$ (typically set to $10^4$) and a binary decision variable $x_{aux}(t_i)$.The Big M method works by defining constraints that represent the conditions in ‘‘if-else’’ statements. The binary decision variable takes on either the value of 1 or 0, and the large constant value is used to penalize the objective function if the conditions are not met. When $x_{aux}(t_i) = 1$, the constraints corresponding to the ‘‘if’’ part of the ‘‘if-else’’ statement are active, otherwise if $x_{aux}(t_i) = 0$ the ‘‘else’’ constraints are active.

This allows to consider the different scenarios represented by the “if-else” conditions, while the optimization problem remains linear [37].

$$M \times x_{aux}(t_i) - \left(p_L^D(t_i) - \gamma_{PV}^{c_0} \times p_{PV}^{MPPT}(t_i)\right) \geq 0 \quad (2.1\text{-}12)$$

$$M \times \left(1 - x_{aux}(t_i)\right) - \left(\gamma_{PV}^{c_0} \times p_{PV}^{MPPT}(t_i) - p_L^D(t_i)\right) \geq 0 \quad (2.1\text{-}13)$$

Where $\gamma_{PV}^{co}$ is the PV converter efficiency, and $p_L^D(t_i)$ is the load demand. In equations (2.1-12) and (2.1-13), $x_{aux}(t_i) = 0$ when $p_{PV}^{MPPT}(t_i) - p_L^D(t_i) \geq 0$ and $x_{aux}(t_i) = 1$ when $p_L^D(t_i) - \gamma_{PV}^{co} \times p_{PV}^{MPPT}(t_i) \geq 0$ . Once $x_{aux}(t_i)$ is determined, the "if-else" conditions are implemented using constraints to control the BESS and utility grid power as follows:

$$p_g^s(t_i) \times \gamma_g^{co}, p_b^d(t_i) \times \gamma_b^{co} \times \mu_d \geq M \times x_{aux}(t_i) \quad (2.1\text{-}14)$$

$$p_g^{in}(t_i)/\gamma_g^{co}, p_b^c(t_i)/\mu_c/\gamma_b^{co} \leq M \times \left(1 - x_{aux}(t_i)\right) \quad (2.1\text{-}15)$$

Where $\gamma_b^{co}$ represents the efficiency of the BESS converter, and $\mu_c$ and $\mu_d$ represent the charging and discharging efficiencies of the battery, respectively. In equations (2.1-12) and (2.1-13), the algorithm determines $p_g^s(t_i) = 0$, $p_b^d(t_i) = 0$ when $x_{aux}(t_i) = 0$ , and $p_g^{in}(t_i) = 0$, $p_b^c(t_i) = 0$ when $x_{aux}(t_i) = 1$ .

The control of the battery discharge and the utility grid supply in order to not exceed the load power within the system is formulated as follows:

$$p_g^s(t_i) \times \gamma_g^{co} + p_b^d(t_i) \times \gamma_b^{co} \times \mu_d + M \times \left(1 - x_{aux}(t_i)\right) \geq -\left(p_L^D(t_i) - \gamma_{PV}^{co} \times p_{PV}^{MPPT}(t_i)\right) \quad (2.1\text{-}16)$$

In the absence of (2.1-16), there is a possibility that the battery can over-discharge beyond the required load demand. This situation arises due to the conditions described in equations (2.1-14), (2.1-15), when $x_{aux}(t_i) = 1$, the optimization algorithm might discharge the BESS more than the load demand (avoid selling energy to utility grid). Additionally, it is important to note that in convex optimization, multiple optimal solutions can exist, but equation (2.1-16)serves the critical purpose of eliminating solutions where the battery is discharged beyond the load demand, ensuring the appropriate power balance.

Lastly, the DC bus net power $p_{bus}(t_i)$ of the system is determined by summing the entering/leaving powers on the DC bus of the microgrid as in equation (2.1-17):

$$p_{bus}(t_i) = p_L^D(t_i) - \gamma_{PV}^{co} \times p_{PV}^{MPPT}(t_i) + p_b^c(t_i)/\mu_c/\gamma_b^{co} + p_b^d(t_i) \times \mu_d \times \gamma_b^{co} + p_g^s(t_i) \times \gamma_g^{co} + \left(p_g^{in}(t_i)\right) \times \gamma_g^{co} \leq 0 \quad (2.1\text{-}17)$$

According to equation (2.1-17), when $p_{bus}(t_i) < 0$ , the produced PV power exceeds the total consumption power, battery charging, and grid selling powers; hence, the surplus generation should be curtailed. On the other hand, when $p_{bus}(t_i) = 0$, the generation and consumption powers are equal, thus there is no surplus generation in the DC microgrid. However, it should be noted that if $p_{bus}(t_i)$ was chosen to be strictly equal to zero in equation (2.1-17) the algorithm would be forced to utilize all the PV power, which means that the excess power should be either injected into the utility grid or stored in the BESS. Therefore, the algorithm in this case increases the capacity of the BESS and reduces the capacity of the PV system to obtain $p_{bus}(t_i) = 0$ for all times. However, this will not be the most cost-effective solution (if the cost of the PV system is lower than BESS), because the algorithm will force increasing the BESS capacity in order to reduce curtailment. To avoid that situation, PV curtailment is allowed by enabling $p_{bus}(t_i) \leq 0$ in equation (2.1-17).

### *2.1.3.2 Objective functions*

The multi-objective optimization problem is formulated to obtain the system's minimal annual LCOE and LCE while ensuring an optimized energy management. The LCOE is the average

cost per unit of producing electricity over the lifetime of a power plant, while LCE is the total amount of $CO_2$ emissions produced over the entire lifecycle of a product. The LCOE is calculated as in:

$$LCOE = \frac{TC \times CRF}{\sum_{t_0}^{tf} p_L^D(t_i) \times \Delta t} \quad (2.1\text{-}18)$$

where $TC$ is the total cost over the project lifetime, $CRF$ is the capital recovery factor. The $CRF$ is a financial metric used to determine the annual capital cost from the project lifetime cost [8]. The $TC$ and the $CRF$ are calculated as follows:

$$TC = C_{inv} + C_{mtn} + C_{rep} + C_{grid} - C_{sv} \quad (2.1\text{-}19)$$

$$CRF = \frac{d(1+d)^Q}{(1+d)^Q - 1} \quad (2.1\text{-}20)$$

where $d$ is the discount rate, $Q$ is the project lifetime, and $C_{inv}$, $C_{mtn}$,$C_{rep}$,$C_{grid}$,$C_{sv}$ are the investment, maintenance, replacement, grid, and salvage value costs, respectively, which are calculated as [15]:

$$C_{inv} = \sum_{k=1}^{K} C_{inv}^k \times N^k + C_{dep} \quad (2.1\text{-}21)$$

$$C_{mtn} = \sum_{k=1}^{K} C_{mtn}^k \times N^k \sum_{q=1}^{Q} \left(\frac{1+\varepsilon}{1+d}\right)^q \quad (2.1\text{-}22)$$

$$C_{rep} = \sum_{k=1}^{K} C_{rep}^k \times N^k \sum_{r=1}^{NOR} \left(\frac{1+\varepsilon}{1+d}\right)^r \quad (2.1\text{-}23)$$

$$C_{grid} = \left(C_{sub} - \Delta t \times \left(\sum_{t_0}^{tf} p_g^s(t_i) \times \lambda^s(t_i) + p_g^{in}(t_i) \times \lambda^{in}\right)\right) \times \sum_{q=1}^{Q} \left(\frac{1+\varepsilon}{1+d}\right)^q \quad (2.1\text{-}24)$$

where $N^k$ is the total number of the $k^{th}$ microgrid component (PV, BESS, etc.), $k$ is the total number of microgrid components, and $C_{inv}^k$ and $C_{dep}$ are the $k^{th}$ component investment cost and the microgrid deployment cost, respectively.

The microgrid deployment cost includes the installation of the microgrid components (such as wiring, concrete, steel, wood, and electrical connections), as well as labour costs and indirect costs associated with the microgrid installation. For the $k^{th}$ microgrid component, $C_{mtn}^k$ is the operation and maintenance cost; ε is the escalation rate; $C_{rep}^k$ is the replacement cost; $NOR$ is the number of rth component replacements over the project lifetime; $q$ and $r$ are the year and replacement indices, respectively; and $\lambda^s$ and $\lambda^{in}$ are the grid tariffs for power supply (buying from the grid) and injection (selling to the grid), respectively. Finally, $C_{sub}$ represents the fixed subscription cost for the utility grid, which is a fixed annual fee imposed by the French utility grid companies [38] and is paid by customers to maintain their connection to the grid, covering infrastructure upkeep and operational expenses. The subscription cost is determined by the utility companies, and its value is taken differently based on the registered maximum power rating (allowed peak consumption) of the grid connection. The salvage cost is considered to be 10% of the PV investment cost and 20% of the battery investment cost [15].

The second objective function is formulated to obtain the system's minimal annual LCE given in equation (2.1-25) as follows:

$$LCE = LCE_{PV} + LCE_{BESS} + LCE_{grid} \quad (2.1\text{-}25)$$

$$LCE_{PV} = \frac{\alpha_{PV} \times p_{PV}^{MPPT}}{Q} \quad (2.1\text{-}26)$$

$$LCE_{BESS} = \frac{\alpha_b \times E_b \times (NOR+1)}{Q} \quad (2.1\text{-}27)$$

$$LCE_{grid} = \sum_{t_i=t_0}^{t_f} p_g^s(t_i) \times \alpha_g(t_i) \times \Delta t \quad (2.1\text{-}28)$$

where $LCE_{PV}, LCE_{BESS}$, and $LCE_{grid}$ are the LCE of the PV system, BESS, and the utility grid, respectively; $\alpha_{PV}$ is the equivalent $CO_2$ emissions of the PV system per kWp; $\alpha_b$ is the equivalent $CO_2$ emissions of the BESS per kWh installed; and $\alpha_g(t_i)$ is the dynamic emissions from the utility grid per kWh.

The optimization problem aims to minimize two objective functions, which are LCE and LCOE. Several approaches are used to solve a multi-objective optimization problem such as weighted-sum, trade off constraint, hierarchical, goal programming, and global criterion methods [39]. In this study, the trade-off constraint approach is used as follows:

$$min(LCOE) \quad (2.1\text{-}29)$$

$$LCE \leq \in \quad (2.1\text{-}30)$$

where $\in$ represents predetermined value that the objective functions are not allowed to surpass. The trade-off methodology, a widely adopted strategy in multi-objective optimization, involves the transformation of one of the two objective functions into an inequality constraint with an upper bound represented by $\in$. By manipulating the parameter $\in$, multiple solutions for the LCOE can be derived. This method effectively converts the original multi-objective optimization problem into a mono-objective form. The motivation for adopting this approach arises from the distinct units of measurement associated with LCOE and LCE. However, this method eliminates the need to convert the units of the two separate objective functions.

The optimization problem in equation (2.1-29) is solved by determining the following decision variables under the constraints in equation (2.1-14) to equation (2.1-17): the BESS capacity $(E_b)$, the number of PV panels $(N_{PV})$, the BESS charge/discharge powers $(p_b^c(t_i)/\, p_b^d(t_i)$ the utility grid supply/inject powers $(p_g^s(t_i)\ /\ p_g^{in}(t_i))$, and the auxiliary variables $(x_{aux}\ (t_i))$; and the capacity of PV, BESS, and the utility grid associated converters $(N_{PV}^{co},\ N_b^{co}, N_g^{co})$.

### 2.1.4 Results and analysis

In this study, the optimization problem is solved using data in a one-hour time resolution (time step of $\Delta t = 1\,h$), and the power profiles of the energy management are determined for a duration of one year (8 760 h). Four types of data are presented in this section, which are meteorological, electrical load, electricity tariff, and energy mix emissions data. The technical and economic parameters used in the study are detailed in Table 2.1-1.

Moreover, the $CO_2$ plays a predominant and substantial role in total greenhouse gas emissions compared to other gases [40]. Therefore, the current analysis focuses exclusively on carbon emissions, and the equivalent $CO_2$ emission data consider the manufacturing, transportation, and end-of-life of components, excluding $CO_2$ contribution of converters, which is negligible, as reported in [18].

The project lifetime is chosen to be 25 years [41] with a discount rate of 4% [42], an escalation rate 3% [41], a deployment cost of 40% of PV cost per year [15]. Lastly, the optimization problem is implemented in Python 3.8 and solved using the CPLEX solver on a desktop computer with an Intel Xeon W-2145 @3.7 GHz processor, 64 GB RAM, and a 64 bit operating system.

**Table 2.1-1 Technical, economic, and environmental parameters.**

| Components | Parameter | Value | Unit | Ref | Parameter | Value | Unit | Ref |
|---|---|---|---|---|---|---|---|---|
| PV | NOCT | 45 | °C | [43] | Conv. efficiency ($\gamma^{\omega}$) | 95 | % | [40] |
| | PV rated power ($\rho_{PV,STC}$) | 200 | Wp | [43] | Conv. lifetime | 15 | years | [44] |
| | Power temperature coefficient ($\gamma$) | −0.45 | %/°C | [43] | Conv. investment cost ($C^{PV}_{inv}$) | 140 | €/kW | [44] |
| | Lifetime | 25 | years | [43] | Conv. maintenance cost ($C^{PV}_{min}$) | 2.5 | €/kW/year | [44] |
| | Investment cost ($C^{PV}_{inv}$) | 90 | € | [43] | Conv. replacement cost ($C^{PV}_{rep}$) | 140 | €/kW | [44] |
| | Maintenance cost ($C^{PV}_{min}$) | 1 | % of cost/year | [15] | | | | |
| | Equivalent $CO_2$ emissions ($\alpha_{PV}$) | 2,625 | kg$CO_2$eq/kWp | [45] | | | | |
| BESS | Charge/discharge efficiency ($\mu_c/\mu_d$) | 0.85 | % | [46] | Conv. efficiency ($\gamma^{\omega}$) | 95 | % | [40] |
| | Lifetime | 5 | years | [46] | Conv. lifetime | 15 | years | [15] |
| | Unit capacity | 1.8 | kWh | [46] | Conv. investment cost ($C^{b}_{inv}$) | 280 | €/kW | [15] |
| | Investment cost ($C^{b}_{inv}$) | 200 | € | [46] | Conv. maintenance cost ($C^{b}_{min}$) | 2 | €/kW/year | [15] |
| | Maintenance cost ($C^{b}_{min}$) | 3 | % of cost/year | [15] | Conv. replacement cost ($C^{b}_{rep}$) | 280 | €/kW | [15] |
| | Replacement cost ($C^{b}_{rep}$) | 200 | € | [46] | Min/Max SOC ($SOC_{min}/SOC_{max}$) | 0.2/0.9 | pu | |
| | Equivalent $CO_2$ emissions ($\alpha_b$) | 55.3 | kg$CO_2$eq/kWh | [18] | Initial SoC | 0.5 | pu | |
| Utility grid interface | Conv. efficiency ($\gamma^{g}$) | 95 | % | [40] | Conv. maintenance cost ($C^{s}_{min}$) | 0.5 | €/kW/year | [44] |
| | Conv. lifetime | 15 | years | [44] | Conv. replacement cost ($C^{s}_{rep}$) | 95 | €/kW | [44] |
| | Conv. investment cost ($C^{s}_{inv}$) | 95 | €/kW | [44] | | | | |

### *2.1.4.1 Meteorological and electrical load data*

The meteorological data for Compiègne, a city located in northern France (latitude: 49.41° North, longitude: 2.82° East), serves as the primary case study for conducting simulations.

The solar irradiation and ambient temperature data, presented in Figure 2.1-3 (a), are acquired through sensors strategically positioned in the study area. The solar irradiation sensor is equipped with a monocrystalline silicon (Si) sensor, featuring a permissible tolerance of ± 5%. Functioning within an extensive temperature range from – 40°C to 85°C, this sensor ensures reliable operation across diverse environmental conditions. The ambient temperature sensor operates within the temperature range of – 40°C to +180°C, with a nominal tolerance of ± 0.8°C, thereby attaining a notable level of precision. Together, these sensors provide indispensable meteorological data and significantly enhance the predictive accuracy of the model.

The electrical load considered in the study is for a university building and its subscribed power limit which is 36 kW as depicted in Figure 2.1-3 (b). The electrical load profile is derived from empirical data, capturing the typical energy consumption patterns exhibited by the building. Analysis of historical data reveals that the university building, affiliated with the Université de Technologie de Compiègne, has exhibited no discernible growth. This absence of growth is attributed to energy-related concerns, particularly those addressed by governmental incentives in France targeting $CO_2$ emissions. These incentives, coupled with global considerations surrounding building consumption, especially for heating, have collectively contributed to the absence of load increase. The observations over the past five years affirm the trend in consumption, substantiating the aforementioned factors. It is noteworthy that the optimization problem remains adaptable to potential load growth scenarios, as an assumption, without impeding its solution.

The objective of limiting the subscribed power from the utility grid is to perform peak shaving, as described in [8]. The cited research that restricts the discharge of BESS when the electrical load is below the maximum grid limit. However, it should be noted that BESS can be discharged all times as long as it is profitable or less polluting compared to utility grid. Therefore, the battery discharge power is not restricted for only peak shaving in this study, it can be also used when the load is less than 36 kW.

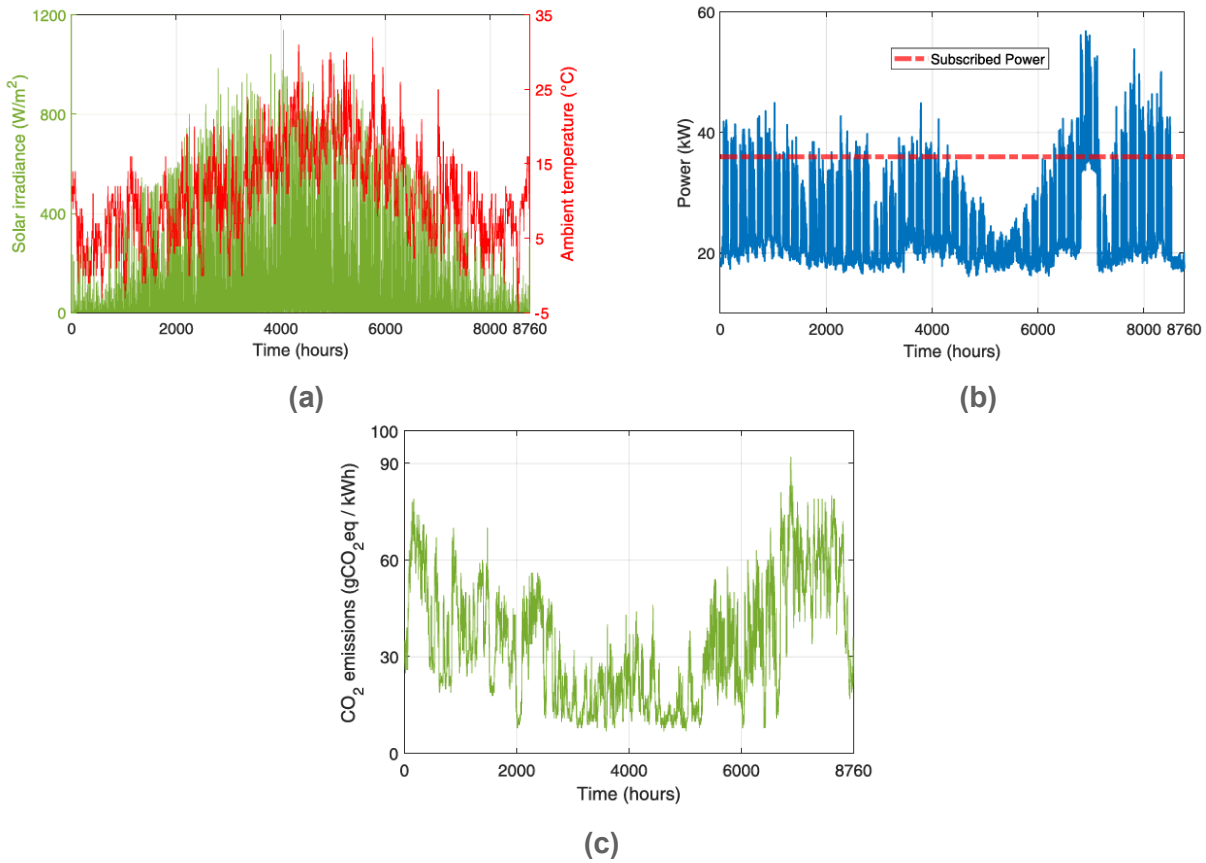


**Figure 2.1-3 Hourly input data from 2021: (a) Solar irradiation and ambient temperature, (b) the electrical load, and (c) utility grid $CO_2$ emissions.**

### *2.1.4.2 Electricity tariffs and energy mix emissions*

TOU electricity price and the cost of grid subscription are taken from one of the electricity service providers in France [38]. Accordingly, the cost of 36 kVA power subscription ($C_{sub}$) for TOU option is 494.92 €/year [38], and TOU tariff is 0.1841 €/kWh for on-peak hours (06:00 A.M – 10:00 P.M) and 0.1470 €/kWh for off-peak hours (10:00 P.M – 06:00 A.M) [47] for the studied location. The grid injection price is fixed at 0.06 €/kWh all times over the year [48]. Figure 2.1-3 (c) displays the utility grid dynamic emissions for the year 2021, where the French transmission system operator RTE provides real-time $CO_2$ emissions data in [49].

### *2.1.4.3 Technical, economic, and environmental results*

The economic and environmental results for $LCE \leq 225{,}000\, kgCO_{2,eq}$ in IMG operating mode and GCMG operations mode are displayed in Table 2.1-2. The system LCE is computed as the LCE sum of the PV, BESS, and utility grid. The results in Table 2.1-2 show that the system's LCOE and LCE are higher in IMG mode compared to GCMG mode.

One reason is that the French electricity grid is heavily dominated by the nuclear power plants which provides cost-efficient and low-carbon electricity services for the end-users. Therefore, the utility grid provides already a clean and cost-efficient solution in GCMG case, where the BESS capacity is mostly determined to provide electricity when the load demand passes the subscribed grid power limit.

Additionally, the specific characteristics of the PV technology, including the incorporation of phase change material [45], make the PV system the primary contributor to the overall system's LCE in both operational modes. The microgrid components' sizes and technical results under identical conditions (where $LCE \leq 225{,}000\ kgCO_{2,eq}$ in IMG operating mode and GCMG operations mode) are presented in Table 2.1-3. The size of BESS and PV for IMG is higher than that of GCMG, with a percentage difference of 160.9% for the PV and a difference of 154% for the BESS.

Larger PV and BESS capacities translate to increased capacities for their associated converters, as illustrated in Table 2.1-3 for the IMG case in comparison with GCMG operation mode. CPLEX computation time for IMG is lower than that of GCMG because the IMG operation mode is based on LP, requiring fewer decision variables and constraints.

In contrast, the GCMG operation mode is a MILP with the addition of a binary decision variable and decision variables related to the utility grid. The outcomes from Table 2.1-2 and Table 2.1-3 are comprehensively analyzed in the following section.

**Table 2.1-2 Economic and environmental results in IMG and GCMG operation modes.**

| Parameter | IMG | GCMG | Unit |
|---|---|---|---|
| System LCOE | 0.98 | 0.22 | €/kWh |
| System LCE | 220,533 | 31,596 | $kgCO_2eq$ |
| PV LCE | 204,099 | 26,621 | $kgCO_2eq$ |
| BESS LCE | 16,434 | 1,839 | $kgCO_2eq$ |
| Utility grid LCE | - | 3,136 | $kgCO_2eq$ |

**Table 2.1-3 Components size and technical results for IMG and GCMG operation modes.**

| Parameter | IMG | GCMG | Unit |
|---|---|---|---|
| **Components size** | | | |
| PV system capacity | 1.94 | 0.21 | MWp |
| BESS capacity | 1.48 | 0.19 | MWh |
| PV converter capacity | 2.2 | 0.24 | MW |
| BESS converter capacity | 0.2 | 0.03 | MW |
| Utility grid converter capacity | - | 0.03 | MW |
| **Technical results** | | | |
| PV output energy | 2,195 | 246 | MWh/year |
| PV curtailed energy | 1,826 | 42 | MWh/year |
| BESS energy | 108 | 33 | MWh/year |
| Grid supplied energy | - | 102 | MWh/year |
| Grid injected energy | - | 58 | MWh/year |
| BESS complete cycles | 73 | 166 | cycles/year |
| CPLEX computation time | 1,853 | 5,652 | seconds |

#### 2.1.4.3.1 Isolated microgrid

Another reason for high LCOE and LCE in the IMG mode is that load shedding is not allowed, as stated in equation (2.1-18). This means that the optimization problem must be able to meet the load demand even during periods of low solar irradiation, such as the winter season.

Figure 2.1-4(a) depicts the energy profiles throughout a year, indicating a significant amount of curtailed power generated by the PV system, particularly during the summer season. Specifically, the curtailed PV energy amounts to about 83% of the total PV output energy. Even though the PV curtailed power is high, the PV contribution to the system still reaches around 60%, with the remaining contribution coming from the BESS. Figure 2.1-5 shows simulation results for August 19 – 20 and November 13 – 14, which are the dates with the highest and lowest solar irradiation levels, respectively. As solar irradiation is typically high during the summer, the battery is not always charging during this period as there is an excess PV generation throughout this time. However, the BESS is configured to maintain its maximum $SOC$ between November 13 and 14 to ensure a continuous supply of power to meet the load demand.

The IMG is sized to match the energy needs between November 13 and 14, which demands significant capacities for both the PV system and BESS. As a result, there is a high amount of energy from the PV system that is being curtailed during the period of August 19 to 20. This high level of energy curtailment (see Table 2.1-3 and Figure 2.1-4 (a)) also affects the size of the PV-associated converter, as it needs to be able to handle the incoming energy from the PV system.

It can be seen in Table 2.1-3 that the BESS has a maximum charging/discharging power that is low in comparison to its capacity, indicating that the BESS does not overcharge or discharge as the charging C-rate equals 0.156 and the discharging C-rate equals 0.044. Avoiding high BESS C-rates is recommended for better safety and lifespan of the battery [50].

Furthermore, the relatively low number of complete BESS cycles is a result of the BESS's substantial capacity. In simpler terms, because the BESS can store a lot of energy, it does not need to cycle through charging and discharging as frequently as a smaller BESS would. Additionally, this demonstrates that the assumption of a fixed battery replacement every five years guarantees a well-operating BESS, as 73 BESS cycles per year will not exceed the cycles to failure in the fifth year for the chosen battery [46].

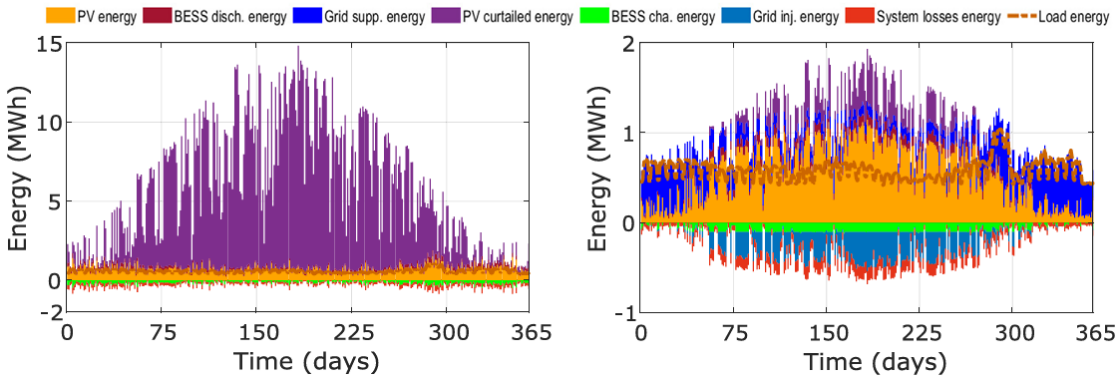


**Figure 2.1-4 Energy profiles over one year for (a) IMG and (b) GCMG operation modes.**

### 2.1.4.3.2 Grid-connected microgrid

The LCOE and LCE have significantly decreased in the GCMG operation mode compared to the IMG mode (see Table 2.1-2). This decrease can be attributed to the lower cost of purchasing power from the utility grid as opposed to increasing the capacity of BESS. Figure 2.1-4(b) demonstrates the power profiles over a simulated year, revealing a noteworthy reduction in curtailed power generated by the PV system compared to the IMG mode. Additionally, the graph highlights the significance of grid injection and battery charging during

the summer season. The load is served directly from the utility grid during periods of low solar irradiation (November 13 – 14, see Figure 2.1-5 (d)), rather than relying on an increased PV and BESS capacities. This results in decreased capacity for PV and BESS capacities and their associated converters in the GCMG mode compared to the IMG mode. Hence, during periods of high solar irradiation (August 19 – 20), as illustrated in Figure 2.1-5 (b), there is a reduction in curtailed power. Overall, the curtailed power decreased to 17% in this operation mode with a PV contribution of 54%. During the summer months, when solar irradiation is abundant, the $SOC$ of BESS is experiencing complete cycles because it is guaranteed that the BESS would be recharged the next day. Conversely, the $SOC$ of BESS is kept at a certain level during the period of November 13 – 14 to maintain a sufficient power supply for the load. The charging/discharging C-rates of the BESS are approximately 0.184 and 0.121, respectively. Although these rates are higher than those of the IMG operation mode, they are still considered low, ensuring that the battery does not overcharge or over discharge, thereby ensuring the safety of the battery. Similar to the IMG operation mode, the BESS cycles of 166 per year ensure a well-operating BESS during the five years considered in this study.

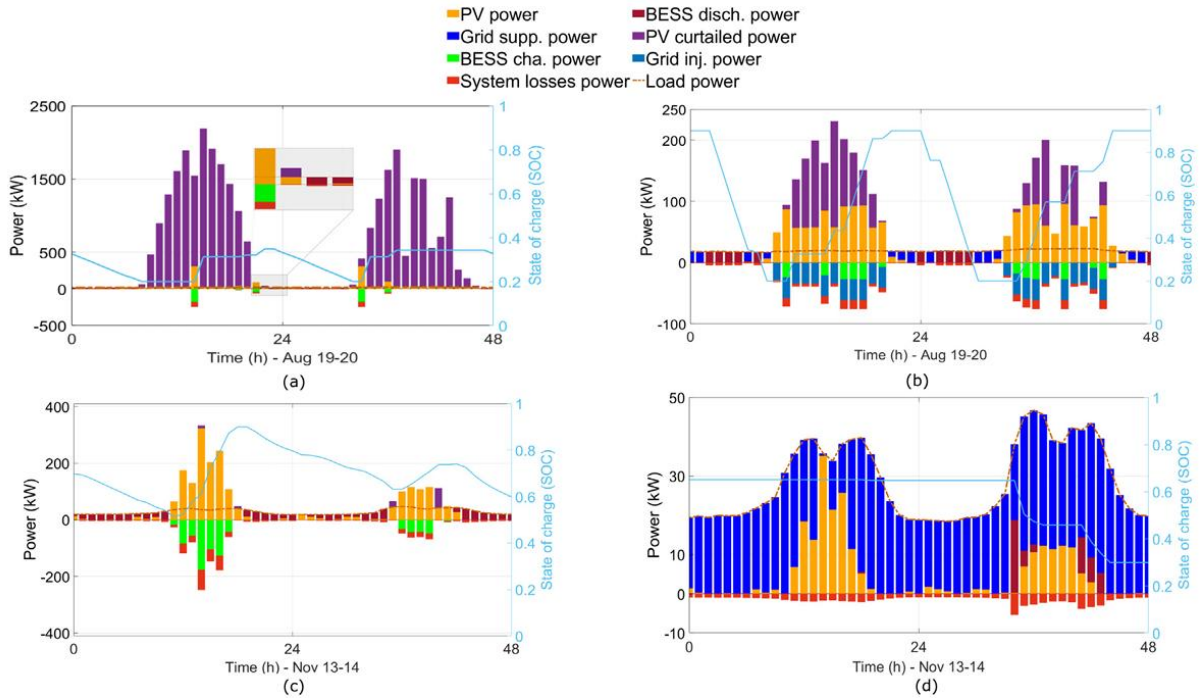


**Figure 2.1-5 Power profiles of Aug 19 – 20 for (a) IMG, (b) GCMG operation modes, and of Nov 13 – 14 for (c) IMG, (d) GCMG operation modes.**

### *2.1.4.4 Analysis of Pareto Fronts*

A key idea in multi-objective optimization is the Pareto front, sometimes referred to as the Pareto set or Pareto frontier. It describes a group of solutions to a problem area that cannot be enhanced for one target without degrading the effectiveness of another objective. In other words, it symbolizes the trade-offs among multiple competing aims. In this study, the Pareto front is determined by manipulating $\epsilon$ (see equation (2.1-30)) where the trade-off between the objectives can be altered, leading to different solutions on the Pareto front. Figure 2.1-6 illustrates the Pareto front along with the variations observed in BESS and PV panels for both IMG and GCMG operation modes.

In the instance of the IMG, there is an approximate 28% difference in both LCOE and LCE between various solutions. For the GCMG mode, these differences amount to about 23% for

LCOE and 17% for LCE. It can be seen that reducing the LCE would necessitate an increase in LCOE and vice versa. This can be explained by the fact that reducing one objective requires sacrificing some of the other objective. Additionally, reducing the LCE of the system can be achieved by increasing the proportion of BESS in the overall system and decreasing the number of PV panels. This finding is consistent with the observation that the LCE of the PV system is slightly greater than that of the BESS in this study.

For the GCMG operation mode, the Pareto front exhibits a generally downward slope from left to right, indicating that it is typically possible to reduce the LCE without substantially increasing the LCOE, but decreasing LCOE often necessitates accepting higher levels of LCE. The variation of the BESS and PV panels is the same for both operation modes, where the BESS increases and the PV decreases whenever the LCE decreases.

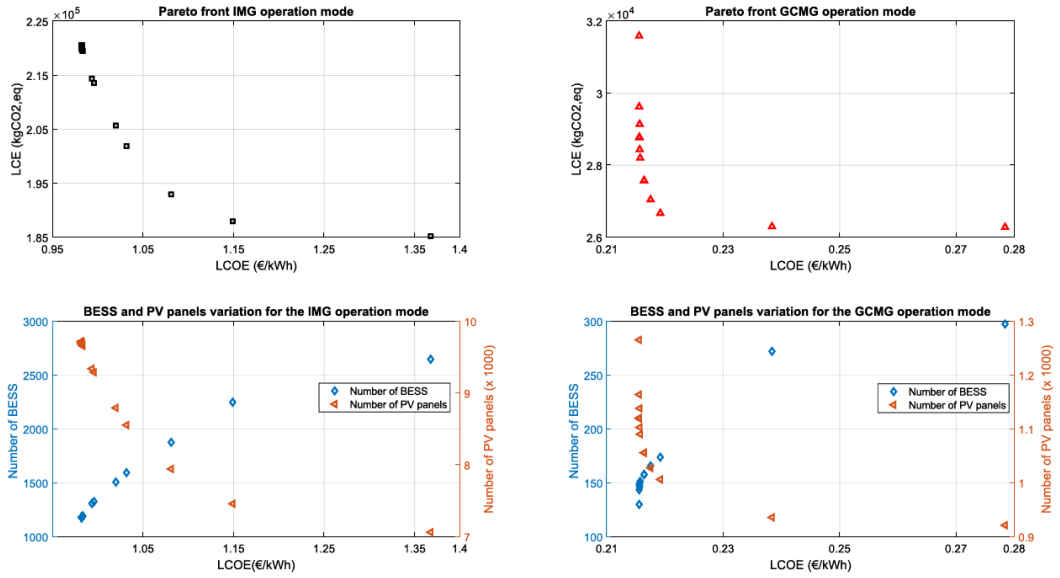


**Figure 2.1-6 Pareto front and the variation of BESS and PV panels for (a) (c) IMG operation mode (b) (d) GCMG operation modes.**

Figure 2.1-7 shows a radar plot that compares the economic indicators such as investment, maintenance, replacement, salvage value, and grid costs (for GCMG operation mode). It can be inferred that when LCOE is the lowest, the investment cost is the highest for both operation modes. This is because the algorithm suggests a microgrid that relies on PV panels, which have a larger investment cost than that of BESS. On the other hand, when LCE is the lowest, the maintenance, replacement, and grid costs are larger compared to the case where LCOE is the lowest. This is because in this case, the algorithm suggests a solution that is more reliant on BESS, which is an only replaced component several times during the project lifetime, in this study.

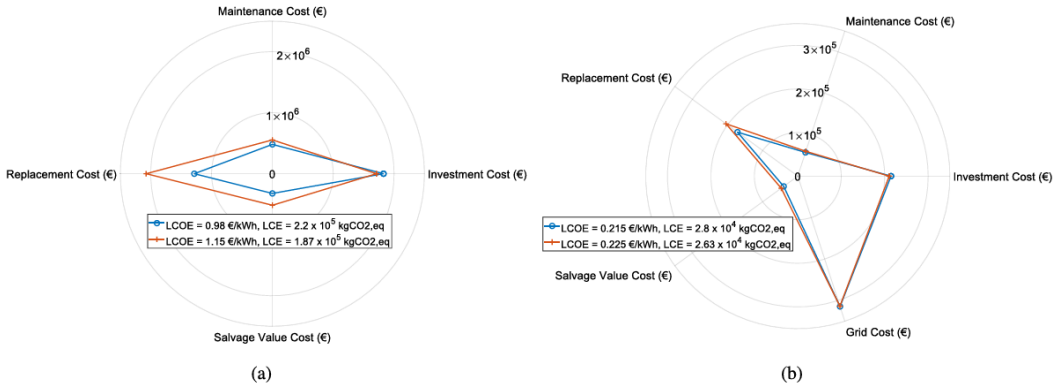


**Figure 2.1-7 Radar plot for economic analysis for (a) IMG (b) GCMG operation modes.**

### *2.1.4.5 Peak shaving strategy impact*

Peak shaving is achieved by varying the maximum subscription limit from 36 kVA to lower limits of 30 kVA, 24 kVA, and 18 kVA by updating subscription cost $C_{sub}$ for each power level [38]. Figure 2.1-8 displays the Pareto fronts for peak shaving strategy with varying utility grid limits and for IMG operation mode. The onset of observable variations in the solution occurs when the LCE for the IMG and GCMG operation modes are less than or equal to 225 000 $kgCO_2,eq$. The results indicate that increasing the utility grid limit results in a reduction in both LCE and LCOE, as evidenced by the upward trend of the Pareto fronts. The average variation between each Pareto curve is calculated in order to determine the impact of the peak shaving on the LCOE and LCE evaluation by varying subscription limit.

It can be seen that when the subscription limit is reduced around 16% (36 kVA to 30 kVA), the LCOE and LCE are increased approximately 12% and 24% due to low-carbon and low-cost French electricity grid. However, it should be noted that this will eventually increase the self-consumption and autonomy in the microgrid around 43% (in parallel to 16% peak reduction) using local PV and BESS due to being less dependent on the utility grid. The optimization algorithm tends to decrease the required BESS capacity as the utility grid limit increases. These findings suggest that it is more economically and environmentally (in terms of $CO_2$ emissions) favourable to rely on the utility grid (which mostly depends on nuclear power plants in France) instead of integrating a local BESS. The Pareto fronts become lower and steeper as the utility grid limit increases. The steeper Pareto front suggests that by relying more on the utility grid, it is possible to reduce the LCE without significantly increasing the LCOE, but reducing LCOE often requires accepting higher levels of LCE.

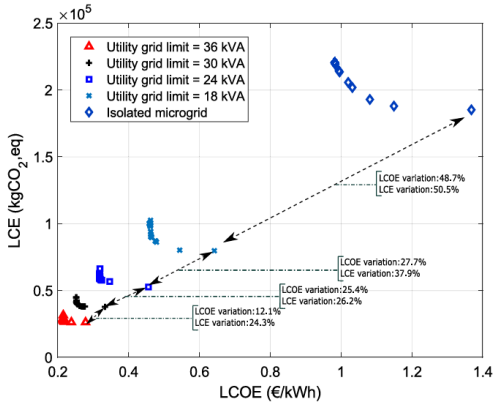


**Figure 2.1-8 The trend of Pareto fronts for peak shaving strategy based on various grid subscription power.**

### *2.1.4.6 Analysis of utilized energy sources in French electricity grid*

The French energy mix has undergone significant decarbonization, primarily attributed to the extensive integration of nuclear power in electricity generation, which emits low levels of $CO_2$ [51]. This investigation illustrates the proportionate contribution of various energy sources to the electricity grid of France, as demonstrated in Figure 2.1-9 for the 36-kVA subscription case study. The results of the scenario of the lowest LCOE are presented in Figure 2.1-9 (a).

The results emphasize the country's substantial dependence on local renewable energy consumption, accounting for 54% of the electricity mix. These findings are in line with the French government's ambitious goals to boost the use of renewable energy sources in electricity generation. Furthermore, the electricity consumption derived from the nuclear grid remains the highest, highlighting the high reliance on nuclear power for electricity production in France.

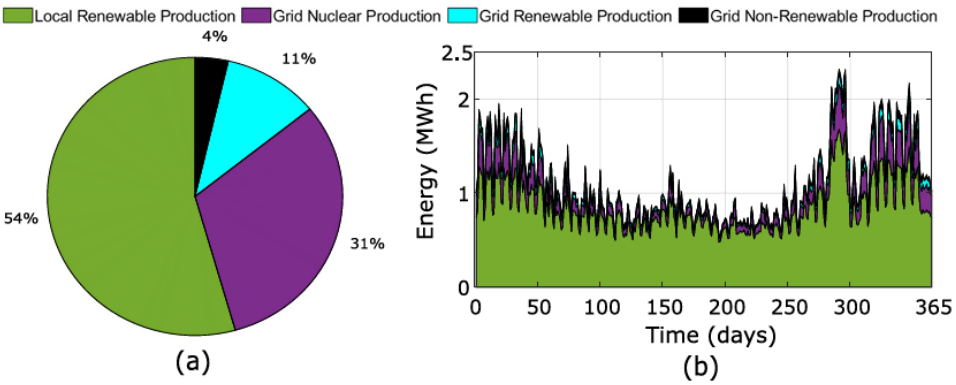


**Figure 2.1-9 (a) The percentage breakdown of the utilized energy sources in the French electricity grid for the case of lowest LCOE, (b) the distribution of energy sources utilized over**

Figure 2.1-9 (b) presents the distribution of energy sources used over the year with a temporal resolution of one day for the lowest LCOE scenario. The results indicate a high reliance on local renewable consumption specifically PV and BESS, followed by nuclear power production. The proportion of nuclear power increases in the winter season due to lower solar irradiation and hence less local renewable consumption.

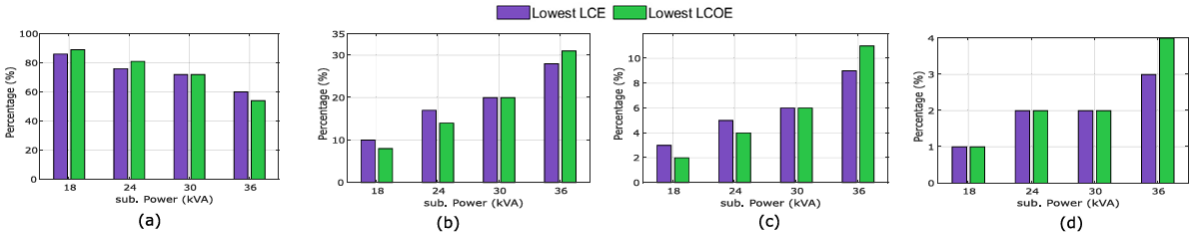


**Figure 2.1-10 Comparative bar chart of the lowest LCOE and lowest LCE scenarios for the (a) local renewable consumption (b), grid nuclear consumption (c), grid renewable consumption (d).**

Figure 2.1-10 compares the scenarios of lowest LCE and lowest LCOE for local renewable consumption (Figure 2.1-10 (a)), grid nuclear consumption (Figure 2.1-10 (b)), grid renewable consumption (Figure 2.1-10(c)), and grid non-renewable consumption (Figure 2.1-10(d)). For both scenarios, the local renewable consumption tends to decrease with an increase in the subscription power from the utility grid. In contrast, the grid nuclear, grid renewable, and grid non-renewable consumptions tend to increase with an increase in the utility grid subscription power.

In the case of local renewable consumption (Figure 2.1-10(a)), for the scenario of the lowest LCOE, the percentage of local renewable consumption is higher than that of the scenario of lowest LCE for subscription powers of 18 kVA, 24 kVA and 30 kVA.

However, this is not the case for the 36-kVA subscription power as the percentage level of local production for the scenario lowest LCE is slightly higher. Regarding nuclear, grid renewable, and grid non-renewable power production (Figure 2.1-10 (b), (c) and (d)) the percentage level for the scenario of lowest LCE is higher than that scenario of lowest LCOE for subscription powers of 18 kVA, 24 kVA and 30 kVA. In contrast, for the 36-kVA subscription power, the percentage level for the scenario of lowest LCOE is higher than that of the scenario where LCE is lowest.

The trend exhibited by the 36-kVA subscription power differs from the remaining cases, primarily attributed to grid injection. As the grid limit increases to 36 kVA, the likelihood of grid injection surpasses that of other capacities such as 18 kVA, 24 kVA and 30 kVA. Consequently, prioritizing the LCOE leads to increased local energy contribution, resulting in a higher grid injection.

The environmental impact of nuclear power generation should be considered when evaluating its feasibility as an energy source. This includes the potential for radioactive pollution of soil and water, which can have long-lasting effects on ecosystems and human health. It is important to consider these impacts when developing objective functions for nuclear power projects.

### 2.1.5 Discussion

In this study, the battery degradation is not formulated in the optimization problem (specifically through depth of discharge constraints) since the battery complete cycles are determined low in both operation modes. As explained previously, the energy capacity of the battery is obtained significantly higher compared to required charge and dis charge powers in BESS converter, hence battery cycle is not performing high number of complete cycles. However, it is aimed to be considered as a future work of this study in order to increase functionality of the presented methodology for the cases where BESS has high number of complete cycles.

Moreover, it should be noted that the presented results are not generic which can vary based on the chosen PV and BESS models, and according to electricity grid characteristics. Therefore, the proposed methodology can/should be used for testing the impact of the various equipment models in different electricity grid which has different emission and price profiles. For instance, when one of the main components, either PV or BESS, has lower costs and emissions in a microgrid with PV systems, BESS, load, and their converters, the solutions and the Pareto front show no variations. In the presented results the PV emissions are comparatively higher due to specific technology characteristics [45], but its cost remains lower. Importantly, it is worth noting that a PV panel with 2 000 $kgCO_2,eq/kWp$, there will not be any differences in the solutions along the Pareto front (single solution) for the chosen BESS technology in this study.

### 2.1.6 Conclusion and perspectives

In this study, a MILP optimization algorithm is presented to co optimize equipment sizing and energy management problems of a DC microgrid for the objectives of cost and emissions reduction. Based on the analysis and results presented in the study, the following conclusions can be drawn:

- In the IMG operation mode, the microgrid exhibits larger component capacities compared to GCMG. This difference is attributed to the necessity of coping with more challenging conditions, such as the absence of a grid connection during periods of low solar irradiation;
- The results reveal that the BESS capacity increases as the LCE decreases, and the number of PV systems is higher when the LCOE is lower for both operation modes. This is due to the fact that the BESS has a slightly lower LCE compared to the PV, and in this study, the LCOE of PV is also lower than BESS;
- From an economic point of view, the solution with a lower LCOE incurs the highest investment cost. Conversely, the solution with the lower LCE incurs the highest replacement cost, as it depends on BESS, which is an only replaced component over the project lifetime in this study;
- As the limit of the utility grid increases, the Pareto fronts for both peak shaving strategy become lower and steeper;
- From an environmental point of view, the findings reveal that 54% of the total production comes from local sources, with the remainder primarily reliant on the grid, which predominantly relies on nuclear power in the French energy mix.

As a future perspective, the Value of Lost Load will be calculated to assess the economic impact of power outages or service interruptions. By assigning a monetary value to the loss of supply reliability, businesses, utilities, and policymakers can better understand the consequences of such disruptions on the economy.

## REFERENCES

[1] S. Matemilola, O. Fadeyi, and T. Sijuade, “Paris Agreement,” in Encyclopedia of Sustainable Management, Springer, Cham, Switzerland, 2023, pp. 1–5. doi: https://doi.org/10.1007/978-3-031-25984-5%E2%82%8516.

[2] M. F. Zia, E. Elbouchikhi, and M. Benbouzid, “Microgrids Energy Management systems: a Critical Review on methods, solutions, and Prospects,” Applied Energy, vol. 222, pp. 1033–1055, 2018, doi: https://doi.org/10.1016/j.apenergy.2018.04.103.

[3] A. S. Brouwer, M. van den Broek, W. Zappa, W. C. Turkenburg, and A. Faaij, "Least-cost Options for Integrating Intermittent Renewables in low-carbon Power Systems," Applied Energy, vol. 161, pp. 48–74, Jan. 2016, doi: https://doi.org/10.1016/j.apenergy.2015.09.090.

[4] L. A. de S. Ribeiro, O. R. Saavedra, Shigeaki. L. Lima, J. G. de Matos, and G. Bonan, "Making Isolated Renewable Energy Systems More Reliable," Renewable Energy, vol. 45, pp. 221–231, Sep. 2012, doi: https://doi.org/10.1016/j.renene.2012.02.014.

[5] D. Wu, X. Ma, S. Huang, T. Fu, and P. Balducci, "Stochastic Optimal Sizing of Distributed Energy Resources for a cost-effective and Resilient Microgrid," Energy, vol. 198, p. 117284, May 2020, doi: https://doi.org/10.1016/j.energy.2020.117284.

[6] C. Shang, D. Srinivasan, and T. Reindl, "Generation-scheduling-coupled Battery Sizing of stand-alone Hybrid Power Systems," Energy, vol. 114, pp. 671–682, Nov. 2016, doi: https://doi.org/10.1016/j.energy.2016.07.123.

[7] S. Sukumar, H. Mokhlis, S. Mekhilef, K. Naidu, and M. Karimi, "Mix-mode Energy Management Strategy and Battery Sizing for Economic Operation of grid-tied Microgrid," Energy, vol. 118, pp. 1322–1333, Jan. 2017, doi: https://doi.org/10.1016/j.energy.2016.11.018.

[8] F. Bagheri, H. Dagdougui, and M. Gendreau, "Stochastic Optimization and Scenario Generation for Peak Load Shaving in Smart District microgrid: Sizing and Operation," Energy and Buildings, p. 112426, Sep. 2022, doi: https://doi.org/10.1016/j.enbuild.2022.112426.

[9] M. Sechilariu and F. Locment, "Connecting and Integrating Variable Renewable Electricity in Utility Grid," in Urban DC Microgrid, Elsevier , 2016, pp. 1–33. doi: https://doi.org/10.1016/b978-0-12-803736-2.00001-3.

[10] N. Nikmehr and S. Najafi Ravadanegh, "Optimal Power Dispatch of Multi-Microgrids at Future Smart Distribution Grids," IEEE Transactions on Smart Grid, vol. 6, no. 4, pp. 1648–1657, Jul. 2015, doi: https://doi.org/10.1109/tsg.2015.2396992.

[11] J. Wasilewski, "Optimisation of Multicarrier Microgrid Layout Using Selected Metaheuristics," International Journal of Electrical Power & Energy Systems, vol. 99, pp. 246–260, 2018, doi: https://doi.org/10.1016/j.ijepes.2018.01.022.

[12] A. T. D. Perera, R. A. Attalage, K. K. C. K. Perera, and V. P. C. Dassanayake, "A Hybrid Tool to Combine multi-objective Optimization and multi-criterion Decision Making in Designing Standalone Hybrid Energy Systems," Applied Energy, vol. 107, pp. 412–425, Jul. 2013, doi: https://doi.org/10.1016/j.apenergy.2013.02.049.

[13] J. Zhou and Z. Xu, "Optimal Sizing Design and Integrated cost-benefit Assessment of stand-alone Microgrid System with Different Energy Storage Employing Chameleon Swarm algorithm: a Rural Case in Northeast China," Renewable Energy, vol. 202, pp. 1110–1137, Jan. 2023, doi: https://doi.org/10.1016/j.renene.2022.12.005.

[14] D. Huo, M. Santos, I. Sarantakos, M. Resch, N. Wade, and D. Greenwood, "A reliability-aware chance-constrained Battery Sizing Method for Island Microgrid," Energy, vol. 251, p. 123978, Jul. 2022, doi: https://doi.org/10.1016/j.energy.2022.123978.

[15] A. Hassan, Y. M. Al-Abdeli, M. Masek, and O. Bass, "Optimal Sizing and Energy Scheduling of grid-supplemented Solar PV Systems with Battery storage: Sensitivity of Reliability and Financial Constraints," Energy, vol. 238, p. 121780, Jan. 2022, doi: https://doi.org/10.1016/j.energy.2021.121780.

[16] F. Khlifi, H. Cherif, and J. Belhadj, "Environmental and Economic Optimization and Sizing of a Micro-Grid with Battery Storage for an Industrial Application," Energies, vol. 14, no. 18, p. 5913, Sep. 2021, doi: https://doi.org/10.3390/en14185913.

[17] J.-L. Duchaud, G. Notton, C. Darras, and C. Voyant, "Multi-Objective Particle Swarm Optimal Sizing of a Renewable Hybrid Power Plant with Storage," Renewable Energy, vol. 131, pp. 1156–1167, Feb. 2019, doi: https://doi.org/10.1016/j.renene.2018.08.058.

[18] M. J. Mayer, A. Szilágyi, and G. Gróf, "Environmental and Economic multi-objective Optimization of a Household Level Hybrid Renewable Energy System by Genetic Algorithm," Applied Energy, vol. 269, p. 115058, Jul. 2020, doi: https://doi.org/10.1016/j.apenergy.2020.115058.

[19] N. Dougier, P. Garambois, J. Gomand, and L. Roucoules, "Multi-objective non-weighted Optimization to Explore New Efficient Design of Electrical Microgrids," Applied Energy, vol. 304, p. 117758, Dec. 2021, doi: https://doi.org/10.1016/j.apenergy.2021.117758.

[20] İ. Çetinbaş, B. Tamyürek, and M. Demirtaş, "Sizing Optimization and Design of an Autonomous AC Microgrid for Commercial Loads Using Harris Hawks Optimization Algorithm," Energy Conversion and Management, vol. 245, p. 114562, Oct. 2021, doi: https://doi.org/10.1016/j.enconman.2021.114562.

[21] M. Alramlawi and P. Li, "Design Optimization of a Residential PV-Battery Microgrid with a Detailed Battery Lifetime Estimation Model," IEEE Transactions on Industry Applications, vol. 56, no. 2, pp. 2020–2030, Mar. 2020, doi: https://doi.org/10.1109/tia.2020.2965894.

[22] A. L. Bukar, C. W. Tan, and K. Y. Lau, "Optimal Sizing of an Autonomous photovoltaic/wind/battery/diesel Generator Microgrid Using Grasshopper Optimization Algorithm," Solar Energy, vol. 188, pp. 685–696, Aug. 2019, doi: https://doi.org/10.1016/j.solener.2019.06.050.

[23] I. Jiménez-Vargas, J. M. Rey, and G. Osma-Pinto, "Sizing of Hybrid Microgrids considering Life Cycle Assessment," Renewable Energy, Nov. 2022, doi: https://doi.org/10.1016/j.renene.2022.11.103.

[24] R. Atia and N. Yamada, "Sizing and Analysis of Renewable Energy and Battery Systems in Residential Microgrids," IEEE Transactions on Smart Grid, vol. 7, no. 3, pp. 1204–1213, May 2016, doi: https://doi.org/10.1109/tsg.2016.2519541.

[25] T. M. Masaud and E. F. El-Saadany, "Correlating Optimal Size, Cycle Life Estimation, and Technology Selection of Batteries: a Two-Stage Approach for Microgrid Applications," IEEE Transactions on Sustainable Energy, vol. 11, no. 3, pp. 1257–1267, Jul. 2020, doi: https://doi.org/10.1109/tste.2019.2921804.

[26] M. R. Jannesar, A. Sedighi, M. Savaghebi, and J. M. Guerrero, "Optimal placement, sizing, and Daily charge/discharge of Battery Energy Storage in Low Voltage Distribution Network with High Photovoltaic Penetration," Applied Energy, vol. 226, pp. 957–966, Sep. 2018, doi: https://doi.org/10.1016/j.apenergy.2018.06.036.

[27] M. Cao, Q. Xu, J. Cai, and B. Yang, "Optimal Sizing Strategy for Energy Storage System considering Correlated Forecast Uncertainties of Dispatchable Resources," International Journal of Electrical Power & Energy Systems, vol. 108, pp. 336–346, Jun. 2019, doi: https://doi.org/10.1016/j.ijepes.2019.01.019.

[28] Agnès François, R. Roche, D. Grondin, and M. Benne, "Assessment of Medium and Long Term Scenarios for the Electrical Autonomy in Island territories: the Reunion Island Case Study," Renewable Energy, vol. 216, pp. 119093–119093, Nov. 2023, doi: https://doi.org/10.1016/j.renene.2023.119093.

[29] G. Soykan, G. Er, and E. Canakoglu, "Optimal Sizing of an Isolated Microgrid with Electric Vehicles Using Stochastic Programming," Sustainable Energy, Grids and Networks, vol. 32, p. 100850, Dec. 2022, doi: https://doi.org/10.1016/j.segan.2022.100850.

[30] F. Boutros, M. Doumiati, J.-C. Olivier, I. Mougharbel, and H. Kanaan, "New Modelling Approach for the Optimal Sizing of an Islanded Microgrid considering Economic and Environmental Challenges," Energy Conversion and Management, vol. 277, p. 116636, Feb. 2023, doi: https://doi.org/10.1016/j.enconman.2022.116636.

[31] A. Malheiro, P. M. Castro, R. M. Lima, and A. Estanqueiro, "Integrated sizing and scheduling of wind/PV/diesel/battery isolated systems," Renewable Energy, vol. 83, pp. 646–657, Nov. 2015, doi: https://doi.org/10.1016/j.renene.2015.04.066.

[32] M. Sechilariu and F. Locment, "Experimental Evaluation of Urban Direct Current Microgrid," in Urban DC Microgrid, Elsevier, 2016, pp. 209–250. doi: https://doi.org/10.1016/b978-0-12-803736-2.00006-2.

[33] M. Sechilariu and F. Locment, "Photovoltaic Source Modeling and Control," in Urban DC Microgrid, Elsevier, 2016, pp. 35–91. doi: https://doi.org/10.1016/b978-0-12-803736-2.00002-5.

[34] C. Yin, H. Wu, F. Locment, and M. Sechilariu, "Energy Management of DC Microgrid Based on Photovoltaic Combined with Diesel Generator and Supercapacitor," Energy Conversion and Management, vol. 132, pp. 14–27, Jan. 2017, doi: https://doi.org/10.1016/j.enconman.2016.11.018.

[35] B. Babaiahgari, H. Ullah, and J. D. Park, "Coordinated Control and Dynamic Optimization in DC Microgrid Systems," International Journal of Electrical Power & Energy Systems, vol. 113, pp. 832–841, Dec. 2019, doi: https://doi.org/10.1016/j.ijepes.2019.05.076.

[36] S. Wang et al., "Impact of Battery Degradation Models on Energy Management of a grid-connected DC Microgrid," Energy, vol. 207, p. 118228, Sep. 2020, doi: https://doi.org/10.1016/j.energy.2020.118228.

[37] F. A. Kassab, B. Celik, F. Locment, M. Sechilariu, and T. M. Hansen, "Combined Optimal Sizing and Energy Management of a DC Microgrid Using MILP," presented at the IEEE Belgrade PowerTech, 2023. doi: https://doi.org/10.1016/j.renene.2024.120186.

[38] "Comparateur Electricité / Comparateur gaz, 2020," Selectra, Mar. 24, 2021. https://selectra.info/energie

[39] L. Sartini and S. F. P. Saramago, “Multiobjective Optimization Techniques Applied to Engineering Problems,” Journal of the Brazilian Society of Mechanical Sciences and Engineering, vol. 32, no. 1, pp. 94–105, Mar. 2010, doi: https://doi.org/10.1590/s1678-58782010000100012.

[40] Hassan, M. Yousif, Shahid Nawaz Khan, A. Abbas, and K. Imran, “A decision-centric Approach for techno-economic Optimization and Environmental Assessment of Standalone and grid-integrated renewable-powered Electric Vehicle Charging Stations under Multiple Planning Horizons,” Energy Conversion and Management, vol. 294, pp. 117571–117571, Oct. 2023, doi: https://doi.org/10.1016/j.enconman.2023.117571.

[41] A. González, J.-R. Riba, and A. Rius, “Optimal Sizing of a Hybrid Grid-Connected Photovoltaic–Wind–Biomass Power System,” Sustainability, vol. 7, no. 9, pp. 12787–12806, Sep. 2015, doi: https://doi.org/10.3390/su70912787.

[42] “Le taux d’actualisation dans l’évaluation des projets d’investissement public | France Stratégie. Available: Here

[43] Z. Liu, Y. Chen, R. Zhuo, and H. Jia, “Energy Storage Capacity Optimization for Autonomy Microgrid considering CHP and EV Scheduling,” Applied Energy, vol. 210, pp. 1113–1125, Jan. 2018, doi: https://doi.org/10.1016/j.apenergy.2017.07.002.

[44] S. Mohseni, R. Khalid, and A. C. Brent, “Metaheuristic-based isolated microgrid sizing and uncertainty quantification considering EVs as shiftable loads,” Energy Reports, vol. 8, pp. 11288–11308, Sep. 2022, doi: https://doi.org/10.1016/j.egyr.2022.08.254.

[45] D. Colarossi, E. Tagliolini, A. Amato, and P. Principi, “Life Cycle Assessment and Circularity Evaluation of a PV Panel Integrated with Phase Change Material,” Renewable Energy, vol. 201, pp. 150–156, Dec. 2022, doi: https://doi.org/10.1016/j.renene.2022.11.076.

[46] “UCG - SOLAR SERIES - 12V,” 2025. https://ultracell.fr/assets/pages/products-ucgseries-12v.html

[47] “Prix De L’électricité En France 2023: tarifs, Comparatif Des offres, 2023.” Available: Here

[48] Yann Colnot, “Tarif Rachat EDF 2022: photovoltaïque, éolien, biométhane..., 2022,” May 11, 2017. Available : Here

[49] “Eco2mix- $CO_2$ Emissions per Kwh of Electricity Generated in France, 2021.” https://www.rte-france.com/ie/

[50] M. Cheng, X. Zhang, A. Ran, G. Wei, and H. Sun, “Optimal Dispatch Approach for second-life Batteries considering Degradation with Online SoH Estimation,” Renewable and Sustainable Energy Reviews, vol. 173, p. 113053, Mar. 2023, doi: https://doi.org/10.1016/j.rser.2022.113053.

[51] “Rapport d’activité 2021 De La CRE, 2021.” Available/ Here

## 2.2 Optimizing Microgrid Sizing, Energy Management, and Electric Vehicle Integration

This section applies the proposed study from Section 2.1 by introducing the EV problem to the previously described methodology and presenting a case study in Compiègne, France. It also analyses the Levelized Cost of Energy (LCOE) and conducts a life cycle emissions (LCE) analysis across various cities[7,8].

### 2.2.1 Introduction

A microgrid offers an efficient solution for integrating distributed energy resources, such as solar power, with the electrical grid. In this context, the increasing demand for electricity is driven by several factors, such as the growth of the electric vehicle (EV) market, which is advancing due to technological innovations and shared societal and political goals aimed at mitigating climate change [1]. Therefore, ensuring the optimal sizing of the microgrids is essential. An undersized microgrid relies on the grid and may not achieve the desired level of autonomy. Moreover, optimizing the microgrid's size helps in reducing the overall cost of the system [2]. The most common goal in the context of optimal microgrid sizing is cost minimization, and to address this problem, software tools, heuristic methods, and linear techniques are commonly utilized.

In the examined literature, various studies consistently apply HOMER commercial software to explore the optimal configurations of microgrids and distributed energy resources. In [3], the research focuses on multi-microgrid component sizing, considering economic and technical factors. Similarly, [4] employs HOMER to design a microgrid with Photovoltaic (PV), wind, batteries, and a diesel generator in Biskra, Algeria. Additionally, in [5], HOMER is used to determine the optimal configurations for PV/Diesel/Pump-hydro and PV/Diesel/Batteries systems and calculate payback periods, emphasizing cost effective solutions. These studies likely yield insights into efficient and economically viable microgrid designs, including resource combinations, cost effectiveness, and anticipated financial returns.

Regarding heuristic optimization methods, these methods are prevalent in the literature due to the complexity of the microgrid sizing problem. Heuristic techniques play a crucial role in reducing the required computational time. In [6], the study introduces three meta-heuristic algorithms: enhanced differential evolution, teaching-learning-based optimization, and the salp swarm algorithm. These algorithms are applied to tackle the sizing optimization problem of a standalone microgrid. In [2], particle swarm optimization is used to address a hybrid microgrid sizing problem by minimizing the Levelized Cost of Energy (LCOE) and maximizing the

---

[7] This study is based on the following publication: F. A. Kassab, B. Celik, S. Cheikh-Mohamad, F. Locment, M. Sechilariu, S. Liaquat and T. M. Hansen, "Optimizing Microgrid Sizing, Energy Management, and Electric Vehicle Integration in Various French Cities," in Electrimacs 2024, 2024, doi: ⟨hal-04772766⟩

[8] The methodology developed is detailed in previous work; refer to the antecedent publication for more details:

F. A. Kassab, B. Celik, F. Locment, M. Sechilariu and T. M. Hansen, "Combined Optimal Sizing and Energy Management of a DC Microgrid using MILP," 2023 IEEE Belgrade PowerTech, Belgrade, Serbia, 2023, pp. 1-6, https://doi.org/10.1109/PowerTech55446.2023.10202939.

F. A. Kassab, B. Celik, F. Locment, M. Sechilariu, S. Liaquat, and T. M. Hansen, "Optimal sizing and energy management of a microgrid: A joint MILP approach for minimization of energy cost and carbon emission," Renewable Energy, vol. 224, p. 120186, 2024, https://doi.org/10.1016/j.renene.2024.120186.

microgrid autonomy. Additionally, in [7], the NSGA II algorithm is implemented for co-optimizing a microgrid in terms of both economic and environmental aspects.

As for linear techniques, the literature frequently features the use of Mixed-Integer Linear Programming (MILP). In [8], cost minimization is achieved through MILP, as this technique ensures a globally optimal solution. Each of these studies also pursues additional objectives, such as load scheduling and the minimization of life cycle emissions (LCE), with a focus on specific regions and types of buildings, encompassing both residential and commercial structures.

Each technique has its own set of limitations. Commercial software packages, such as HOMER, fall short in certain aspects. They lack the capability to perform multi-objective optimization or effectively address intra-hour-based variability. Furthermore, when confronted with more intricate design scenarios, they often demand a significant amount of computational time or do not converge [9]. Heuristic approaches do not guarantee global optimal solutions for optimization problems [10]. MILP techniques, on the other hand, can entail high computational time, especially for complex problems where linearizing equations becomes challenging, potentially necessitating trade-offs between optimality and computational efficiency.

This research is a continuation of the work in [11],[12], where a MILP algorithm that ensures a global optimal solution was introduced to optimize both the sizing and energy management of a microgrid, considering the yearly solar irradiation and the yearly load demand of a tertiary building in the university campus. The study is extended by including the modeling and consideration of EV loads, where the microgrid is tested in various cities. Additionally, the study calculates the LCE for the proposed solutions across different cities.

The research is organized as follows: In Section 2.2.2, the system modeling is described. The optimization problem is presented in Section 2.2.3, Section 2.2.4 covers the results and analysis, and Section 2.2.5 presents the conclusions.

## 2.2.2 System Modelling

The studied microgrid (Figure 2.2-1) comprises several components, including PV panels, a battery energy storage system (BESS), a grid connection (EG), a tertiary building, and EV loads. The same PV and BESS equations from [11], [12] are used for calculating their power outputs. Additionally, the EV charging models are included in this study.

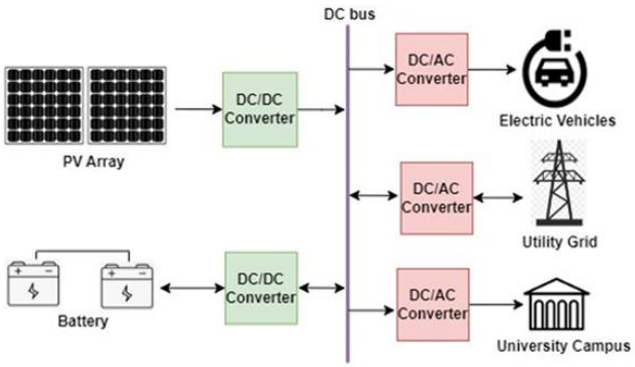


**Figure 2.2-1 The studied microgrid structure.**

### *2.2.2.1 EV Charging model*

It is crucial to develop sophisticated models that consider factors such as the EV's plug-in time ($t_p$) and initial state of charge ($SOC_{EV\,init}$ ). In [13], data is collected for a university campus to

illustrate the probability density functions (PDFs) of $t_p$ and $SOC_{EV\,init}$ for private EVs. The findings revealed that the Generalized Extreme Value (GEV) PDF closely aligns with the collected data. The GEV PDF equation is obtained as follows:

$$f(x;\mu,\sigma,\varepsilon) = \begin{cases} \frac{1}{\sigma}[1+\varepsilon\left(\frac{x-\mu}{\sigma}\right)]^{-\frac{1}{\varepsilon}-1} \times exp\left\{-\left[1+\varepsilon\left(\frac{x-\mu}{\sigma}\right)\right]^{-\frac{1}{\varepsilon}}\right\}, if\ \varepsilon \neq 0 \\ \frac{1}{\sigma} exp-\left(\frac{x-\mu}{\sigma}\right), if \varepsilon = 0 \end{cases} \quad (2.2\text{-}1)$$

Here, $f(x;\mu,\sigma,\varepsilon)$ represents the GEV PDF, where $x$ is the random variable, μ is the location parameter, σ is the scale parameter, and \varepsilon is the shape parameter. For the $SOC_{EV\,init}$, the GEV PDF parameters are: $\varepsilon = 0.0629$, $\sigma = 0.5493$,$\mu = 8.9068$ , while for $t_p$, the GEV PDF parameters are: $\varepsilon = 0.0474$,$\sigma = 7.9015$, $\mu = 12.8820$.

The duration required for charging the EV varies based on the connection time, and the period needed to attain the maximum $SOC$ for the EV $SOC_{EV\,max}$, is computed as follows:

$$T_{char,a} = \frac{\left(SOC_{EV\,max,a} - SOC_{EV\,init,a}\right)\times EV_{cap,a}}{P_{cs}} \quad (2.2\text{-}2)$$

where $T_{char,a}$, $SOC_{EV\,max,a}$, and $EV_{cap,a}$ are the charging duration ($h$), maximum $SOC$, and battery capacity (kWh) of the EV $a$, respectively; and $P_{cs}$ is the charging station power (kW).

The plug-out time for EV is determined using a uniform distribution that ranges from zero to three hours after the EV charging time needed to reach the maximum $SOC$. This consideration is incorporated into the optimization problem to introduce a margin of flexibility, enabling the scheduling of EV charging. Without this margin, if the unplugging time coincides exactly with the EV charging duration, scheduling EV charging sessions would be unfeasible. The EV charging power demand is calculated as follows:

$$p_{EV,a}(t) = \begin{cases} \frac{\left(SOC_{EV\,max,a} - SOC_{EV\,init,a}\right)\times EV_{cap,a}}{T_{char,a}} \ if\ t \geq t_p \\ 0, \quad otherwise \end{cases} \quad (2.2\text{-}3)$$

Equation (2.2-3) calculates the charging power of each EV, denoted as $p_{EV,a}$, after the plug-in time $t_p$. The energy needed to charge the EV is divided by the rounded-up charging duration ($T_{char,a}$) to calculate the actual EV power. This method is chosen because the study operates on an hourly time scale, and charging the EV at a steady power rate might risk pushing the battery's $SOC$ beyond its permitted maximum level.

### 2.2.3 Formulation of the optimization problem

The optimization problem is designed to achieve a dual objective: the first objective is to minimize the LCOE, and the second is to determine the optimal size of microgrid components and efficiently manage energy within the microgrid. As this study is a continuation of [11][12], the optimization problem and its formulation are already detailed in those researches. However, the algorithm introduced in this chapter considers the EV demand. For that, this section introduces the equations that are modified, and the rest can be seen considered from [11][12].

#### *2.2.3.1 Constraints*

The BESS charge/discharge power ($p_b^c(t)$ / $p_b^d(t)$) are not limited to a specific power level. This allows for optimal sizing of the BESS converter, as restricting the charging/discharging power would fix the converter's size. In contrast, the grid supply/injection powers

$(p_{EG}^{s}(t)/p_{EG}^{in}(t))$ are constrained to a maximum power level to represent the subscribed maximum power from the French grid.

$$p_b^c(t) \geq 0,\ p_b^d(t) \leq 0 \tag{2.2-4}$$

$$-p_{EG}^{max} \leq p_{EG}^{s}(t) \leq 0 \tag{2.2-5}$$

$$0 \leq p_{EG}^{in}(t) \leq p_{EG}^{max} \tag{2.2-6}$$

In (2.2-4), there is no strict maximum limit imposed on the power of the BESS, allowing the BESS associated converter to be determined by the algorithm. The "Big M" technique, used for optimizing energy management in the microgrid, simplifies complex decision making, similar to how "If Else" statements are employed in programming. For a detail understanding of the constraints and BESS energy calculations, refer to the reference [11]. The converters capacity is determined based on the maximum output power obtained by the connected resources as follows:

$$p_{PV}^{MPPT}(t) \times N_{PV} \leq M_{PV}^{DC/DC} \tag{2.2-7}$$

$$-p_b^d(t) \times \mu_d + p_b^c(t)/\mu_c\ /\gamma_b^{DC/DC} \leq M_b^{DC/DC} \tag{2.2-8}$$

$$-p_{EG}^{s}(t) + p_{EG}^{in}(t)/\gamma_{EG}^{DC/AC} \leq M_{EG}^{AC/DC} \tag{2.2-9}$$

$$p_{EV}(t)/\gamma_{EV}^{DC/AC} \leq M_{EV}^{DC/AC} \tag{2.2-10}$$

$$p_{build}(t)/\gamma_{build}^{DC/AC} \leq M_{build}^{DC/AC} \tag{2.2-11}$$

where $p_{PV}(t)$ is the power output of a PV panel, $N_{PV}$ is the total PV panel number, and $\mu_c$ and $\mu_d$ denote the charge and discharge efficiency of the BESS. Additionally, $\gamma_k^x$ and $M_k^x$ represent the efficiency and capacities of the $x^{th}$ component associated with the $k^{th}$ component respectively, and $p_{build}(t)$ is the consumption power. The net power on the DC bus, denoted as $p_{bus}(t)$, is calculated as given below:

$$\begin{aligned} p_{bus}(t) = p_{buil}(t)/\gamma_{build}^{DC/AC} + p_{EV}(t)/\gamma_{EV}^{DC/AC} - \gamma_{PV}^{DC/DC} \times p_{PV}^{MPPT}(t) \\ +p_b^c\ (t)/\mu_c \times \gamma_b^{DC/DC} + p_b^d(t) \times \gamma_b^{DC/DC} \times \mu_d \\ +p_{EG}^{s}(t) \times \gamma_{EG}^{AC/DC} + p_{EG}^{in}(t)/\gamma_{EG}^{DC/AC} \leq 0 \end{aligned} \tag{2.2-12}$$

Enforcing $p_{bus}(t) \leq 0$ implies curtailing negative power and prohibiting load shedding.

### *2.2.3.2 Objective function*

The objective function aims to minimize the LCOE and the LCE calculated as follows:

$$LCOE = \frac{TC \times CRF}{\sum_{t_0}^{t_f} p_L^D(t) \times \Delta t} \tag{2.2-13}$$

$$LCE = LCE_{PV} + LCE_{BESS} + LCE_{EG} + LCE_{cables} \tag{2.2-14}$$

In Equation (2.2-13), $TC$ is the total cost which considers several factors, including initial capital investment, maintenance, replacement costs, potential salvage value of electrical components, and the expenses associated with energy procurement from the grid. The capital recovery factor is $CRF$, $p_L^D(t)$ denotes the load (which includes EV and building loads), and $t_0$, $t_f$ and $\Delta t$ represent the initial, final, and the step time of the simulation, respectively.

In Equation (2.2-14), $LCE_{PV}$, $LCE_{BESS}$, $LCE_{EG}$ and $LCE_{cables}$ are the LCE of the PV system, BESS, utility grid and the cables, respectively. Readers are referred to [11],[12] for detailed equations related to equations (2.2-13) and (2.2-14).

The optimization problem is addressed by determining the following decision variables:

- BESS capacity ($E_b$);
- the number of PV panels ($N_{PV}$);
- BESS charge/discharge powers ($p_b^c(t)/p_b^d(t)$);
- EG supply/inject powers ($p_{EG}^s(t)/p_{EG}^{in}(t)$);
- Auxiliary variables ($x_{aux}(t)$).

Additionally, the capacities of PV, BESS, EG, EV, and building associated converters ($M_{PV}^{DC/DC}, M_b^{DC/DC}, M_{EG}^{AC/DC}, M_{EV}^{DC/AC}, M_{build}^{DC/AC}$ are also determined.

### 2.2.4 Results and Analysis

In the studied microgrid, the load distribution encompasses the EVs and the university building. The charging infrastructure for EVs comprises five EV charging terminals, each equipped with two 7 kW chargers, allowing for a maximum of 10 EVs to be charged simultaneously.

Additionally, plugging in the EV is subject to an SOC limitation, ranging from 20% to 100%. The EV battery capacity is assumed to be 50 kWh. The daily arrival of EVs is determined using a uniform distribution. On weekdays, there are between seven to ten EV arrivals, while on weekends, there are one to two EV arrivals. During the vacation month of August, there can be one to four EV arrivals.

The load profile of the university building is sourced from empirical data collected at a specific building within Université de Technologie de Compiègne in 2023. Both the EVs and university building's load characteristics are visually represented in Figure 2.2-2.

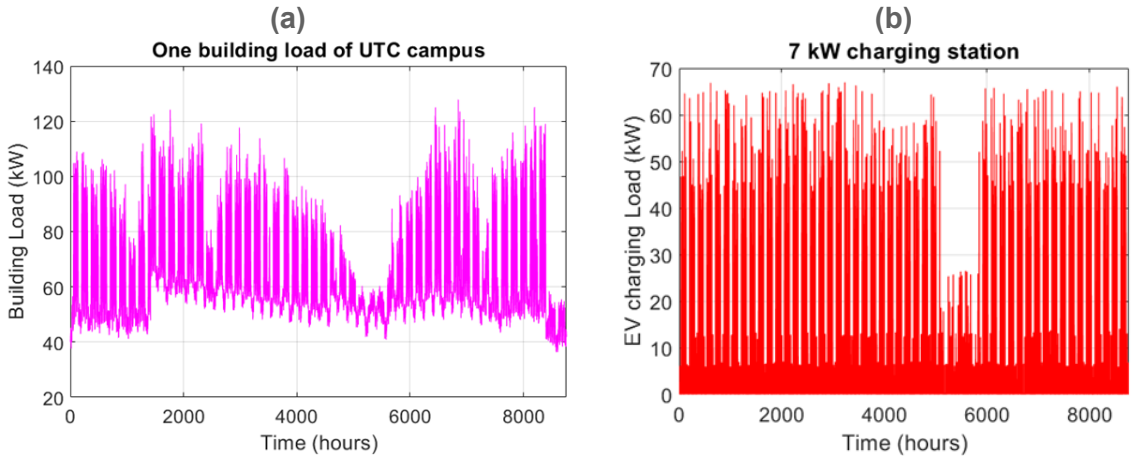


**Figure 2.2-2 (a) Building load and (b) EV load**

The EG $CO_2$ emissions are considered dynamic as it is provided by the French transmission system operator. In this study, a load growth of 1% is considered to anticipate potential future increases in demand and to ensure the resilience of the microgrid, while the EG tariffs remain the same.

The optimization horizon covers one year (8 760) with an hourly timestep while considering the project's 20-year economic lifespan.

The problem is formulated using Python 3.8 and CPLEX optimization solver. The computations are carried out on a super computer equipped with an AMD EPYC 7763 64-Core Processor, 256 cores, and 1 510 GB of RAM, all running on the "RockyLinux9.1" operating system.

### *2.2.4.1 Case study – Compiègne, France*

The optimization algorithm has been applied to the case study of Compiègne, France, using the input described in the above section and a combination of several PV and BESS technologies. The technical, economic, and environmental data utilized for this analysis are presented in Table 2.2-1.

**Table 2.2-1 Input parameters data of the microgrid system.**

| Parameter | Value | Unit | Parameter | Value | Unit |
|---|---|---|---|---|---|
| | **DualSun PV** | | | **SunPower PV** | |
| PV module-rated power | 400 | Wp | PV module-rated power | 315 | Wp |
| Lifetime | 25 | years | Lifetime | 25 | years |
| Investment cost | 612 | € | Investment cost | 550 | € |
| Maintenance cost | 1 | % of Investment cost/year | Maintenance cost | 1 | % of Investment cost/year |
| $CO_2$ emissions | 507.5 | $kgCO_2$,eq/kWp | $CO_2$ emissions | 685 | $kgCO_2$,eq/kWp |
| | **JASolar PV** | | | **Voltec PV** | |
| PV module-rated power | 310 | Wp | PV module-rated power | 300 | Wp |
| Lifetime | 25 | years | Lifetime | 25 | years |
| Investment cost | 450 | € | Investment cost | 480 | € |
| Maintenance cost | 1 | % of Investment cost/year | Maintenance cost | 1 | % of Investment cost/year |
| $CO_2$ emissions | 1,349 | $kgCO_2$,eq/kWp | $CO_2$ emissions | 776 | $kgCO_2$,eq/kWp |
| | **Li-Ion BESS** | | | **Lead Acid BESS** | |
| Unit Capacity | 2.55 | kWh | Unit Capacity | 1.8 | kWh |
| Lifetime | 10 | years | Lifetime | 5 | years |
| Investment cost | 1,084 | € | Investment cost | 200 | € |
| Maintenance cost | 3 | % of Investment cost/year | Maintenance cost | 3 | % of Investment cost/year |
| Replacement cost | 1,084 | € | Replacement cost | 200 | € |
| $CO_2$ emissions | 102 | $kgCO_2$,eq/kWp | $CO_2$ emissions | 146 | $kgCO_2$,eq/kWp |
| | **DC/DC & AC/DC & DC/AC converters** | | | **System** | |
| Efficiency | 95 | % | Cable $CO_2$ emissions | 17,680 | $kgCO_2$,eq |
| Lifetime | 10 | years | Project Lifetime | 20 | years |
| Investment cost | 80 | €/kW | Discount rate | 7 | % |
| Maintenance cost | 2 | % of Investment cost/year | Escalation rate | 3 | % |
| Replacement cost | 80 | €/kW | Installation cost | 40 | % of PV Investment cost |
| | **EG** | | | **EV Charging Station & EV** | |
| Grid power limit | 140 | kVA | Charging station power | 7 | kW |
| Inject tariff | 0.07878 | €/kWh | EV battery capacity | 50 | kWh |
| Fixed subscription cost | 1,000 | €/year | EV max SOC | 100 | % |
| Peak hour supply tariff | 0.2460 | €/kWh | EV min SOC | 20 | % |
| Off-Peak hour supply tariff | 0.1824 | €/kWh | | | |

DualSun offers the lowest cost among the available PV panel options. The Table 2.2-2 presents the optimization results for DualSun PV in combination with both BESS technologies Lead Acid and Lithium-Ion (Li-Ion).

In terms of LCOE, the combination of Lead Acid batteries with DualSun results in a lower LCOE compared to the Li-Ion/DualSun configuration. However, the Li-Ion/DualSun system achieves a lower LCE than the Lead Acid/SunPower case when considering the latter's higher grid supply, which is due to the smaller PV capacity.

The Li-ion/DualSun system is designed with excess capacity, as the optimization algorithm increases the PV size to reduce LCE. This result leads to a higher amount of curtailed PV power. Conversely, the higher PV capacity in the Li-Ion/DualSun system also results in higher grid injection, as more power is available for feeding back into the grid.

**Table 2.2-2 Optimization results for DualSun/Lead Acid and DualSun/Li-Ion.**

| Parameter | Lead Acid | Li-Ion | Unit |
|---|---|---|---|
| LCOE | 0.36 | 0.54 | €/KWh |
| LCE | 57,221 | 52,182 | $kgCO_2$,eq |
| PV capacity | 0.385 | 0.86 | MWp |
| BESS capacity | 1.87 | 0.77 | MWh |
| PV energy | 316 | 710 | MWh/year |
| PV curtailment | 0.05 | 133 | MWh/year |
| Grid supplied energy | 446.5 | 379 | MWh/year |
| Grid injected energy | 6.75 | 167 | MWh/year |
| BESS energy | 93.3 | 121 | MWh |

The Figure 2.2-3 illustrates the energy distribution over one year within the microgrid for the two studied combinations.

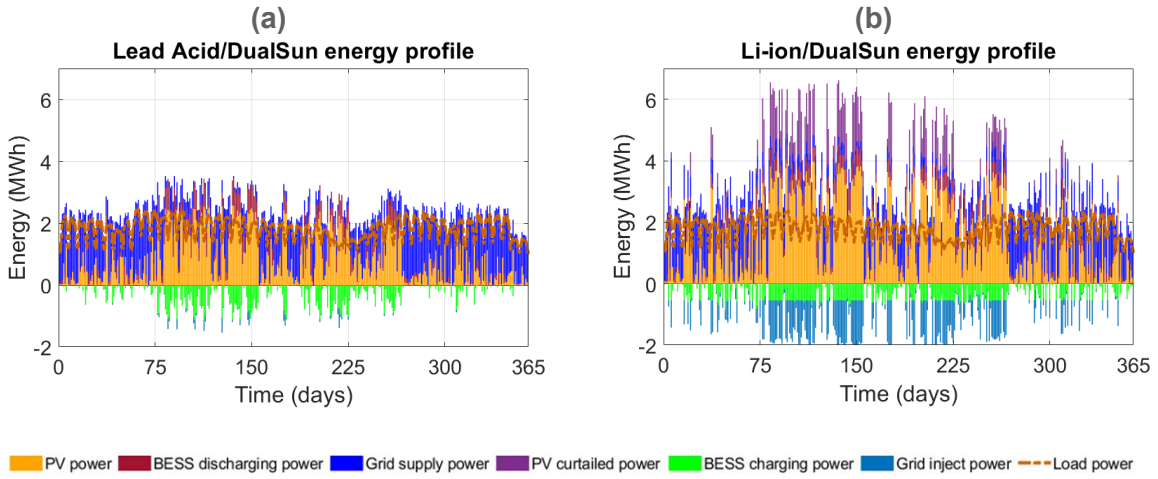


**Figure 2.2-3 Energy distribution over one-year (a) Lead Acid/DualSun and (b) Li-Ion/DualSun.**

The Lead acid/DualSun system is well-proportioned, resulting in minimal PV curtailment thanks to the high capacity of the BESS. In comparison, the energy generated in the Li-Ion/DualSun case is nearly double the amount produced in the Lead acid/DualSun case, highlighting the superior performance of the Li-Ion system in terms of energy production.

The Figure 2.2-4 presents a zoomed-in view of the energy distribution when using the Lead Acid/DualSun BESS over one week in February and one week in July.

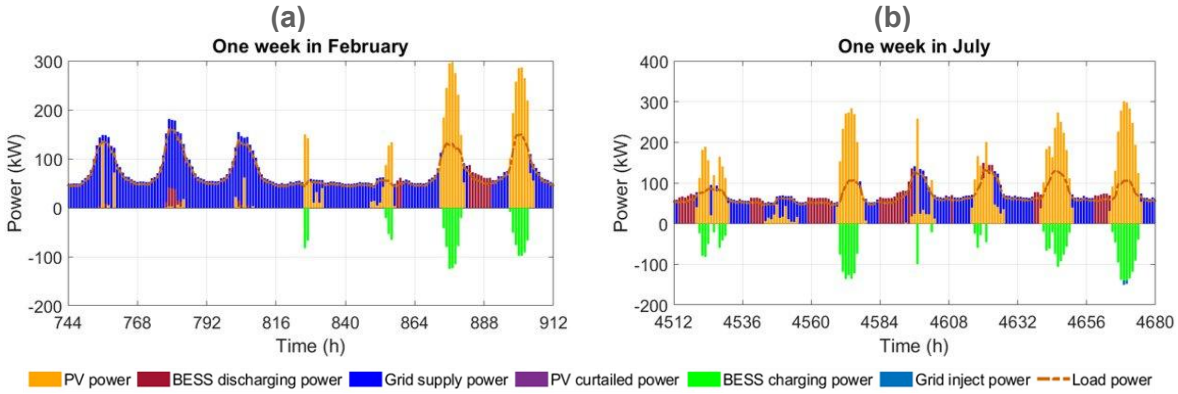


**Figure 2.2-4 (a) One-week in February and (b) one-week in July of the one-year simulation.**

The Figure 2.2-4 highlights the fact that during the summer, the BESS experiences significantly higher discharge levels compared to the winter months. In contrast, grid interventions are more frequent during the winter, primarily due to lower solar irradiation. The surplus PV power generated in both seasons is mainly used to recharge the Lead Acid/DualSun BESS, ensuring a continuous and reliable energy supply.

#### 2.2.4.1.1 LCOE and LCE Results

The optimization process involves studying various PV and BESS technologies to assess their impact on the dimensioning and energy management of the microgrid. Figure 2.2-5 (a) and (b) illustrate the LCOE and LCE, respectively.

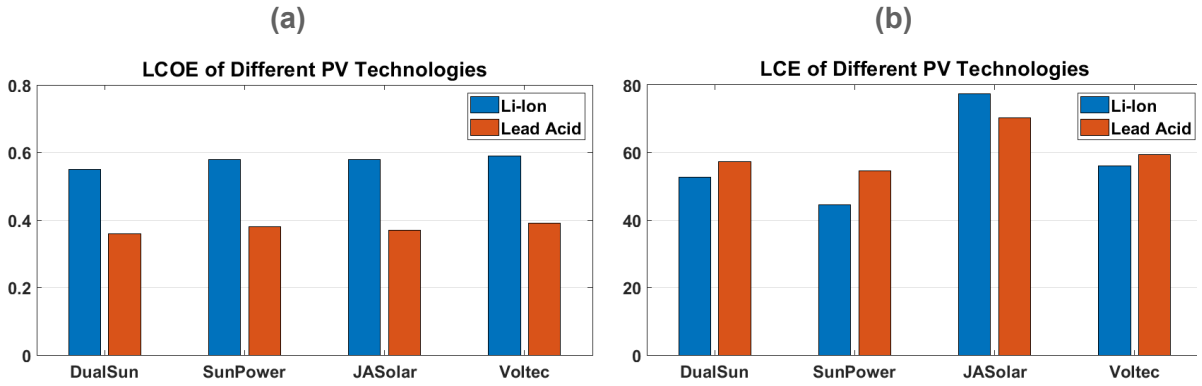


**Figure 2.2-5 (a) LCOE and (b) LCE results of different PV technologies.**

When Lead Acid batteries are used, the LCOE is lower compared to systems incorporating Li-Ion batteries. Among the analyzed configurations, the Voltec/Li-Ion system exhibits the highest LCOE, while the DualSun/Lead Acid system achieves the lowest. However, the reliance on Lead Acid batteries leads to the highest grid costs, primarily due to the smaller PV capacity. In contrast, investment costs are highest when Li-Ion batteries are utilized, as they are generally paired with larger PV capacity systems.

The analysis further highlights that the JASolar configuration yields the highest LCE. Notably, Lead Acid/PV systems consistently exhibit higher LCE values than Li-Ion/PV systems, with the exception of the Li-Ion/JASolar combination. However, JASolar is also associated with the highest emissions ($kgCO_2$,eq), which explains why the PV capacity for the Li-Ion/JASolar configuration is significantly lower than in other cases. Additionally, emission sources vary depending on the BESS type: in Li-Ion/PV scenarios, PV-related emissions represent the largest share, whereas in Lead Acid/PV scenarios, the primary contributor to emissions is the BESS.

### *2.2.4.2 Geographical Analysis*

To go further, the study progressed by applying the optimization algorithm to several cities in France and worldwide. Table 2.2-3 presents the average solar irradiation for the considered regions over the course of one year, as retrieved from [14].

**Table 2.2-3 Solar irradiation and Ambient temperature average in different cities.**

| City | Solar irradiation (kWh/m$^2$) | Ambient temperature (°C) | City | Solar irradiation (kWh/m$^2$) | Ambient temperature (°C) |
|---|---|---|---|---|---|
| Adelaide, AU | 1,758 | 14.98 | Madrid, ES | 1,991 | 14.94 |
| Ajaccio, FR | 1,769 | 12.36 | Marseille, FR | 1,375 | 16.59 |
| Bamako, ML | 2,300 | 27.89 | Nagoya, JP | 1,775 | 14.94 |
| Bern, CH | 1,658 | 9.12 | New Delhi, IN | 2,027 | 27.17 |
| Brest, FR | 810 | 12.81 | Poitiers, FR | 968 | 13.81 |
| Cairo, EG | 2,624 | 22.18 | Rabat, MA | 2,259 | 18.72 |
| Compiègne, FR | 838 | 12.74 | Strasbourg, FR | 964 | 12.44 |
| Dijon, FR | 987 | 12.5 | Toronto, CA | 1,634 | 8 |
| Doha, QA | 2,323 | 27.7 | Toulouse, FR | 1,697 | 14.89 |
| Le Havre, FR | 873 | 12.17 | Tripoli, LB | 2,165 | 19.37 |
| Lille, FR | 820 | 12.16 | Twente, NL | 1,313 | 11.58 |
| Lisbon, PT | 1,983 | 16.9 | Washington, US | 1,868 | 11.5 |

The optimization encompasses all cities specified in Table 2.2-3, where the same load (EV and building) is used for each city.

The capacity analysis of the microgrid components and the detailed energy dispatch for some cities with high solar irradiation are presented in Table 2.2-4. Additionally, the power profiles

of these cities for one week in July are depicted in Figure 2.2-6. Rabat, Tripoli, and Lisbon are identified as the cities with a high solar irradiation among the selected cities.

**Table 2.2-4 The microgrid components capacities and energy of the selected cities with high solar irradiation.**

| Parameter/City | Rabat | Tripoli | Lisbon |
|---|---|---|---|
| **Microgrid components capacities** | | | |
| PV capacity (kWp) | 381 | 303 | 389 |
| BESS capacity (kWh) | 226 | 461 | 270 |
| PV converter capacity (kW) | 410 | 302 | 413 |
| BESS converter capacity (kW) | 57 | 94 | 67 |
| EG converter capacity (kW) | 147 | 140 | 147 |
| EV converter capacity (kW) | 66 | 66 | 66 |
| Building converter capacity (kW) | 164 | 164 | 164 |
| **Energy dispatch** | | | |
| PV output energy (MWh/year) | 824 | 623 | 602 |
| Curtailed energy (MWh/year) | 18.5 | 0.4 | 0 |
| BESS energy (MWh/year) | 63 | 101 | 116 |
| EG supplied energy (MWh/year) | 362 | 375 | 368 |
| EG injected energy (MWh/year) | 257 | 94 | 63 |
| System losses energy (MWh/year) | 93 | 87 | 88 |

It can be seen that, the curtailed energy from the PV system is relatively small compared to the PV output energy. This observation indicates that the BESS capacity and EG power limits are sufficient to absorb most of the PV surplus. Additionally, the EG supply is always higher than the EG injection rate, highlighting the reliance on the EG. This suggests that the EG in France offers a more cost-effective solution compared to BESS, primarily due to the high investment cost of batteries. Furthermore, the EG limit is close to the maximum load peak, which explains the increased EG contribution in the microgrid. It should be noted that system losses include converters for PV, BESS, the electrical grid, EV load, and building load.

Figure 2.2-6 represents one week (the first week of July) of the one-year simulation for Rabat, Tripoli, and Lisbon.

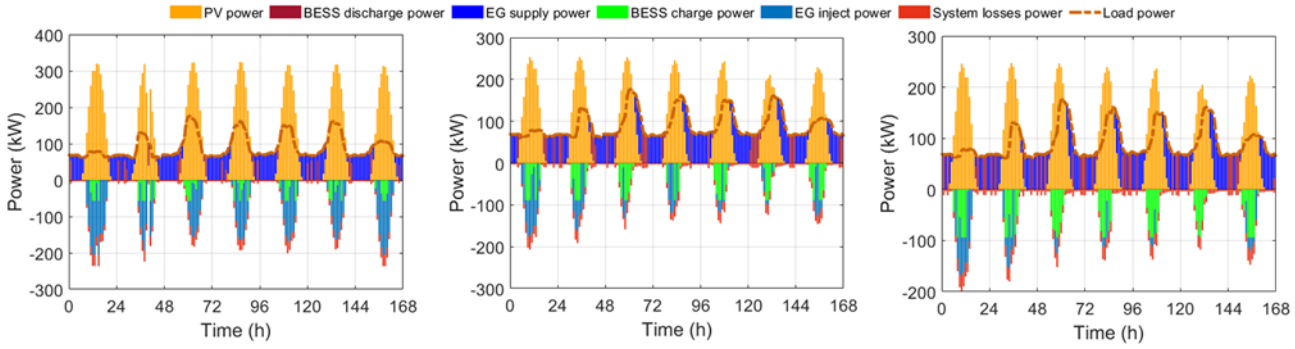


**Figure 2.2-6 One-week (1st of July's week) of the one-year simulation for (a) Rabat (b) Tripoli (c) Lisbon.**

For all these cities, the load is primarily covered by PV during the daytime and by the BESS and EG supply during the night-time. On the other hand, Brest, Le Havre, and Marseille are identified as cities with low solar irradiation. The capacity analysis of the microgrid components and the detailed energy dispatch for these cities are presented in Table 2.2-5. Additionally, the power profiles of these cities for one week in July are depicted in Figure 2.2-7.

**Table 2.2-5 The microgrid components capacities and energy of the selected cities with Low solar irradiation.**

| Parameter/City | Brest | Marseille | Le Havre |
|---|---|---|---|
| **Microgrid components capacities** | | | |
| PV capacity (kWp) | 1,146 | 457 | 1,060 |
| BESS capacity (kWh) | 2,732 | 1,160 | 1,611 |
| PV converter capacity (kW) | 1,130 | 460 | 1,052 |
| BESS converter capacity (kW) | 425 | 181 | 351 |
| EG converter capacity (kW) | 147 | 140 | 147 |
| EV converter capacity (kW) | 66 | 66 | 66 |
| Building converter capacity (kW) | 164 | 164 | 164 |
| **Energy dispatch** | | | |
| PV output energy (MWh/year) | 920 | 614 | 915 |
| Curtailed energy (MWh/year) | 133 | 0.07 | 138 |
| BESS energy (MWh/year) | 280 | 189 | 247 |
| EG supplied energy (MWh/year) | 327 | 350 | 352 |
| EG injected energy (MWh/year) | 139 | 37 | 160 |
| System losses energy (MWh/year) | 158 | 110 | 150 |

The energy dispatch analysis in Brest, Marseille, and Le Havre shows that the curtailed energy is generally higher than that in Rabat, Tripoli, and Lisbon. This leads to the conclusion that a city with low solar irradiation will result in higher curtailed energy rates due to the greater PV capacity needed to cover the load. A higher PV capacity will result in higher curtailed energy and greater system energy losses, as Table 2.2-5.

Figure 2.2-7 represents one week (the first week of July) of the one-year simulation for Brest, Marseille, and Le Havre.

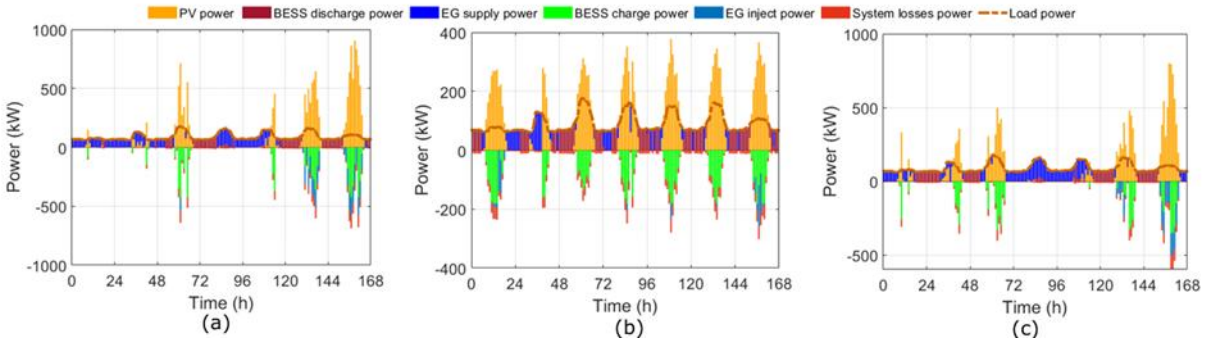


**Figure 2.2-7 One-week (1st of July's week) of the one-year simulation for (a) Brest (b) Marseille (c) Le Havre.**

### *2.2.4.3 LCOE and LCE results*

The heat maps Figure 2.2-8 presented represent the Solar Irradiation, LCOE, and LCE values, respectively, for various cities. These visual aids highlight significant variability in both energy costs and carbon emissions across different locations.

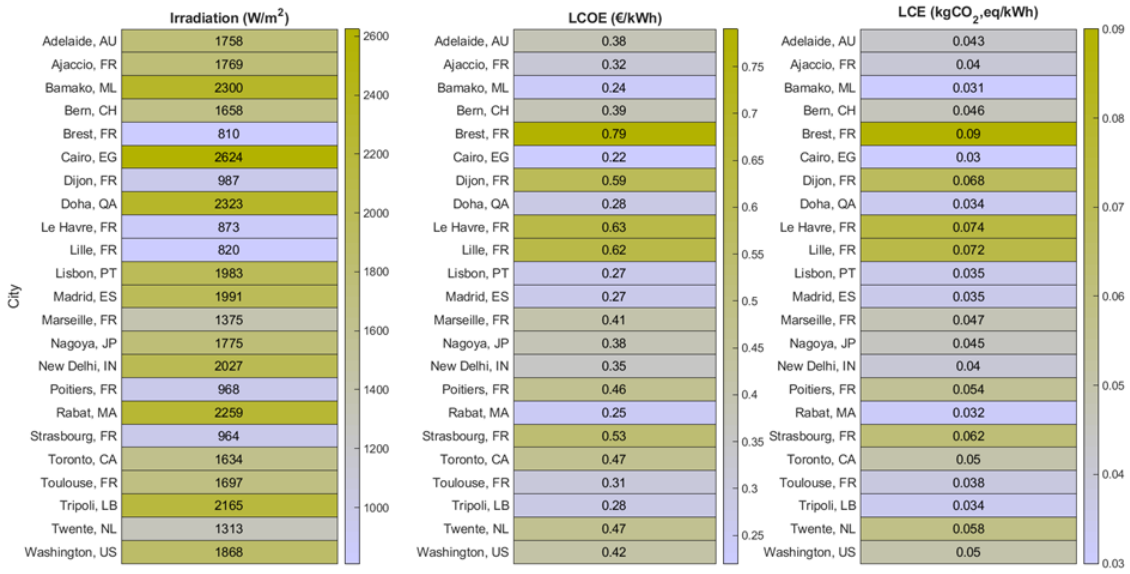


**Figure 2.2-8 Heat map for the Solar irradiation, LCOE, LCE values of different studied cities.**

These visual aids demonstrate considerable variability in both energy costs and carbon emissions across different locations. The heat map presented in Figure 2.2-8 shows stable LCOE values, indicating more predictable and affordable energy costs under these conditions. Cities like Cairo, EG (0.22 €/kWh), Doha, QA (0.28 €/kWh), and Lisbon, PT (0.27 €/kWh) maintain relatively low LCOE values, suggesting more efficient energy production. They also exhibit low LCE values (0.03 $kgCO_{2,eq}$/kWh, 0.034 $kgCO_{2,eq}$/kWh, and 0.035 $kgCO_{2,eq}$/kWh, respectively), indicating more sustainable and environmentally friendly energy production practices.

The colour gradients facilitate quick visual assessments, identifying areas where strategic interventions might be necessary to mitigate costs and reduce carbon emissions. This information is crucial for informed decision-making in energy investments and policy-making, aimed at carbon reduction initiatives. These results are consistent with the data presented in Table 2.2-3, which indicates that Cairo has the highest average solar irradiation. However, the ranking based on average solar irradiation does not consistently match the order of cities based on LCOE and LCE. This discrepancy is primarily due to variations in solar irradiation across different months and seasons rather than solely depending on the annual average solar irradiation.

For example, although Dijon has a higher average solar irradiation than Poitiers, Poitiers achieves a lower LCOE and LCE. Figure 2.2-9 illustrates this phenomenon by presenting the monthly solar irradiation data for both Dijon and Poitiers.

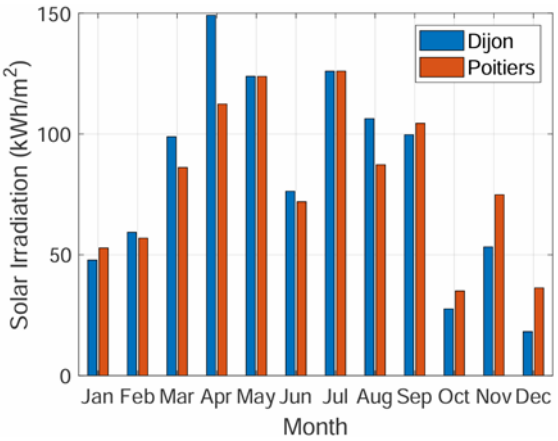


**Figure 2.2-9 The monthly solar irradiation data for both Dijon and Poitiers.**

Notably, during the summer and spring seasons, Dijon experiences higher levels of solar irradiation compared to Poitiers. However, during the autumn and winter seasons, Dijon's solar irradiation is lower than that of Poitiers. As a result, to meet the load demand during the autumn and winter months in Dijon, the optimization algorithm increases the PV capacity. In contrast, while Poitiers' solar irradiation in summer and spring is not as high as that of Dijon, it remains sufficient to cover the load requirements. Moreover, the significantly higher solar irradiation in Poitiers during the autumn and winter seasons allows for a lower PV capacity compared to Dijon. Thus, LCOE and LCE can vary significantly between different cities, even when the load remains the same. This highlights the importance of seasonal and monthly variations in solar irradiation in determining the optimal energy strategy.

### 2.2.5 Conclusions

In this study, a MILP algorithm is developed to optimize the size and energy management of microgrids across various cities and technologies. The case study is based on the energy load of a university building, including the consumption by EVs. The optimization problem considers the economic horizon over the project's lifetime, with the objective of minimizing both the LCOE and LCE. The results indicate that cities with high solar irradiation exhibit lower LCOE and LCE compared to cities with low solar irradiation. It is also observed that the ranking of cities based on average solar irradiation does not necessarily correlate with the ranking of LCOE and LCE. Monthly and daily fluctuations in solar irradiation significantly impact these results. The study highlights the importance of a well-sized combination of renewable resources to optimize the economic and environmental performance of energy systems in different cities. There is no universal solution; therefore, a thorough assessment of local conditions and available resources is essential for making decisions tailored to each specific city. Regarding the technologies, locally produced PV panels positively contribute to the overall LCE of the microgrid. Additionally, the LCE associated with BESS plays a dominant role in determining the total LCE of the configurations.

## REFERENCES

[1] A. K. Fadi and F. Bruno, "Holistic Approach for Prioritizing Emergency EV Charging in an Existing Distribution Network," IET Conference Proceedings, vol. 2022, no. 3, pp. 6–10, Jun. 2022, doi: https://doi.org/10.1049/icp.2022.0649.

[2] J.-L. Duchaud, G. Notton, C. Darras, and C. Voyant, "Multi-Objective Particle Swarm Optimal Sizing of a Renewable Hybrid Power Plant with Storage," Renewable Energy, vol. 131, pp. 1156–1167, Feb. 2019, doi: https://doi.org/10.1016/j.renene.2018.08.058.

[3] D. Khan Ngwashi, A. Kafatiya Arnold, S. Godwill Ndeh, and E. Tanyi, "Optimal design and sizing of a multi-microgrids system: Case study of Goma in The Democratic Republic of the Congo," Scientific African, vol. 22, p. e01913, Nov. 2023, doi: https://doi.org/10.1016/j.sciaf.2023.e01913.

[4] Ardjouna. Chebabhi, Ilyes. Tegani, A. Djoubair. Benhamadouche, and Okba. Kraa, "Optimal Design and Sizing of Renewable Energies in Microgrids Based on Financial Considerations a Case Study of Biskra, Algeria," Energy Conversion and Management, vol. 291, p. 117270, Sep. 2023, doi: https://doi.org/10.1016/j.enconman.2023.117270.

[5] B. K. Das, M. Hasan, and F. Rashid, "Optimal Sizing of a grid-independent PV/diesel/pump-hydro Hybrid system: a Case Study in Bangladesh," Sustainable Energy Technologies and Assessments, vol. 44, p. 100997, Apr. 2021, doi: https://doi.org/10.1016/j.seta.2021.100997.

[6] A. Khan et al., "Enhanced Evolutionary Sizing Algorithms for Optimal Sizing of a Stand-Alone PV-WT-Battery Hybrid System," Applied Sciences, vol. 9, no. 23, p. 5197, Nov. 2019, doi: https://doi.org/10.3390/app9235197.

[7] Y. Wang et al., "Optimal Design of Integrated Energy System considering economics, Autonomy and Carbon Emissions," Journal of Cleaner Production, vol. 225, pp. 563–578, Jul. 2019, doi: https://doi.org/10.1016/j.jclepro.2019.03.025.

[8] C. O. Okoye and O. Solyalı, "Optimal Sizing of stand-alone Photovoltaic Systems in Residential Buildings," Energy, vol. 126, pp. 573–584, May 2017, doi: https://doi.org/10.1016/j.energy.2017.03.032.

[9] N. Dougier, P. Garambois, J. Gomand, and L. Roucoules, "Multi-objective non-weighted Optimization to Explore New Efficient Design of Electrical Microgrids," Applied Energy, vol. 304, p. 117758, Dec. 2021, doi: https://doi.org/10.1016/j.apenergy.2021.117758.

[10] D. Huo, M. Santos, I. Sarantakos, M. Resch, N. Wade, and D. Greenwood, "A reliability-aware chance-constrained Battery Sizing Method for Island Microgrid," Energy, vol. 251, p. 123978, Jul. 2022, doi: https://doi.org/10.1016/j.energy.2022.123978.

[11] F. A. Kassab, B. Celik, F. Locment, M. Sechilariu, and T. M. Hansen, "Combined Optimal Sizing and Energy Management of a DC Microgrid Using MILP," presented at the IEEE Belgrade PowerTech, 2023. doi: https://doi.org/10.1016/j.renene.2024.120186.

[12] F. A. Kassab, B. Celik, F. Locment, M. Sechilariu, S. Liaquat, and T. M. Hansen, "Optimal Sizing and Energy Management of a microgrid: a Joint MILP Approach for Minimization of Energy Cost and Carbon Emission," Renewable Energy, vol. 224, pp. 120186–120186, Feb. 2024, doi: https://doi.org/10.1016/j.renene.2024.120186.

[13] H. U. Shabieh, M. Yousif, S. Nawaz Khan, A. Abbas, and K. Imran, "A decision-centric Approach for techno-economic Optimization and Environmental Assessment of Standalone and grid-integrated renewable-powered Electric Vehicle Charging Stations under Multiple Planning Horizons," Energy Conversion and Management, vol. 294, pp. 117571–117571, Oct. 2023, doi: https://doi.org/10.1016/j.enconman.2023.117571.

[14] "PVGIS 5.3 Calculateur de panneau solaire," 2020. https://pvgis.com/fr

# 3 PVCS: INTELLIGENT CONTROL AND NEW SERVICES

As the adoption of EVs accelerates worldwide, their integration into the energy ecosystem introduces both challenges and opportunities. Among the most pressing concerns is how to satisfy the increased power demand of EVs in a way that aligns with sustainability goals. Meeting this demand through clean energy sources is essential to minimizing carbon emissions and ensuring the long-term viability of the smart grid.

In parallel, the evolution of the EV market has brought forth new services and models, such as Vehicle-to-Grid (V2G) and Battery Swapping, that require dedicated analysis. These emerging approaches not only redefine the relationship between EVs and the grid but also open new avenues for energy management, flexibility, and user convenience.

The following two sections explore these key developments.

The first section delves into the concept of V2G, examining how EVs can support the grid by returning stored energy during peak periods.

The second section focuses on battery swapping, an alternative model that offers rapid energy replenishment and addresses some limitations of traditional charging infrastructure.

Together, these sections aim to shed light on how these innovations contribute to the evolving role of EVs within a smarter, more sustainable energy landscape.

## 3.1 Energy Cost Optimization via V2G Services

This study introduces an energy management algorithm of a PVCS formulated with mixed-integer linear programming to minimize the total energy cost of the participation of EV users in V2G service. Simulation results demonstrate that the proposed optimization method satisfies EV user demands while providing V2G service and highlights the benefits of the V2G service where the determined costs of the proposed algorithm perform significantly better compared to the baseline scenario (simulation without optimization)[9,10].

### 3.1.1 Introduction

Photovoltaic (PV) - powered charging stations (PVCS) are designed for charging electric vehicles (EV) using clean energy sources that can be installed on car parking shades and/or building rooftops. Charging EVs with renewable energy sources, particularly PV sources, is a crucial factor in enhancing their environmental benefits and reducing their greenhouse gas emissions [1]. To achieve defined objectives such as minimizing charging costs and providing a satisfactory charging process for EV users [2], it is necessary to implement an energy management system that can control and monitor the energy flows within the PVCS. A feasibility study of a PVCS has been conducted by analysing its effectiveness based on technical, economic, and environmental aspects by comparing the impact of different geographical areas on the installation location in [3]. The study investigates how a PVCS can contribute to charging EVs with different energy mixes and compares the produced $CO_2$ emissions of charging EV batteries solely from the grid, from the PVCS, and with internal combustion engine vehicles. They have found that the PVCS concept is more efficient in countries with high annual average irradiance and significant $CO_2$ emissions in their grid, but it remains economically unfeasible due to expensive storage systems. In [4], a supervision control system is presented for smart charging of an EV fleet in a PVCS-based research building. The proposed control strategy is based on a real-time operation to satisfy EV users using PV forecasting and EV charging historical records over four years to predict the EV power profiles. A user-friendly smart charging method, which includes interactions with EV users via an interface, has been developed in [5], where the EV user is a key player in the process of choosing the best scenario among uncoordinated charging, smart charging, and bidirectional smart charging control in a PVCS. The proposed methodology is based on real-time rule-based control and a predictive linear optimization control. The results showed that bidirectional charging control had the best cost reduction, while uncoordinated charging control costs the most. In [6], mixed-integer programming was investigated to minimize the cost of energy traded to a PVCS, where the intermittency of PV power can be compensated by EVs which can also discharge energy to the PVCS, where it does not integrate stationary storage. The EVs are classed in three categories according to their charging behaviour, and the results showed that an increase of green EVs, the only category of EVs for which the users can allow discharging of energy into the charging station, could reduce the total cost of the PVCS. In [7],

[9] This chapter is based on the following publication:

S. Cheikh-Mohamad, B. Celik, M. Sechilariu, and F. Locment, 'PV-Powered Charging Station with Energy Cost Optimization via V2G Services', Applied Sciences, vol. 13, no. 9, 2023, http://doi.org/10.3390/app13095627.

[10] This work has been achieved within the framework of the EE4.0 project (Energie Electrique 4.0). EE4.0 is co-financed by the French State and the French Region of Hauts-de-France. This research was also funded by ADEME France, project T-IPV grant number # 2308D0002.

mixed-integer linear programming (MILP) has been applied to optimize the sizing of a PVCS components (PV, stationary storage, and transformer) in order to minimize the investment cost and the total cost considering the uncertainties of PV and EV charging power profiles. The simulation results, with a 1 hour step time, showed that EV charging stations powered by PV are more cost-effective than EV charging stations powered by the grid.

However, large-scale EV charging will pose difficulties from a power point of view for grid operators [8]. Therefore, charging of EVs should be controlled intelligently in order to reduce the negative impact on the connected public grid [9]. Additionally, EVs remain in an idle state for a long time. As a result, they can serve as energy storage systems and assist the grid by providing energy when they are plugged in. In this way, EVs can be charged during off-peak periods and discharged during peak periods to support the public grid and/or a microgrid. This approach enables EVs to be utilized as a flexible load, with their charging and discharging being controlled. Therefore, vehicle-to-grid (V2G) services have emerged as a promising technology in the field of smart grids [10], where they can improve frequency [11] and voltage regulations while providing benefits to the EV users [12], and this depends on the number of available EVs [13,14]. Additionally, such services can enhance power quality and promote the integration of renewable energy with developed smart control algorithms [15,16,17]. In [18], the benefits are highlighted for V2G service participants, as these services can decrease the total ownership cost of EVs. For the grid operator, V2G is seen as a power source that is able to mitigate fluctuations caused by renewable energy sources and provide ancillary services. As for EV owners, participating in V2G services should have financial incentives without limiting their travel needs.

Moreover, V2G optimization plays a crucial role in maximizing the benefits. In [19], the authors found that total cost of EV ownership could be reduced by implementing V2G service in the Flanders region of Belgium. This service helped to smooth out electricity demand by filling in valleys and reducing power peaks, ultimately leading to improved grid stability. A charging and discharging strategy for EVs proving the effectiveness of their V2G operation in different cities in China with different trip patterns was developed in [20]. Their aim was to minimize the cost of operation of the distribution grid considering grid congestion and voltage constraints. These factors were particularly important, given the variation in the distribution of EVs across areas of operations. The potential locations for EV charging and their participation in V2G service have been predicted in [21] using automated machine learning, based on historical data collected over 42 weeks. The authors of [22] have demonstrated that the participation of EVs in V2G services, when they are idle at charging stations, can reduce the demand for charging EVs. In [23], an improved harmony particle swarm optimization problem was investigated in a bi-level model (low level: EV cluster scheduling, upper level: planning) to determine the optimal allocation of distributed generation and charging stations within a V2G service. The results indicated that the optimized model could satisfy the charging demand of EV users, improve the voltage quality, mitigate load fluctuations, encourage the use of renewable energy, and improve the global performance of the planning scheme. An optimization framework has been developed in [24] to reduce greenhouse gases and intensive electricity imports in the Switzerland power system with controlled charging/discharging of EVs. To jointly install EV charging stations and distributed energy resources in a distribution system in China, an optimization model has been presented in [25], where V2G service is considered with minimized annual costs (considering also social aspects). An optimization problem has been modelled in [26] as a nonlinear stochastic programming problem with uncertainty of PV energy. The EVs can operate in V2G mode, where this allows EVs to charge during off-peak hours and discharge during peak hours to reduce energy costs. The proposed problem can optimize the operation of EVs and minimize the cycles of their batteries to reduce battery degradation

speed. A novel control system has been presented in [27] to underpin V2G service by deploying a fleet of EVs, which allows a V2G aggregator to provide voltage and frequency services while reducing the charging cost with the minimization of battery-level degradation. A case study of an EV charging station based on a university campus in Jordan has been presented in [28], which investigates the feasibility of a V2G service to minimize the global consumption of energy drawn from the public grid. A computational model of an EV with battery degradation has been studied in [29] to supply power to the grid while gaining profit for the EV owner by alleviating the load on the main grid. The results show that the potential benefits from V2G are greater than the cost of battery degradation.

On the other hand, research studies have investigated the optimization of V2G service in a PVCS. In [30], a dynamic searching peak-and-valley algorithm was proposed to determine the optimal charging and discharging start time of EVs based on their initial state-of-charge ($SOC$), arrival time, charging mode, departure time, and the tariffs in peak hours. The aim of this optimization was to reduce the burden on the public grid and lower its energy cost. A control scheme using a grid-connected inverter was developed in [31] to improve the voltage and frequency stability of a PVCS with V2G operation. This inverter can identify unusual faults of the microgrid and functions in islanding mode. The authors in [32], have modelled a PVCS to provide ancillary services where EV users can receive rewards for their V2G participation. The results proved that EVs participating in V2G service could provide high availability of service. Furthermore, in [33], an energy management strategy has been examined for the real-time control of multi-source EV charging to lower the operating cost, taking into consideration battery degradation of stationary storage and EVs for their V2G participation. In [34], a PVCS was designed with V2G service to lower the stress on the public grid and to enhance its stability during peak hours. The authors also discussed possible financial incentives that can motivate EV users to participate in the demand response. Additionally, an energy management and control system has been introduced in [35] for an EV charging station with V2G integration. This charging station featured a PV system, wind turbine, and fuel cell with grid connection. A MILP model has been proposed in [36] for a parking lot of EVs powered with a microgrid, based on PV sources, wind turbines, hydrogen energy, and a stationary storage system to minimize the total sustainability cost, as well as economic and environmental costs. The EVs can operate in V2G mode to participate in demand response, thus encouraging EV users to charge in off-peak periods instead of on-peak periods. In [37], a day-ahead operation planning method that incorporates EVs with V2G service in a microgrid was investigated to minimize the daily operation costs. A multi-objective optimization model has been proposed in [38] for a microgrid integrating EVs with V2G service. Their objectives were maximizing the use of renewable energy, maximizing the benefits for EV users, and minimizing grid load fluctuation. A heuristic optimization problem has been studied in [39] to optimize the sizing of a hybrid PV sources, battery, and diesel generator for an EV parking lot with V2G service, where EVs are considered as a flexible load. A two-stage smart charging algorithm (first stage: optimization problem, second stage: real-time control) has been proposed in [40] for buildings integrating EVs, PV sources, a storage system, and a heat pump. The optimization problem is formulated as a non-linear programming model to optimize the operation of EVs. The results show the benefits of V2G service as primary frequency regulation reserve while participants achieve energy cost reductions; however, the degradation of Lithium – Ion (Li-Ion) batteries is non-negligible. The authors in [41] have proposed an effective strategy using adjustable robust optimization to enhance the operation stability and economic cost of a microgrid by enabling V2G service during peak periods and charging for valley filling at off-peak periods to minimize the cost of operation under various constraints.

The references cited earlier have highlighted the role of V2G in serving as a spinning reserve source and power regulation to lower the impact of the peak load on the grid and its associated services. Yet, their optimization problems are mostly based on day-ahead prediction of EV profiles modelled with a probability distribution function, whereas the proposed optimization algorithm in this study is actualized at every arrival of a new EV, considering the impact of the uncertainties in real-time simulation. This study is an extension of [42], where V2G is realized with a rule-based control scheme, whereas in this extended version, the focus is on the energy cost optimization problem with V2G implementation in the PVCS. In this study, a PVCS with five chargers that can support three charging modes, slow, average, and fast charging, is presented. The PVCS combines PV sources, a stationary storage system, a public grid connection, and EVs as a flexible load that can operate in V2G mode. The human–machine interface (HMI) allows the EV users to interact with the PVCS and choose their preferences, such as charging mode, desired state of charge $SOC$ at departure, and willingness to participate in V2G service. Additionally, EV users arrive arbitrarily at the PVCS, and their arrivals are unpredictable. In [43], the authors presented a control mechanism aimed at minimizing the discomfort of EV users for a charging station equipped with PV sources and connected to a public grid, but without a stationary storage system. However, their study differs from ours in several ways. Firstly, only one charging mode—namely, the slow mode—is allowed, whereas three different charging modes are offered in the present work. Secondly, their focus is on maximizing social welfare and minimizing the discomfort of EV users, while the objective in this study is to minimize the total energy cost of the PVCS, with optimization being updated for each EV arrival. Furthermore, the energy injected into the grid from EVs and the energy distribution for each EV charging from each power source are being analyzed to provide a more comprehensive understanding of the system's energy dynamics. To sum up, the main contributions of this study are:

- Proposing an energy cost optimization problem in a PVCS with V2G service, taking into consideration the uncertainty of the arrival time of EVs in a real-time simulation;
- Actualizing the optimization problem formulated via MILP at every arrival of a new EV; the arrival of EVs is not modelled based on day-ahead prediction; instead it is randomly generated as unpredicted events in MATLAB;
- Assessing the energy consumption of every EV from each power source and the energy participation among the power sources (PV, energy storage, and grid).

The study is organized as follows: Section 3.1.2 introduces the PVCS with V2G energy cost optimization. 3.1.3 develops the energy cost optimization problem. Section 3.1.4 describes the different simulation cases with V2G service. Section 3.1.5 analyses the energy cost results. Section 3.1.6 concludes the study.

### 3.1.2 PV-Powered Charging Station with V2G Service

The PVCS infrastructure consists of PV modules, a stationary storage system, and a connection with the public grid [42], as illustrated in Figure 3.1-1.

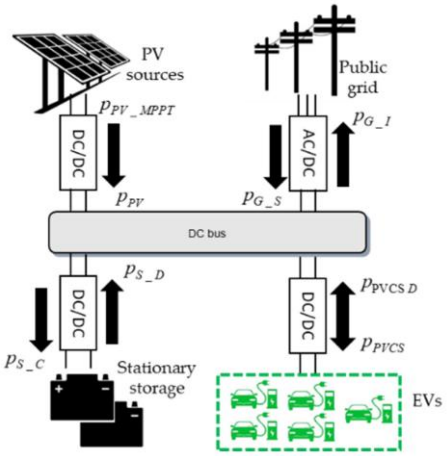


**Figure 3.1-1 Scheme of PV-powered charging station with V2G service.**

In Figure 3.1-1, $p_{PV-MPPT}$ is the PV power operating in maximum-power point-tracking (MPPT) mode, $p_{PV}$ is the PV power after shedding (if it is necessary), $p_{G-I}$ is the power injection into the public grid, $p_{G-S}$ is the power supply from the public grid, $p_{S-C}$ is the charging power of the stationary storage$p_{S-D}$ is the discharging power of the stationary storage, $p_{PVCS-D}$ is the total demand power of EVs, and $p_{PVCS}$ is the total charging power of EVs after shedding (if it is necessary). The PVCS is designed such that the public grid can provide power to charge EVs and also absorb power in case of excess energy from PV sources or discharging EVs. Each component of the PVCS is connected to the DC bus using dedicated converters. The EVs' batteries are considered as controllable loads because they can be charged or discharged at variable or constant power. To ensure a consistent power supply and reduce the difference between power production and load, the public grid connection is formed through a bidirectional AC/DC converter. The stationary storage is charged solely by PV sources and can be discharged to provide power for EVs' load.

### *3.1.2.1 PV-Powered Charging Station with V2G Service without Energy Cost Optimization*

The PVCS can operate without energy cost optimization based on the storage priority algorithm shown in Figure 3.1-2. In this case, the EVs are charged using PV sources first, followed by the stationary storage system, and finally by the public grid. The surplus PV production is used to charge the stationary storage system. However, if the storage system has reached its capacity or charging power limit and there is still unused excess PV power, the remaining power is injected into the public grid. Participating in a V2G service allows EV users to discharge their EVs for up to 15 min or until the battery is fully discharged during peak periods. Following the V2G operation, the EVs will then be charged to achieve the desired $SOC$ at departure. The charging can be performed using any available power, regardless of the initial charging mode, as long as the charging terminal can support variable power up to 50 kW.

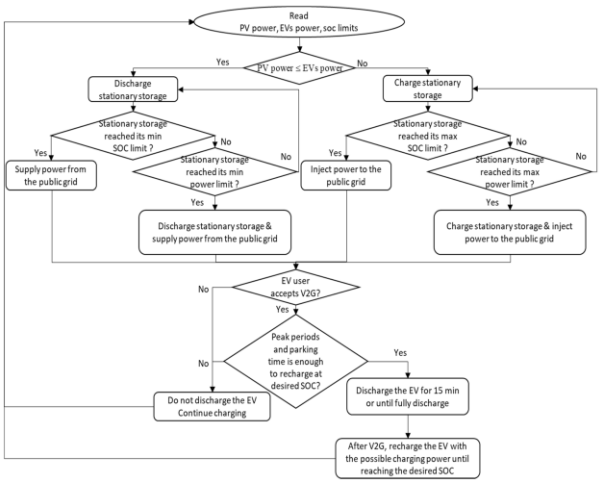


**Figure 3.1-2 PV-powered charging station energy management via $V2G$ service without optimization.**

### *3.1.2.2 PV-Powered Charging Station with V2G Service with Energy Cost Optimization*

On the other hand, the PVCS can operate with energy cost optimization. In this case, Figure 3.1-3 describes the supervisory control system for the PVCS [44]. The supervisory control system of the PVCS is composed of four layers: prediction, energy cost optimization, operation, and HMI. The control block has been designed and implemented to interact with EV users and maintain power balance at the DC bus through the energy cost optimization and operation layers.

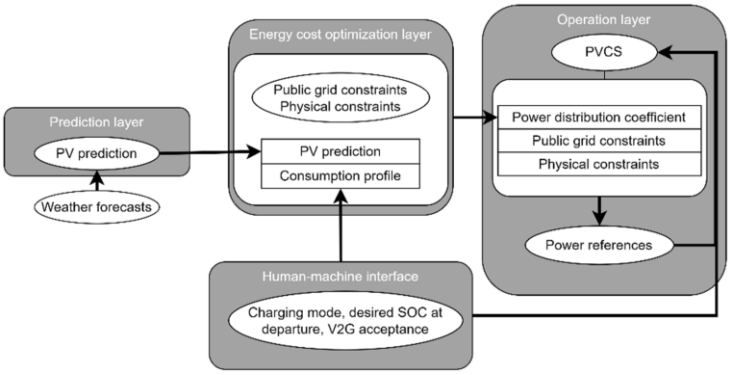


**Figure 3.1-3 Supervisory control system for the PVCS [44].**

The prediction layer utilizes weather forecasts. From the interaction with the HMI, the user of an EV $v$ selects their desired $SOC$ at departure charging mode, participates in the V2G service, and obtains the $SOC$ of their EV at arrival in real-time. The energy cost optimization relies on the production prediction, which depends on the hourly solar irradiation predictions and consumption profile communicated from the HMI. Moreover, the power limits of the connected public grid, energy pricing, and energy system limits are communicated. The MILP formulation is used to reduce the total energy cost of the PVCS. This supervisory control system has the advantage of interacting with EV users for optimization; yet, if the choices of the EV users are not practical, they must be adjusted in order to enable optimization [45]. For instance, if an EV user arrives at the charging station and requests fast charging, but the available power cannot support it, the HMI will communicate with the user to suggest charging in average or slow mode, waiting for available power, or leaving the charging station altogether. Similarly, if the

EV user mistakenly inputs an invalid $SOC$ at departure (e.g., 180%), the HMI will alert the user to enter a valid $SOC$ interval below 100%. Whenever a new EV arrives, the optimization process is updated with the new inputs from the HMI and physical constraints. Therefore, the process is repeated each time a new EV arrives.

Dealing with the unpredicted arrival of EVs is the main challenge. The power references for the public grid, stationary storage, and EVs are sent to the operation layer based on the optimization results. The operation layer is responsible for maintaining the power balance while respecting the system's constraints and physical limitations [46]; furthermore, it sets the PV power limitation and applies EV shedding if needed.

#### 3.1.2.2.1 Prediction Layer

In the prediction layer, hourly solar irradiation predictions are provided by Météo France to calculate the PV power prediction. The PV power prediction is based on solar irradiation ($g$) and the ambient temperature ($T_{amb}$) from forecasted data [47]. Therefore, the PV power prediction $p_{PV-MPPT-pred}$ is calculated in MPPT mode for each time instant $t_i$ [48] as in Equations (3.1-1) and (3.1-2), and it is introduced into the energy cost optimization layer:

$$p_{PV-MPPT-pred} = P_{PV-STC} \times \frac{g(t_i)}{1{,}000} \times [1 + \gamma \times (T_{PV}(t_i) - 25)] \times N_{PV} \quad (3.1\text{-}1)$$

$$with t_i = t_0, t_0 + \Delta t, t_0 + 2\Delta t, \cdots, t_F$$

$$T_{PV}(t_i) = T_{amb}(t_i) + g(t_i) \times (NOCT - T_{air-test})/G_{test} \quad (3.1\text{-}2)$$

where $P_{PV-STC}$ is the PV power in standard test conditions (STC), $\gamma$ is the power coefficient of temperature (-0.29%/°C), $N_{PV}$ is the number of PV panels, $T_{PV}$ is the PV cell temperature, and $t_0$, $\Delta t$, and $t_F$ are the initial time instant, time interval between two samples, and time instant at the end of operation, respectively. $NOCT$ is the nominal operating cell temperature (41°C), $G_{test}$ is the fixed solar irradiation (800 W/m$^2$), and $T_{air-test}$ is the fixed air temperature (20°C).

#### 3.1.2.2.2 Human–Machine Interface

This layer interacts with the EV users, allowing them to choose their preferred charging mode $M_v$ among slow, average, and fast. It should be noted that all EVs have the same energy capacity and can handle fast charging. The HMI obtains the $SOC$ of the EVs at their arrivals $SOC_{EV-arr_v}$ and assists the users in selecting their desired $SOC$ at departure $SOC_{EV-des}$ , as well as their participation in V2G service $V2G_{EV}$ in real-time. Therefore, the estimated charging time $t_{est-ch_v}$, which indicates the time required to reach the desired $SOC$, is determined in Equation (3.1-3):

$$t_{est-ch_v} = \left(SOC_{EV-dep_v} - SOC_{EV-arr_v}\right) \times \frac{E}{P_{EV-max_v}} \quad (3.1\text{-}3)$$

where $E$ is the EV battery capacity, and $P_{EV-max_v}$ is the maximum power of EV charging based on the charging mode selected by the user. The HMI for the PVCS is explained thoroughly in [49], and once the user preferences are set in the HMI, these data are communicated simultaneously to the operation layer and to the energy cost optimization layer to actualize the optimization with these data.

#### 3.1.2.2.3 Energy Cost Optimization

This layer interacts with the prediction layer and the HMI to carry out the optimization to minimize the total energy cost. This layer, the power references for the stationary storage, the public grid, and the EVs, which are the decision variables, are sent to the operational layer.

The optimization has several benefits, such as minimizing the energy cost, determining the optimal contribution of the stationary storage or the public grid, and avoiding EV and PV shedding. The energy pricing is considered for on-peak and off-periods with fixed tariffs, and the limits for public grid power injection and supply are defined with the public grid operators. Moreover, the physical limitations of the stationary storage should be respected to avoid its damage. The energy cost optimization problem is detailed in Section 3.1.3.

#### 3.1.2.2.4 Operation Layer

From the energy optimization layer, the optimal power flow for the sources and the EVs considering $p_{PV-MPPT-pred}$ and $p_{PVCS}$ is found. The optimized powers for the stationary storage and the public grid are obtained through the optimization layer. However, these optimized powers are not sent directly into the operation layer. Instead, the power distribution coefficient $k_D$ is identified and introduced into the operation layer to account for uncertainties in the forecasted data. The power distribution coefficient $k_D$ determines the power share between the public grid and the stationary storage. Thus, if PV power is insufficient for EV charging, either the public grid or the stationary storage or both can continue supplying power to charge the EVs based on the value of $k_D$ (see Section 3.1.5). The upside of $k_D$ is coupling easily the energy management with the operation layer while respecting all constraints [47].

The operation layer must ensure robustness and be able to withstand uncertainties in the forecast data. After that, this layer defines the power references and applies PV or EV shedding when needed. To maintain the DC bus at the reference voltage $V_{ref}$, the actual operating conditions are used to determine the power reference $P_{ref}$ using (3.1-4) and (3.1-5) :

$$p_{ref}(t_i) = p_{PV}(t_i) - p_{PVCS-D}(t_i) - C_P \times \left(V_{ref} - v_{DC-bus}\right) \quad (3.1\text{-}4)$$

$$p_{ref}(t_i) = p_{G-ref}(t_i) + p_{S-ref}(t_i) \quad (3.1\text{-}5)$$

where $C_P$ is the proportional controller gain, and $v_{DC-bus}$ is the actual voltage of the DC bus. The power reference for the public grid $p_{G-ref}$ and the stationary storage $p_{S-ref}$ can be obtained by (3.1-6), and the power distribution coefficient $k_D$ is given by (3.1-7):

$$p_{S-ref}(t_i) = k_D(t_i) \times p_{ref}(t_i) \quad (3.1\text{-}6)$$

$$k_D(t_i) = \frac{p_{S-C}(t_i)+p_{S-D}(t_i)}{p_{S-C}(t_i)+p_{S-D}(t_i)+p_{G-I}(t_i)+p_{G-S}(t_i)} \quad with\ k_D \in [0,1] \quad (3.1\text{-}7)$$

### 3.1.3 Energy Cost Optimization with $V2G$ Service

The principal objective of the formulated optimization problem is to minimize the total energy cost while satisfying various constraints [47]. The constraints and objective function are explained in detail in the following subsections.

#### *3.1.3.1 PV Sources*

PV system can operate in two modes: MPPT or limited-power mode. The latter mode is used in case of excessive surplus PV production which exceeds the total EV load, the allowed stationary storage charging power, and the public grid injection power. In the MPPT mode, there is no need to shed any PV power, and thus PV shedding $p_{PV-S}$ is zero. However, in the power-limitation mode, $p_{PV-S}$ becomes positive, indicating the amount of PV power that needs to be shed to ensure that the total power injected into the grid does not exceed the limits. Accordingly, $p_{PV}$ is calculated [47] as given by (3.1-8) with the constraint of $p_{PV-S}$ in (3.1-9) and (3.1-10):

$$p_{PV}(t_i) = p_{PV-MPPT}(t_i) - p_{PV-S}(t_i) \quad (3.1\text{-}8)$$

$$p_{PV}(t_i) > 0 \quad (3.1\text{-}9)$$

$$0 < p_{PV-S}(t_i) < p_{PV-MPPT}(t_i) \quad (3.1\text{-}10)$$

### 3.1.3.2 Stationary Storage

In order to extend the lifetime of the Li-Ion batteries as a stationary storage method and protect them from overcharging or over-discharging, the maximum and minimum $SOC$ of the storage, $SOC_{S-max}$, $SOC_{S-min}$as well as the maximum storage power $P_{S-max}$ must be respected as given by (3.1-11) and (3.1-12) [47]-[50]. The $SOC$ of the storage $soc_S$ can be simplified as in [51], neglecting the effects of self-discharge and temperature, and is given by (3.1-13) below:

$$-P_{S-max} \leq p_S(t_i) \leq P_{S-max}, where\ p_S(t_i) = p_{S-C}(t_i) - p_{S-D}(t_i) \quad (3.1\text{-}11)$$

$$SOC_{S-min} \leq soc_S(t_i) \leq SOC_{S-max} \quad (3.1\text{-}12)$$

$$soc_S(t_i) = SOC(t_0) + \frac{1}{3\,600 \times E_{Bat}} \int_{t_0}^{t} p_S(t_i)\, dt \quad (3.1\text{-}13)$$

where $E_{Bat}$ and $p_S$ are the energy capacity (kWh) and power of the stationary storage, respectively.

### 3.1.3.3 Grid Connection

The maximum limits for the grid supply and injection $P_{G-S-max}$ and $P_{G-I-max}$, set by the public grid, should be respected [47], as given by (3.1-14), where $p_G$ is the public grid power:

$$-P_{G-S-max} \leq p_G(t_i) \leq P_{G-I-max}, where\ p_G(t_i) = p_{G-I}(t_i) - p_{G-S}(t_i) \quad (3.1\text{-}14)$$

### 3.1.3.4 Electric Vehicles

When the stationary storage and public grid have reached their limits, it may not be possible to fully supply EV batteries, which represent the entire load of the PVCS. In such cases, the charging of EVs can be shed [47]. Moreover, it should be noted that $p_{PVCS}$ can be negative when an EV is in the process of discharging into the grid during V2G service. In situations where there is enough PV power available, there is no need to shed any PV production. Similarly, when there is sufficient charging capacity available, there is no need to shed any EV charging power. Moreover, the stationary storage could be charged, and/or the public grid could absorb power when PV production is higher than load demand. On the other hand, when the load demand exceeds the PV production, the stationary storage can be discharged, and/or the public grid can supply power. Therefore, the constraints given by (3.1-15) and (3.1-16) must be respected.

$$if\ p_{PV-MPPT}(t_i) \geq p_{PVCS-D}(t_i)\ then \begin{cases} p_G(t_i) \geq 0 \\ p_S(t_i) \geq 0 \end{cases} \quad (3.1\text{-}15)$$

$$if\ p_{PV-MPPT}(t_i) \leq p_{PVCS-D}(t_i)\ then \begin{cases} p_{PV-S}(t_i) = 0 \\ p_G(t_i) \leq 0 \\ p_S(t_i) \leq 0 \end{cases} \quad (3.1\text{-}16)$$

The PVCS interface allows EV users to make choices regarding their charging mode and other preferences. The constraints given in (3.1-17) – (3.1-34) reflect the interaction between EV users and the supervisory control system.

#### 3.1.3.4.1 V2G Mode

The following constraints given below in (3.1-17) – (3.1-23) are included in the optimization problem for the EV users who accept providing V2G services.

$$disch_{min} \times \frac{60}{\Delta t} \leq \sum V2G_{bin_v}(t_i) \leq disch_{max} \times \frac{60}{\Delta t} \qquad \forall t_i \in [t_{arr_v}, t_{dep_v}] \qquad (3.1\text{-}17)$$

$$V2G_{SW_v}(t_i) \geq V2G_{bin_v}(t_i) - V2G_{bin_v}(t_{i-1}) \qquad \forall t_i \in [t_{arr_v}, t_{dep_v}] \qquad (3.1\text{-}18)$$

$$G2V_{SW_v}(t_i) \geq G2V_{bin_v}(t_i) - G2V_{bin_v}(t_{i-1}) \qquad \forall t_i \in [t_{arr_v}, t_{dep_v}] \qquad (3.1\text{-}19)$$

$$G2V_{bin_v}(t_i) + V2G_{bin_v}(t_i) \leq 1 \qquad \forall t_i \in [t_{arr_v}, t_{dep_v}] \qquad (3.1\text{-}20)$$

$$-P_{EV-fast-max} \times V2G_{bin_v}(t_i) \leq p_{EV_v}(t_i) \qquad \forall t_i \in [t_{arr_v}, t_{dep_v}] \qquad (3.1\text{-}21)$$

$$p_{EV_v}(t_i) \leq P_{EV-fast-max} \times G2V_{bin_v}(t_i) \qquad \forall t_i \in [t_{arr_v}, t_{dep_v}] \qquad (3.1\text{-}22)$$

$$p_{EV_v}(t_i) - p_{EV_v}(t_{i-1}) \leq Limit \times \frac{\Delta t}{60} \times G2V_{bin_v}(t_i) \qquad \forall t_i \in [t_{arr_v}, t_{dep_v}] \qquad (3.1\text{-}23)$$

where $disch_{min}$(5min) and $disch_{max}$ (15min) are the minimum and maximum duration for the EV's discharge, while $t_{arr_v}$ and $t_{dep_v}$ are the time of arrival and departure of vehicle $v$, respectively. $G2V_{bin_v}$ and $V2G_{bin_v}$are binary decision variables for charging/discharging times; $G2V_{SW_v}$ and $V2G_{SW_v}$ are binary decision variables for the switching times between charging/stop and discharging/stop; $p_{EV_v}$ is the EV charging power of vehicle $v$; $P_{EV-fast-max}$ is the fast charging power at maximum; and $Limit$ is the ramp-up charging power (15 kW/min). Constraint (3.1-17) determines the discharging period of the EV, while Constraints (3.1-18) and (3.1-19) determine that the discharging and charging times of the EV, respectively, should be successive. Constraint (3.1-20) specifies that the EV can either charge, discharge, or be idle at any given time. Constraints (3.1-21) and (3.1-22) refer to the discharging and charging power of the EV, respectively. Lastly, Constraint (3.1-23) helps to reduce the charging fluctuations of the EV.

#### 3.1.3.4.2 EV Charging Mode

If the EV user does not want to participate in the V2G service, Constraints (3.1-24) – (3.1-27) are used for charging the EV battery, where the charging power is determined by the charging mode selected by the EV user as follows:

$$if\ M_v = 1\ then\ 0 \leq p_{EV_v}(t_i) \leq P_{EV-fast-max} \qquad \forall t_i \in [t_{arr_v}, t_{dep_v}]\ With\ v = 1,2,\cdots,N_v \qquad (3.1\text{-}24)$$

$$if\ M_v = 2\ then\ 0 \leq p_{EV_v}(t_i) \leq P_{EV-aver-max} \qquad \forall t_i \in [t_{arr_v}, t_{dep_v}] \qquad (3.1\text{-}25)$$

$$if\ M_v = 3\ then\ 0 \leq p_{EV_v}(t_i) \leq P_{EV-slow-max} \qquad \forall t_i \in [t_{arr_v}, t_{dep_v}] \qquad (3.1\text{-}26)$$

$$p_{EV_v}(t_i) = 0 \qquad \forall t_i \notin [t_{arr_v}, t_{dep_v}] \qquad (3.1\text{-}27)$$

where $N_v$ is the total number of EVs, $P_{EV-aver-max}$ is the average charging power at maximum, and $P_{EV-slow-max}$ is the slow charging power at maximum. The total EV charging power in (3.1-28) and the $SOC$ calculation with its constraints in (3.1-29) – (3.1-34) are given:

$$p_{PVCS}(t_i) = \sum_v^{N_v} p_{EV_v}(t_i) \qquad \forall t_i \in [t_{arr_v}, t_{dep_v}] \qquad (3.1\text{-}28)$$

$$SOC_{EV-min} \leq soc_{EV_v}(t_i) \leq SOC_{EV-max} \qquad \forall t_i \in [t_{arr_v}, t_{dep_v}] \qquad (3.1\text{-}29)$$

$$soc_{EV_v}(t_i) = 0 \qquad \forall t_i \notin [t_{arr_v}, t_{dep_v}] \qquad (3.1\text{-}30)$$

$$soc_{EV_v}(t_i) = SOC_{EV_{arr_v}} \qquad \forall t_i = t_{arr_v} \qquad (3.1\text{-}31)$$

$$SOC_{EV_{arr_v}}(t_i) \geq SOC_{EV-min} \qquad \forall t_i = t_{arr_v} \qquad (3.1\text{-}32)$$

$$soc_{EV_v}(t_i) = SOC_{EV_{arr_v}}(t_i) + \frac{1}{3\,600 \times E} \int_{t_{arr_v}}^{t_{dep_v}} p_{EV_v}(t_i)\, dt \qquad (3.1\text{-}33)$$

$$soc_{EV_v}(t_i) = SOC_{EV_{des_v}} \qquad \forall t_i = t_{dep_v} \qquad (3.1\text{-}34)$$

where $soc_{EV_v}$ is the $SOC$ of vehicle $v$, and $SOC_{EV-min}$ and $SOC_{EV-max}$ are the minimum and maximum battery $SOC$ of vehicle $v$, respectively. The dynamic $SOC$ evolution $soc_{EV_v}$ is given by (3.1-33). Similar to the stationary storage, Constraint (3.1-29) determines the $SOC$ limit. Additionally, Constraint (3.1-30) refers to the absence of an EV, while Constraint (3.1-31) assigns the $SOC$ of an EV at its arrival time, requiring it to be greater than the limit specified in Constraint (3.1-32). Finally, Constraint (3.1-34) refers to the $SOC$ of an EV at its departure time, which should be lower than or equal to the desired $SOC$ of the EV at departure.

### *3.1.3.5 Power Balancing*

All the production and consumption should be equal on the DC bus; therefore, an equation for power balancing should be included in the formulation. The power balancing equation [47], where all power signs are assigned positives, is be given by (3.1-35):

$$p_{PV}(ti) + p_{S-D}(t_i) + p_{G-S}(t_i) = p_{PVCS}(t_i) + p_{S-C}(t_i) + p_{G-I}(t_i) \qquad (3.1\text{-}35)$$

### *3.1.3.6 Objective Function*

The total energy cost $C_{total}$ takes into consideration the cost of the power supplied from the public grid, the profit from the power injected into the public grid, the cost of the stationary storage, the penalty cost in case the EV has not reached the desired $SOC$ at departure, and the cost associated with shedding power from the PV sources. To prevent excessive switching during charging or discharging, a switching penalty $C_{SW}$ is introduced to ensure that the action is completed in the fewest cycles possible. Therefore, the objective function minimizes $C_{total}$, as given by Equations (3.1-36) – (3.1-41):

$$min\ C_{total} = C_G + C_S + C_{PVS} + C_{EV-penalty} + C_{SW} \qquad (3.1\text{-}36)$$

$$C_G = \sum_{t_i=t_0}^{t_F} \left[c_G(t_i) \times \Delta t \times \left(-p_{G-I}(t_i) + p_{G-S}(t_i)\right)\right] \qquad (3.1\text{-}37)$$

$$c_G = \begin{cases} c_{G_{NH}} for\ t \in normal\ hours \\ c_{G_{NH}} for\ t \in peak\ hours \end{cases}$$

$$C_S = \sum_{t_i=t_0}^{t_F} \left[c_S(t_i) \times \Delta t \times \left(p_{S-C}(t_i) + p_{S-D}(t_i)\right)\right] \qquad (3.1\text{-}38)$$

$$C_{PVS} = \sum_{t_i=t_0}^{t_F} [c_{PVS}(t_i) \times \Delta t \times p_{PVS}(t_i)] \qquad (3.1\text{-}39)$$

$$C_{EV-penalty} = \sum_{v}^{N_v} \left[c_{EV_p} \times \left(SOC_{EV-des_v} - SOC_{EV-dep_v}\right) \times E\right] \qquad (3.1\text{-}40)$$

$$C_{SW} = \sum_{t_i=t_0}^{t_F} \sum_{v}^{N_v} \left[c_{SW}(t_i) \times \left(V2G_{SW_v}(t_i) + G2V_{SW_v}(t_i)\right)\right] \qquad (3.1\text{-}41)$$

where $C_G$, $C_S$, $C_{PVS}$, $C_{EV-penalty}$, and $C_{SW}$ are the public grid, stationary storage, PV shedding, EV penalty, and switching penalty costs, respectively; and $c_G$, $c_S$, $Cc_{PVS}$, $c_{EV_p}$, and $c_{SW}$ are the public grid, stationary storage, PV shedding, EV penalty, and switching penalty tariffs, respectively. The energy cost optimization problem is formulated to minimize the objective

function in (3.1-36) with respect to Constraints (3.1-8) – (3.1-35) , determining the decision variables: $p_G, p_S, p_{PV-S}, p_{EV_v}, V2G_{bin_v}, G2V_{bin_v}, V2G_{SW_v}$ and $G2V_{SW_v}$.

### 3.1.4 Simulation Results for PVCS with V2G Service

Several simulation cases are presented to demonstrate the effectiveness of the energy cost optimization method. Finally, the cases with optimization, denoted as "Sim w/ opti", are compared with the cases without optimization, denoted as "Sim w/o opti". The "Sim w/o opti" is operated under a simple control scheme based on a storage priority, where $k_D$ is set to one in this operation mode [52]. The optimization problem is solved by CPLEX [53], where CPLEX is a high-performance mathematical programming solver for linear programming, mixed-integer programming, quadratic programming, and convex optimization, developed by IBM. The optimization is performed with 1min intervals, while the simulation is performed with 1s intervals. The data for the irradiance and ambient temperature were recorded at 10s intervals using proper instruments of measurement, and through interpolation, the data are reduced to 1s intervals.

In this section, two case studies are presented for a PVCS that includes five chargers, with EVs equipped with 50 kWh Li-Ion batteries. The PVCS has 84 PV panels with 28.9 kWp, and the stationary storage has a capacity of 130 Ah, with 288 V providing 37.44 kWh. However, there is no defined power injection limit for the public grid. Table 3.1-1 lists the parameters that are used in the following simulation cases for the PVCS with V2G service.

**Table 3.1-1 Parameter values used in the simulations for the V2G service.**

| Parameter | Value | Parameter | Value | Parameter | Value |
|---|---|---|---|---|---|
| $P_{G-I-max}$ | - | $SOC_{S-min}$ | 20 % | $c_{G-NH}$ | 0.1 €/kWh |
| $P_{G-S-max}$ | 50 kW | $SOC_{S-max}$ | 80 % | $c_{G-PH}$ | 0.7 €/kWh |
| $P_{S-max}$ | 7 kW | $SOC_{EV-min}$ | 20 % | $c_S$ | 0.01 €/kWh |
| $P_{EV-fast-max}$ | 50 kW | $SOC_{EV-max}$ | 100 % | $c_{PVS}$ | 1.2 €/kWh |
| $P_{EV-aver-max}$ | 22 kW | $SOC_{S_0}$ | 50 % | $c_{EV_p}$ | 2.5 €/kWh |
| $P_{EV-slow-max}$ | 7 kW | $v_S$ | 288 V % | $c_{SW}$ | 0.05 € |
| $E$ | 50 kWh | $C_{Bat}$ | 130 Ah % | $p_{PV_{MPPT}}$ | 28.9 kWp |

Table 3.1-2 presents the EV users' data and preferences. $SOC_{EV-arr_v}$ , $t_{arr_v}$, $M_v$, and V2G participation are generated randomly. $SOC_{EV-arr_v}$ and $SOC_{EV-des_v}$ are generated in the intervals [20%,50%] and [70%,100%], respectively. It is assumed that EV battery capacity is capable of handling fast charging.

**Table 3.1-2 Data and preferences of EV users [43].**

| EVs | $SOC_{EV-arr}$ | $SOC_{EV-des}$ | $t_{arr}$ | $t_{est-ch}$ | Mode | V2G |
|---|---|---|---|---|---|---|
| EV1 | 31 % | 85 % | 09:20 | 03 h 52 min | Slow | Yes |
| EV2 | 35 % | 75 % | 10:00 | 00 h 24 min | Fast | No |
| EV3 | 50 % | 80 % | 12:05 | 02 h 08 min | Slow | Yes |
| EV4 | 25 % | 78 % | 13:45 | 01 h 13 min | Average | No |
| EV5 | 29 % | 72 % | 14:25 | 03 h 05 min | Slow | No |

Additionally, two scenarios in each study case are taken into consideration:

- Scenario a: during peak periods, EVs discharge at a constant power and then recharge with the same constant charging power as set by the user until departure time;
- Scenario b: during peak periods, EVs discharge at a maximum power of 50 kW and then recharge again with a variable charging power, irrespective of the charging mode selected by the user, to achieve the desired $SOC$ at departure after V2G service.

### *3.1.4.1 Case 1: Sunny Day*

For case 1, a day with high irradiance was considered, specifically, 29 June 2019 in Compiegne. The real and predicted PV power are shown in Figure 3.1-4, where it can be observed that the predicted PV power is slightly higher than the real PV power and follows the same trend. As a result, this uncertainty has an impact on the optimization results, which will potentially lead to supplying energy from the public grid instead of discharging energy from the stationary storage. In this case, two scenarios are conducted, which involve constant and variable charging/discharging powers.

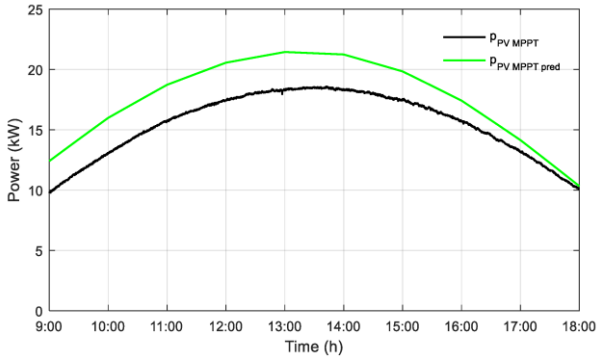


**Figure 3.1-4 Real PV power $p_{PV-MPPT}$ and predicted PV power $p_{PV-MPPT-pred}$ – 29 June 2019.**

#### 3.1.4.1.1 Scenario a: Constant Power

Figure 3.1-5 and Figure 3.1-6 show the power and $SOC$ of the EVs with V2G service at constant power with the “Sim w/o opti” and “Sim w/ opti” algorithms, respectively.

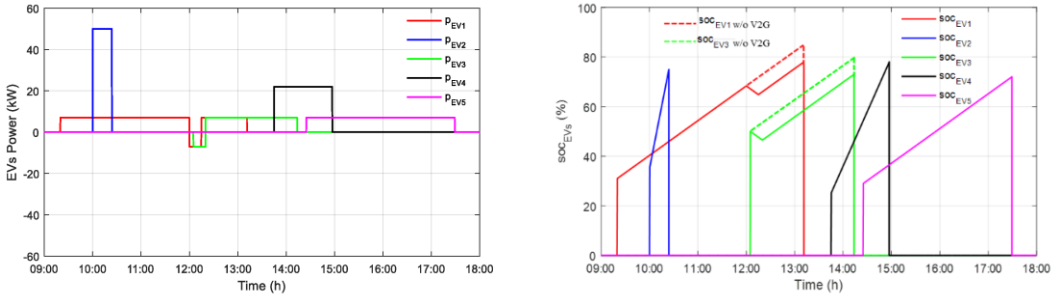


(a) (b)

**Figure 3.1-5 Power (a) and $SOC$ of the EVs (b) – scenario a in “Sim w/o opti”.**

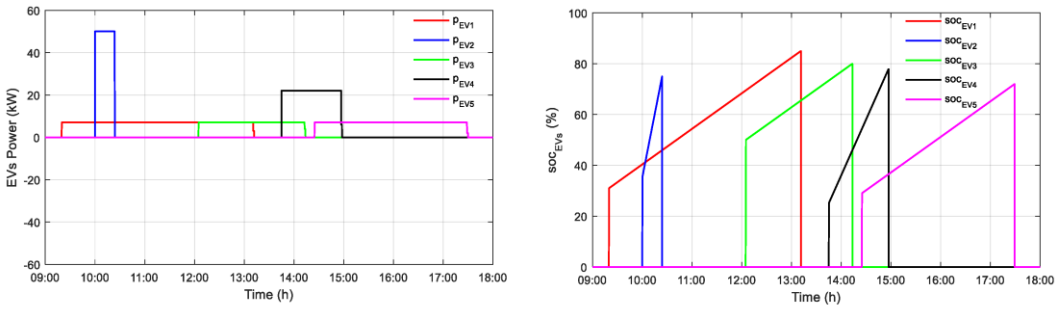


(a) (b)

**Figure 3.1-6 Power (a) and $SOC$ of the EVs (b) – scenario a in "Sim w/ opti".**

Figure 3.1-5 (a) shows that EV1 as well EV3 are discharged at peak hours with 7 kW each for 15 min; they are then charged after providing V2G service directly until their departure time with the same constant power. As a result, EV1 and EV3 failed to achieve their desired $SOC$ values at departure. Specifically, EV1 only reached 71% instead of the desired 85%, and EV3 reached 68.33% instead of 80%, as shown in Figure 3.1-5 (b). The dashed points represent the $SOC$s of the EVs that should be reached with respect to user preferences. On the other hand, Figure 3.1-6 (a) shows that all the EVs are charging according to user preferences, and the desired $SOC$ at departure is reached even when EV users opt to participate in V2G service, as shown in Figure 3.1-6 (b). However, discharging the EVs is not possible because it would prevent the desired $SOC$ from being achieved, and hence meeting the requirements of EV users is given priority over discharging energy via V2G into the grid.

#### 3.1.4.1.2 Scenario b: Variable Power

The power flow of the PVCS with V2G service at variable power with the "Sim w/o opti" and "Sim w/ opti" algorithms is presented in Figure 3.1-7, where the predicted PV power is used only to run the optimization, and the real PV power is used in both simulation scenarios.

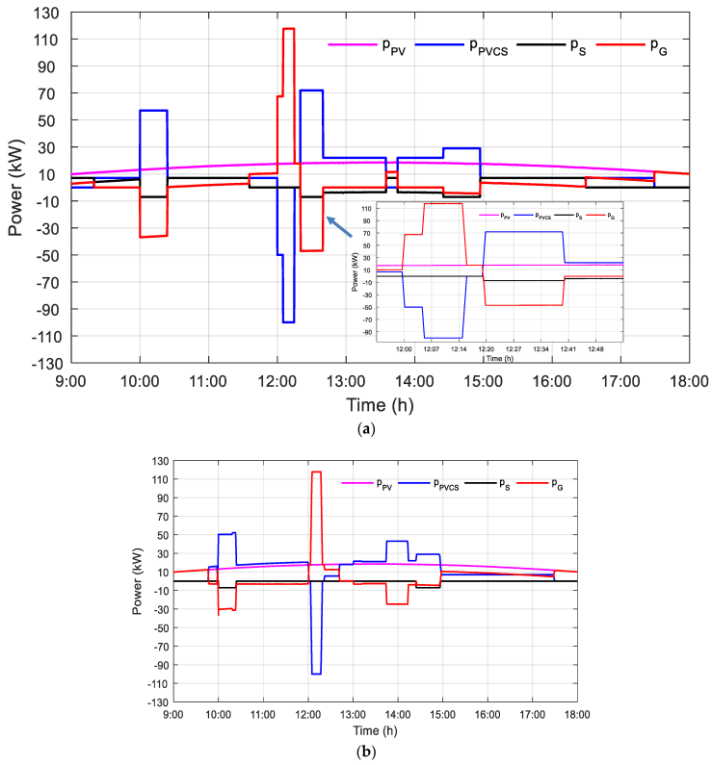


**Figure 3.1-7 Power flow with V2G service – scenario b (a) in "Sim w/o opti" and (b) in "Sim w/ opti".**

Figure 3.1-7 shows that EV1 as well EV3 are discharged at peak periods for 15 min at 50 kW each, and then they are recharged with the appropriate charging power after V2G service to meet the needs of the users while considering the duration of the remaining parking time. The PVCS operates in storage-priority mode, meaning that any excess PV power is initially used to charge the stationary storage. Once the stationary storage is either full or its maximum charging power is reached, which occurs around 11:00 A.M till 11:30 A.M and from 03:00 P.M until 06:00 P.M, any additional PV power is then injected into the public grid. Furthermore, the public grid provides power when EV2 charges in fast mode and during peak periods when EV1 and EV3 recharge after V2G. Thus, charging EVs during peak periods will increase the energy cost. Sharp variations in power levels might lead to stability issues. To prevent this, Constraint (3.1-23) limits steep power variations, which can be seen in Figure 3.1-7 (a)'s zoom-in during the peak hour of 12:00 P.M to 01:00 P.M. On the other hand, in Figure 3.1-7 (b), EV1 and EV3 are discharged simultaneously during peak periods (serving a total of 100 kW power to the grid), and then each EV recharges after V2G with the optimized power to meet user preferences. EV1 and EV3 are primarily charged by PV power. However, due to uncertainty in the PV power prediction, the public grid may supply power to the EVs between 10:25 A.M and 12:00 P.M, although it is not very significant. The injection of power into the public grid is determined by the optimization result to maximize profits in the event of excess PV power, which occurs before 10:00 A.M during V2G service and from 03:00 P.M until 06:00 P.M. The power and $SOC$ of the EVs in "Sim w/o opti" and "Sim w/ opti" are shown in Figure 3.1-8 and Figure 3.1-9, respectively.

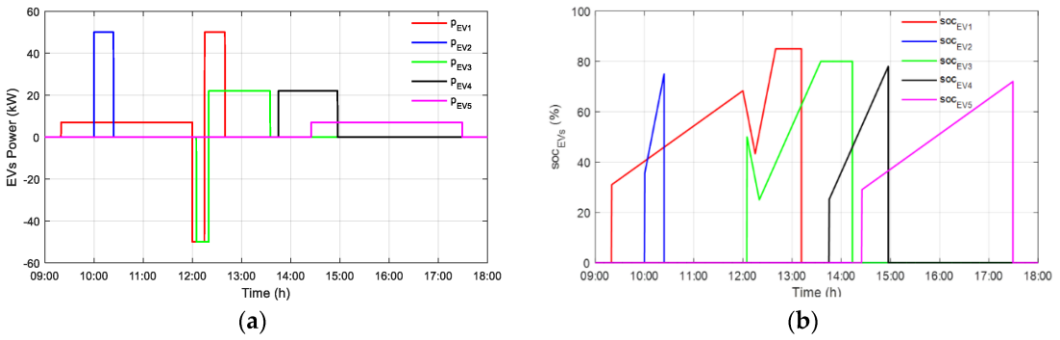


**Figure 3.1-8 Power (a) and $SOC$ of the EVs (b) – scenario b in "Sim w/o opti".**

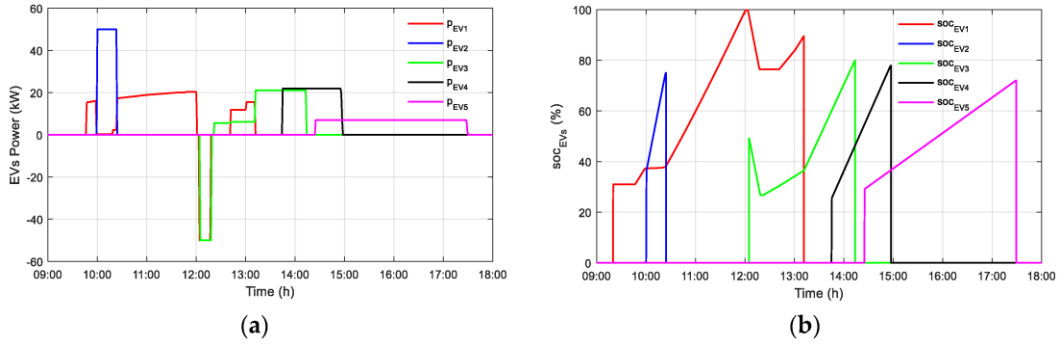


**Figure 3.1-9 Power (a) and $SOC$ of the EVs (b) – scenario b in "Sim w/ opti".**

Figure 3.1-8 (a) shows that EV1 begins discharging 50 kW and then recharges with 50 kW to reach the desired $SOC$ at the time of departure. The EVs have enough remaining charging time after V2G to recharge with 22 kW. In Figure 3.1-9 (b), the optimized charging/discharging profiles of EV1 and EV3 allow them to participate in V2G service, reach the desired $SOC$ at departure, and satisfy the users with minimization of the cost. When EV2 arrives, the optimization is actualized again, and as a result, EV1's charging power is dropped to reduce the total power demand because EV2 charges in fast mode. After EV2 leaves, EV1 starts recharging again, which helps to discharge power during peak periods. After providing V2G service, EV1 resumes charging its battery to achieve the desired $SOC$ at the time of departure. In the same way, the optimization is actualized every time a new EV comes to the PVCS, and thus the optimization procedure is realized five times during the day in this case. The power provided to recharge EV1 and EV3 is synchronized with PV power, even during peak periods. Consequently, all EVs have achieved their desired $SOC$ values at the time of departure, as shown in Figure 3.1-8 (b) and Figure 3.1-9 (b).

Scenario a, where the charging/discharging power is constant, is proved to be impractical because EVs will never achieve their desired $SOC$ at the time of departure. On the other hand, scenario b proves its feasibility by allowing EVs to recharge with variable power after participating in V2G service, irrespective of their initially selected charging mode, in order to satisfy the EV user. Therefore, only the variable charging/discharging scenario is considered in the following case studies, and the "Sim w/ opti" is compared to the "Sim w/o opti".

### *3.1.4.2 Case 2: Cloudy Day*

For case 2, a cloudy day with high irradiation was considered, specifically, 10 May 2019 in Compiegne. The real and predicted PV powers are shown in Figure 3.1-10, where it can be observed that the predicted PV power is slightly higher than the real PV power, and the

fluctuations are hard to predict due to hourly provision of forecasts and their inconsistent trends. As a result, these uncertainties have an impact on the optimization results that potentially lead to supplying power from the public grid instead of discharging energy from the stationary storage. In this case, the power flow of the PVCS with V2G service in "Sim w/o opti" and "Sim w/ opti" is shown in Figure 3.1-11, where the predicted PV power is used only to run the optimization, and the real PV power is used in both simulation scenarios.

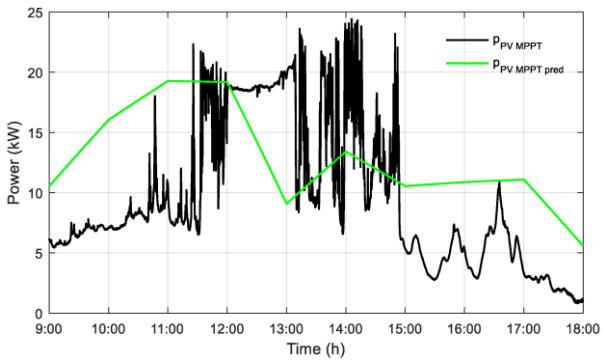


**Figure 3.1-10 Real PV power $p_{PV-MPPT}$ and predicted PV power $p_{PV-MPPT-pred}$ – 10 May 2019.**

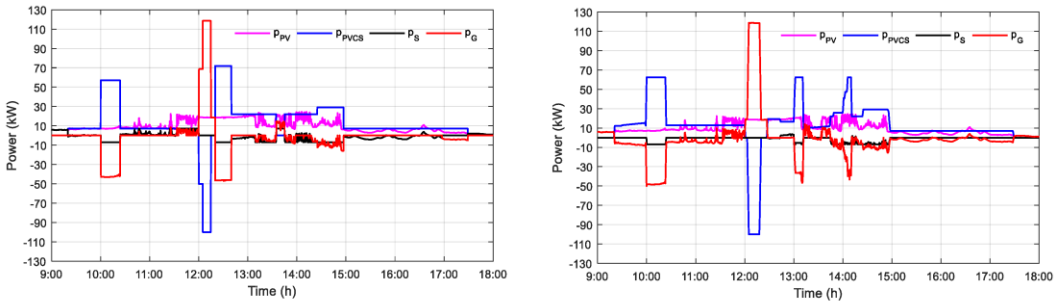


**Figure 3.1-11 Power flow with V2G service – case 2 (a) in "Sim w/o opti" and (b) in "Sim w/ opti".**

Figure 3.1-11 (a) shows that EV1 and EV3 are discharged at peak periods for 15 min with 50 kW each, and they are then recharged after V2G with the appropriate charging power to meet the needs of the users. As the PV power is not very significant and is fluctuating, the stationary storage is discharged to support the charging of EVs. The PVCS operates in storage-priority mode, meaning any excess PV power is initially used to charge the stationary storage. Once the stationary storage is either full or its maximum charging power is reached, which occurs at around 11:30 A.M, any additional PV power is injected into the public grid. However, once the storage is empty, which occurs around 05:00 P.M, the public grid supplies power to continue charging the EVs. Furthermore, the public grid supplies power when EV2 charges in fast mode and during peak periods, when EV1 and EV3 recharge after V2G. Therefore, charging EVs during peak periods will increase the energy cost. On the other hand, in Figure 3.1-11 (b), EV1 and EV3 are discharged simultaneously during peak periods (serving total 100 kW power to the grid), and they are then recharged after V2G with optimized power to meet the needs of the users. The power injected into the public grid is defined by the optimization result to maximize profits in the event of excess PV power, which occurs before 09:30 A.M, around 11:30 A.M during V2G service, and from 01:15 P.M until 01:45 P.M. Figure 3.1-12 and Figure

3.1-13 show the power and $SOC$ of the EVs for the "Sim w/o opti" and "Sim w/ opti" algorithms, respectively.

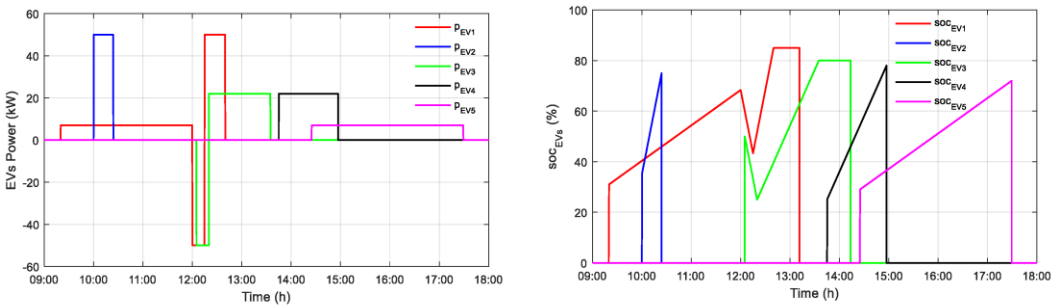


(a) (b)

**Figure 3.1-12 Power (a) and $SOC$ of the EVs (b) – case 2 in "Sim w/o opti".**

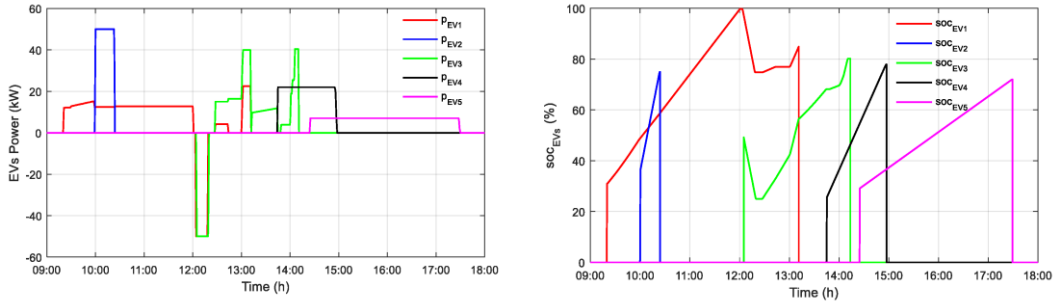


(a) (b)

**Figure 3.1-13 Power (a) and $SOC$ of the EVs (b) – case 2 in "Sim w/ opti".**

In Figure 3.1-12 (a), similarly to case 1 scenario b under "sim w/o opti", EV1 and EV3 are discharged at peak periods for 15 min at 50 kW each, and then they continue charging until their departure times to meet the needs of the EV users at 50 kW and 22 kW, respectively. However, in Figure 3.1-13 (a), the charging and discharging profiles of EV1 and EV3 are the optimized profiles that allow them to participate in V2G service, reach the desired $SOC$ at the time of departure, and satisfy the users with the lowest cost. PV power is not very significant; therefore, EV1 keeps charging even when EV2 comes to charge in fast mode. During peak periods, the charging power of EV1 and EV3 is provided by PV sources. Consequently, all EVs have achieved their desired $SOC$ at the time of departure, as shown in Figure 3.1-12 (b) and Figure 3.1-13 (b). Figure 3.1-14 compares the dynamic $SOC$ of the stationary storage for case 1, scenario b, and case 2.

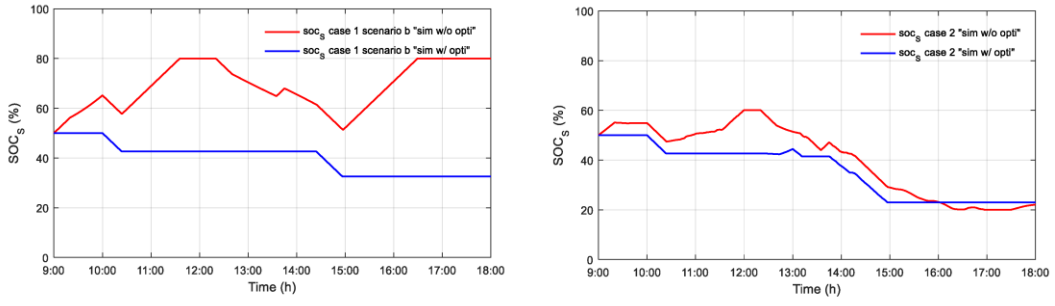


(a) (b)

**Figure 3.1-14 $SOC$ of the stationary storage in (a) case 1, scenario b and (b) – case 2.**

For Figure 3.1-14 (a), the dynamic $SOC$ of the stationary storage is shown for case 1, where the real PV power is high. In “sim w/o opti”, where the storage priority is applied, the storage is always used for either charging or discharging. The storage becomes full around 11:30 A.M and 04:30 P.M, when the charging demand of EVs is not significant. In contrast, in sim w/ opti”, the storage is used only at the moments decided by the optimization algorithm – for example, during peak hours (02:30 P.M – 03:00 P.M) and when the charging demand of EVs is high, such as the case where EV2 charges in fast mode simultaneously with EV1.

On the other hand, Figure 3.1-14 (b) shows the dynamic $SOC$ of the stationary storage for case 2 where the real PV is highly fluctuating. In “sim w/o opti”, the storage is always used for either charging or discharging, but it is never at full capacity and becomes empty around 04:00 P.M. In contrast, in “sim w/ opti”, the behaviour of the storage is similar to case 1 in “sim w/ opti” and becomes empty at 03:00 P.M.

### 3.1.5 Energy Cost Analyses for PV-Powered Charging Station with V2G Service

Table 3.1-3 demonstrates the energy injected into the grid for the two case studies. The energy is injected into the grid during V2G, where the EVs’ contribution is significantly greater in the variable charging/discharging power scenario than the constant charging/discharging power scenario. The contribution of EVs is higher than 65% in the variable charging/discharging power scenario. Even in “Sim w/ opti”, the energy share from EVs is similar to that in “Sim w/o opti” and considered significant.

**Table 3.1-3 Energy injected into the public grid for the different cases.**

| Operation Case | | Energy Injected into the Public Grid during V2G Period | | | | | |
|---|---|---|---|---|---|---|---|
| | | PV (kWh) | EVs (kWh) | Total Energy during V2G (kWh) | % EV/Total | % PV/Total | Energy Injected into the Grid during the Day (kWh) |
| Case 1 - constant power scenario | Sim w/o opti | 5.88 | 2.91 | 8.79 | 33.10% | 66.90% | 44.03 |
| | Sim w/ opti | 0 | 0 | 0 | 0 | 0 | 58.85 |
| Case 1 - variable power scenario | Sim w/o opti | 5.88 | 20.83 | 26.71 | 77.98 % | 22.02 % | 50.95 |
| | Sim w/ opti | 5.88 | 23.33 | 29.21 | 79.87% | 20.13 % | 68.34 |
| Case 2 - variable power scenario | Sim w/o opti | 6.21 | 20.83 | 27.04 | 77.04 % | 22.96 % | 30.52 |
| | Sim w/ opti | 7.45 | 25 | 32.45 | 77.04% | 22.96 % | 40.91 |

Furthermore, “Sim w/o opti” and “Sim w/ opti” are compared with an ideal case, which is considered as a reference: “Opti for real conditions”. In this reference case, it is assumed that the real PV MPPT power production and the arrival times of all EVs are known, and hence there will be no uncertainty issues related to forecasting errors. Therefore, the optimization is executed only one time because the arrival times of EVs are considered known in “Opti for real conditions”. The total energy costs of “Sim w/ opti” are closer to the ideal case than “Sim w/o opti” in the two cases, which indicates the effectiveness of the proposed optimization algorithm during different meteorological conditions.

Table 3.1-4 presents the energy costs for the case studies. Only in case 1 “Sim w/o opti”, with constant charging/discharging power, is the obtained dissatisfaction cost for EV users positive due to not having the desired $SOC$ at the departure time. In the variable charging/discharging power scenario, the total energy cost is negative, which refers to selling energy to the public grid. Moreover, in “Sim w/ opti” the total energy cost is better due to power injection into the public grid, bringing more profits. In case 1 “Sim w/ opti”, with constant charging/discharging power, the total cost is negative, as there is no penalization due to injecting power to the public grid. However, there is no V2G participation even though the users accept participating to meet the user requirement (minimum $SOC$ of EV) at departure time.

**Table 3.1-4 Energy costs for the different cases.**

| Operation Case | | Public Grid Cost (c€) | Stationary Storage Cost (c€) | EV Penalty (c€) | Total Cost (c€) |
|---|---|---|---|---|---|
| Case 1 - constant power scenario | Sim w/o opti | -1106 | 32 | 1750 (Dissatisfied client - Risk of losing client) | -1074 |
| | Sim w/ opti | -1247 | 9 | 0 | -1238 |
| Case 1 - variable power scenario | Sim w/o opti | -1006 | 40 | 0 | -966 |
| | Sim w/ opti | -2942 | 6 | 0 | -2936 |
| | Opti for real conditions | -4210 | 10 | 0 | -4200 |
| Case 2 - variable power scenario | Sim w/o opti | -571 | 28 | 0 | -543 |
| | Sim w/ opti | -1745 | 11 | 0 | -1734 |
| | Opti for real conditions | -2710 | 11 | 0 | -2699 |

Table 3.1-3 and Table 3.1-4 prove the unfeasibility of the constant charging/discharging scenario, as the energy injected into the public grid from EVs is not significant because they charge/discharge with constant power. The total final cost for this scenario is calculated without including the EV penalty cost, which is only included to optimization for modeling the dissatisfaction of the EV users. A high EV penalty indicates that EV users will be dissatisfied due to having low battery energy at departure time, which can cause risks of rejection of enabling V2G services by EV users or even losing clients in the future. The distribution of energy for EVs in “sim w/o opti” and “sim w/ opti” is also assessed in Figure 3.1-15 and Figure 3.1-16 for case 1b and 2 respectively.

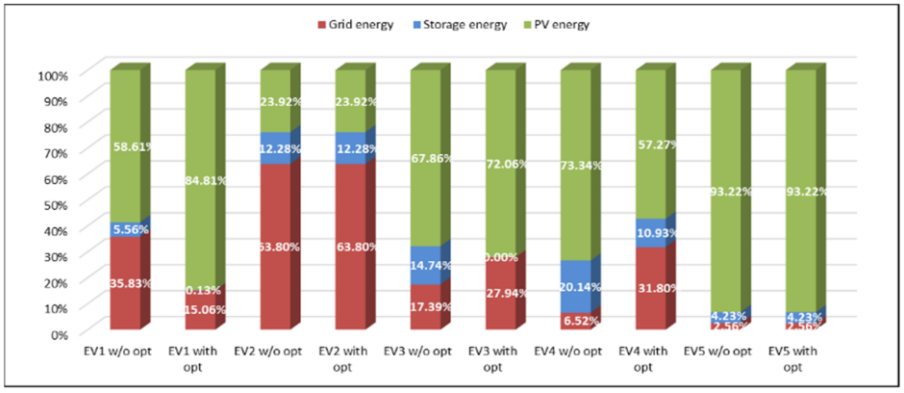


**Figure 3.1-15 Distribution of energy for EVs in “sim w/o opti” and “sim w/ opti” for case 1b.**

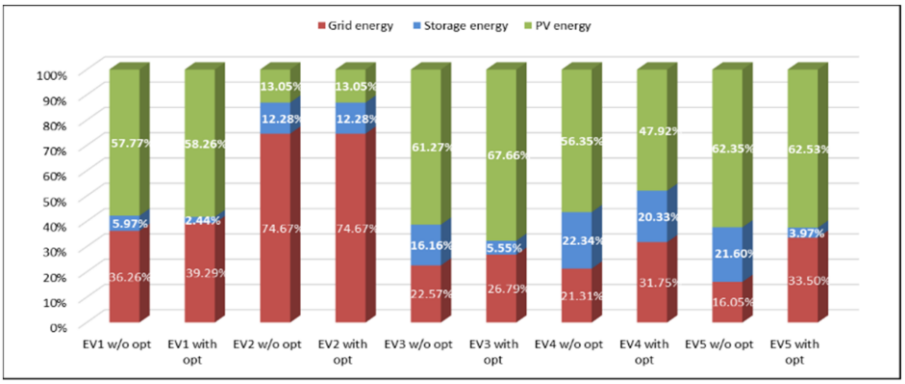


**Figure 3.1-16 Distribution of energy for EVs in “sim w/o opti” and “sim w/ opti” for case 2.**

In Figure 3.1-15 and Figure 3.1-16, PV sources mainly charge EV1 and EV3. Moreover, in the “sim w/ opti” scenario, the amount of PV energy used for charging EV1 is significantly higher than in the “sim w/o opti” scenario, as shown in case 1. Given that EV2 is charging in fast

mode, the primary source of its charging power is the public grid. On the other hand, because EV4 is charged in average mode, it depends on PV and stationary storage energy. Similarly, because EV5 is charged in slow mode, it is mainly charged by PV sources. However, in case 2, EVs require frequent charging from the public grid due to the fluctuation of PV power.

V2G service can improve the energy efficiency of EVs by allowing the EV batteries to be used as a source of energy for the grid during times of high grid demand (and/or high-tariff, low-renewable production) and then recharge from the grid during times of low grid demand (and/or low-tariff, high-renewable production). By providing energy back to the grid, EVs can help balance the electrical load, which can improve the overall efficiency and reliability of the distribution grid. As for the EV users, V2G can provide a way to earn revenue by selling energy stored in their EV batteries back to the grid during peak times. Additionally, the EV batteries can be charged with clean and low-cost renewable resources (e.g., photovoltaics) and can be discharged later to the grid at high-grid-consumption moments via V2G; thus, the electricity grid can use local renewable production more efficiently.

### 3.1.6 Conclusions

In conclusion, a PVCS with energy cost optimization and V2G service can provide a sustainable and cost-effective solution for EV charging/discharging, which can help grid operators by discharging EV batteries via with V2G services, leading to a more efficient system. The focus of the study is to minimize energy costs, prevent EV penalization and PV shedding, and consider prediction errors in real-time simulations. Additionally, the research analyses energy distribution for the system and each EV to gain a better understanding of the system's functionality. However, there are still some challenges to be addressed in order to optimize the energy cost of the charging station. One of the main challenges is the optimal scheduling of the charging and discharging of the EV batteries to minimize the energy cost and to maximize the charging of EVs with PV power. Furthermore, the cost of implementing and maintaining a PVCS and V2G system can be high, and there is a need to establish standardization and protocols for integration with the existing public grid and communication networks. In addition, the type of an EV can affect the energy cost in the case of V2G because each type of EV has a different battery size, charging and discharging power characteristics, and energy efficiency. Battery EVs have larger batteries with higher power ratings than plug-in EVs and hybrid EVs, which means they can provide more flexibility for charging/discharging operations, and eventually they provide more energy to support the electricity grid. Although V2G operation is possible for FCEVs, the consumption/production of hydrogen can be inefficient compared to battery-based vehicles due to the low efficiency of fuel cells and electrolyzers.

The simulation results show that variable charging and discharging power have major advantages over constant charging/discharging, as no penalization was imposed, and the EV users were satisfied. In addition, optimizing the charging/discharging power is cost-effective because EVs are charged during off-peak hours and discharged during on-peak hours into the public grid, resulting in greater profitability. Furthermore, the energy that EVs inject into the public grid during V2G service is significant, accounting for over 75% of the total energy injected into the public grid during V2G service. The optimization problem is applicable to both private (domestic, work) charging stations and public ones, regardless of their size. By participating in V2Gservices, EV owners and/or charging station operators can generate revenue and reduce the total energy cost of EV charging, while also providing grid services to improve the reliability and efficiency of the public grid. The HMI allows for the operation of both a single EV and multiple EVs, and the number of EVs that can be operated is only limited by the number of charging terminals. However, the size of the charging station can affect the

applicability of optimization problems for V2G services. For example, a small charging station (e.g., one EV in a residential building) can participate in V2G service to support the electricity grid and earn revenue in return for its services; however, it will have limited power support capacity, and hence it may not be able to provide significant aid individually. In contrast, a large charging station (e.g., 100 EVs in a university parking lot) will have more power capacity, which can enable more significant V2G services for the electricity grid based on its requirements.

For future research, the degradation impact on EV batteries will be studied, as well as the environmental impact. Moreover, more case studies will be conducted to validate the optimization method and demonstrate its feasibility in real-time experimental tests under the concept of power hardware in the loop. Furthermore, annual simulation will be considered where optimization and real-time simulation consider annual irradiation profiles, temperatures, and EV profiles.

## REFERENCES

[1] A. Galati, N. Adamashvili, and M. Crescimanno, “A Feasibility Analysis on Adopting Electric Vehicles in the Short Food Supply Chain Based on GHG Emissions and Economic Costs Estimations,” Sustainable Production and Consumption, vol. 36, pp. 49–61, Mar. 2023, doi: https://doi.org/10.1016/j.spc.2023.01.001.

[2] Y. Yang et al., “Optimal Design and Energy Management of Residential Prosumer Community with Photovoltaic Power Generation and Storage for Electric Vehicles,” Sustainable Production and Consumption, vol. 33, pp. 244–255, Sep. 2022, doi: https://doi.org/10.1016/j.spc.2022.07.008.

[3] A. Sierra Rodriguez, T. Santana, I. MacGill, N. J. Ekins-Daukes, and A. Reinders, “A Feasibility Study of Solar PV-powered Electric Cars Using an Interdisciplinary Modeling Approach for the Electricity balance, CO2emissions, and Economic aspects: the Cases of the Netherlands, Norway, Brazil, and Australia,” Progress in Photovoltaics: Research and Applications, vol. 28, no. 6, pp. 517–532, Nov. 2019, doi: https://doi.org/10.1002/pip.3202.

[4] B. Robisson, S. Guillemin, L. Marchadier, G. Vignal, and A. Mignonac, “Solar Charging of Electric Vehicles: Experimental Results,” Applied Sciences, vol. 12, no. 9, pp. 4523–4523, Apr. 2022, doi: https://doi.org/10.3390/app12094523.

[5] R. Razi, K. Hajar, A. Hably, and S. Bacha, “A user-friendly Smart Charging Algorithm Based on energy-awareness for Different PEV Parking Scenarios,” in 29th Mediterranean Conference on Control and Automation (MED), Puglia, Italy, 2021, pp. 392–397. doi: https://doi.org/10.1109/med51440.2021.9480287.

[6] W. Tushar, C. Yuen, S. Huang, D. B. Smith, and H. V. Poor, “Cost Minimization of Charging Stations with Photovoltaics: an Approach with EV Classification,” IEEE Transactions on Intelligent Transportation Systems, vol. 17, no. 1, pp. 156–169, Jan. 2016, doi: https://doi.org/10.1109/TITS.2015.2462824.

[7] D. Yan and C. Ma, “Optimal Sizing of a PV Based Electric Vehicle Charging Station under Uncertainties,” in IECON 2020 the 46th Annual Conference of the IEEE Industrial Electronics Society, Lisbon, Portugal, 2019, pp. 4310–4315. doi: https://doi.org/10.1109/iecon.2019.8926749.

[8] Q. Chen, W. Wang, H. Wang, Y. Dong, and S. He, “Information gap-based Coordination Scheme for Active Distribution Network considering charging/discharging Optimization for Electric Vehicles and Demand Response,” International Journal of Electrical Power & Energy Systems, vol. 145, pp. 108652–108652, Feb. 2023, doi: https://doi.org/10.1016/j.ijepes.2022.108652.

[9] J. Wang, N. Zhou, Q. Wang, and H. Liu, “Hierarchically Coordinated Optimization of Power Distribution Systems with Soft Open Points and Electric Vehicles,” International Journal of Electrical Power & Energy Systems, vol. 149, p. 109040, Jul. 2023, doi: https://doi.org/10.1016/j.ijepes.2023.109040.

[10] W. Kempton and J. Tomić, “Vehicle-to-grid Power implementation: from Stabilizing the Grid to Supporting large-scale Renewable Energy,” Journal of Power Sources, vol. 144, no. 1, pp. 280–294, Jun. 2005, doi: https://doi.org/10.1016/j.jpowsour.2004.12.022.


[11] Y. Yoo, Y. Al-Shawesh, and A. Tchagang, "Coordinated Control Strategy and Validation of Vehicle-to-Grid for Frequency Control," Energies, vol. 14, no. 9, p. 2530, Apr. 2021, doi: https://doi.org/10.3390/en14092530.

[12] S. Habib, M. M. Khan, F. Abbas, L. Sang, M. U. Shahid, and H. Tang, "A Comprehensive Study of Implemented International Standards, Technical Challenges, Impacts and Prospects for Electric Vehicles," IEEE Access, vol. 6, pp. 13866–13890, 2018, doi: https://doi.org/10.1109/access.2018.2812303.

[13] E. Mortaz and J. Valenzuela, "Optimizing the Size of a V2G Parking Deck in a Microgrid," International Journal of Electrical Power & Energy Systems, vol. 97, pp. 28–39, Apr. 2018, doi: https://doi.org/10.1016/j.ijepes.2017.10.012.

[14] P. Fan et al., "A Load Frequency Coordinated Control Strategy for Multimicrogrids with V2G Based on Improved MA-DDPG," International Journal of Electrical Power & Energy Systems, vol. 146, p. 108765, Mar. 2023, doi: https://doi.org/10.1016/j.ijepes.2022.108765.

[15] S. Habib, M. Kamran, and U. Rashid, "Impact Analysis of vehicle-to-grid Technology and Charging Strategies of Electric Vehicles on Distribution Networks – a Review," Journal of Power Sources, vol. 277, pp. 205–214, Mar. 2015, doi: https://doi.org/10.1016/j.jpowsour.2014.12.020.

[16] L. Noel, G. Z. de Rubens, J. Kester, and B. K. Sovacool, Vehicle-to-grid: a Sociotechnical Transition beyond Electric Mobility. Switzerland: Springer International Publishing: Cham, 2019. Available: Here.

[17] G. Saldaña, J. I. San Martin, I. Zamora, F. J. Asensio, and O. Oñederra, "Electric Vehicle into the Grid: Charging Methodologies Aimed at Providing Ancillary Services considering Battery Degradation," Energies, vol. 12, no. 12, p. 2443, Jun. 2019, doi: https://doi.org/10.3390/en12122443.

[18] S. S. Ravi and M. Aziz, "Utilization of Electric Vehicles for Vehicle-to-Grid Services: Progress and Perspectives," Energies, vol. 15, no. 2, p. 589, Jan. 2022, doi: https://doi.org/10.3390/en15020589.

[19] D. Huber, Q. De Clerck, C. De Cauwer, N. Sapountzoglou, T. Coosemans, and M. Messagie, "Vehicle to Grid Impacts on the Total Cost of Ownership for Electric Vehicle Drivers," World Electric Vehicle Journal, vol. 12, no. 4, p. 236, Nov. 2021, doi: https://doi.org/10.3390/wevj12040236.

[20] S. Qi et al., "Research on Charging-Discharging Operation Strategy for Electric Vehicles Based on Different Trip Patterns for Various City Types in China," World Electric Vehicle Journal, vol. 13, no. 1, pp. 7–7, Dec. 2021, doi: https://doi.org/10.3390/wevj13010007.

[21] R. Shipman, J. Waldron, S. Naylor, J. Pinchin, L. Rodrigues, and M. Gillott, "Where Will You Park? Predicting Vehicle Locations for Vehicle-to-Grid," Energies, vol. 13, no. 8, p. 1933, Apr. 2020, doi: https://doi.org/10.3390/en13081933.

[22] H.-S. Han, E. Oh, and S.-Y. Son, "Study on EV Charging Peak Reduction with V2G Utilizing Idle Charging Stations: the Jeju Island Case," Energies, vol. 11, no. 7, p. 1651, Jun. 2018, doi: https://doi.org/10.3390/en11071651.

[23] L. Liu, F. Xie, Z. Huang, and M. Wang, "Multi-Objective Coordinated Optimal Allocation of DG and EVCSs Based on the V2G Mode," Processes, vol. 9, no. 1, p. 18, Dec. 2020, doi: https://doi.org/10.3390/pr9010018 .

[24] L. Di Natale et al., "The Potential of Vehicle-to-Grid to Support the Energy Transition: a Case Study on Switzerland," Energies, vol. 14, no. 16, p. 4812, Aug. 2021, doi: https://doi.org/10.3390/en14164812.

[25] L. Luo, Z. Wu, W. Gu, H. Huang, S. Gao, and J. Han, "Coordinated Allocation of Distributed Generation Resources and Electric Vehicle Charging Stations in Distribution Systems with vehicle-to-grid Interaction," Energy, vol. 192, p. 116631, Feb. 2020, doi: https://doi.org/10.1016/j.energy.2019.116631.

[26] H. Mehrjerdi and E. Rakhshani, "Vehicle-to-grid Technology for Cost Reduction and Uncertainty Management Integrated with Solar Power," Journal of Cleaner Production, vol. 229, pp. 463–469, Aug. 2019, doi: https://doi.org/10.1016/j.jclepro.2019.05.023.

[27] S.-A. Amamra and J. Marco, "Vehicle-to-Grid Aggregator to Support Power Grid and Reduce Electric Vehicle Charging Cost," IEEE Access, vol. 7, pp. 178528–178538, 2019, doi: https://doi.org/10.1109/access.2019.2958664.

[28] A. AbuElrub, F. Hamed, and O. Saadeh, "Microgrid Integrated Electric Vehicle Charging Algorithm with Photovoltaic Generation," Journal of Energy Storage, vol. 32, p. 101858, Dec. 2020, doi: https://doi.org/10.1016/j.est.2020.101858.

[29] T. Steffen, A. Fly, and W. Mitchell, "Optimal Electric Vehicle Charging considering the Effects of a Financial Incentive on Battery Ageing," Energies, vol. 13, no. 18, p. 4742, Sep. 2020, doi: https://doi.org/10.3390/en13184742.

[30] D. Wang, M. Sechilariu, and F. Locment, "PV-Powered Charging Station for Electric Vehicles: Power Management with Integrated V2G," Applied Sciences, vol. 10, no. 18, p. 6500, Sep. 2020, doi: https://doi.org/10.3390/app10186500.

[31] Y. Jang et al., "Grid-Connected Inverter for a PV-Powered Electric Vehicle Charging Station to Enhance the Stability of a Microgrid," Sustainability, vol. 13, no. 24, p. 14022, Dec. 2021, doi: https://doi.org/10.3390/su132414022.

[32] Y. Wang and D. Gladwin, "Power Management Analysis of a Photovoltaic and Battery Energy Storage-Based Smart Electrical Car Park Providing Ancillary Grid Services," Energies, vol. 14, no. 24, p. 8433, Dec. 2021, doi: https://doi.org/10.3390/en14248433.

[33] U. Abronzini, C. Attaianese, M. D'Arpino, M. Di Monaco, and G. Tomasso, "Cost Minimization Energy Control Including Battery Aging for Multi-Source EV Charging Station," Electronics, vol. 8, no. 1, p. 31, Jan. 2019, doi: https://doi.org/10.3390/electronics8010031.

[34] A. Ul-Haq, C. Cecati, and E. Al-Ammar, "Modeling of a Photovoltaic-Powered Electric Vehicle Charging Station with Vehicle-to-Grid Implementation," Energies, vol. 10, no. 1, p. 4, Dec. 2016, doi: https://doi.org/10.3390/en10010004.

[35] S. Mumtaz, S. Ali, S. Ahmad, L. Khan, S. Hassan, and T. Kamal, "Energy Management and Control of Plug-In Hybrid Electric Vehicle Charging Stations in a Grid-Connected Hybrid Power System," Energies, vol. 10, no. 11, p. 1923, Nov. 2017, doi: https://doi.org/10.3390/en10111923.

[36] V. C. Onishi, C. H. Antunes, and J. P. F. Trovão, "Optimal Energy and Reserve Market Management in Renewable Microgrid-PEVs Parking Lot Systems: V2G, Demand Response and Sustainability Costs," Energies, vol. 13, no. 8, p. 1884, Apr. 2020, doi: https://doi.org/10.3390/en13081884.

[37] B. Aluisio, A. Conserva, M. Dicorato, G. Forte, and M. A. Trovato, "Optimal Operation Planning of V2G-equipped Microgrid in the Presence of EV Aggregator," Electric Power Systems Research, vol. 152, pp. 295–305, Nov. 2017, doi: https://doi.org/10.1016/j.epsr.2017.07.015.

[38] T. Zhou and W. Sun, "Research on multi-objective Optimisation Coordination for large-scale V2G," IET Renewable Power Generation, vol. 14, Art. no. 3, 2020, doi: https://doi.org/10.1049/iet-rpg.2019.0173.

[39] A. Modarresi Ghazvini and J. Olamaei, "Optimal Sizing of Autonomous Hybrid PV System with Considerations for V2G Parking Lot as Controllable Load Based on a Heuristic Optimization Algorithm," Solar Energy, vol. 184, pp. 30–39, May 2019, doi: https://doi.org/10.1016/j.solener.2019.03.087.

[40] W. Vermeer, G. R. Chandra Mouli, and P. Bauer, "Real-Time Building Smart Charging System Based on PV Forecast and Li-Ion Battery Degradation," Energies, vol. 13, no. 13, p. 3415, Jul. 2020, doi: https://doi.org/10.3390/en13133415.

[41] R. Shi, S. Li, P. Zhang, and K. Y. Lee, "Integration of Renewable Energy Sources and Electric Vehicles in V2G Network with Adjustable Robust Optimization," Renewable Energy, vol. 153, pp. 1067–1080, Jun. 2020, doi: https://doi.org/10.1016/j.renene.2020.02.027.

[42] M. Kajanova and P. Bracinik, "The Vehicle-to-Grid Concept with Respect to the Preferences of Electric Vehicle Drivers and Charging Station Operators," Applied Sciences, vol. 12, no. 11, p. 5476, May 2022, doi: https://doi.org/10.3390/app12115476.

[43] Saleh Cheikh-Mohamad, M. Sechilariu, and Fabrice Locment, "PV-Powered Charging Station: Energy Management with V2G Operation and Energy Cost Analysis," in 2022 7th International Conference on Smart and Sustainable Technologies (SpliTech), Split , Croatia, Jul. 2022, pp. 1–6. doi: https://doi.org/10.23919/splitech55088.2022.9854343.

[44] S. Cheikh-Mohamad, M. Sechilariu, and F. Locment, "Real-Time Power Management Including an Optimization Problem for PV-Powered Electric Vehicle Charging Stations," Applied Sciences, vol. 12, no. 9, p. 4323, Apr. 2022, doi: https://doi.org/10.3390/app12094323.

[45] S. Cheikh-Mohamad, M. Sechilariu, and F. Locment, "PV-Powered Charging Station: Energy Management and Cost Optimization," in 2021 IEEE 30th International Symposium on Industrial Electronics (ISIE), Kyoto,Japan, Jun. 2021, pp. 1–6. doi: https://doi.org/10.1109/isie45552.2021.9576324.

[46] M. Sechilariu, N. Molines, G. Richard, H. Martell-Flores, F. Locment, and J. Baert, “Electromobility framework study: infrastructure and urban planning for EV charging station empowered by PV-based microgrid,” IET Electrical Systems in Transportation, vol. 9, Art. no. 4, 2019, doi: https://doi.org/10.1049/iet-est.2019.0032.

[47] M. Sechilariu and F. Locment, “Direct Current Microgrid Power Modeling and Control,” in Urban DC Microgrid, Elsevier, 2016, pp. 133–170. doi: https://doi.org/10.1016/B978-0-12-803736-2.00004-9.

[48] M. Sechilariu and F. Locment, “Experimental Evaluation of Urban Direct Current Microgrid,” in Urban DC Microgrid, Elsevier, 2016, pp. 209–250. doi: https://doi.org/10.1016/B978-0-12-803736-2.00006-2.

[49] C. E. Montaño-Salcedo, M. Sechilariu, and F. Locment, “Human-System Interfaces for PV-Powered Electric Vehicles Charging Station,” in 2021 IEEE 30th International Symposium on Industrial Electronics (ISIE), Kyoto, Japan, 2021, pp. 1–6. doi: https://doi.org/10.1109/ISIE45552.2021.9576251

[50] F. Marra, G. Y. Yang, C. Træholt, E. Larsen, C. N. Rasmussen, and S. You, “Demand Profile Study of Battery Electric Vehicle under Different Charging Options,” in 2012 IEEE Power and Energy Society General Meeting, San Diego, CA, USA, 2012, pp. 1–7. doi: https://doi.org/10.1109/PESGM.2012.6345063.

[51] M. Sechilariu and F. Locment, “Backup Power Resources for Microgrid,” in Urban DC Microgrid, Elsevier, 2016, pp. 93–132. doi: https://doi.org/10.1016/b978-0-12-803736-2.00003-7.

[52] D. Wang, F. Locment, and M. Sechilariu, “Modelling, Simulation, and Management Strategy of an Electric Vehicle Charging Station Based on a DC Microgrid,” Applied Sciences, vol. 10, no. 6, p. 2053, Mar. 2020, doi: https://doi.org/10.3390/app10062053.

[53] “IBM CPLEX Optimizer.” https://www.ibm.com/fr-fr/products/ilog-cplex-optimization-studio.

## 3.2 Solar charging swappable EV batteries

The integration of PV with swappable battery systems offers a promising solution to align solar energy integration into EV charging needs. This approach enhances grid flexibility, reduces overall system costs, and supports wider PV adoption[11].

### 3.2.1 Introduction

The use of photovoltaics (PV) to charge electric vehicle (EV) batteries plays a crucial role in the cost-competitive mitigation of greenhouse gas emissions linked to transportation. However, the temporal mismatch between solar generation peaks and charging needs may hinder some of its benefits. The use of swappable batteries, by decoupling battery charging from vehicle use, overcomes this mismatch [1],[2]. Furthermore, it also facilitates a more extensive integration of photovoltaics within both the realm of electric mobility and the broader electricity demand of consumers. This integration, in turn, leads to a substantial reduction in the overall costs associated with the combined power and transport systems.

The concept of swappable batteries has recently remerged with the increasing adoption of electric vehicles and the challenges of synchronizing the development of plug-in charging infrastructure and EV sales. Recent literature reviews have presented the battery swapping concept, highlighting its impact on the decrease in energy refuelling duration as well as its potential for regulating grid load and extending battery life [4]-[6]. Techno-economic assessments have repeatedly shown that the swappable batteries approach is cost-competitive for a range of assumptions and geographies [7]-[10] pointing out some of the challenges to overcome such as the need for battery standardization [4]-[6]. For an in-depth discussion of the potential benefits and challenges to the adoption of the swappable battery approach [2].

### 3.2.2 Assumptions

In this model, vehicles swap their low-charge batteries for charged ones at battery swapping stations (BSS), mostly an evolution of the traditional fuel service stations. The batteries received are inserted into rack-mounted chargers and remain grid-connected for long periods (typically 24 hours). They are charged at a relatively low rate (0.25 kW/kWh, or 4 hours) at times of solar excess generation and lowest energy prices. Thus, EV battery charging is decoupled from vehicle use, and its load to the electric system is flexible (within their residence time). This flexibility is a powerful tool for PV integration: most of the electricity for battery charging will concentrate on solar peak hours [1].

A typical battery swapping station swaps about 0.4 million batteries per year [2]. Assuming that their useful life for e-mobility corresponds to about 2 000 full charge cycles, then some 200 batteries/year will be declared unfit for loading into EVs. Perhaps half will be classified as healthy and fit for second-life use; the other 100 are further diagnosed, and with some

[11] This work is based on the participation of A.M Vallera and M.C Brito from Faculdade de Ciências da Universidade de Lisboa, Portugal in Task17 activities and was funded by the Portuguese Fundação para a Ciência e a Tecnologia (FCT) I.P./MCTES through national funds (PIDDAC) – UIDB/50019/2020 https://doi.org/10.54499/UIDB/50019/2020, UIDP/50019/2020 https://doi.org/10.54499/UIDP/50019/2020 and LA/P/0068/2020 (https://doi.org/10.54499/LA/P/0068/2020).

intervention/repair, many will still be fit for second-life, the others are sent for recycling. This means that every battery swapping station has a continuous pipeline of second-life batteries, and will naturally use them in rack-mounted bidirectional inverter modules, on the premises, for increased PV integration and grid service. These resident second-life batteries may further substitute grid energy with cheaper and cleaner locally produced PV also away from the solar hours, extending their usefulness even to fast, high power, battery-to-grid services such as reserve power, increasing grid resilience and balance.

To illustrate the impact of swappable batteries on PV penetration, the approach was applied to an idealized small region of 200 000 inhabitants, served by the national electric grid and relying solely on PV as the viable renewable resource [3]. The fraction of energy required to meet both transport and general electricity demand (with general demand excluding mobility) that could be economically supplied by local PV generation was studied.

Two key research questions are addressed here. First, the optimal fraction of PV generation that can be effectively utilized for EV battery charging is determined. Additionally, the feasibility of using excess generation to satisfy general demand, thereby reducing imported grid energy, is investigated. Second, these results are compared with alternative models, as summarized in Table 3.2-1.

**Table 3.2-1 Description of models under study.**

| | Model | Description |
|---|---|---|
| 1 | Business as usual (BAU) | Transport relies on fossil diesel and petrol |
| 2 | Plug-in | Vehicles are all battery electric and charge by connecting a plug into the socket of a charger |
| 3 | Plug-in Flex + Storage | As above, with 10% demand flexibility and added second-life battery storage |
| 4 | BSwap Flex | Vehicles refuel by swapping their low-charge batteries by charged batteries at the BSS |
| 5 | BSwap Flex + Storage | As above, with added second-life battery storage |
| 6 | BSwap Flex + Double Storage | As above, with twice the previous storage capacity |

The optimum PV capacity that should be installed is determined by the minimum of the global cost function which includes estimates of all costs (or cost differences between models), as summarized in Table 3.2-2. For details on the modelling methodology and assumptions check [3].

**Table 3.2-2 Summary of costs considered for the analysis within the small region under study.**

| Cost component | Values | Description |
|---|---|---|
| Imported energy | 70 €/MWh + 100 €/t$CO_{2eq}$<br>0.25 €/t$CO_{2eq}$/MWh | Dynamic hourly prices centred on this reference value, to which carbon emissions cost is added.<br>Emissions per unit of grid electric energy are also dynamic, centred on this reference value. |
| PV generation | 35 €/MWh | |
| Fuel | 65 €/MWh + 100 €/t$CO_{2eq}$ | A reference cost for an average of diesel oil and petrol, special taxes excluded. Emissions costs are also added. |
| Charging infrastructure | Plug-in: 11.1 M€/year<br>BSS: 17.1 M€/year | Annualized costs of Plug-in chargers and BSSs in the region. |
| Battery rack modules for the second life batteries | Plug-in: 6.85 M€/year<br>BSS: 6.85 M€/year<br>BSS (double storage): 12 M€/year | Annualized costs of bidirectional B2G modules (cost of batteries excluded) in the region. |
| Vehicles (cost difference) | ICE: 0 M€/year<br>Plug-in: 5.7 M€/year<br>BSwap: 6.1 M€/year | Annualized costs,imputed to the region considered, including, besides upfront vehicle cost, the costs of repair and maintenance, and substitution of important parts such as batteries. |

### 3.2.3 Results

Results are presented in Figure 3.2-1 showing that, compared with the business-as-usual model of internal combustion engine vehicles, the plug-in model reduces the overall cost of energy and transport, whilst allowing for higher integration of PV generation, from 40% to 60% (rigid demand, no storage) or 80% (10% flexibility and storage) of the general demand. The decrease in overall cost is essentially due to the higher efficiency of electric when compared to ICE motors (substitution of fuels for electric energy, similarly priced but with a large efficiency gain).

The battery-swapping model, however, can achieve even lower cost and higher PV integration. In fact, higher PV integration, substituting grid energy for lower cost, cleaner, solar energy, essentially explains the further cost reduction below Plug-in: with battery swapping, the flexibility of battery charging demand concentrates it mostly under the solar peaks. Notice that the demand for transport is 42% of the general demand for models 2 to 6, and therefore the total electric energy consumption is 142% of the general demand. As expected, the higher the installed storage capacity, the larger the optimal integration of PV in the system. The precise values of course depend on the detailed model assumptions, but the qualitative trends would be reproduced by most other reasonable models.

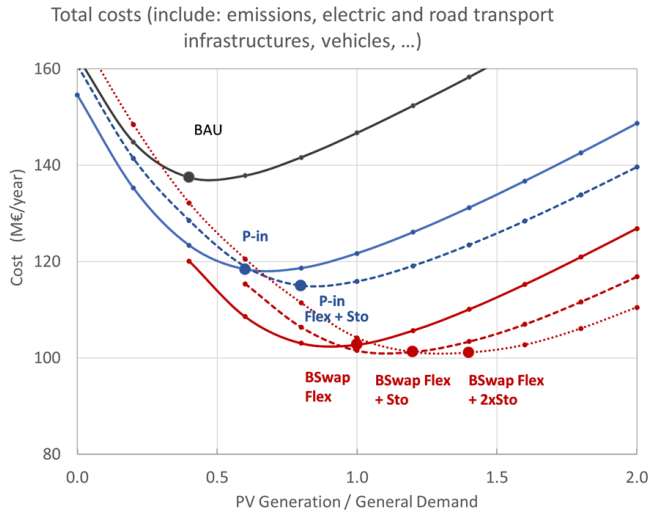


**Figure 3.2-1 Total costs of the electricity and transport sectors for the region under study. Notice that the vertical axis does not start at the origin to enhance readability.**

Considering the optimal installed PV capacity, one-year hourly demand and PV-generation time series allow determining annual energy curtailment, import and use for the general and transport demand, as shown in Figure 3.2-1. The results show that the need to import grid energy falls dramatically with the battery-swapping models, from 1.42 (business as usual with no PV) down to 0.63 (44% of total demand) in the pure flexibility model, and to 0.44 and 0.26 (31 and 18%) in the case of the battery swapping models including second-life batteries with bidirectional coupling to the grid. As a consequence, emissions are also reduced by an estimated 1.3 tCO2eq/capita for the central battery-swapping model.

Integration of PV reaches very high values in the battery-swapping models, and this causes total export and curtailment of PV generation to be in the range of 15% to 16% of the total energy consumption. On the other hand, PV generation satisfies 56%, 69% and 82% of the total, transport and general, demand for each of the battery-swapping models considered.

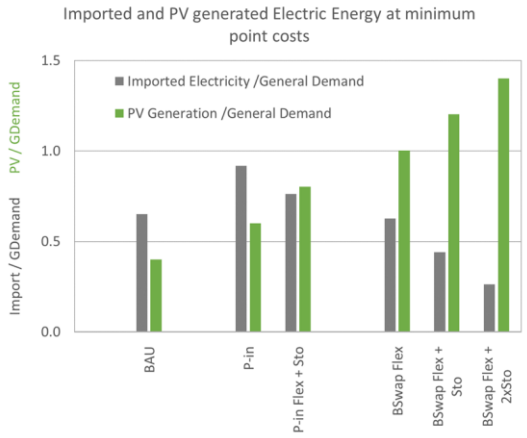


**Figure 3.2-2 The annual energy (grey) imported from the national grid and (green) locally generated by PV**

Overall, the battery-swapping approach has a significant impact on the overall cost of electricity (for general and mobility demand) and on GHG emissions, as shown in Figure 3.2-3.

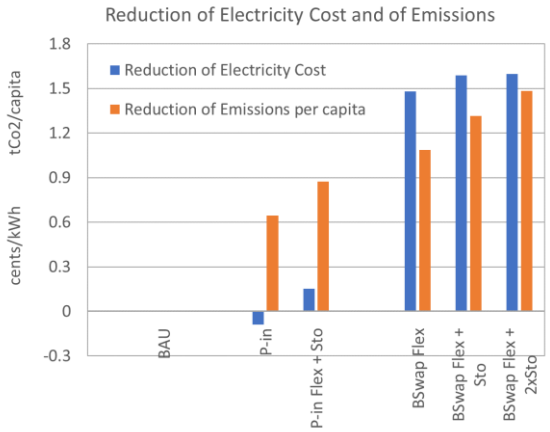


**Figure 3.2-3 The decrease in electricity cost (blue) and GHG emissions (orange), compared to the business-as-usual model with optimum PV capacity.**

### 3.2.4 Conclusion

This case study has shown that battery-swapping models in most systems are expected to lead to the highest levels of PV integration with the lowest costs for electric energy, both for EV battery charge and for general consumers, while providing a stable and resilient electric system with a large fraction of flexible load and high power, fast response reserve capacity.

## REFERENCES

[1] A. M. Vallera, P. M. Nunes, and M. C. Brito, “Why we need battery swapping technology,” Energy Policy, vol. 157, p. 112481, Oct. 2021, doi: https://doi.org/10.1016/j.enpol.2021.112481.

[2] A. M. Vallêra, The transition: Why We Need Battery Swapping for the Future Energy and Transport Systems. Universidade De Lisboa, Faculdade De Ciências, Instituto Dom Luiz, Lisboa, Portugal, 2023. doi: https://doi.org/10.56526/10451/55274.

[3] A. M. Vallera and M. C. Brito, “In preparation,” 2024.

[4] W. Zhan, Z. Wang, L. Zhang, P. Liu, D. Cui, and D. G. Dorrell, “A Review of siting, sizing, Optimal scheduling, and cost-benefit Analysis for Battery Swapping Stations,” Energy, vol. 258, p. 124723, Nov. 2022, doi: https://doi.org/10.1016/j.energy.2022.124723.

[5] D. Cui et al., “Operation Optimization Approaches of Electric Vehicle Battery Swapping and Charging station: a Literature Review,” Energy, vol. 263, p. 126095, Jan. 2023, doi: https://doi.org/10.1016/j.energy.2022.126095.

[6] F. Ahmad, M. Alam, I. Alsaidan, and S. M. Shariff, “Battery Swapping Station for Electric Vehicles: Opportunities and Challenges,” IET Smart Grid, vol. 3, no. 3, Apr. 2020, doi: https://doi.org/10.1049/iet-stg.2019.0059.

[7] Y. Deng, Z. Chen, P. Yan, and R. Zhong, “Battery Swapping and Management System Design for Electric Trucks considering Battery Degradation,” Transportation Research Part D: Transport and Environment, vol. 122, p. 103860, Sep. 2023, doi: https://doi.org/10.1016/j.trd.2023.103860.

[8] F. Zhu et al., “Does the Battery Swapping Energy Supply Mode Have Better Economic Potential for Electric heavy-duty trucks?,” eTransportation, vol. 15, p. 100215, Jan. 2023, doi: https://doi.org/10.1016/j.etran.2022.100215.

[9] M. O. Tarar, N. U. Hassan, and I. H. Naqvi, “On the Economic Feasibility of Battery Swapping Model for Rapid Transport Electrification,” in IEEE PES Innovative Smart Grid Technologies Europe (ISGT-Europe), 2021, pp. 1–5. doi: https://doi.org/10.1109/ISGTEurope52324.2021.9639986.

[10] Z. Wang, Y. Liu, Z. Lin, H. Hao, and S. Li, “Techno-economic Comparison on Charging Modes of Battery heavy-duty Vehicles in short-haul delivery: a Case Study of China,” Journal of Cleaner Production, vol. 425, pp. 138920–138920, Nov. 2023, doi: https://doi.org/10.1016/j.jclepro.2023.138920.

[11] J. Sindha, J. Thakur, and M. Khalid, “The Economic Value of Hybrid Battery Swapping Stations with Second Life of Batteries,” Cleaner Energy Systems, vol. 5, p. 100066, Aug. 2023, doi: https://doi.org/10.1016/j.cles.2023.100066.

[12] M. R. Sarker, H. Pandžić, and M. A. Ortega-Vazquez, “Electric Vehicle Battery Swapping station: Business Case and Optimization Model,” in 2013 International Conference on Connected Vehicles and Expo (ICCVE), Dec. 2013, pp. 289–294. doi: https://doi.org/10.1109/ICCVE.2013.6799808.

[13] M. Zhang, S. Yu, H. Yu, P. Li, W. Li, and H. M. Khalid, “Dispatchable Capacity Optimization Strategy for Battery Swapping and Charging Station Aggregators to Participate in Grid Operations,” Energy Reports, vol. 10, pp. 734–743, Nov. 2023, doi: https://doi.org/10.1016/j.egyr.2023.07.022.A. Galati, N. Adamashvili, and M. Crescimanno, “A Feasibility Analysis on Adopting Electric Vehicles in the Short Food Supply Chain Based on GHG Emissions and Economic Costs Estimations,” Sustainable Production and Consumption, vol. 36, pp. 49–61, Mar. 2023, doi: https://doi.org/10.1016/j.spc.2023.01.001.

# 4 ELECTRIC BUS CHARGING STATIONS

The electrification of public transportation plays a pivotal role in the global transition toward sustainable, low-emission mobility systems. Among the various solutions, electric buses (e-buses) have emerged as a key component in reducing urban air pollution, lowering greenhouse gas emissions, and improving the energy efficiency of transport networks.

Unlike private EVs, e-buses operate on fixed routes with high daily mileage, making their integration into energy and transport infrastructures both impactful and technically demanding. The deployment of electric bus fleets presents unique challenges and opportunities in terms of charging strategies, battery management, grid interaction, and operational planning.

This chapter presents a preliminary study on the integration of e-buses in urban areas, with a focus on their energy modeling, consumption patterns, and the various charging methods proposed in the literature. The study also highlights the potential role of PV systems in supporting e-bus charging infrastructure.

## 4.1 Modelling of Electric Bus Operation and Charging Process: Potential Contribution of Local Photovoltaic Production

This study assesses the transition from diesel to electric buses, focusing on charging strategies' impacts on service quality and the utility grid. Through comprehensive modeling of an urban bus network in Compiègne, France, it evaluates various charging infrastructure configurations. Additionally, it explores the potential benefits of local photovoltaic (PV) energy production to reduce grid strain[12,13].

### 4.1.1 Introduction

Urban public transport is essential for carrying millions of people for their daily trips; however, it has a significant impact on greenhouse gas (GHG) emissions. Therefore, the electrification of urban buses is an efficient way to reduce emissions, as long as the supplied electricity is provided by low carbon energy sources. Additionally, electric buses (e-buses) provide supplementary benefits compared to conventional buses such as a reduction of air pollution (fine particle matter), noise, and on-board vibrations [1]. Their maintenance is also easier and cheaper; however, the integration of e-buses is a challenging procedure due to the increased power demand which adds additional stress to the electricity network.

The location of charging infrastructures and charging periods can induce negative impacts on the utility grid. The three main locations for static-charging infrastructures are bus depots, line terminals, and bus stops. Most of the time, e-buses are charged at the bus depot during the night [2]. Therefore, buses require sufficient battery capacity to perform their daily service of around 200–300 km [3]. The consumption of an e-bus varies between 0.76 and 2.79 kWh/km for a standard bus with an average of 1.65 kWh/km [4]. Therefore, at least 150 kWh battery capacity is required to complete the daily service. Such an on-board battery pack weights approximately one ton considering the energy density around 150 Wh/kg for lithium-ion batteries. Ji et al. have shown that an increase of the on-board battery capacity from 50 kWh to 400 kWh induces a raise in the bus' energy consumption by 25% [5]. A larger battery capacity will thus increase the available energy to perform a long trip without frequently charging the battery. However, it will also lead to an increased energy consumption due to higher bus weight. Battery capacity has also an impact on the capacity of passengers, as a higher battery capacity requires more space in the bus [6]. The TOSA project has shown that decreasing the battery capacity leads to a reduction on the battery weight by 5 – 7 tons, an increase of the passengers' capacity of 15 – 30% and a reduction in the energy consumption of 10% [7].

Charging at the bus depot is usually performed once per daily service during several hours in the night at a power of 24 – 180 kW [1]. Currently, the majority of e-bus fleets is very small, around 15 e-buses per bus fleet in Europe [2] and 6 in the United States [8]. However, in the future, the penetration of a higher number of e-bus fleets is expected, hence a higher amount

[12] This study is based on the following publication: N. Dougier, B. Celik, S.-K. Chabi-Sika, M. Sechilariu, F. Locment, and J. Emery, "Modelling of Electric Bus Operation and Charging Process: Potential Contribution of Local Photovoltaic Production," Applied Sciences, vol. 13, 2023, https://doi.org/10.3390/app13074372.

[13] This research was funded by ADEME France, project T-IPV, grant number #2308D0002.

of power consumption will most likely be observed during the night period. Although it is not a peak power consumption period for the utility grid, charging during the night might prevent transformers from cooling down and accelerating the degradation of these units.

Alternatively, e-bus batteries can also be charged on-route at line terminals or bus stops (also called opportunity charging). Charging at terminals can occur around 20 times per daily service for a few minutes at a power of 150 – 600 kW [1]. On the other hand, charging at bus stops can occur around 200 times per daily service for a few seconds at a power up to 600 kW. From this perspective, the on-board battery capacity can be reduced with on-route charging, and it will lead to lower bus energy consumption. However, the short charging times imposed by passengers' transportation require high power to supply enough energy to the bus battery in a few seconds/minutes. A significant number of e-buses in the fleets could impact the stability of the utility grid and create a risk of increasing the peak power consumption in the local area. A large number of e-buses could also cause an overloading of utility grid transformers and induce the use of carbon-based fuel supplies, which release high GHG emissions.

One solution to reduce the impacts on the utility grid is to produce electricity locally with photovoltaic (PV) panels. If the e-buses charge during the daylight, the PV production can reduce the bus consumption peak. On the other hand, if they charge during the night, an additional stationary battery could help to reduce grid impact by storing surplus PV production during the day to use it at night. The charging scenario must be adapted in order to maximize PV self-consumption ratio, i.e., to increase the percentage of the bus load covered by the PV production. However, charging during the daylight at a low power to maximize PV self-consumption ratio might induce additional charging time, which can cause delays in the service. All of these factors show that the location and the size of charging infrastructures, as well as the charging strategy, can have a significant impact on both the utility grid and the transport network, which need to be carefully analysed with a detailed model of the bus transportation network.

The aim of this study is to focus on the influence of sizing and placement of charging infrastructures on both the utility grid and transportation network. This preliminary study simulates a bus fleet operation with several scenarios, which differ according to the location of chargers (depot, terminals, or stops) and their rated power. First, the bus network is modelled and the operation of buses is simulated. After that, charging stations are placed on the transportation network – at depot, terminals, or stops – and charging rules are applied. Performance indicators are defined to compare studied configurations. The main contributions of this work are listed as follows:

- A bus consumption model that considers the influence of the battery capacity on the bus gross weight and thus on the bus consumption;
- Modelling of a bus network is presented based on General Transit Feed Specification (GTFS) data;
- A sequential simulation of the e-bus operation is performed in order to analyse the influence of the charging scenarios on the quality of transportation services (delay indicator);
- A comparison between bus energy demand and PV production in order to assess the potential of PV energy to reduce impacts of e-bus charging on the utility grid.

The rest of the study is structured as follows. Section 4.1.2 analyses the scientific literature to underline the research gaps. Section 4.1.3 presents the modelling and simulation approach for the buses' operation and charging. The case study is introduced in Section 4.1.4. Section

4.1.5 displays the simulation results, and Section 4.1.6 analyses them. Finally, Section 4.1.7 contains a conclusion and perspectives for future works.

## 4.1.2 State of the Art of Scientific Literature

This section analyses the scientific literature to underline trends and gaps. The literature survey focuses on public transport planning, sizing of charging infrastructures, and PV supply of charging stations

### *4.1.2.1 Research Positioning*

The planning of public transportation can be divided into three main phases: strategic (horizon of years), tactical (one year to days), and operational (real time). As described by Perumal et al.[9], the planning process starts by determining the infrastructure, the lines, the frequencies, and the bus fleet investment. The tactical planning phase consists of the definition of the timetables, the vehicle scheduling (assignation of buses to the timetabled trips), the crew scheduling, and eventually the crew rostering. Recovery plans and real-time control strategies are also often implemented to reduce the impact of disruptions. From a transportation point of view, the present study concerns the strategic planning (sizing and placement of charging infrastructures) and its impact on the operational planning (e.g., bus delay). According to Manzolli et al. [10], e-bus studies can be divided into five categories: vehicle technology, battery technology, energy management, fleet operation, and sustainability. The present research concerns both the vehicle technology, in particular the charging power, and the fleet operation.

### *4.1.2.2 Sizing of Charging Infrastructures*

Scientific publications about e-bus charging either focus on the infrastructures' sizing [11] and/or the scheduling of the battery charging power [12][13]. A charging strategy can be defined as the choices of charging frequency, power, start time, and duration [6]. Few studies tackle both the sizing and management problems. Gao et al. [14] compared the impact of normal charging at 90 kW and ultra-fast charging at 480 kW on the on-board battery capacity for improving the autonomy of the bus. Fast charging has been shown to reduce the battery capacity and increase the autonomy. Leone et al. [15] have demonstrated that two 150 kW charging stations and an opportunity charger of 350 kW are needed at the terminals in order to reduce the cost and environmental impact compared to current diesel buses. Hasan et al. [16] have focused on the energy management of the bus and the charging strategy. The developed "ECO-charging" strategy, using pulsed charging to lessen the battery cooling needs, reduces the average grid load by more than 10% and shifts the charging to off-peak periods. On the other hand, a two-phase optimization framework is proposed to size the charging infrastructure and schedule the charging of e-buses with the objective to minimize the total system cost in [6]. The developed rolling-horizon-based charging strategy, which adjusts charging scheduling in real-time based on e-bus consumption and travel time, reduces the total charging cost by 68.3% compared to uncontrolled charging. In several studies, the sizing of a battery storage is combined with the determination of charging schedules [17]-[19]. Most studies only consider the sizing of the charger's rated power and the capacity of stationary storage. They usually consider that the size of the on-board battery of the bus is known. However, [6] investigated the charger deployment, the on-board battery capacity, the charging schedules, and charging costs, and the study shows the importance of considering the on-board battery.

Many studies about e-bus charging consider the influence on transportation or on the utility grid, but not both at the same time [20]. For example, in order to improve the traffic, Bie et al. have analysed passenger loading to optimize the vehicle scheduling plan, locations of starting, and terminal stations for short-turning lines and charging strategies [21]. The proposed strategy led to reduce the total passenger travel time (dwell times at stops and inter-stop travel times) of 15%. On the other hand, Akaber et al. have considered mainly grid constraints to optimize the objectives of bus operators such as load balancing via peak shaving and cost minimization with load shifting. The presented methodology is achieved to reduce the peak consumption and total charging cost by 50% and 27%, respectively. Lin et al. optimized the bus planning process considering jointly the transportation system and utility grid [23], and Tomizawa et al. studied the feasibility of simultaneously minimizing the power and the energy of surplus PV production [24]. Both studies showed that joint optimization reduces the charging cost, prevents later conflicts between transportation objectives and electricity network constraints, and increases the rate at which e-buses charge using local renewable energy.

#### *4.1.2.3 Photovoltaic Integration for Bus Charging*

Charging infrastructures of e-buses are often supplied only by the utility grid [25]; however, Arif et al. also included local PV production and/or electricity storage in order to improve the energy management [26]. Regarding a PV-storage-based charging station at the depot, the authors showed that limiting the supplied power from the grid to 5 kW can maximize the bus depot operator profit while minimizing the charging power causing transformer overloading. Rafique et al. also presented an optimal energy management system using a weighted multi-objective stochastic optimization to minimize the cost of electricity while aiming to reduce battery degradation [27]. Zhuang et al. studied the stochastic energy management of bus charging stations for reducing charging costs with PV production and battery storage considering bus-to-grid energy flows [28]. Szczesniak et al. adopted another point of view, attempting to find an optimal bus charging schedule at line terminals or depots in order to locally smooth the PV production fluctuations [29]. The proposed method was compared to uncontrolled charging and a cost minimization strategy. Results showed that operating costs increased marginally compared to the cost minimization strategy, but that utility grid power fluctuations were significantly reduced.

Concerning the design of PV power plants related to battery charging of e-buses, Santos et al. focused on the suitable locations of PV implantation at bus shelters [30]. Based on the solar irradiation, the potential of each bus shelter in Lisbon to supply electronic devices with PV panels was analysed. Almost 54% of bus shelters were found to be able to receive small devices such as lighting or remote small-scale sensors, but only 4% could provide at least 100 W and 2.4 kWh per day in order to supply a refrigerated vending machine. Dalala et al. performed an economic and environmental feasibility study about the installation of PV panels near a bus route [25]. With the right placement of PV panels, supplying e-buses with PV panels was found economically and environmentally interesting. However, the investment cost can be huge, as shown by Islam et al. who designed an off-grid PV system to balance the consumption of a bus depot in Malaysia [31]. Sizing results showed that 7 350 PV modules (6.5MWp in total), a battery capacity of 118 200 Ah, and 23 200 $m^2$ area were needed to offset a peak demand of 466.5 kW. Ren et al. [32] determined the optimal size and location of rooftop PV panels and capacity of storage near the line terminals of neighbouring communities. A case study in Hong Kong showed that the infrastructure (PV and stationary battery) deployment achieved the shortest payback period of 3.98 years and addressed the design issues such as battery oversizing with PV and battery misallocation. In [33], Ren et al. focused on the optimization of the charging strategy in the same community-based bus network to increase

the on-site consumption of PV production. All of these studies have showed the importance of both infrastructure location and charging strategy to lower the cost.

#### *4.1.2.4 Discussion on the State of the Art*

The literature review shows that the sizing of charging infrastructures and the management of the charging process have a significant influence on the economic and the environmental performances of the bus charging. Many studies tackle the sizing or the management problems, but rarely both at the same time. Similarly, impacts of e-bus charging on the utility grid and the transport network are not simultaneously considered, although the deployed charging strategies have significant impacts on both networks. Joint consideration of these two aspects could show benefits for the integration of renewable energy.

Several researchers analysed the integration of PV panels and stationary energy storage system to charge e-buses with reduced GHG emissions. Where PV production on bus shelters seems insufficient to supply bus energy consumption, large power plants at the depot show opportunity for balancing the energy consumption or reducing the peak demand. The designed infrastructures present a reduced energy cost but a higher investment cost compared to a diesel bus network. The sizing and the placement of charging infrastructures and PV production have an influence on both electricity and transport networks. Therefore, it is important to model the e-buses' network and operation precisely in order to identify the various impacts.

### 4.1.3 Modelling of the Bus Transportation Network

In this section, the modelling approach of the transportation network is presented to determine the charging powers and time delays of e-buses. First, the technical terms used to characterize the bus network are defined, then the utilized input data are presented with the deployed models and the simulation approach. The modelling steps are presented in Figure 4.1-1 . The inputs represent the bus network, the bus fleet operation, the solar irradiation, and the assumptions made on the bus technology and the charging infrastructures. General Transit Feed Specification (GTFS) data are used for modelling the bus network accurately. Models of bus consumption, charging process, and PV production are then integrated into a simulation process to analyse the operation of a bus fleet.

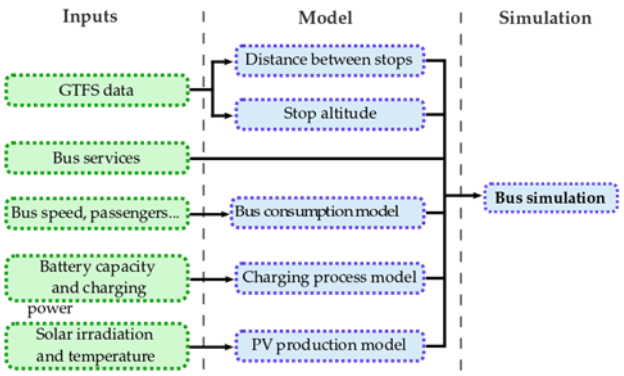


**Figure 4.1-1 Flow chart of the modelling approach with the inputs and the computation steps.**

### *4.1.3.1 Definitions*

Several specific terms which are used for the modelling of bus transportation network are introduced to ease the comprehensibility of the presented method (see Figure 4.1-2). The first components of a bus network are bus stops where the bus will stop during the day to board or alight passengers. The travel of a bus from one stop to another is named as a segment. A succession of segments is a route defined by its ordered sequence of stops. A route can belong to various bus lines that are official paths with intermediate stops between one or several terminals at the end of a line.

Public transport along a line is characterized by a timetable which indicates the times when a bus will stop at each bus stop. Based on the timetable, bus operators define the different bus trips that are combinations of routes and time sequences. This means that a bus can run through the same route several times during the day; however, each time will represent a different bus trip. Eventually, the succession of trips represents the daily service. Services can vary according to the period of the year (e.g., weekdays, weekends, or bank holidays). A service is composed of commercial trips and deadheading ones such as travelling from a bus depot to the beginning of a line without carrying passengers. These terms are illustrated on Table 4.1-1, which is the timetable of the bus line “ARC Express” in Compiègne, France [34]. The first column shows the stop sequence for bus line ARC Express, from the “Gare” terminal to the “Aramont” terminal. Then each column is a bus trip, starting at a different time. It can be noticed that bus trips 1,2,3,6,10 and 11 correspond to the same stops sequence, as well as trips 4,5, and 7. Therefore, 11 trips are represented on the table with only 4 routes. These trips are assigned to the services of two buses, represented on the first row. It is worth noticing that studies may use a different vocabulary to present the bus transportation network from a passenger point of view.

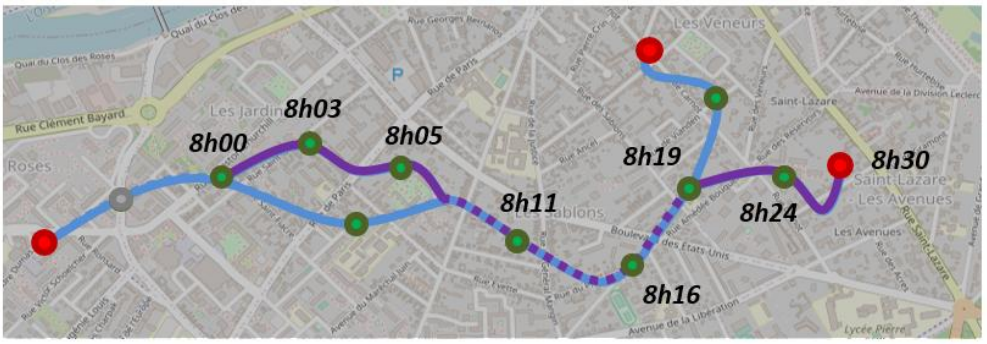


**Figure 4.1-2 Scheme of a bus line with three terminals (in red), intermediate bus stops (in green), two routes (in blue and purple), and the time schedule of one trip on the purple route.**

**Table 4.1-1 Timetable of bus line "ARC Express" in Compiègne, France [34].**

| **Service n°** | 1 | 1 | 1 | 2 | 2 | 2 | 2 | 2 | 2 | 2 | 1 |
|---|---|---|---|---|---|---|---|---|---|---|---|
| **Trip n°** | 2 | 3 | 4 | 5 | 6 | 7 | 8 | 9 | 10 | 11 | |
| **Bus stops** | **Time Schedule** | | | | | | | | | | |
| Gare | 06:42 AM | 07:54 AM | 08:36 AM | 09:36 AM | 10:00 AM | 12:10 PM | 02:10 PM | 03:41 PM | 04:00 PM | 04:49 PM | 05:36 PM |
| Couttolenc | 06:47 AM | 07:59 AM | 08:44 AM | 09:41 AM | 10:05 AM | 12:15 PM | 02:15 PM | 03:44 PM | 04:05 PM | 04:54 PM | 05:41 PM |
| Rés. Univ. | 06:51 AM | 08:03 AM | 08:46 AM | 09:45 AM | 10:09 AM | 12:19 PM | 02:19 PM | 03:44 PM | 04:08 PM | 04:58 PM | 05:46 PM |
| Denielou | 06:55 AM | 08:07 AM | 08:51 AM | 09:49 AM | 10:13 AM | 12:25 PM | 02:23 PM | 03:48 PM | 04:12 PM | 05:04 PM | 05:51 PM |
| Mercières | 06:58 AM | 08:12 AM | 08:55 AM | 09:52 AM | 10:16 AM | 12:28 PM | 02:26 PM | 03:51 PM | 04:16 PM | 05:08 PM | 05:55 PM |
| Parc Tertiaire | 07:00 AM | 08:15 AM | 08:58 AM | 09:55 AM | 10:19 AM | 12:30 PM | 02:29 PM | 03:53 PM | 04:19 PM | 05:11 PM | 05:58 PM |
| Longues | 07:04 AM | 08:18 AM | 09:02 AM | | | 12:33 PM | 02:33 PM | 03:57 PM | 04:35 PM | 05:16 PM | 06:02 PM |
| Lecuru | 07:10 AM | 08:25 AM | 09:10 AM | | | 12:40 PM | | | 04:05 PM | | |
| Z.A. | 07:18 AM | | 09:18 AM | | | 12:49 PM | | | 05:31 PM | | 06:18 PM |
| Automne | 07:21 AM | 08:30 AM | 09:21 AM | | | 12:52 PM | | | 05:34 PM | | 06:23 PM |
| Église | 07:25 AM | 08:40 AM | 09:25 AM | | | 12:56 PM | | | 05:38 PM | | 06:25 PM |
| Aramount | 07:28 AM | 08:42 AM | 09:29 AM | | | 01:00 PM | | | 05:42 PM | | 06:29 PM |

### *4.1.3.2 Bus Consumption Modelling*

E-bus energy consumption varies according to several parameters: bus speed, weight, traffic, number of passengers, road slope, etc. Bus consumption also depends on heating, ventilation, and air-conditioning (HVAC), and other auxiliaries, as well as on the implementation of a deceleration and braking energy recovery system. Therefore, a bus consumption model is needed to assess the energy demand of each e-bus in the fleet. Physical (also called white-box) models rely on the analysis of physical and chemical processes in the energy transmission and storage components of the vehicle [35]. Data-driven (also called black-box) models deduce the bus consumption based on large amounts of experimental or real-world operation data [35]. Eventually, intermediate grey-box models combine experimental data with mechanical insight [36].

#### 4.1.3.2.1 Consumption Model

Data-driven models require gathering a high amount of data, which can be collected through sensors. High-resolution data can be used [37][38], but they are often hard to collect and replicate for other locations. Low-resolution data [39] can also be used; however, they decrease the accuracy of the consumption model. Comparatively, physical models apply Newton's second law of motion in order to model the electricity consumption of e-bus. In this category, longitudinal dynamic models consider only the traction of the bus and require driving profiles of e-buses as input (i.e., a time series of velocity and elevation) [40]. Jefferies and Göhlich [41] have indicated that driving profiles may come from real-world operation [14] or standard dynamometer driving cycles [42][43]. Moreover, HVAC and other auxiliaries' consumption (lighting and other support systems) can be also considered for more detailed modelling of an electricity consumption profile [44]-[47]. This study implements an existing physical model [35]. The model needs to be fast enough to compute, to require accessible data, and to consider both the traction and the auxiliaries' consumption, considering the influence of the latter on the bus' consumption. It should be noted that the presented method does not consider the regenerative braking, the curves of the road, the number of crossroads, the meteorological conditions, or the driver's behaviour. The total consumed power by the bus $P_{tot}(t)$ is defined by Equation (4.1-1) (as the sum of the power needed for vehicle motion $P_{ldm}(t)$ and for auxiliary systems $P_{aux}(t)$ at each time step $t$.

$$P_{tot}(t) = P_{ldm}(t) + P_{aux}(t) \quad (4.1\text{-}1)$$

$$P_{ldm}(t) = v(t) \times \Big( m(t) \times g \times sin(\alpha) + m(t) \times g \times C_r \times cos(\alpha) + \frac{1}{2} \times \rho \times v^2(t) \times A_{front} \times C_d + m(t) \times a(t) \Big) \quad (4.1\text{-}2)$$

$$P_{aux}(t) = P_{HVAC}(t) + P_{other}(t) = P_{HC}(t) + P_{ventilation}(t) + P_{other}(t) \quad (4.1\text{-}3)$$

where $v(t)$ is the bus speed, $m(t)$ is the mass of the bus, $g = 9.81\, m/s^2$ is the standard acceleration of gravity, α is the slope, $C_r$ is the coefficient of rolling resistance, $\rho = 1.2\, kg/m^3$ is the air density,$A_{front}$ is the frontal area of the bus, and $C_d$ is the drag coefficient. The auxiliary consumption is modelled as the sum of the consumption of HVAC (the sum of $P_{ventilation}$ and $P_{HC}$ [35]) and the other auxiliaries $P_{other}$ . It should be noted that the total bus weight $m(t)$ consists of the bus curb ($m_{bus}$), battery pack ($m_{battery}$ ), and the total number of passengers ($m_{passengers}$) inside the bus $m = m_{bus} + m_{battery} + m_{passengers}$ at time $t$ .

#### 4.1.3.2.2 Speed Profile

The speed of the bus must be determined based on the distances and travel times between bus stops taken from the GTFS data in order to calculate the power consumption. Inspired by SORT standard driving cycles [48]-[50], the present study considers a speed profile with a trapezoid shape between two consecutive bus stops, as seen on Figure 4.1-3.

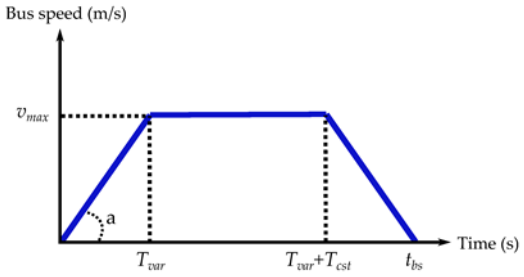


**Figure 4.1-3 Bus speed profile in trapeze representing the travel between two bus stops.**

The trapezoid is defined by the maximal speed $v_{max}$ and the acceleration $a$. Travel time and the distance between two bus stops $t_{bs}$ and $d_{bs}$ are determined using GTFS data. The spatial and temporal constraints of the bus travel can be determined from the speed profile. The distance between the consecutive stops is therefore determined as follows:

$$d_{bs} = 2 \times d_{var} + d_{cst} \quad (4.1\text{-}4)$$

$$d_{var} = \int_0^{T_{var}} v(t) \times dt = \int_0^{T_{var}} a \times t \times dt = \frac{a}{2} \times T_{var}^2 \quad (4.1\text{-}5)$$

$$d_{cst} = \int_{T_{var}}^{T_{var}+T_{cst}} v(t) \times dt = v_{max} \times T_{cst} \quad (4.1\text{-}6)$$

where $d_{var}$ and $d_{cst}$ are the distances travelled during the acceleration/deceleration and constant speed phases, respectively. $T_{var}$ is the acceleration/deceleration time, $T_{cst}$ is the time at constant speed, and $v(t)$ is the bus speed. The time to travel between the two stops is described below:

$$t_{bs} = 2 \times T_{var} + T_{cst} \quad (4.1\text{-}7)$$

$$T_{var} = \frac{v_{max}}{a} \quad (4.1\text{-}8)$$

Therefore, using Equations (4.1-7) and (4.1-8) with the value of discriminant of the quadratic equation $\Delta = t_{bs}^2 - 4a \times d_{bs}$ , the maximal speed $v_{max}$ is determined by:

$$\frac{v_{max}^2}{a} - t_{bs} \times v_{max} + d_{bs} = 0$$

$$v_{max} = \begin{cases} \frac{t_{bs} - \sqrt{t_{bs}^2 - \frac{4}{a} \times d_{bs}}}{2} \times a & if\ \Delta > 0 \\ \frac{t_{bs}}{2} \times a & if\ \Delta < 0 \end{cases} \quad (4.1\text{-}9)$$

If a delay is anticipated for arriving to the next stop on the route, the e-bus is assumed to increase its speed and acceleration up to limits. If the maximal speed – computed based on the real departure time of the bus from one stop and the theoretical arrival time to another – is above the speed limit, the speed is capped to a maximal value $v_{lim}$ and a new acceleration is computed. If the new acceleration is also above its limit, then it is capped to $a_{lim}$ and the bus is considered to be late arriving to the next stop.

### *4.1.3.3 Modelling of Charging Process*

The state of charge ($SoC$) of the bus battery $soc_{bus}(t)$ at each time $t$ depends on the bus consumption and the charged energy. The evolution of $soc_{bus}(t)$ is determined by:

$$soc_{bus}(t) = soc_{bus}(t - \Delta t) + \frac{\left(P_{conso}(t) + P_{charged}(t)\right) \times \Delta t}{E_{batt}} \quad (4.1\text{-}10)$$

$$soc_{min} < soc_{bus}(t) < soc_{max} \quad (4.1\text{-}11)$$

Where $P_{conso}(t)$ is the power consumed by the bus (negative), $P_{charged}(t)$ is the power used for battery charging (positive), $E_{batt}$ is the e-bus battery capacity, $soc_{min}$ and $soc_{max}$ , are, respectively, the minimal and maximal $SoC$ limits of the e-bus battery.

### *4.1.3.4 PV Production*

PV power is considered to be utilized for a local and clean energy source for charging the e-bus' battery. The PV power is determined according to [51] as below:

$$p_{PV}(t) = \eta_{syst} \times P_{STC} \times N_{PV} \times \frac{g(t)}{g_{STC}} \times [1 + \gamma \times T_{PV}(t) - 25] \quad (4.1\text{-}12)$$

$$T_{PV}(t) = T_{amb}(t) + g(t) \times \frac{NOCT - T_{air-test}}{G_{Test}} \quad (4.1\text{-}13)$$

where $\eta_{syst}$ is a yield considered to represent the system losses in the cables and converters, $P_{STC}$ is the PV power at standard test conditions (STC), $N_{PV}$ is the number of PV panels, $g(t)$ is the solar irradiation, $g_{STC}$ is the standard solar irradiation value at STC, $\gamma$ is the power temperature coefficient of PV module, $T_{PV}(t)$ is the PV cell temperature, $T_{amb}(t)$ is the ambient temperature, $NOCT$ is the nominal operating cell temperature of PV module, $T_{air-test}$ is the fixed air temperature at $NOCT$ condition, and $G_{Test}$ is the fixed solar irradiation at $NOCT$ condition.

#### *4.1.3.5 Bus Network Modelling*

This subsection deals with the modelling of the network, which consists of the bus stops, routes, trips, services, and lines. The GTFS data format is used in order to analyse the operation of the bus fleet on a transportation network.

##### 4.1.3.5.1 GTFS Data

The GTFS format was initially developed by Google and has since become a de facto standard. Open data in GTFS format are generated by urban transport organizing authorities. They are composed of several tables gathering information about bus schedules and line topography [52] via various text files. The major advantages of GTFS files are that they are open access and the data are provided in the same format for the transportation network of different cities. However, they must be combined with a description of bus services to simulate the operation of buses. The location information (i.e., latitude and longitude) of bus stops can be found in GTFS data but the distances and slopes between stops must be computed with the post-treatment as in the following section.

##### 4.1.3.5.2 Post-Treatment of GTFS Data

The GTFS data are used to determine the list of all routes and trips. As GTFS data only consider trips to model buses' operations and do not use the concept of routes defined in Section 4.1.3.1, all trips must be analysed to identify their corresponding route. After that, the distance between consecutive stops of each route is determined using Open Street Map, which is a free editable geographic database of the world [53]. The elevation of each stop is retrieved from Open Elevation Software. GTFS data also allows analysing the time spent between two consecutive bus stops. This duration can vary during a day mainly due to the hourly/daily traffic conditions.

Firstly, the distance between stops are determined. Based on the latitude and longitude information, a path between two bus stops is generated on Open Street Map using a "bus" transportation mode. To generate the path, Open Street Map creates a sequence of intermediate points on the road between the two stops with a higher density in curved portions (see Figure 4.1-4), and defines the total distance as the sum of distances between each intermediate point. This matches quite accurately the real path of the bus; however, it requires manual verification that the path proposed by Open Street Map fits the one on the bus network map.


**Figure 4.1-4 Path between two bus stops generated using Open Street Map with intermediate points.**

Secondly, determination of the altitude is performed. The bus consumption also depends on the slope of the road. Therefore, the Open Elevation software has been used to compute the altitude of all stops based of their latitude and longitude [54]. However, only the mean slope between consecutive stops is accessible in this way. The limit is the resolution of topographic map, around 200 m for open-source maps. This means that all points in a square of 200 m per side will have the same altitude, and that slope variations in this area might be hidden.

#### 4.1.3.5.3 Simulation of the Operation of Buses

The operation of bus trips is defined by timetables, which are provided by urban transport organizing authorities to bus operators. Bus operators determine which bus will perform which trip to complete their daily service. This step is called the “vehicle scheduling problem” and e-bus services which are gathered as the output of scheduling problem are used as the inputs of the presented simulations in this study.

Simulation inputs are the transport network modelling (GTFS data) and the bus fleet operation (bus services). The distance that a bus has to travel from each stop to the next charging station can be calculated for each bus service. The energy needed to reach the next charging station can be calculated based on this distance. Therefore, it is possible to ensure that a bus does not leave a charging station until it has enough energy to complete its service. The procedure of calculation of bus power consumption on a transportation network is presented in the flow chart in Figure 4.1-5. Inputs are first initialized such as bus services, trips, and routes. Then, for each time step of the simulated period, the status of each bus is determined successively: its position, speed, acceleration, service, trip, route, energy consumption, charged energy (if the bus is at a charging station), remaining dwell time (if the bus is at a stop), and battery $SoC$.

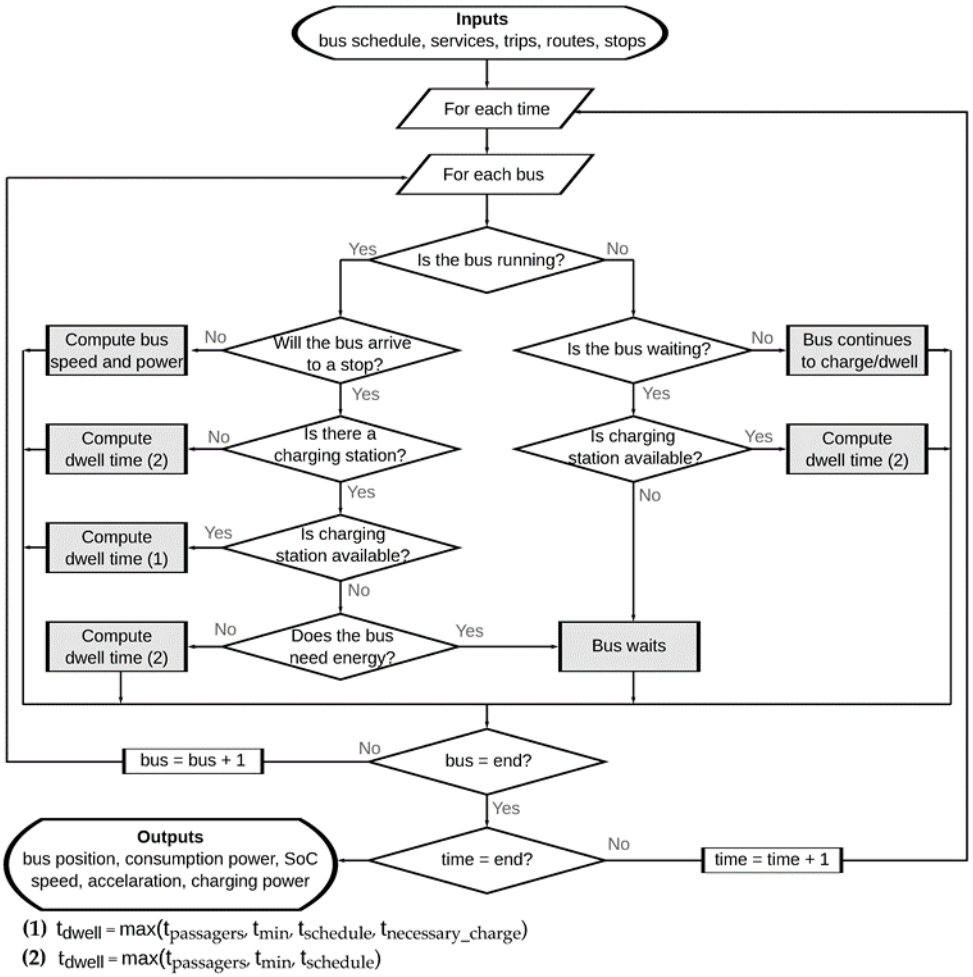


**Figure 4.1-5 Flow chart of the simulation of the bus fleet operation.**

The process to compute the new status of a specific bus depends on the inputs. If the bus was previously being charged or stopped, it continues this way until its dwell time reaches zero. However, if the bus has to run at this time step (it was running previously or its dwell time at a bus stop is over), then its position and speed need to be assessed. When the bus starts running between two stops, its maximal speed and acceleration on the current segment are computed and its trapezoid-shaped speed profile is deduced. Then, the bus energy consumption is assessed for all the time steps. If the bus arrives at a stop at the next time step, its dwell time must be computed considering the required energy needed to reach the next charging station.

The dwell time is computed in two different ways depending on whether the bus is charging or not. The passengers boarding/alighting time $t_{passegers}$ is defined as the time taken by the passengers to board or alight from the bus. The minimal dwell time $t_{min}$ is defined as a necessary idle time for transportation reasons (e.g., to change driver). The theoretical dwell time $t_{schedule}$ is the difference between the time when the bus arrives at a stop and the theoretical time at when it is supposed to leave according to the timetable. In the case when the bus is not charging, dwell time is the maximal value among $t_{passegers}$ , $t_{min}$, and $t_{schedule}$ . In the case when the bus is charging, the dwell time additionally depends on the time necessary to charge the battery to a sufficient level to travel to the next charging station

$t_{necessary_{charge}}$. This case requires computing the distance to the next charging station and assuming an average consumption for the following trip.

Bus delay can be computed in two manners: charging delay and scheduling delay. The charging delay $delay_{charge}$ is the additional dwell time of a bus due to charging the bus battery, and the scheduling delay $delay_{schedule}$ occurs because of other reasons which cause the bus to leave a bus stop late.

$$delay_{charge}(t) = t_{dwell} - max(t_{min}, t_{passegers}, t_{schedule})$$

$$delay_{schedule} = t_{arrival_{real}} - t_{arrival_{theroy}}$$

Where $t_{dwell}$ is the computed dwell time, $t_{min}$ is the minimal dwell time at a stop, $t_{passegers}$ is the necessary dwell time for passengers' boarding/alighting, $t_{schedule}$ is the theoretical dwell time before the next trip, $t_{arrival_{real}}$ is the time at which the bus arrives at the next stop, and $t_{arrival_{theroy}}$ is the theoretical arrival time at the next stop (according to the timetable).

### 4.1.4 Case Study

In this study, the GTFS data are gathered for the city of Compiègne in France. The bus line "ARC EXPRESS", which is 20 km long and composed of 12 bus stops, is chosen as the case study (see Figure 4.1-6). According to GTFS data, there are 11 routes and 36 trips used for providing transportation services over a day. The services of two buses were defined manually, so they matched the timetable. In order to realize all the trips defined on the timetable, the first bus "bus n°1" begins its service at 06:30 A.M and ends it at 07:15 P.M. It performs 11 trips, including 2 between the bus depot and the line terminals. The second bus "bus n°2" operates from 06:10 A.M to 06:50 P.M and performs 15 trips. Both buses have long idle period in the middle of the day. The cumulative distance travelled by bus n°1 and bus n°2 are 149 km and 219 km, respectively. Concerning the speed profile between two bus stops, the acceleration is assumed to be constant at $a = 1\,m/s^2$ [55]. Speed and acceleration limits are assumed as $v_{lim} = 40\,km/h$ and $a_{lim} = 1.5\,m/s^2$ , considering the need of passenger comfort [56].

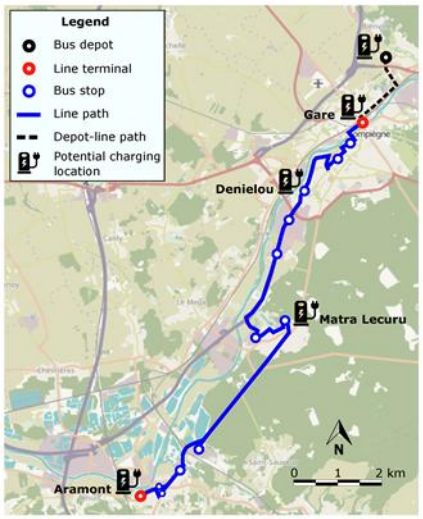


**Figure 4.1-6 Bus line ARC EXPRESS in Compiègne [57].**

The 12 m bus model from BYD has been chosen for this case study [58], and its characteristics are given in Table 4.1-2. This e-bus is equipped with a 422-kWh battery adding 2.8 tons (assuming 150 Wh/kg for lithium iron phosphate battery [1]) to the normal bus weight of 16.7

tons (total weight 19.5 tons). Average power values are assumed for the ventilation $P_{ventilation}$ and the other auxiliaries $P_{other}$ [35]. The initial $SoC$ of the e-bus battery is arbitrarily set to 90%.

Available charging powers are taken from the ABB's chargers. Buses can be charged at the depot using a Combined Charging System plug with a power of 100 kW or 150 kW [59]. They can also be charged overnight at the depot with a pantograph at 50 kW [60]. Eventually, on-route charging at bus stops and terminals can be performed via ABB's HVC-Opportunity charger at the power ratings of 150 kW, 300 kW, 450 kW, or 600 kW [60]. Scenarios described hereafter consider a power of 50 kW at the depot and 150 kW, 300 kW, 450 kW, and 600 kW for opportunity charging.

**Table 4.1-2 Characteristics of the BYD-12m bus and the PV panels. (LFP: Lithium Iron Phosphate)**

| BYD-12 m Bus | | PV Panel | |
|---|---|---|---|
| **Characteristics** | **Value** | **Characteristics** | **Value** |
| Length | 12.2 m | Power Output | 345 W |
| Width | 2.55 m | Panel Efficiency | 290 |
| Height | 3.30 m | Solar Irradiance | 1000 W/m$^2$ |
| Gross Vehicle Weight | 19.5 t | Temperature Coefficient | 0.29 %/°C |
| Maximal Passenger Capacity | 85 | NOCT | 41.5 °C |
| Battery Capacity | 422 kWh | $T_{\text{air-test}}$ | 20 °C |
| Battery Technology | LFP | $G_{\text{test}}$ | 800 W/m$^2$ |
| $soc_{\min}$ | 20% | $n_{\text{syst}}$ | 85% |
| $soc_{\max}$ | 90% | | |
| $P_{\text{ventilation}}$ | 0.5 kW | | |
| $P_{\text{other}}$ | 2 kW | | |

The number of boarding/alighting passengers is chosen arbitrarily, and the passenger flow is fixed for all routes of the same length. The number of passengers boarding/alighting is summarized in Table 4.1-3 for different lengths of bus sequence and one example for a bus route composed of 10 stops is displayed in Figure 4.1-7 . The passage rate is assumed to be one passenger every four seconds [35]. An average passenger weight of 68 kg is considered. When computing the necessary energy to reach the next charging station, an arbitrary consumption of 1.3 kWh/km is chosen in order to keep a safety margin for considering the uncertainty on the future bus consumption.

**Table 4.1-3 Number of passengers boarding (B) and alighting (A) from the bus at each stop according to the length of the bus sequence.**

| Stop | 1 | 2 | 3 | 4 | 5 | 6 | 7 | 8 | 9 | 10 | 11 | 12 |
|---|---|---|---|---|---|---|---|---|---|---|---|---|
| B | 30 | 15 | 5 | 2 | 0 | 0 | 0 | | | | | |
| A | 0 | 0 | 10 | 10 | 15 | 15 | 17 | | | | | |
| B | 20 | 25 | 15 | 10 | 10 | 5 | 2 | 0 | | | | |
| A | 0 | 0 | 5 | 10 | 20 | 15 | 10 | 22 | | | | |
| B | 20 | 25 | 15 | 10 | 5 | 10 | 5 | 1 | 0 | | | |
| A | 0 | 1 | 5 | 6 | 14 | 15 | 9 | 20 | 21 | | | |
| B | 25 | 20 | 10 | 15 | 5 | 0 | 5 | 3 | 0 | 0 | | |
| A | 0 | 1 | 3 | 10 | 2 | 15 | 7 | 18 | 12 | 15 | | |
| B | 30 | 15 | 20 | 10 | 5 | 0 | 5 | 0 | 2 | 1 | 0 | 0 |
| A | 0 | 2 | 0 | 15 | 10 | 5 | 10 | 5 | 3 | 15 | 10 | 13 |

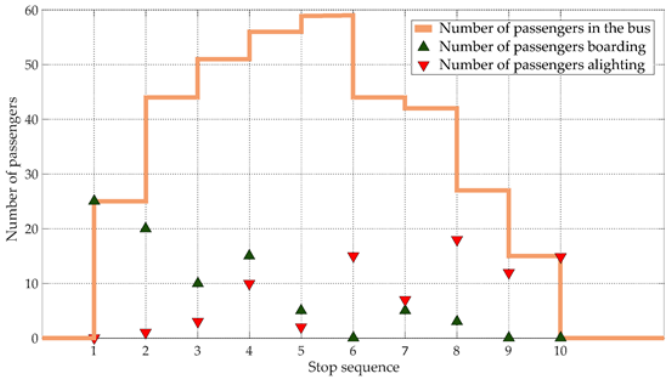


**Figure 4.1-7 Number of passengers boarding, alighting, and on the bus at each stop of route n°1.**

Local PV production has been considered and compared to the energy needs of the buses. Irradiation and ambient temperature data have been gathered on the STELLA experimental platform of the Université de Technologie de Compiègne with a time step of 10 s. The PV power plant is assumed to operate without stationary storage. The electricity produced is primarily supplied to the bus charging stations and the surplus is injected into the utility grid. However, buses charge automatically when they reach an available charging station without a charging strategy. The objective is to determine the temporal adequacy between the PV production and the bus consumption according to the charging scenario. The data from two days, one in January and one in July, have been used. A 100-kWp PV installation, corresponding to a realistic surface of a bus depot, is considered in this example. The parameters of the PV panel are presented in Table 4.1-2. It is assumed in this study that all charging stations and PV panels are connected to the same substation of the electric distribution network.

Simulations are performed and presented for three main scenarios with three additional sub-scenarios that differ only by their charging power. Charging scenarios are identified as follows:

- Scenario 1: two chargers at the depot;
- Scenarios 2 and 2bis: two chargers at the depot and a charger at “Gare” and “Aramont” line terminals;
- Scenarios 3, 3bis, and 3ter: chargers at the terminals “Gare” and “Aramont”, and bus stops “Denielou” and “Matra Lecuru”.

The number and location of charging stations are chosen arbitrarily. Charging powers at each location are presented in Table 4.1-4. The on-board battery capacity varies according to the scenarios from 70 kWh to 422 kWh. The simulations are performed over a day horizon with a two-second time step.

**Table 4.1-4 Location and power of charging stations in the different scenarios.**

| Scenarios | 1 | 2 | 2bis | 3 | 3bis | 3ter |
|---|---|---|---|---|---|---|
| Bus depot | $2 \times 50$ kW | $2 \times 50$ kW | $2 \times 50$ kW | – | – | – |
| Line terminal | – | 150 kW | 300 kW | 150 kW | 450 kW | 600 kW |
| Bus stops | – | – | – | 150 kW | 450 kW | 600 kW |
| Battery Capacity | 422 kWh | 422 kWh | 70 kWh | 70 kWh | 70 kWh | 70 kWh |

### 4.1.5 Results

#### *4.1.5.1 Scenario 1 – Charge at the Bus Depot*

In this scenario, 2 buses with 422 kWh batteries realize their services over 1 day. A charging station is located at the bus depot with two 50 kW chargers. Figure 4.1-8 shows the cumulative distance travelled by each bus and the $SoC$ of the bus's battery. Horizontal portions represent dwell times at bus stops and line terminals. The dwell times at bus stops can be seen more easily on the zoomed-in Figure 4.1-8 (a) as they are very short (around twenty seconds). $SoC$ decreases over time as there are no charging points on the road. It can be noticed that, even with a 422-kWh battery, the battery SoC of bus n°2 with the highest daily consumption goes below 38%. As expected, buses are fully recharged at the depot during the night after completing daily service. The total energy consumption is 373 kWh—respectively, 155 kWh and 218 kWh for buses n°1 and 2—which represents an average consumption per travelled distance of 1.01 kWh/km.

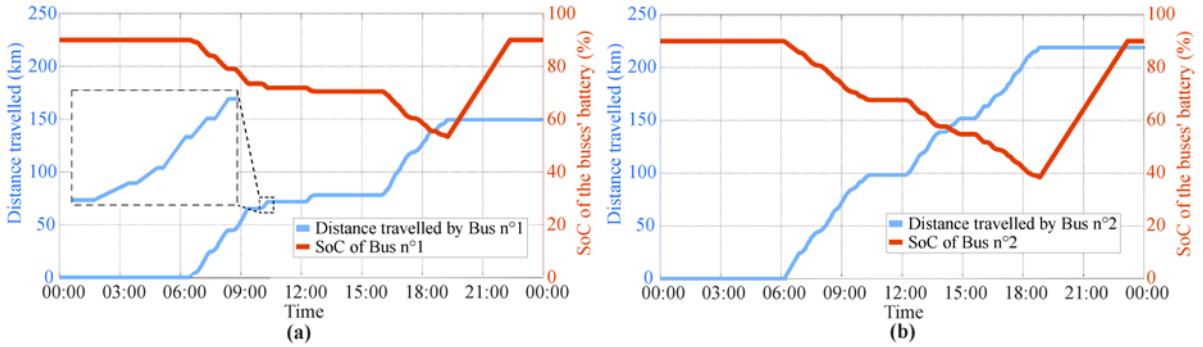


**Figure 4.1-8 Travelled distance and battery $SoC$ of buses n°1 (a) and n°2 (b) – scenario 1.**

Figure 4.1-9 shows the total charging power at each time step, i.e., the sum of the charging power of all charging stations with the PV production on the 15 January and the 17 July. The charging starts at 06:50 P.M when bus n°2 arrives to the depot. The charging power increases from 50 kW to 100 kW at 07:15 P.M when both buses are at the depot for the night. The daily PV production is 108 kWh in January and 500 kWh in July, which makes it possible to balance the buses' consumption only in July. PV energy could be stored in an additional stationary storage during the day and then used to charge the e-buses' batteries at night.

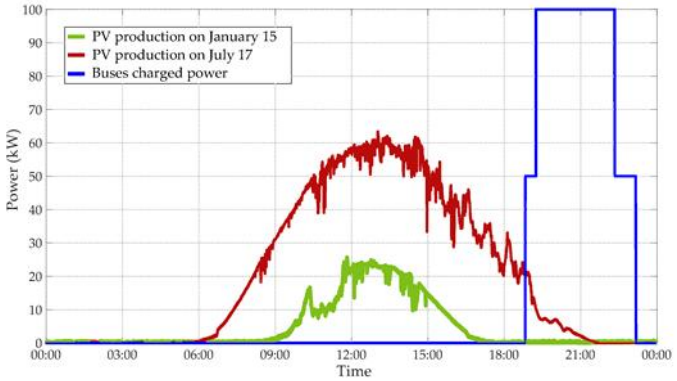


**Figure 4.1-9 Total charging power and PV production over time – scenario 1.**

### *4.1.5.2 Scenario 2 – Charge at the Line Terminals*

In the second scenario, two additional 150 kW chargers are located at the line terminals Gare and Aramont (see Figure 4.1-6). The batteries' $SoCs$ of the buses are given in Figure 4.1-10. Buses recharge during their dwell time between consecutive trips without a delay. According to the number of times they pass through a charging station, bus n°1 charges approximately ten times and bus n°2 twelve times (cf. Section 4.1.4). The minimal values of the batteries' $SoCs$ are obtained at 79% for bus n°1 and 73% for bus n°2. This means that the on-board battery capacity can be reduced if charging stations are located at the line terminals. The total energy consumption is 373 kWh, which represents an average consumption per travelled distance of 1.01 kWh/km.

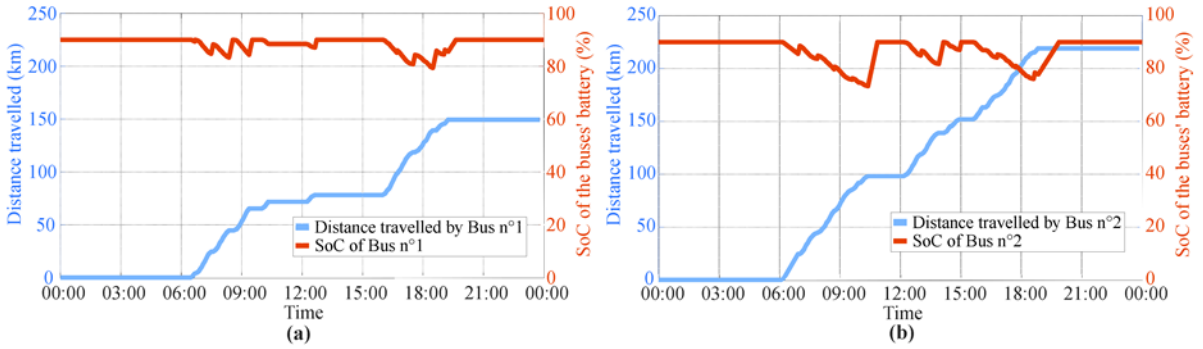


**Figure 4.1-10 Travelled distance and battery $SoC$ of buses n°1 (a) and n°2 (b) – scenario 2.**

It can be seen in Figure 4.1-11 that the two buses recharge during a short period at line terminals, usually not at the same time. However, the total charging power reaches 300 kW for 4 min at 06:36 P.M when both buses are charging at bus terminals and 200 kW for 3 min at 07:02 P.M when bus n°2 arrives at the terminal and bus n°1 is at the depot. The charging process occurs mainly during the day, when electricity is produced by PV panels. As for PV energy, 81 kWh are used directly to charge buses during the day, but additional stationary storage would increase the PV share during the day and allow the use of PV energy during the night.

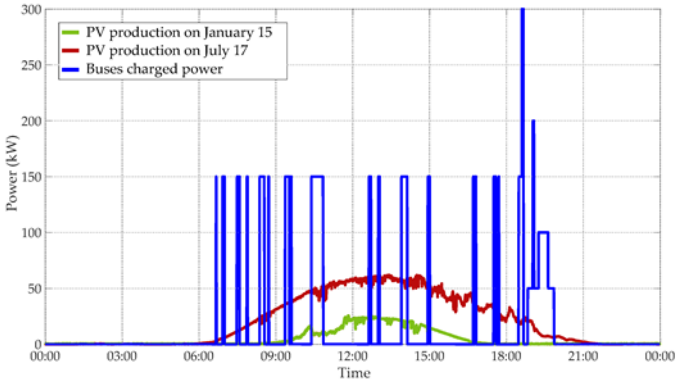


**Figure 4.1-11 Total charging power and PV production over time – scenario 2.**

### *4.1.5.3 Scenario 3 – Charge at Several Bus Stops*

In scenario 3, the battery capacity of the bus is reduced to 70 kWh. Charging stations are located at line terminals Gare and Aramont, and at bus stops Denielou and Matra Lecuru. The charging power is limited to 150 kW. Therefore, there is a delay of 84 s in the dwell time due

to the charging process at 09:49 A.M and 10:08 A.M. Figure 4.1-12 shows the cumulative distance travelled by bus n°2 in scenario 1 and scenario 3. The black dotted line is shifted twice compared to the orange one. The reason why this delay does not spread is because the simulation authorizes the bus to accelerate (up to a limit) to reach the next bus stop on time, as explained in Section 4.1.3.2. Case studies with more frequent buses would probably show a more significant impact on the transport due to the waiting time of buses when they need to charge at a bus stop but the charging station is occupied. The delay could be avoided by increasing the on-board battery capacity, increasing the charging power, and/or adding new charging points on the road to reduce the required energy between two charges.

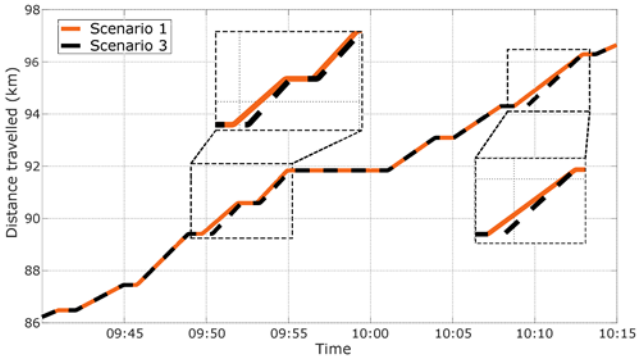


**Figure 4.1-12 Comparison between the distance travelled by bus n°2 in scenario 1 and scenario 3.**

Figure 4.1-13 shows that the $SoC$ of the 70-kWh battery of bus n°2 reaches 22.2% in scenario 3. This means that there is almost no security margin to ensure that the $SoC$ will not fall below $soc_{min}$ in case of a higher consumption. The total energy consumption is 337 kWh—respectively, 140 kWh and 197 kWh for buses n°1 and 2—which represents an average consumption per travelled distance of 0.91 kWh/km.

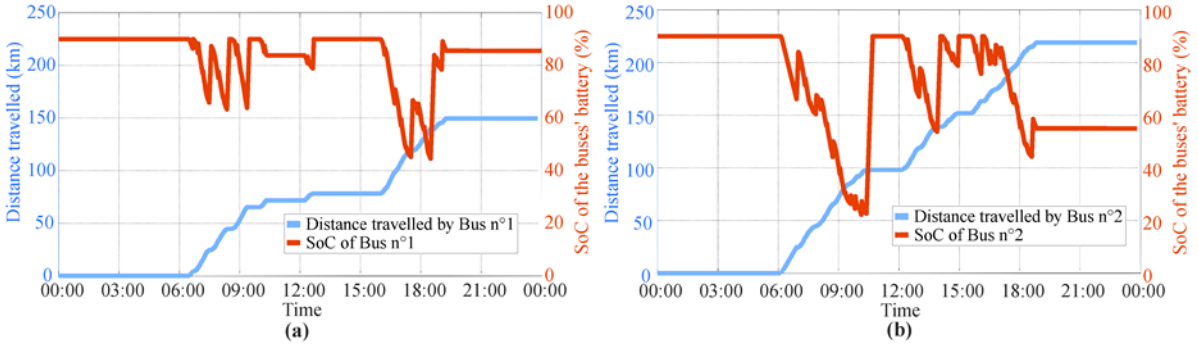


**Figure 4.1-13 Travelled distance and battery $SoC$ of buses n°1 (a) and n°2 (b) – scenario 3.**

Concerning the charging power, Figure 4.1-14 shows that most charges occur at different times with a power of 150 kW (the rated power of one charger). Rarely, 2 buses are charging at the same time, with a cumulative power of 300 kW when both buses are at bus stops (but not necessarily the same stop). The assumption here is that all chargers are connected to the same substation on the utility grid. Otherwise, the technical constraints would differ for each portion of the network where the chargers are located. Regarding PV energy, charging during the daylight at terminals and stops increases the PV self-consumption compared to scenarios 1 and 2. Additional storage would increase the PV benefits. Considering the reasonable amount of energy needed as the next charging station is close and the high charging power

required due to the short duration of charges at bus stops, supercapacitors with a high-power density could be used to store the solar energy but with an increased cost.

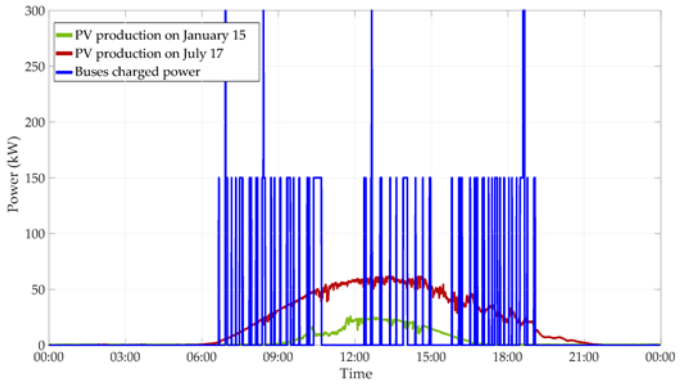


**Figure 4.1-14 Total charging power and PV production over time – scenario 3.**

### 4.1.6 Discussion

In this section, performances of all the scenarios are summarized in Table 4.1-5 and the results are discussed focusing on the impacts on the utility grid in terms of energy and power with/without considering the presence of PV panels. First of all, the charging of e-buses shows that the determined average bus consumption in terms of kWh/km is consistent with the literature data [4] which validates the presented model. However, it should be noted that there is a potential for further improvement of the presented model, through an analysis of the GTFS and Open Street Map data, by defining classes of roads according to the number of curves, intersections, and traffic lights. Additionally, the obtained energy consumption is 36 kWh (9.4%) less in scenario 3 (where a 70 kWh battery weighs 467 kg) compared to scenarios 1 and 2 (where a 422 kWh battery weighs 2.8 tons). Therefore, the total energy consumption of the two buses during their daily operation decreases based on the capacity of on-board battery. Secondly, analysing the minimal $SoC$ of the on-board battery allows assessing the adequacy between the capacity of the batteries and the charging scenario. For instance, in scenario 2, the minimal battery $SoC$ of bus n°2 is determined at 73.3% which indicates that the battery is oversized or that it can be charged less frequently and/or at a lower power. On the other hand, in scenario 3 in which buses operate with a lower battery capacity, the $SoC$ of bus n°2 decreases until it reaches 22.2%, which might increase charging time of the battery for next trip and cause delays in case of higher consumption. Lastly, the maximal charging power of the bus fleet is analysed for each scenario. The highest total power is determined at 1 200 kW in scenario 3ter where the two buses charge their battery simultaneously on route. Although the peak power only lasts a few seconds/minutes, it can jeopardize the reliability of the utility grid due to severe changes in grid consumption in the case of a massive deployment of e-buses. Utilization of PV energy can be considered low, which occurs because it is not able to charge the e-buses' batteries on the road. Therefore, the utilization of the hybrid energy system which is formed by PV panels and stationary storage is essential for increasing clean energy utilization for e-buses. On the other hand, the PV panels might be integrated into the roof of the e-buses in order to use produced PV power directly while moving on the road. However, in that case, the surrounding buildings around the road which e-buses use to perform their services are required to be modelled in detail to consider the impact of the buildings' shadows over the PV panels of the e-bus.

Concerning the utilization of local PV energy, simulation results show that only a small fraction of PV energy is directly supplied to e-buses and the rest of the energy is injected back into the

grid. The obtained self-consumption of the PV energy varies according to the scenarios as seen in Table 4.1-5. The highest utilization of the PV energy is obtained in scenario 2 (charging at terminals/depot) with 81 kWh, while the minimum is determined in scenario 1 (charging at depot) due to charging only at night. Moreover, it can be seen that the total energy production on January the 15$^{th}$ is lower than the buses' energy consumption. On the other hand, the produced PV energy in July is sufficient to supply all buses' consumption during the day if an additional stationary storage system is deployed.

Overall, this study presents a methodology for modelling and analysing the consumption power of the e-bus fleet for various scenarios. The potential impacts of the e-buses charging on the utility grid are discussed considering a local PV production without trying to minimize them via an optimization. However, results show that optimal planning and management are required for minimizing the grid impacts while maximizing the potential benefits. The main indicators that could be used as decision criteria for the implementation of a scenario are the e-buses' maximal charging power, grid supplied energy/power, and charging times. Based on the criteria, an optimal sizing of PV-storage-based charging infrastructure with an intelligent energy management algorithm can be developed for efficient public bus services that aims to increase renewable energy utilization by storing surplus production during the day and/or summer seasons and using it during low PV production times.

### 4.1.7 Conclusions

This study analyses the performance of various charging infrastructure placements. The proposed method considers a modelling of the bus network based on GTFS data and a sequential simulation of the bus operation. The method is applied to the operation of two buses on one bus line in Compiègne, France. Scenarios with charging stations at the depot, line terminals, and bus stops are compared. Results show the relevance of the method to estimate the impacts on both the transport delay and the power supplied from the grid. Charging at the depot implies having a larger on-board battery pack whereas on-route charging at bus stops and terminals helps reduce the battery capacity by 83%, and thus the bus consumption by 9.4% due to a reduction in the bus weight. However, on-route charging with a high power can have an impact on the utility grid, especially during the peaks of charging power. On the other hand, a lower charging power can generate some transport delay due to the slow charging process. The potential of a local PV production to reduce the impacts on the grid is shown. Nevertheless, the PV self-consumption remains very low during winter and PV energy cannot balance the buses consumption. During summer additional energy storage would increase PV benefits.

**Table 4.1-5 Performance indicators per scenarios.**

| Scenarios | 1 | 2 | 2bis | 3 | 3bis | 3ter |
|---|---|---|---|---|---|---|
| **Bus charging** | | | | | | |
| Average consumption of the buses (kWh/km) | 1.01 | 1.01 | 0.91 | 0.92 | 0.91 | 0.91 |
| Consumed energy of bus n°1 (kWh) | 155 | 155 | 140 | 140 | 140 | 140 |
| Consumed energy of bus n°2 (kWh) | 218 | 218 | 197 | 197 | 197 | 197 |
| Minimal SoC of bus n°1 (%) | 53.3 | 79.4 | 45.0 | 44.6 | 65.5 | 69.1 |
| Minimal SoC of bus n°2 (%) | 38.4 | 73.3 | 27.9 | 22.2 | 63.5 | 66.2 |
| Max. total charging power (kW) | 100 | 300 | 350 | 300 | 900 | 1200 |
| **Influence of PV production on 15 January** | | | | | | |
| PV energy production (kWh) | 108 | 108 | 108 | 108 | 108 | 108 |
| PV energy used for direct charging (kWh) | 1 | 14 | 6 | 13 | 4 | 3 |
| **Influence of PV production on 17 July** | | | | | | |
| PV energy production (kWh) | 500 | 500 | 500 | 500 | 500 | 500 |
| PV energy used for direct charging (kWh) | 17 | 81 | 42 | 69 | 24 | 18 |

Future work will simulate the charging process with stationary storage and smarter charging strategies. Furthermore, charging stations and PV power plants will be positioned on the utility grid to model more realistically the impacts on each portion of the network. The operation of larger fleets will be simulated to underline different impacts. An annual time horizon will allow analysing the evolution of the solar irradiation, external temperature, passenger flow, and bus services according to the period of the year and thus to simulate more realistically the operation of buses. Eventually, several performance indicators will be implemented in an optimization algorithm for the sizing and management of PV-storage-based charging infrastructures of an e-bus network.

## REFERENCES


[1] "Guide Bus Électriques ," Avere France, Sep. 2021. Available: Here , Accessed: Dec. 12, 2022.

[2] "Clean Bus Report - an Overview of Clean Buses in Europe Clean Bus Report," UITP ASSURED. Available: Here, Accessed: Dec. 12, 2022.

[3] "ZeEUS eBus Report #2 an Updated Overview of Electric Buses in Europe," ZeEUS , 2018. Available: Here, Accessed: Dec. 12, 2022.

[4] A. L. P. Rodrigues and Sonia. R. C. Seixas, "Battery-electric Buses and Their Implementation barriers: Analysis and Prospects for Sustainability," Sustainable Energy Technologies and Assessments, vol. 51, p. 101896, Jun. 2022, doi: https://doi.org/10.1016/j.seta.2021.101896.

[5] J. Ji, Y. Bie, Z. Zeng, and L. Wang, "Trip Energy Consumption Estimation for Electric Buses," Communications in Transportation Research, vol. 2, p. 100069, Dec. 2022, doi: https://doi.org/10.1016/j.commtr.2022.100069.

[6] Y. He, Z. Liu, and Z. Song, "Integrated Charging Infrastructure Planning and Charging Scheduling for Battery Electric Bus Systems," Transportation Research Part D: Transport and Environment, vol. 111, p. 103437, Oct. 2022, doi: https://doi.org/10.1016/j.trd.2022.103437.

[7] "TOSA: Geneva's Electrical Bus Innovation," Energy Cities. Available: Here, Accessed: Dec. 12, 2022.

[8] "ZEROING IN ON ZEBS," Calstart, 2020. Available Here, Accessed: Dec. 12, 2022.

[9] S. S. G. Perumal, R. M. Lusby, and J. Larsen, "Electric Bus Planning & scheduling: a Review of Related Problems and Methodologies," European Journal of Operational Research, vol. 301, no. 2, pp. 395–413, Sep. 2022, doi: https://doi.org/10.1016/j.ejor.2021.10.058.

[10] J. A. Manzolli, J. P. Trovão, and C. H. Antunes, "A review of electric bus vehicles research topics – Methods and trends," Renewable and Sustainable Energy Reviews, vol. 159, p. 112211, May 2022, doi: https://doi.org/10.1016/j.rser.2022.112211.

[11] T. Boonraksa, P. Boonraksa, and B. Marungsri, "Optimal Capacitor Location and Sizing for Reducing the Power Loss on the Power Distribution Systems due to the Dynamic Load of the Electric Buses Charging System using the Artificial Bee Colony Algorithm," Journal of Electrical Engineering & Technology, vol. 16, no. 4, pp. 1821–1831, 2021, doi: https://doi.org/10.1007/s42835021007184.

[12] K. Liu, H. Gao, Y. Wang, T. Feng, and C. Li, "Robust Charging Strategies for Electric Bus Fleets under Energy Consumption Uncertainty," Transportation Research Part D: Transport and Environment, vol. 104, p. 103215, Mar. 2022, doi: https://doi.org/10.1016/j.trd.2022.103215.

[13] E. Toniato, P. Mehta, S. Marinkovic, and V. Tiefenbeck, "Peak load minimization of an ebus depot: impacts of userset conditions in optimization algorithms," Energy Informatics, vol. 4, no. 3, p. 23, 2021, doi: https://doi.org/10.1186/s42162021001744.

[14] Z. Gao et al., "Battery Capacity and Recharging Needs for Electric Buses in City Transit Service," Energy, vol. 122, pp. 588–600, Mar. 2017, doi: https://doi.org/10.1016/j.energy.2017.01.101.

[15] C. Leone, L. Sturaro, Giacomo Geroli, M. Longo, and Wahiba Yaici, "Design and Implementation of an Electric Skibus Line in North Italy," Energies, vol. 14, no. 23, pp. 7925–7925, Nov. 2021, doi: https://doi.org/10.3390/en14237925.

[16] M. M. Hasan, N. Avramis, M. Ranta, A. Saez-de-Ibarra, M. El Baghdadi, and O. Hegazy, "Multi-Objective Energy Management and Charging Strategy for Electric Bus Fleets in Cities Using Various ECO Strategies," Sustainability, vol. 13, no. 14, p. 7865, Jul. 2021, doi: https://doi.org/10.3390/su13147865.

[17] M. Lotfi, P. Pereira, N. G. Paterakis, H. A. Gabbar, and Joao, "Optimal Design of Electric Bus Transport Systems with Minimal Total Ownership Cost," IEEE Access, vol. 8, pp. 119184–119199, Jan. 2020, doi: https://doi.org/10.1109/access.2020.3004910.

[18] A. Kunith, R. Mendelevitch, and D. Goehlich, "Electrification of a City Bus network – An Optimization Model for cost-effective Placing of Charging Infrastructure and Battery Sizing of fast-charging Electric Bus Systems," International Journal of Sustainable Transportation, vol. 11, no. 10, pp. 707–720, Mar. 2017, doi: https://doi.org/10.1080/15568318.2017.1310962.

[19] F. Trocker, O. Teichert, M. Gallet, A. Ongel, and M. Lienkamp, "City-scale Assessment of Stationary Energy Storage Supporting end-station Fast Charging for Different bus-fleet Electrification Levels," Journal of Energy Storage, vol. 32, p. 101794, Dec. 2020, doi: https://doi.org/10.1016/j.est.2020.101794.

[20] N. Qin, A. Gusrialdi, R. Paul Brooker, and A. T-Raissi, "Numerical Analysis of Electric Bus Fast Charging Strategies for Demand Charge Reduction," Transportation Research Part A: Policy and Practice, vol. 94, pp. 386–396, Dec. 2016, doi: https://doi.org/10.1016/j.tra.2016.09.014.

[21] Y. Bie, M. Hao, and M. Guo, "Optimal Electric Bus Scheduling Based on the Combination of All-Stop and Short-Turning Strategies," Sustainability, vol. 13, no. 4, p. 1827, Feb. 2021, doi: https://doi.org/10.3390/su13041827.

[22] P. Akaber, T. Hughes, and S. Sobolev, "MILP-based customer-oriented E-Fleet charging scheduling platform," IET Smart Grid, vol. 4, no. 2, pp. 215–223, Mar. 2021, doi: https://doi.org/10.1049/stg2.12034.

[23] Y. Lin, K. Zhang, Z.-J. M. Shen, B. Ye, and L. Miao, "Multistage large-scale charging station planning for electric buses considering transportation network and power grid," Transportation Research Part C: Emerging Technologies, vol. 107, pp. 423–443, Oct. 2019, doi: https://doi.org/10.1016/j.trc.2019.08.009.

[24] Y. Tomizawa et al., "Multipurpose Charging Schedule Optimization Method for Electric Buses: Evaluation Using Real City Data," IEEE Access, vol. 10, pp. 56067–56080, Jan. 2022, doi: https://doi.org/10.1109/access.2022.3177618.

[25] Z. Dalala, O. Al Banna, and O. Saadeh, "The Feasibility and Environmental Impact of Sustainable Public Transportation: A PV Supplied Electric Bus Network," Applied Sciences, vol. 10, no. 11, p. 3987, Jun. 2020, doi: https://doi.org/10.3390/app10113987.

[26] S. M. Arif, T. T. Lie, B. C. Seet, S. M. Ahsan, and H. A. Khan, "Plug-In Electric Bus Depot Charging with PV and ESS and Their Impact on LV Feeder," Energies, vol. 13, no. 9, p. 2139, Jan. 2020, doi: https://doi.org/10.3390/en13092139.

[27] S. Rafique, M. S. H. Nizami, U. B. Irshad, M. J. Hossain, and S. C. Mukhopadhyay, "A two-stage multi-objective stochastic optimization strategy to minimize cost for electric bus depot operators," Journal of Cleaner Production, vol. 332, p. 129856, Jan. 2022, doi: https://doi.org/10.1016/j.jclepro.2021.129856.

[28] P. Zhuang and H. Liang, "Stochastic Energy Management of Electric Bus Charging Stations With Renewable Energy Integration and B2G Capabilities," IEEE Transactions on Sustainable Energy, vol. 12, no. 2, pp. 1206–1216, Apr. 2021, doi: https://doi.org/10.1109/TSTE.2020.3039758.

[29] J. Szczesniak, T. Massier, M. Gallet, and A. Sharma, "Optimal Electric Bus Charging Scheduling for Local Balancing of Fluctuations in PV Generation," in 2019 IEEE Innovative Smart Grid Technologies - Asia (ISGT Asia), Chengdu, China, May 2019, pp. 2799–2804. doi: https://doi.org/10.1109/isgt-asia.2019.8881445.

[30] T. Santos, K. Lobato, J. Rocha, and J. A. Tenedório, "Modeling Photovoltaic Potential for Bus Shelters on a City-Scale: A Case Study in Lisbon," Applied Sciences, vol. 10, no. 14, p. 4801, Jul. 2020, doi: https://doi.org/10.3390/app10144801.

[31] S. M. M. Islam, A. A. Salema, and J. M.-Y. Lim, "Design and Sizing of Solar PV Plant for an Electric Bus Depot in Malaysia," E3S Web of Conferences, vol. 160, p. 02003, 2020, doi: https://doi.org/10.1051/e3sconf/202016002003.

[32] H. Ren, Z. Ma, A. Ming Lun Fong, and Y. Sun, "Optimal Deployment of Distributed Rooftop Photovoltaic Systems and Batteries for Achieving net-zero Energy of Electric Bus Transportation in high-density Cities," Applied Energy, vol. 319, p. 119274, Aug. 2022, doi: https://doi.org/10.1016/j.apenergy.2022.119274.

[33] H. Ren, Z. Ma, C. Fai Norman Tse, and Y. Sun, "Optimal Control of solar-powered Electric Bus Networks with Improved Renewable Energy on-site Consumption and Reduced Grid Dependence," Applied Energy, vol. 323, p. 119643, Oct. 2022, doi: https://doi.org/10.1016/j.apenergy.2022.119643.

[34] "ARC Express - Timetable," Agglomération De La Région De Compiègne., Nov. 2021. Available: Here, Accessed: Dec. 12, 2022.

[35] O. A. Hjelkrem, K. Y. Lervåg, S. Babri, C. Lu, and C.-J. Södersten, "A battery electric bus energy consumption model for strategic purposes: Validation of a proposed model structure with data from bus fleets in China and Norway," Transportation Research Part D: Transport and Environment, vol. 94, p. 102804, May 2021, doi: https://doi.org/10.1016/j.trd.2021.102804.

[36] X. Li, T. Wang, J. Li, Y. Tian, and J. Tian, "Energy Consumption Estimation for Electric Buses Based on a Physical and Data-Driven Fusion Model," Energies, vol. 15, no. 11, p. 4160, Jun. 2022, doi: https://doi.org/10.3390/en15114160.

[37] X. Ma, R. Miao, X. Wu, and X. Liu, "Examining influential factors on the energy consumption of electric and diesel buses: A data-driven analysis of large-scale public transit network in Beijing," Energy, vol. 216, p. 119196, Feb. 2021, doi: https://doi.org/10.1016/j.energy.2020.119196.

[38] N. A. El-Taweel, A. Zidan, and Hany, "Novel Electric Bus Energy Consumption Model Based on Probabilistic Synthetic Speed Profile Integrated With HVAC," IEEE Transactions on Intelligent Transportation Systems, vol. 22, no. 3, pp. 1517–1531, Mar. 2021, doi: https://doi.org/10.1109/tits.2020.2971686.

[39] Hatem Abdelaty and M. Mohamed, "A framework for BEB energy prediction using low-resolution open-source data-driven model," Transportation Research Part D: Transport and Environment, vol. 103, pp. 103170–103170, Feb. 2022, doi: https://doi.org/10.1016/j.trd.2022.103170.

[40] J. Asamer, A. Graser, B. Heilmann, and M. Ruthmair, "Sensitivity analysis for energy demand estimation of electric vehicles," Transportation Research Part D: Transport and Environment, vol. 46, pp. 182–199, Jul. 2016, doi: https://doi.org/10.1016/j.trd.2016.03.017.

[41] D. Jefferies and D. Göhlich, "A Comprehensive TCO Evaluation Method for Electric Bus Systems Based on Discrete-Event Simulation Including Bus Scheduling and Charging Infrastructure Optimisation," World Electric Vehicle Journal, vol. 11, no. 3, p. 56, Aug. 2020, doi: https://doi.org/10.3390/wevj11030056.

[42] D. Göhlich, T.-A. Fay, D. Jefferies, E. Lauth, A. Kunith, and X. Zhang, "Design of urban electric bus systems," Design Science, vol. 4, 2018, doi: https://doi.org/10.1017/dsj.2018.10.

[43] A. Lajunen and T. Lipman, "Lifecycle cost assessment and carbon dioxide emissions of diesel, natural gas, hybrid electric, fuel cell hybrid and electric transit buses," Energy, vol. 106, pp. 329–342, Jul. 2016, doi: https://doi.org/10.1016/j.energy.2016.03.075.

[44] F. Cigarini, T.-A. Fay, N. Artemenko, and D. Göhlich, "Modeling and Experimental Investigation of Thermal Comfort and Energy Consumption in a Battery Electric Bus," World Electric Vehicle Journal, vol. 12, no. 1, p. 7, Jan. 2021, doi: https://doi.org/10.3390/wevj12010007.

[45] J. Vepsäläinen, K. Kivekäs, K. Otto, A. Lajunen, and K. Tammi, "Development and validation of energy demand uncertainty model for electric city buses," Transportation Research Part D: Transport and Environment, vol. 63, pp. 347–361, Aug. 2018, doi: https://doi.org/10.1016/j.trd.2018.06.004.

[46] K. Kivekas, A. Lajunen, F. Baldi, J. Vepsalainen, and K. Tammi, "Reducing the Energy Consumption of Electric Buses With Design Choices and Predictive Driving," IEEE Transactions on Vehicular Technology, vol. 68, no. 12, pp. 11409–11419, Dec. 2019, doi: https://doi.org/10.1109/tvt.2019.2936772.

[47] L. Kessler and K. Bogenberger, "Dynamic traffic information for electric vehicles as a basis for energy-efficient routing," Transportation Research Procedia, vol. 37, pp. 457–464, 2019, doi: https://doi.org/10.1016/j.trpro.2018.12.218.

[48] Wojciech GIS, Stanisław KRUCZYŃSKI, S. TAUBERT, and Andrzej WIERZEJSKI, "Studies of energy use by electric buses in SORT tests," Silniki Spalinowe/Combustion Engines, vol. 170, no. 3, pp. 135–138, Aug. 2017, doi: https://doi.org/10.19206/ce-2017-323.

[49] N. Kammuang-lue and J. Boonjun, "Energy consumption of battery electric bus simulated from international driving cycles compared to real-world driving cycle in Chiang Mai," Energy Reports, vol. 7, pp. 344–349, Sep. 2021, doi: https://doi.org/10.1016/j.egyr.2021.07.016.

[50] V. Algin, A. M. Goman, and A. S. Skorokhodov, Main Operational Factors Determining the Energy Consumption of the Urban Electric bus: Schematization and modelling. 2019. doi: https://doi.org/10.13140/RG.2.2.32154.80328.

[51] M. Sechilariu and F. Locment, Intelligent Control and Power Flow Optimization. Elsevier, 2016. doi: https://doi.org/10.1016/b978-0-12-803736-2.00002-5.

[52] " Google Transit - Static Transit - GTFS Reference," Google Developers. Available: Here , Accessed: Dec. 12, 2022.

[53] "OpenStreetMap." https://www.openstreetmap.org Accessed: Dec. 12, 2022.

[54] "Open-Elevation API." https://open-elevation.com Accessed: Dec. 12, 2022.

[55] O. Czogalla and U. Jumar, "Design and control of electric bus vehicle model for estimation of energy consumption," IFAC-PapersOnLine, vol. 52, no. 24, pp. 59–64, 2019, doi: https://doi.org/10.1016/j.ifacol.2019.12.381.

[56] C. Fiori, M. Montanino, S. Nielsen, M. Seredynski, and F. Viti, "Microscopic Energy Consumption Modelling of Electric buses: Model development, calibration, and Validation," Transportation Research Part D: Transport and Environment, vol. 98, p. 102978, Sep. 2021, doi: https://doi.org/10.1016/j.trd.2021.102978.

[57] "ARC Peri-Urban Lines Map," Jul. 2021. Available: Here, Accessed: Dec. 12, 2022.

[58] "BYD Europe - 12 m eBus," 2025. https://bydeurope.com/pdp-bus-model-12 Accessed: Dec. 12, 2022.

[59] "Electric Bus Charging Station | Electric Truck Charging," Electric Vehicle Charging Infrastructure. https://new.abb.com/ev-charging/depot-connector-charging Accessed: Dec. 12, 2022.

[60] "Pantograph Bus | Pantograph Up," Electric Vehicle Charging Infrastructure. https://new.abb.com/ev-charging/pantograph-up Accessed: Dec. 12, 2022.

# CONCLUSIONS AND FUTURE WORKS

This report has explored various aspects of EV charging infrastructure and energy management systems, with emphasis on optimization approaches and their practical implications.

As the number of EVs and the complexity of charging scenarios grow, scalability becomes a critical concern. Addressing this, a series of modifications to the MILP formulation were proposed to reduce computational burden. By employing linear cuts and reformulating the problem as a linear program under simplified assumptions, substantial reductions in solving time were achieved without sacrificing solution quality. Additionally, a distributed computation scheme was introduced, further enhancing scalability for large-scale implementations. These adjustments demonstrated that it is possible to efficiently manage thousands of vehicles while maintaining near-optimal performance, making real-time or near real-time operation increasingly viable.

Beyond individual vehicle charging, the optimization of microgrids that incorporate renewable energy sources and storage systems was also examined. When sizing components and managing energy flows within DC microgrids, it was observed that operation in islanded mode led to larger capacity requirements compared to grid-connected scenarios. This is primarily due to the need to maintain supply reliability under variable generation conditions. Economic analysis revealed trade-offs between lower levelized cost of electricity (LCOE) and higher investment or replacement costs, with battery energy storage systems (BESS) playing a pivotal role in both cost and emissions profiles. Environmentally, the systems contributed significantly to local energy production, but grid reliance remained essential, particularly in the context of the French energy mix.

The location of deployment also plays a key role, as shown in a comparative study across multiple cities using different solar irradiation levels. The results highlighted that optimal system configurations vary significantly with local resource availability. Cities with higher solar irradiation achieved better economic and environmental performance, although temporal fluctuations in solar availability affected outcomes. These findings reinforce the need for site-specific designs and emphasize the value of tailoring renewable resource integration based on local conditions. Technologies such as locally produced PV panels and BESS were shown to have a dominant influence on the life-cycle emissions of the systems.

Energy cost optimization and vehicle-to-grid (V2G) services offer additional avenues to improve system efficiency and sustainability. Incorporating real-time simulations that account for prediction errors, it was demonstrated that dynamic scheduling of charging and discharging could minimize costs and enhance grid support. V2G-enabled systems were especially effective in reducing peak grid demand and increasing profitability, with EVs providing the greatest flexibility. However, challenges remain in standardizing communication protocols, addressing battery degradation, and managing integration costs. Future research aims to deepen these analyses through annual-scale simulations and hardware-in-the-loop testing to better understand long-term impacts and system behaviour under realistic conditions.

Finally, the charging infrastructure for electric buses was assessed, considering the implications of different charging station placements on transport efficiency and grid impact. While depot charging required larger battery capacities and incurred higher energy consumption due to increased vehicle weight, on-route charging offered significant benefits by reducing battery size and overall energy usage. Nevertheless, such strategies introduced new

challenges, such as potential grid stress during high-power charging events and increased transport delays with slower charging rates. The potential of local PV generation was also explored, though seasonal variability limited its contribution during certain periods. Future developments will involve integrating stationary storage, refining charging strategies, and modeling broader grid interactions to inform the optimal design and management of e-bus charging networks.

Taken together, the studies in this report highlight the multifaceted nature of EV charging systems and energy management, showing that advances in optimization, infrastructure sizing, and system integration are key to achieving both economic and environmental goals. Moving forward, continued interdisciplinary research and real-world validation will be essential to unlock the full potential of sustainable electric mobility.